NEW GENERATION MULTI-FUNCTIONAL CEMENTITIOUS COMPOSITES WITH PHOTOCATALYTIC DEGRADATION CAPABILITY

FOTOKATALİTİK İNDİRGEME KABİLİYETİNE SAHİP YENİ NESİL ÇOK FONKSİYONLU ÇİMENTO BAĞLAYICILI KOMPOZİTLER

EMRAH BAHŞİ

PROF. DR. MUSTAFA ŞAHMARAN

Supervisor

Submitted to

Graduate School of Science and Engineering of Hacettepe University

as a Partial Fulfilment to the Requirements

for be Award of the Degree of **Doctor of Philosophy**

in Civil Engineering

2022

ABSTRACT

NEW GENERATION MULTI-FUNCTIONAL CEMENTITIOUS COMPOSITES WITH PHOTOCATALYTIC DEGRADATION CAPABILITY

Emrah BAHŞİ

Doctor of Philosophy, Department of Civil Engineering

Supervisor: Prof. Dr. Mustafa ŞAHMARAN

March 2022, 216 pages

Today, air quality continues to be an important issue affecting public health, environment, and economy around the world. One of the most fundamental problems faced by industrialized societies is air pollution caused by high amounts of nitrogen oxides (NO_x) released from crowded cities and industrial areas to the atmosphere. Thanks to remarkable technological developments, such problems are reduced using ultraviolet (UV) rays from solar energy, and new solutions are tried to be produced for large surface areas of building materials. Considering that concrete is the most widely used material after water, it can be said that one of the main ways to overcome the air pollution faced by modern societies is to develop innovative, functional, and economical building materials reducing air pollutants by chemically binding them. In this context, titanium dioxide (TiO_2), a type of photocatalytic material and also a semiconductor, comes to the fore with some of its properties such as its strong oxidation capacity under UV light irradiatons, its chemical stability when exposed to acidic and basic compounds, its chemical inertness in the absence of UV lights, and its non-toxicity. Due to these properties, it is an important photocatalyst material that can be used in construction applications. Within the scope of this thesis study, TiO_2-added photocatalytic cementitious composites were developed by considering many parameters at different scales (nano and micro scales) at the same time,

which can offer applicable solutions to the abovementioned environmental problems. In this context, first of all, an efficient mixing method to be used in experimental studies of this thesis was developed in order to homogeneously disperse TiO_2 particles of different sizes (especially nanoscale) throughout cement-based materials. After that, TiO_2 particles under different crystal phases (anatase and rutile) were substituted into the cement-based systems at the rates of 2.5%, 5%, 7.5%, and 10% of the total weight of binder to investigate their effects on composite materials' properties and the most appropriate usage rate of TiO_2 was determined. Then, the optimum particle size distribution (PSD) of TiO_2 particles was determined by using TiO_2 particles with three different size ranges (nano, submicron and micron) in combination at the optimum substitution rate by adjusting their PSDs with three different PSD moduli (q): 0.1, 0.5, and 0.9. Finally, the photocatalytic degradation capability of TiO_2 particles under different crystal phases (anatase and rutile) were investigated by incorporating them into the cementitious systems and the most suitable combination of anatase and rutile TiO_2 particles was determined.

Keywords: NO_x reduction, Titanium dioxide, Photocatalytic performance, Particle size distrubution, Optimum substitution rate, Optimum combination, Anatase and rutile phase.

ÖZET

FOTOKATALİTİK İNDİRGEME KABİLİYETİNE SAHİP YENİ NESİL ÇOK FONKSİYONLU ÇİMENTO BAĞLAYICILI KOMPOZİTLER

Emrah BAHŞİ

Doktora, İnşaat Mühendisliği Bölümü
Tez Danışmanı: Prof. Dr. Mustafa ŞAHMARAN
Mart 2022, 216 sayfa

Günümüzde dünya genelinde hava kalitesi; halk sağlığını, çevreyi ve ekonomiyi etkileyen önemli bir husus olmaya devam etmektedir. Gelişmiş sanayi toplumlarının karşılaştığı en temel problemlerden birisi kalabalık şehirlerden ve sanayi bölgelerinden atmosfere salınan yüksek miktardaki nitrojen oksitlerden (NO_x) kaynaklanan hava kirlilikleridir. Dikkate değer teknolojik gelişmeler sayesinde bu tip sorunlar güneş enerjisinden gelen ultraviyole (UV) ışınlarından yararlanılması ile azaltılmakta ve yapı malzemelerinin geniş yüzey alanlarına yönelik olarak yeni çözümler üretilmeye çalışılmaktadır. Hacimsel olarak sudan sonra en çok kullanılan malzemenin beton olduğu düşünüldüğünde, modern toplumların karşı karşıya kaldığı hava kirliliklerini aşmanın temel yollarından birisinin de var olan temel yapı malzemelerini havada kirliliği oluşturan maddeleri kimyasal olarak bağlayarak azaltacak nitelikte, yenilikçi, fonksiyonel ve ekonomik tasarımlar ile geliştirmek olduğu söylenebilir. Bu kapsamda fotokatalitik malzemelerin bir türü ve aynı zamanda bir yarı iletken olan titanyum dioksit (TiO_2) bazı özellikleri ile ön plana çıkmaktadır. Bunlar, UV ışınları altındaki güçlü oksidasyon kapasitesi, asidik ve bazı temel bileşiklere maruz kaldığı durumlarda kimyasal stabilitesini koruyabilmesi, UV ışıklarının yokluğunda aktive olmaması ve toksik herhangi bir özellik göstermemesidir.

Sahip olduğu bu özelliklerinden dolayı TiO_2 inşaat uygulamalarında kullanılabilecek önemli bir fotokatalizör malzeme olarak karşımıza çıkmaktadır. Tez çalışmaları kapsamında, bahsedilen çevre problemlerine uygulanabilir çözümler sunabilen, geleneksel yöntemlerden farklı olarak, tasarımında aynı anda farklı ölçeklerde (nano ve mikro ölçekler) birçok parametre dikkate alınarak, TiO_2 katkılı çimento bağlayıcı kompozitler geliştirilmiştir. Bu bağlamda öncelikle, farklı boyutlardaki özellikle nano ölçekli TiO_2 taneciklerinin homojen olarak dağıtılabilmesi amacı ile uygun pratik karıştırma yöntemleri üzerinde çalışmalar yapılarak verimli karıştırma yöntemleri geliştirilmiş ve tez boyunca bu yöntem uygulanmıştır. Daha sonra farklı kristal fazlardaki (anataz ve rutil) TiO_2 partilülleri, toplam bağlayıcı ağırlığının %2,5, %5, %7,5 ve %10 oranlarında ikame edilmiş ve kompozit malzemeler üzerindeki etkileri araştırılarak, en uygun kullanım oranı tespit edilmiştir. Daha sonra optimum ikame oranında, farklı dağılım modülleri (q:0,1- 0,5 ve 0,9) kullanılarak optimum dağılım modülü belirlenmiştir. Son olarak, farklı kristal fazlardaki (anataz ve rutil) TiO_2 taneciklerinin birlikte farklı kombinasyonlarda çimentolu sistemlere dahil edilmesiyle elde edilen kompozitlerin, fotokatalitik etkileri araştırılarak, en uygun kombinasyon belirlenmiştir.

Anahtar Kelimeler: NO_x indirgeme, Titanyum dioksit, Fotokatalitk performans, Parçacık boyut dağılımı, Optimum ikame oranı, Optimum kombinasyon, Anataz ve rutil fazı.

,

ACKNOWLEDGEMENT

Foremost, I would like to express my deep gratitude to my supervisor Prof. Dr. Mustafa ŞAHMARAN for supporting and guiding me with his vast knowledge and experience throughout my thesis study. It was a great honour and pleasure to work with him.

I also want to extend my thanks to Prof. Dr. İsmail Özgür YAMAN, Prof. Dr. İlhami DEMİR, Assoc. Prof. Dr. Alper ALDEMİR, Assoc. Prof. Dr. Gürkan YILDIRIM for being in my thesis jury.

I would like to thank all members of the Advanced Concrete Research Laboratory at Hacettepe University for their support and valuable friendship. Especially, I would like to thank my friends Oğuzhan ŞAHİN, Muhammed Faruk GÜNAL and Samed BAY for their encouragements and support.

I would also like to thank the project numbered 118M197 within the scope of the 1001 program of the Scientific and Technical Research Council of Turkey (TÜBİTAK) for the financial support it has provided, part of which is my thesis work.

Finally, I am grateful to my mother Elif BAHŞİ, my father Ali Rıza BAHŞİ, who passed away recently, and my brothers and sisters for their endless support, encouragement, and precious love. I would also like to thank my dear wife Tuğba BAHŞİ, my daughter Elif Vera BAHŞİ, my mother-in-law Şerife YAĞCI and my father-in-law Ahmet YAĞCI, who supported and motivated me throughout this process.

EMRAH BAHŞİ

March 2022, Ankara

TABLE OF CONTENTS

LIST OF FIGURES

LIST OF TABLES

SYMBOLS AND ABBREVIATIONS

Symbols

D	Pore Diameter
^{o}C	Centigrade Degree
Z	Electrical Impedance
γ	Surface Tension of the Mercury
θ	Contact Angle Between the Mercury and the Pore Wall
μm	Micrometer
ρ	Resistance
ϕ	Phase Angle

Abbreviations

$Ca(OH)_2$	Calcium Hydroxide
CdO	Cadmium Oxide
CdS	Cadmium Sulfide
CO	Carbon Monoxide
CO_2	Carbon Dioxide
C-S-H	Calcium Silicate Hydrate
CTD	Computed Tomography Device
D P25	Degussa Evonik P25
e^-/h^+	Electron-Hole Pairs
EDX	Energy Dispersive X-Ray Analysis
EEA	European Environment Agency
E_g	Band Gap Energy
EPA	United States Environmental Protection Agency
EU	Europe
eV	Electronvolt
Fe_2O_3	Iron Oxide
LOI	Loss on Ignition

MA	Micron Anatase
MA	Micron Rutile
MIP	Mercury Intrusion Porosimetry Test
MR	Micron Rutile
NA	Nano Anatase
nm	Nanometer
NO	Nitrogen Monoxide
NO_2	Nitrogen Dioxide
NO_x	Nitrogen Oxide
O^{2-}	Superoxide Radical
OH*	Hydroxyl Radicals
PAA	Polyacrylic Acid
ppb	Parts Per Billion
ppm	Parts Per Million
PSD	Particle Size Distribution
Rpm	Revolutions Per Minute
SEM	Scanning Electron Microscopy
SMA	Sub-micron Anatase
SMR	Sub-micron Rutile
SO_2	Sulfur Dioxide
SP	Superplasticizer
TGA	Thermogravimetric Analysis
TiO_2	Titanium Dioxide
UV	Ultraviolet
w/c	Water-to-Cement Ratio (by weight)
WHO	World Health Organization
WO_3	Tungsten Trioxide
WPC	White Portland Cement
XRD	X-ray Diffraction Analysis
XRF	X-ray Fluorescence Analysis
ZnO	Zinc Oxide

1. INTRODUCTION

1.1. Problem Definition

As a consequence of the rapidly increasing urbanization, population, number of vehicles, advancing industry among many other reasons, air pollution has reached serious levels and become one of the most pressing environmental issues facing the nations in the world. The World Health Organization (WHO) reported that air pollution is responsible for the death of 8 million people around the world annually and 9 out of 10 people living in low- and middle-income countries are exposed to environmental air pollution (WHO, 2020), pointing out the disturbing effect of air pollution on the quality of life of our society, which is increasingly urbanizing every day.

Air pollution is caused by different types of solid, liquid, and gaseous materials suspended in the air; the most important of which are the harmful gases of carbon monoxide (CO), sulfur dioxide (SO_2), and nitrogen oxides (NO_x). These gases are particularly important, because if inhaled without any protection up to certain level, they can be very dangerous health-wise, especially for the upper respiratory tract given their toxic nature. In order to reduce/eliminate the amount of these gases, several solutions focusing on their reduction/elimination on the source level and their existence after their production have been attempted. Given the situation of these gases, however, it is evident that current measures are not adequate and needed to require advancements to be made.

Among air pollutant gases that are harmful to human health, NO_x requires special attention since they are highly reactive, odorless, colorless and water-insoluble. They are generated in the compound forms of NO and NO_2. The exhaust gases of vehicles are one of the main contributors to the world's NO_x emission alongside with industrial activities (Cunha-Lopes et al., 2019). It has been stated by a report related to the worsening in air quality of the São Paulo State of Brazil that major factors found responsible for the air pollution are around 2000 industrial establishments located in the city and around 9.7 million registered vehicles. It was also reported that the NO_x release amount from these sources was around 376k tons in 2009, and the vehicles were responsible for approximately 96% of the NO_x-related air pollution (Prodesp, 2009). According to a report published by the South Korea National Air Pollutants Emission Service (National

Air Pollutants Emission Service of Korea. Emission Rate Inquiry, 2020), NO_x emitted from different sources, which is the substance with the highest emission rate, is responsible for about 26% of the total pollution. Total NO_x emission in South Korea measured in 2017 was about 1189k tons, and the road transport had the biggest share with 434k tons/year. Considering that the cases in regard to NO_x emission in other countries are similar to the above examples, many developed countries have taken measures to limit/reduce their NO_x emission over the years. So as to control/limit the rate of NO_x emission to the atmosphere, United States Environmental Protection Agency (EPA,2010, 2018) has set a one-hour ambient air quality standard for NO_2 at a level of 100 parts per billion (ppb) and an annual NO_2 standard at a level of 53 ppb based on annual average NO_2 concentrations, and strict control measures were applied to interested parties to properly comply with this matter. NO_x release is a major concern in European countries (The United Kingdom and EU-27) as well. They have made a number of adjustments to limit NO_x emission rates and minimize its detrimental effects. For the European countries, the determined critical/limit value for NO_x concentration in air is 40 $\mu g/m^3$ as an annual average. The vegetation critical level set for the protection of vegetation (beyond/above this level, direct adverse impacts on sensitive vegetation may happen) is 30 $\mu g/m^3$ as an annual average and the official 1-hour NO_2 standard is for a level at or below 200 $\mu g/m^3$ (EEA, 2018; EU, 2008; WHO, 2000). Owing to such adjustments related with NO_x, the rate of decrement in the amount of NO_x emission from 2017 to 2018 was 4.1% and this decrement rate was 60% for 1990–2018 (EEA, 2020). Despite the availability of measures taken to combat the high levels of NO_x, additional solutions must be sought since the problem of air pollution is far from being reduced currently.

1.2. Scope and Objectives

One innovative and new-generation way to eliminate NO_x in the air is using photocatalysts in photocatalytic degradation reactions via photoactivation. Photocatalysts induce the formation of photoinduced negative electrons and positive holes (surface charge carriers) when exposed to visible or ultraviolet light (UV). A series of reduction and oxidation reactions (redox) are initiated by these surface charge carriers resulting in the generation of reactive radical species (mainly hydroxyl and/or superoxide radicals) and these radicals exhibit capability to oxidize/degrade various pollutants such as NO_x (Nishikawa and Takahara, 2001; Martyanov and Klabunde, 2003; Ohama and Gemert, 2011). There are various photocatalyst materials used in the photocatalytic applications

like cadmium oxide (CdO), titanium dioxide (TiO_2), zinc oxide (ZnO) etc.. Among them, TiO_2 is one of the most popular photocatalysts, most probably because of its enhanced photocatalytic activity (Hager et al., 2000), safety, chemical inertness while not being exposed to irradiation, cost-efficiency, and nontoxicity (Zhao and Yang, 2003; Wang et al., 2007; Husken and Brouwers, 2008). Moreover, it's a commonly used material in a variety of applications like as different self-cleaning purposes including water and air purification, cancer treatment, development of dye-sensitized solar cells, sterilization, development of antifogging surfaces, water splitting, and CO_2 reduction (Fujishima et al., 1986; Cai et al., 1991, 1992; Anpo et al., 1995; Blake et al., 1999; Fujishima et al., 2000; Mills et al., 2003; Mor et al., 2006; Supeno and Siburian, 2018). It also has very wide and rapidly expanding area of use in many subbranches of different industries through its superior photocatalytic degradation capability.

The photocatalytic degradation capability of TiO_2 has become of interest particularly to those working on the construction-related sectors utilizing construction materials heavily. This is mainly because of the structural members have large surface areas that can be easily subjected to irradiation from the sun and/or any other artificial source to trigger photocatalytic activity and can be useful instruments for air purification purposes. In line with this idea, incorporation of photocatalysts (e.g., nano-TiO_2) into cementitious systems has been an option to provide air purification property for the construction materials in favor of achieving multi-functionality alongside the improvement of other performance indicators (e.g., strength, permeability, durability, material greenness).

Within the scope of this thesis study, it is aimed to develop new generation multifunctional cementitious systems with high photocatalytic performance and NO_x reduction capability without endangering fundamental engineering properties by using a multi-scale design approach. With this thesis work carried out, some of the superior properties of cement-based systems is integrated with the functions of photocatalyst materials to combat environmental (air) pollution. In this context, new generation photocatalytic cement-based systems are developed for the decomposition of polluting agents that cause air pollution, especially in city centers, and their conversion into the harmless products. In order for achieving a long-term stable photocatalytic performance, superior photocatalytic efficiency and NO_x reduction capability, TiO_2-incorporated

cement-based systems are designed through a holistic approach evaluating many parameters simultaneously. It is expected that the outputs obtained from this study will contribute to the improvements in life standards when considering the air pollution has seriously threatened human life all over the world.

So as to get at the primary of this thesis study, the following particular objectives are determined.

- Determination of a cost-effective, practical and feasible mixing method allowing proper dispersion of TiO_2 particles throughout the cement-based systems.
- Determination of the optimum utilization rate of TiO_2 particles in terms of different engineering properties of the cement-based systems (especially for photocatalytic performance)
- Determination of optimum TiO_2 particle size distribution of TiO_2 particles in a wide range of sizes incorporated into cement-based systems in terms of the engineering properties of cementitious systems and/or the degree of photocatalytic reactions in favor of NO_x degradation capability.
- Determination of the optimum combination of anatase and rutile TiO_2 particles providing the optimum NO_x reduction capability for photocatalytic cement-based systems.

1.3. Thesis Outline

The content of the five main sections of this thesis is summarized below.

In the first section, the main problems that are the subject of the studies carried out within the scope of the thesis are defined and the aim, scope and objectives of the thesis study are explained. Generel content of the thesis study is also detailed under this section.

Within the scope of the second section, a detailed literature review on the TiO_2 as a photocatalyst and its NO_x reduction mechanism, the factors affecting the photocatalytic performance of the systems, and the use of TiO_2 in cementitious systems is presented.

In the third section, detailed information about the materials used, the preparation of the specimens, the mixing methods investigated, and the tests performed are given.

The fourth section is the main section in which the results obtained from the experimental studies are presented. This section is comprised of the determination of (i) best mixing method achieving the most homogeneous distribution of TiO_2 particles throughout the cement-based systems, (ii) the optimum utilization rate of TiO_2 particles in the cement-based systems in order to provide efficient photocatalytic degradation process, (iii) the optimum TiO_2 particle size distribution to develop microstructure of the cement-based systems in favor of photocatalytic performance, and (iv) the optimum combination of anatase and rutile TiO_2 particles.

Finally, within the scope of the fifth section, the important conclusions obtained within the framework of the experimental studies of thesis are summarized.

2. LITERATURE REVIEW

2.1. Introduction

In this section, the properties of the TiO_2 materials, the photocatalytic reaction mechanism of the TiO_2 particles and parameters affecting the photocatalyic reduction effectiveness of TiO_2 particles/TiO_2-incorporated systems are explained. In addition, studies from the current literature mainly focusing on the photocatalytic systems are summarized extensively outlining the current understanding, situation, and research directions to equip cementitious systems with the air purification property.

2.2. TiO_2 as a Photocatalyst

Photocatalytic reactions occur as a result of the activation of heterogeneous semi-conductive photocatalysts through irradiation. Owing to their considerably high activity in NO_x degradation through photocatalytic reactions, TiO_2, ZnO and CdO are often preferred as photocatalysts (Juan and Xudong, 2003; Chen et al., 2008). Among these materials, TiO_2 is the most commonly used semi-conductive photocatalyst, given its superior characteristics including its enhanced photocatalytic activity (Hager et al., 2000), safety, chemical inertness while not being exposed to radiation, cost-efficiency, and nontoxicity (Zhao and Yang, 2003; Wang et al., 2007; Husken et al., 2009). Under this title, detailed information in regard to the use of TiO_2 as a photocatalytic material are shared.

2.2.1. Structure of TiO_2

There are three crystalline phases of TiO2 in nature, under atmospheric pressure; anatase (tetragonal), rutile (tetragonal), and brookite (orthorhombic) (Gamboa and Pasquevich, 1992; Mo and Ching, 1995; Ding et al., 1996; Ghosh et al., 2003; Smith et al., 2009) crystallographic structures of which are shown in Figure 2.1. Rutile is the most stable thermodynamically and is the most prevalent type (Gouma and Mills, 2001; Lin et al., 2013; Mayabadi et al., 2014; Fazli et al., 2017;). Anatase can transform into rutile phase at elevated temperatures and this transformation is not reversible. There are also other phases of TiO_2 formed under high pressure, which are TiO_2 II or srilankite, cubic fluorite, pyrite-type, monoclinic baddeleyite-type and cotunnite-type phases (Hanaor and Sorrell,

2011). The generation of brookite phase is more difficult, therefore, its presence is less common compared to other natural phases of TiO_2, which led researchers to focus on more common phases of metastable anatase and stable rutile. Anatase and rutile phases have a tetragonal ditetragonal dipyramidal crystal system, where Ti^{4+} is bonded with six O^{2-} resulting in the formation of TiO_6 octahedra chain (oxygen atoms around a titanium atom), with different lattice parameters of a=0.378nm; b=0.951nm and a=0.459nm; b=0.296nm, respectively (Cromer and Herrington, 1955; Burdett et al., 1987; Peters and Vill, 1989; Fisher and Egerton, 2001; Austin and Lim, 2008). They are both inert and insoluble in water (Fisher and Egerton, 2001). The number of atoms per unit cell (Z) is 4 for anatase and 2 for rutile (Cromer and Herrington, 1955; Burdett et al., 1987; Peters and Vill, 1989; Mo and Ching, 1995). It can be seen from lattice parameters of these two forms of TiO2 that rutile has a relatively shorter and wider lattice structure compared to anatase making it different in terms of physical and chemical properties. The unit cell volumes (volumes of the lattices) of rutile and anatase phases are approximately 0.0624 and 0.1363 nm^3 (Burdett et al., 1987; Peters and Vill, 1989; Hanaor and Sorrell, 2011; Hanson, 2014), while their hardnesses are 5.5-6 and 6-6.5 Mohs, respectively (Hanaor and Sorrell, 2011; Oi et al., 2016). While rutile can be excited by both visible and UV light, anatase is only excited by the UV light (Hanson, 2014). Anatase and rutile have bandgap energies (Eg) of 3.2 eV and 3.0 eV, respectively, which correspond to wavelengths of 388 nm and 413 nm (Daude et al., 1977; Kavan et al., 1996; Reddy et al., 2003; Wang and Lewis, 2005; Beltrán et al., 2006; Serpone, 2006; Hanaor and Sorrell, 2011).

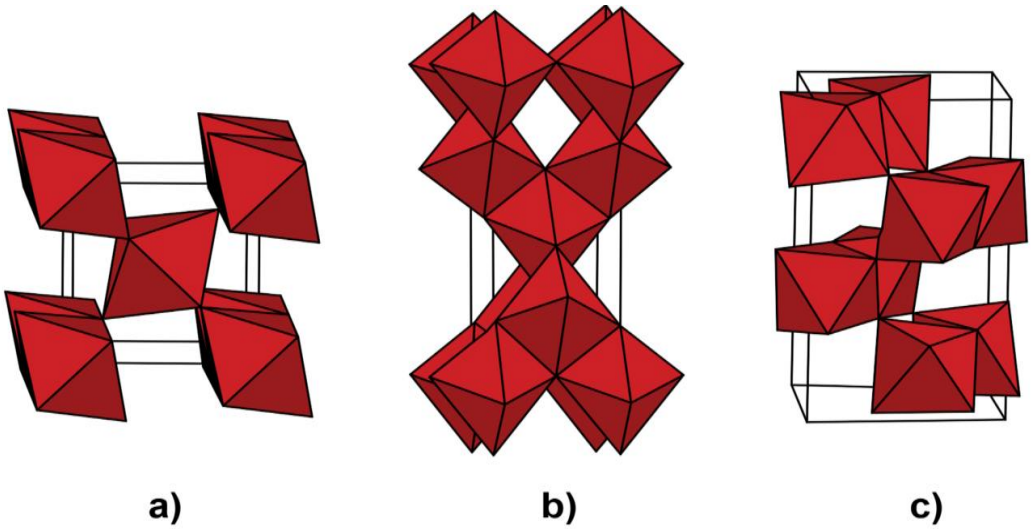

Figure 2.1. Illustration of crystallographic structure of (a) anatase, (b) rutile, (c) brookite.

2.2.2. Utilization of TiO_2 for air purification

There are several photocatalyst used for air purification purposes including TiO_2, ZnO, Fe_2O_3, WO_3, CdS, CdO, and bismuth (Bi) and others. (Zhao and Yang, 2003; Chen et al., 2008; Ibhadon and Fitzpatrick, 2013). Band energies and beam wavelengths of some of these semi-conductive materials are presented in Table 2.1.

Table 2.1 Band energies and beam wavelengths of some semi-conductive photocatalysts.

Semi-conductive photocatalysts	**Wavelength (nm)**	**Band Energy (eV)**
Titanium Dioxide (TiO_2) – rutile	413	3.0
Titanium Dioxide (TiO_2) – anatase	388	3.2
Zinc Oxide (ZnO)	388	3.2
Zinc Sulfide (ZnS)	335	3.6
Cadmium Sulfide (CdS)	516	2.4
Hematite (Fe_2O_3)	539	2.3
Tungsten Trioxide (WO_3)	443	2.8

Photocatalytic reaction is a photochemical process, where semiconductive photocatalyst absorbs energy of the incident light, which is stimulated to be used especially in removing air/water pollution. Photocatalytic activity of semiconductive materials, used as a catalyst, under light irradiation depends on the amount of energy difference between the valence band and conduction band. Although the band energy required for the stimulation of TiO_2 (Table 2.1) is somewhat higher than that for the CdS, Fe_2O_3 and WO_3; TiO_2 is more preferred than other semiconductors. This is partly because of the fact that the wavelength required for the activation of TiO_2 falls in the range of 315-400 nm, which is the range of UV-A rays emitting from the sun and reaching to the atmosphere and TiO2 is photochemically stable, chemically inert in the absence of irradiation, safe, cost-efficient, nontoxic and with enhanced photocatalytic activity (Hager et al., 2000; Zhao and Yang, 2003; Wang et al., 2007; Husken and Brouwers, 2008). Enhanced photocatalytic activity of TiO_2 which brings about effective NO_x degradation capability (Husken and Brouwers, 2008), is largely dependent on the shape, size, phase, type, and

particle properties of TiO_2 (Znaidi et al., 2001). Given both anatase and rutile phases of TiO_2 are thermally/chemically stable, have high oxidation capability, permeability against visible rays and high hydrophilic properties, their use as photocatalytic materials in numerous applications has been more comment compared to other semiconductive photocatalysts (Sakai et al., 2004; Banerjee et al., 2006).

2.2.3. Photocatalytic property of TiO_2

2.2.3.1. NO_x degradation mechanism of TiO_2

A photocatalyst is a material capable of improving the quality of atmospheric air, which degrades or removes air pollutants such NO_x by absorbing the energy of light (i.e. UV irradiation) to stimulate a chemical reaction called photocatalytic degradation. It is necessary to trigger this photochemical degradation process via UV and/or visible light irradiation having a photon energy equivalent to or greater than the energy of the band-gap of the semiconductive photocatalysts. Mechanism of photocatalytic degradation process of TiO_2 is explained step-by-step below and schematized in Figure 2.2.

- First, photons emitted from an irradiation source reach the surface of photocatalysts to start the photochemical degradation process. When the photons' energy (hv) is equal to or greater than the photocatalysts' electronic band gap value (Eg) ($hv \geq Eg$), the photocatalysts absorb the light energy (visible light or UV rays). A gap in the valence band of the photocatalyst is formed in this first step of the photocatalytic reaction, which is aided by a photon from an irradiation source, as a result of electron movement from the valence band of the photocatalyst to the conduction band. In this way, photo-generated electron hole (e^-/h^+) pairs are formed (Zhu and Zhou, 2019) following the reaction below:

$$TiO_2 + h_v \leftrightarrow h^+ + e^-$$

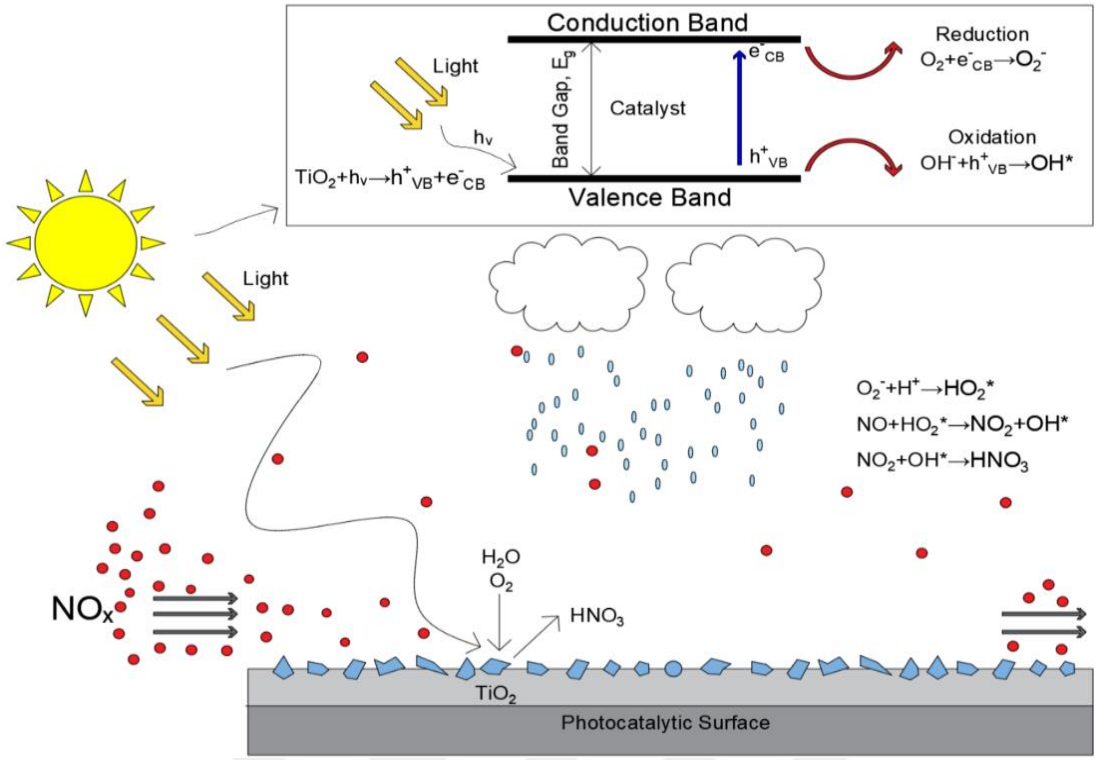

Figure 2.2. Mechanism of photocatalytic degradation process of TiO_2 (Poon and Cheung, 2007; Dylla et al., 2011; Boonen and Beeldens, 2013; Janus and Zając, 2016).

- The photogenerated holes (h^+) are one of the critical reactive oxidation species stimulating oxidation of electron donors in photocatalytic degradation process. In the second step, the holes oxidize the hydroxyl groups to form highly active hydroxyl radicals (OH*) (Yang et al., 2007; Zhao et al., 2007). Another critical highly reactive oxidation specie for the photodegradation process is superoxide radical (O^{2-}) obtained from the reduction of oxygen (O_2) by using the free electron available in the conduction band as an electron acceptor (Banerjee et al., 2006; Husken and Brouwers, 2008; Zhu and Zhou, 2019). This oxidation-reduction process which is schematized in Fig. 2.2 takes place following the reactions given below. It is of significance to stress that generally, in the absence of O_2, photocatalytic degradation process stops almost completely. Since the resulting superoxide ion (O_2^-) obtained from the reduction of O_2 is highly active, it either directly attacks the pollutant molecules oxidizing and decomposing them, or causes the formation of hydroxyl radicals. Therefore, oxygen is very important for the photocatalytic degradation process.

$$\text{Hole trapping, } OH^- + h^+ \rightarrow OH^*$$

$$\text{Electron trapping, } O_2 + e^- \rightarrow O_2^-$$

- Finally, highly reactive hydroxyl radicals oxidize the pollutants such as NO_x. The photocatalytic particles can adsorb airborne pollutants via reactions, the processes of which are:

$$O_2^- + H^+ \rightarrow HO_2^*$$
$$NO + HO_2^* \rightarrow NO_2 + OH^*$$
$$NO_2 + OH^* \rightarrow HNO_3$$

2.2.3.2. Factors affecting photocatalytic activity

There are numerous factors affecting the photocatalytic activity of TiO_2 particles including photocatalyst-related parameters such as specific surface area/particle size, crystal structure, crystallite size, type of phase, and operational parameters such as amount of TiO_2, concentration of the pollution, type/intensity/wavelength/duration of the irradiation, temperature/humidity/pH of the ambient, amount/type of substituted metal/non-metal materials. All these factors play incontrovertible and essential role on the formation of effective photocatalytic degradation and are mainly influential on the energy released through the combination/recombination of electrons and holes, photon (light) absorption rate of TiO_2, concentration/number of active surface sites and diffusion/capture rates of pollutant compounds. The influence of some of these factors on the photocatalytic degradation capability is detailed in the following sections.

2.2.3.2.1. Specific surface area and particle size of TiO_2

Photocatalytic activity of TiO_2 is in direct relationship with its surface morphology, specific surface area and particle size, which are influential on the amount of available active sites for the photocatalytic reactions to take place, light absorption rate, photon conversion efficiency, photoactivation of electron-hole pairs on its surface, carriage of the photoinduced charges (electron [e^-] and hole [h^+]) on its surface, recombination of e^- and h^+ and mass transfer of reactants to its surface reaction sites (Serpone et al., 1995; Lin et al., 2006; Kočí et al., 2009, 2012) However, there are several other material-, production-, target substance- and operation-related parameters having clear effect on the photocatalytic activity of TiO_2 apart from the abovementioned parameters TiO_2 itself. Therefore, different photocatalytic activity results are generally observed in the available literature studies. In accordance with Vorontsov et al., (2018), the particle size and

specific surface area of TiO_2 particles are only secondary factors affecting the photocatalytic activity while the production-related parameters such as calcination temperature and pH are more influential on photocatalytic activity (Vorontsov et al., 2018). Several studies reported that the reduction in particle size of TiO_2 particles up to a certain level has a positive effect on the photocatalytic activity, although different particle size levels have been reported to be optimum in these studies. For example, Zhang et al. (1998) stated that the optimum particle size of TiO_2 for photocatalytic decomposition activity for chloroform ($CHCl_3$) (oxidation of $CHCl_3$ in liquid phase) is about 10 nm (Zhang et al., 1998). Maira et al. (2000) found that optimum particle size of TiO_2 for the photocatalytic degradation of trichloroethylene (TCE) in gas phase is 7 nm (Maira et al., 2000). There are also other TiO_2 particle size and/or size ranges that are reported to be optimum from different studies for the photocatalytic degradation of different substances. For example, Almquist and Biswas (2002) stated that the optimum particle size range of TiO_2 for the oxidation of phenol is 25–40 nm (Almquist and Biswas, 2002), while Wang et al. (1997) stated that 11 nm is the optimum particle size for the liquid-phase decomposition of chloroform (Wang et al., 1997). Studies from the literature therefore clearly show that there is no unified particle size and/or range of TiO_2, as there are many other parameters being influential on the achievement of effective photocatalytic activity.

Decrement in the particle size of TiO_2 causes increment in the specific surface area and the large specific surface area of smaller particles contributes to the enhanced photocatalytic activity, most probably due to modifications in the physical and electrochemical properties of TiO_2 resulting in higher photon energy absorption, stimulation of the radiation-free transfer of the absorbed photon energy, a rise in the number of places on the surface where pollutant molecules can be absorbed and thereby higher electron–hole generation and higher rate of surface reaction of e^- and h^+ (Yamashita et al., 1996; Kominami et al., 1998; Xu et al., 1999; Jang et al., 2001; Dodd et al., 2006; Lin et al., 2006; Chou et al., 2007; Kim et al., 2007; Carneiro et al., 2010; Cheng et al., 2014; Retamoso et al., 2019). Although the increase in particle size improves the optical properties of TiO_2, which is beneficial for its photocatalytic activity, the gain in the photocatalytic activity due to improved optical properties is compromised because of decrements in the specific surface area of TiO_2 when the particle size increases (Lin et al., 2006). Moreover, the conduction band energy and the band gap energy of photocatalysts increase with the decreasing particle size (Brus, 1986; Lippens and

Lannoo, 1989; Retamoso et al., 2019). Increments in the conduction band energy level lead to increments in the redox potential stimulating the reduction of oxygen on the catalyst surface and contribute to the efficient photocatalytic degradation (Wang et al., 2000; Abreu et al., 2012). This increment in the band gap energy can lead to a decrease in the photocatalytic activity (Koči et al., 2009, 2012). However, some studies have stated that the observed increments in the band energy are not possible when the particle size of TiO_2 gets smaller than a certain limit and under such cases, band energy can decrease (Lin et al., 2006). It is also known that when the particle size of the photocatalyst is smaller, the charges of e^- and h^+ are closer to each other, and this closeness can increase the interaction between them (Anpo et al., 1984).Photogenerated electron–hole (e^-/h^+) pairs are also formed sufficiently close to the surface, when the particle size of the photocatalyst is smaller, leading the pairs to reach the surface more quickly (Zhang et al., 1998). The closeness in the charges of e^- and h^+ can increase the rate of surface recombination (Harada and Ueda, 1984; Wang et al., 1997; Zhang et al., 1998; Almquist and Biswas, 2002; Yeung et al., 2003; Cheng et al., 2014; Yuangpho et al., 2015) and accumulation of charge carriers (Gao and Zhang, 2001; Yeung et al., 2003; Pellegrino et al., 2017; Zhu et al., 2017). As the particle size decreases, the density of recombination centers increases and thus the recombination of photoinduced charges (e^- and h^+) is also enhanced (Grela and Colussi, 1996; Lin et al., 2006). Below a certain particle size, the surface recombination process is more dominant than the carriage of photoinduced charges, which affects the photocatalytic activity negatively. This is most probably the reason why an optimum particle size is reported in numerous studies for the achievement of the best photocatalytic activity (Zhang et al., 1998; Dodd et al., 2006) and is in line with the literature, which states that the surface reactions and recombination of charge carriers (e^- and h^+) should be balanced to guarantee the achievement of highly effective photocatalytic activity of semiconductors (Zhang et al., 1998; Asilturk et al., 2006; Kominami and Ohtani, 2010). In addition, decrement in particle size of TiO_2 beyond a certain limit can ease the formation of rapid flocculation and agglomeration, reducing the availability of active surface areas and interaction of pollutants on the surface of the photocatalyst, thereby lowering the photocatalytic activity (Maira et al., 2000; Lin et al., 2006; Yuangpho et al., 2015; Pellegrino et al., 2017).

2.2.3.2.2. Crystal structure, crystallite size and crystalline phase of TiO_2

TiO_2 is a widely preferred photocatalytic material and has two polymorphs (phases), namely, anatase and rutile. Although there are disputed results about the photocatalytic activity of these two phases in the literature, it is generally reconciled that anatase has a more effective photocatalytic degradation capability (Brown et al., 1985; Sclafani et al., 1990; Tanaka et al., 1991; Augustynski, 1993; Fox and Dulay, 1993; Linsebigler et al., 1995; Safarzadeh-Amiri et al., 1996; Jung and Park, 1999; Blimes et al., 2000; Hassan et al., 2010 a,b; Arunmetha et al., 2013; Etacheri et al., 2015; Wang et al., 2015; Garcia-Segura and Brillas, 2017; Ilie et al., 2017). Despite this general agreement in the literature, it has also been reported by several other researchers that rutile has a better photocatalytic activity than anatase (Mills et al., 2003; Watson et al., 2003; Jia et al., 2018; Vijayarangamuthu et al., 2018). Furthermore, a number of studies have reported that the combined use of anatase and rutile phases leads to a better photoelectrochemical activity and degradation of pollutant compounds than the single use of anatase phase (Bacsa and Kiwi, 1998; Muggli and Ding, 2001; Ohno et al., 2001; Poon and Cheung, 2007; Kim and Ehrman, 2009).

The differences between the photocatalytic activities of anatase and rutile phases of TiO_2 are directly related to their crystal structure, which affects the kinetic behavior of the charge carriers, including their optical and transport properties. It was reported that the band gaps of rutile and anatase TiO_2 are 3.00 and 3.20 eV, respectively, indicating that the conduction band of anatase phase is 0.2 eV more than that of rutile phase. Thanks to the excess electrons in the conduction band of anatase resulting in lower oxygen absorption capacity and higher degree of hydroxylation (Maruska and Ghosh, 1978; Tanaka et al., 1991; Gerischer and Heller, 1992), the reduction of reactants is more stimulated in the anatase phase than the rutile phase (McLendon, 1983; Banerjee et al., 2006; Reza et al., 2017). Anatase also exhibits longer lifetimes of photogenerated excess charge carriers because of its lower recombination rate and higher specific surface area owing to the presence of differently oriented facets on its surface, resulting in better photocatalytic degradation capability than rutile (Schindler and Kunst, 1990; Xu et al., 2011; Schneider et al., 2014). Another possible reason for the better photocatalytic activity of anatase is related to the wider optical absorption gap and smaller electron effective mass of anatase, which provide higher mobility of photogenerated e^- and h^+

compared to rutile (Mo and Ching, 1995; Banerjee et al., 2006). Although it has been reported in many studies that anatase has a more effective photocatalytic activity in general, it should be kept in mind that there are many other factors other than phase type largely affecting the photocatalytic activity such as crystal size, surface area, defects, porosity, and pore size distribution of photocatalyst and others.

2.2.3.2.3. Amount of TiO_2

In photocatalytic degradation, the amount of TiO_2 is one of the key factors for the photocatalytic activity of the process. The utilization of TiO_2 at optimum levels is necessary in order to ensure complete/efficient absorption of the photons on the surface of TiO_2 particles and lower the excess use of TiO_2 in favor of achieving cost-efficiency. The optimum amount of TiO_2 to be used for the achievement of a more effective photocatalytic activity varies in accordance with the material-, production-, target substance–, and operation-related factors such as the process of synthesis, particle size/ specific surface area of the photocatalyst, concentration, and structure of degraded substances together with the concentration of the pollution (Krýsa et al., 2004).

Many studies in literature have reported that an increment in the amount of photocatalyst leads to a rise in the rate/amount of photocatalytic activity (Hung and Yuan, 2000; Saquib and Muneer, 2003; Qamar et al., 2005; Saggioro et al., 2011; Kumar and Pandey, 2017a, 2017b, 2017c). On the other hand, some other studies claimed that the increase in the photocatalytic activity is valid up to a certain TiO_2 amount, after which, there was either decrement or no change in the photocatalytic activity (Wei and Wan, 1991; Neppolian et al., 2002; Zhang et al., 2002; Daneshvar et al., 2003; Chen and Liu, 2007; Coleman et al., 2007; Sohrabi and Ghavami, 2008; Huang and Wen, 2019). As the amount of photocatalyst increases above the optimum level, although some of the photocatalyst particles can be activated as a result of the stimulation through the irradiation reaching their surface, there is a likelihood that some particles cannot be activated due to inadequate interaction with the irradiation, resulting in lower overall photocatalytic activity (Chun et al., 2000). Moreover, TiO_2 particles are prone to agglomeration and sedimentation, which limits the interaction of the particles with photons and thereby the formation of further photocatalytic reactions especially in the presence of high dosages of TiO_2 (So et al., 2002; Garcia and Takashima, 2003; Kaneco et al., 2004; Li et al., 2010;

Pellegrino et al., 2017). It was also reported that in the presence of high concentrations of photocatalyst, photoinduced and nonphotoinduced particles can collide with each other before they allow photocatalytic reactions to occur, resulting in the inactivation of induced particles (Neppolian et al., 2002; Asilturk et al., 2006). All these findings from the literature therefore clearly show that there is an optimum amount of TiO_2 for the achievement of effective photocatalytic activity, and this situation is also closely related to other influential parameters.

2.2.3.2.4. Pollutant concentration

TiO_2's photocatalytic activity is influenced by the pollutant type and concentration as well. It was stated that the increment in the pollutant (substrate) concentration up to a specific level increments the pollutant degradation rate of the photocatalyst although there are studies found that increment in pollutant concentration causes continuous increments (Mazierski et al., 2017) or decrements (Behnajady et al., 2011; Martinez et al., 2011; Tayeb and Hussein, 2015; Thennarasu and Sivasamy, 2016; Lucas, 2017) in degradation rate. However, once the pollutant concentration rises over a specific threshold, the photocatalytic degradation rate decreases (Kiriakidou et al., 1999; Augugliaro et al., 2002; Sakthivel et al., 2003; Saquib and Muneer, 2003; Sivalingam et al., 2003; Kabra et al., 2004; Sohrabi et al., 2009). One of the possible reasons for the reported decrement in photocatalytic activity is that higher pollutant concentrations prevent the irradiation-based induction of the active surface areas on the photocatalysts' surface, hindering further generation of OH* and O^{2-} radicals required for the photocatalytic degradation process (Kiriakidou et al., 1999; Augugliaro et al., 2002; Saquib and Muneer, 2003; Chong et al., 2010; Tayeb and Hussein, 2015; Kumar and Pandey, 2017a, 2017b; Mazierski et al., 2017). One of another possible reason reported for the decrement in photocatalytic degradation rate with increased pollutant concentration is unavailability of sufficient active sites and thereby intermediate products to meet available pollutant substrates for an efficient degradation process (Lucas, 2017). Another possible reason is that when there are a lot of pollutants in the air, a lot of the irradiation that causes photocatalytic degradation reactions is absorbed by the pollutants rather than TiO_2 molecules. This means that the formation of OH* and O2- radicals that help to get pollutant molecules off the photocatalyst surface is blocked, which slows down the rate of photocatalytic reactions (Jun et al., 2006; Tayeb and Hussein, 2015).

2.2.3.2.5. Temperature

Reaction temperature has significant role in the kinetic behavior of charge carriers, which are influential on photocatalytic degradation of the pollutants. For a more effective photocatalytic degradation process, the balance between the adsorption and desorption processes needs to be ensured. Considering the effect of temperature on these processes, there is an optimum temperature range and/or value for the photocatalytic degradation process, as reported by the literature (Pichat and Hermann, 1989; Ollis et al., 1992; Hermann, 1999; Kim and Hong, 2002; Gogate and Pandit, 2004; Soares et al., 2007; Kumar and Pandey, 2017a). In general, when the temperature rises, the rate of electron-hole pair recombination on the photocatalyst surface increases (Moser et al., 1987; Zeltner and MA, 1993; Kumar and Pandey, 2017a, 2017b). Due to the competitive nature of the processes involving the combination and recombination of charge carriers, excessively high temperatures limit photocatalytic activity by preventing the creation of redox reactions on the photocatalyst surface.

Lowering the temperature promotes the adsorption of reactants (e.g., NO, NO_2, dye) and final reaction product. Moreover, increase in the temperature increments the desorption of the final reaction product of the redox reactions from the surface of the photocatalyst inhibiting the reactions, thereby reducing the number of radicals formed on the photocatalyst surface. Therefore, the desorption of the final reaction products determines the level of reaction in the case of low reaction temperatures while adsorption of reactants determines the level of reaction in the case of high reaction temperatures (Fu et al., 1996; Peral et al., 1997; Hashimoto et al., 2005; Soares et al., 2007; Hussein, 2016).

2.2.3.2.6. Irradiation

The light absorption intensity of a photocatalyst is significantly effective on its photocatalytic performance and the photocatalytic activity of a photocatalyst improves with the increased light absorption intensity (Zhang et al., 2020). One of the main requirements for the initiation of the photocatalytic activity is to have the energy of photons reached to the surface of photocatalyst to be equivalent to or greater than its electronic band gap. Therefore in addition to the light absorption performance of the photocatalysts, irradiation-related factors affect photon absorption rate of a photocatalyst and thereby the photocatalytic reaction process. For one of these factors, namely, the

intensity of light irradiation, it was reported that the reaction rates of photocatalyst increases with the increased light intensity, which results in higher amount of light absorption and further electron–hole formation (Aguado et al., 1994; Bahnemann, 1999; Hung and Yuan, 2000; Curcó et al., 2002; Xiao et al., 2007). However, despite the availability of increased number of photons with the increased light intensity resulting in further potential for photon activation, owing to limited number of activation areas, the increase in the reaction rates becomes limited and after a certain level; therefore the increments in the light intensity become ineffective on the photocatalytic degradation rate (Ollis and Al-Ekabi, 1993; Xiao et al., 2007; Reza et al., 2017). In addition, exposure to higher light intensity can lead to increments in the rate of recombination of electron–hole pairs (Aguado et al., 1994).

2.2.3.2.7. Humidity

Water molecules have a very significant role to play in the photocatalytic degradation process of pollutants, namely, transforming the pollutant molecules into harmless products (Zhang et al., 2020). The presence of water molecules in the photocatalytic reaction medium is a necessity for the photocatalytic degradation. Briefly, upon irradiation of the photocatalyst with light, the interaction of the photocatalyst with water molecules is a critical step for the photocatalytic oxidation to take place, which leads to the formation of reactive radical species (mainly hydroxyl and/or superoxide radicals) (Kim et al., 2002). Moreover, the water molecules also increase the rate of recombination of photoinduced charges (e^- and h^+) (Fox and Dulay, 1993; Mark et al., 1993). There is also a tough competition between the water molecules and pollutant molecules for adsorption on the catalyst surface sites decreasing the generation of the number of radicals (Luo and Ollis, 1996; D'Hennezel et al., 1998; Wang et al., 1998; Kim and Hong, 2002; Assadi et al., 2012; Héquet et al., 2018; Zhang et al., 2020). The concentration of water molecules also affects the generation of carbon deposits on the surface of photocatalyst, which decrease the activity of photocatalyst (Einaga et al., 1999, 2002). At higher humidity levels, formation of a film on the surface of the photocatalyst is also possible, which decreases the adsorption of pollutant molecules and thereby blocks the photodegradation reactions (Zhang, et al., 2007; Rismanchian et al., 2014; Zhang, et al., 2020). It can be stated in this regard that humidity can impact the photodegradation rate of a pollutant both positively and negatively, depending on its level,

hydrophilic/hydrophobic characteristics of the pollutant compounds, and other factors as concluded by several studies available in the literature (Einaga et al., 1999, 2002; Kim et al., 2002; Ao et al., 2003; Maggos et al., 2007; Zhang et al., 2007; Hay et al., 2015; Zhang et al., 2020). Therefore in order to ensure an ideal and stable photocatalytic degradation process, the humidity level of the reaction environment needs to be balanced.

2.3. Utilization of TiO_2 in Cementitious Systems for Air Purification Purposes

Researchers with innovative opinions who consider themselves responsible for contributing to sustainability have achieved remarkable progress in developing new generation advanced construction materials in recent years. Environment-friendly multi-functional construction materials with air purification capability act as valuable options in contributing to the sustainability perspectives, and there are increasing efforts in the route of solving/combating the problems related to low air quality, which affects our lives as a whole. The incorporation of different types of photocatalysts into the cement-based mixtures, with the aim of equipping the resultant construction material with NO_x degradation capability, is one of the initiatives to tackle air pollution. Large surface areas of structural/nonstructural members manufactured by the use of cement-based mixtures make them unique and ideal options that can be used for the stimulation of photocatalytic reactions.

One of the most important challenges to achieve effective photocatalytic activity from TiO_2-based cementitious composites is to allow the irradiation to reach all surfaces together with the in-depth regions of cement-based specimens/elements. Therefore, for an effective photocatalytic activity in the case of cementitious systems, optimized design, development, and production processes are required by taking into account all related factors. There are numerous studies available in the current literature focusing on the usage of TiO_2 particles within cementitious systems to develop sustainable photocatalytic construction materials with NO_x degradation capability. In the following sections, these studies are reviewed, especially from the perspectives of material-, production-, and operation-related parameters.

2.3.1. Relationship between the quality of distribution of TiO_2 particles in the cement-based systems and NO_x degradation capability

Agglomeration of nanomaterials including nano-TiO_2 is a general problem, which arises because of high surface area/energy of the nanomaterials triggering very strong attractive forces and intense surface interactions among nanosized particles (Kawashima et al., 2014). Cement-based systems are also very alkaline and have a lot of calcium, which makes it easier for nano-TiO_2 particles to stick together. Agglomeration leads to the formation of nonhomogeneous microstructure, thereby reducing the UV light reachable photocatalyst surface area in the photocatalyst-incorporated matrix, lowering the number of active sites and leading to the occurrence of weak zones in the matrix. Therefore, one of the most important requirements to obtain the optimum photocatalytic performance and make sure reliable reproducibility of TiO_2-based photocatalytic systems identically is the achievement of homogeneous dispersion of nano-TiO_2 particles along the cementitious matrix (Figure 2.3).

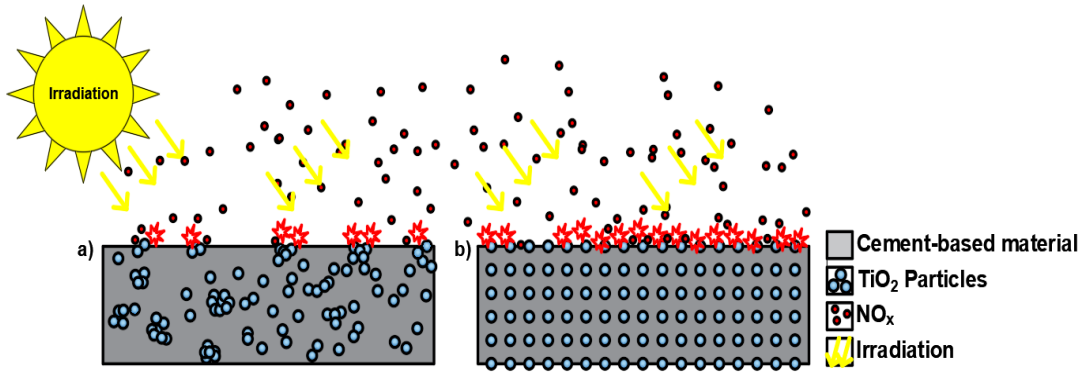

Figure 2.3. Nano-TiO_2-incorporated cementitious systems with (a) nonhomogeneous and (b) homogeneous dispersion of nano-TiO_2 particles.

Other characteristic properties of TiO_2-incorporated photocatalytic cementitious systems such as microstructure, mechanical properties, etc., are also affected by the homogeneous distribution of TiO_2. As in the case of other nanomaterials, selection of proper treatment method to ensure homogeneous dispersion of nano-TiO_2 particles along the cement-based systems requires specific attention, especially in order not to risk the chemical state of the cement-based systems and hydration process. Several studies available in the literature approve the significance of surface charge on the distribution of nano-TiO_2 in cementitious systems and show that pH of the environment can markedly change the magnitude of the surface charge and hence affect the degree of distribution of

photocatalyst (Folli et al., 2010; Cárdenas et al., 2012; MacPhee and Folli, 2016). The attraction or repulsion of nano-TiO_2 particles determines the stability and distribution quality/state of the system depending on their electrical charge (Oliveira, 2000; Folli et al., 2010). Therefore, an environment with specific/proper pH is usually required to obtain negatively or positively charged surface properties, which leads to the effective dispersion of nano-TiO_2 particles. When the pH of the environment increases, a negatively charged surface is obtained, on the contrary, when the pH decreases, a positively charged surface is obtained. Thus, via surface charging, particles repellent to each other are obtained so as to avoid agglomeration; and the larger the magnitude of charge, the stronger the repulsion and nonagglomeration property of nano-TiO_2 particles is (Figure. 2.4) (MacPhee and Folli, 2016).

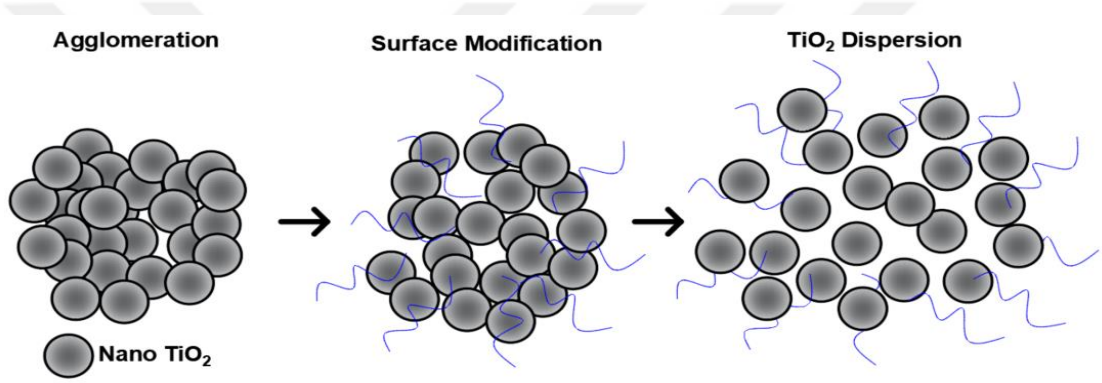

Figure 2.4 Nano-TiO_2 distribution through surface modification (surface charging) (Source: Redrawn after Li et al., 2018).

Zeta potential is an indicator of the surface charge status of the particles and measurement of the magnitude of zeta potential of a system gives valuable information about the stability and surface properties. At pH levels, where the zeta potential is or close to zero, an environment in which the particles can agglomerate, resulting in instability and insufficient distribution can be obtained (Suttiponparnit et al., 2011). Positive and/or negative threshold values for the zeta potential, that can eliminate the agglomeration of particles, have been reported in the available literature such as |25–30| mV (Mandzy et al., 2005), <−30 mV (Cárdenas et al., 2012), ±30 mV (Jiang et al., 2008; Cárdenas et al., 2012; Pérez-Nicolás et al., 2017), although these values have the potential to be seriously affected by different conditions. It is therefore essential to obtain an environment with an appropriate distribution-oriented pH value (i.e., zeta potential value), considering the characteristics of the developed systems, especially alkaline medium of cementitious paste together with the presence of complex ions in this

environment. Accordingly, various studies have been carried out to research the distribution of nano-TiO_2 particles throughout the cementitious systems and its effects on the properties of such systems specifically considering the photocatalytic activity (Yousefi et al., 2013; MacPhee and Folli, 2016; Dantas et al., 2019; Şahin et al., 2021;). Different procedures have been utilized in the literature in order to uniformly distribute nano-TiO_2 particles throughout the cementitious systems with the aim of acquiring photocatalytic capability through manipulating the status of surface charge of the particles. Such procedures include optimization by curing process (Strini et al., 2016), proper selection of the constituents (Strini et al., 2016; Giosuè et al., 2018), mixing of the mixture ingredients with high-shear energy (Dantas et al., 2019) or handheld electric mixer (Jin et al., 2019), incorporation of TiO_2 particles as suspension instead of powder form (Hunger et al., 2008), particle surface modification/treatment through chemical and physical processes including the implementation of different mixing procedures via sonication (Yousefi et al., 2013; Karapati et al., 2014; Rhee et al., 2018; Xu et al., 2020 a, 2020b; Şahin et al., 2021;), utilizing different surfactant materials such as modified polycarboxylate polymer (Cárdenas et al., 2012; Pérez-Nicolás et al., 2018), polyacrylic acid– and polycarboxylic ether–based superplasticizer (Şahin et al., 2021), incorporating saturated $Ca(OH)_2$ solution (Yousefi et al., 2013), doping different metal/nonmetal materials such as P–OH surface modification (Folli et al., 2010), Fe doping (Pérez-Nicolás et al., 2017), etc. In more details about some of these studies which are directly focused on ensuring of effective dispersion of TiO_2 powder in cementitious systems, Dantas et al. (2019) evaluated the TiO_2 dispersion capability of two different dispersion procedures based on two different mixing equipment including “standard energy mix” (standard shear energy) and “high energy dispersion” (high shear energy) and observed that mixing with “high energy dispersion” is more efficient more deagglomeration providing better dispersion quality than that with “standard energy mix.” Şahin et al. (2021) investigated five different mixing procedures created with combination of different surfactant material content (single or binary utilization of polyacrylic acid– and polycarboxylic ether–based superplasticizer) and different type of mixing equipment (conventional cement mixer, high-speed kitchen-type hand blender, ultrasonic mixer and mixer combinations) to evaluate their TiO_2 dispersion capability in cement pastes. According to their results, the mixing procedure based on ultrasonication operation and dual usage of surfactant (mentioned above) provides more homogeneous cementitious system with higher photocatalytic activity compared to those prepared with

other mixing methods. They claimed that increasing the fluidity of cementitious systems may increase the uniform dispersion of components in the system. Yousefi et al. (2013) also made some efforts to obtain a method for efficient dispersion of nano-TiO_2 powder in cement media. They prepared nano-TiO_2 dispersions by using two different dispersants (deionized water and saturated $Ca(OH)_2$ solution) and two different mixing methods (mechanical stirring or ultrasonication) and obtained better nano-TiO_2 dispersion capability from the suspension prepared with saturated $Ca(OH)_2$ solution and ultrasonication. Pérez-Nicolás et al. (2018) experimented with different superplasticizer molecules to evaluate their compatibility with cement-based systems in terms of dispersion of nanosized photocatalytic particles. According to their findings, using polycarboxylate-based superplasticizers effectively prevented the agglomeration of TiO_2 particles, whereas using a naphthalene sulfonate formaldehyde polycondensate resulted in the production of significant agglomerations of nanosize TiO_2 particles.

2.3.2.Relationship between the particle size of TiO_2 in the cement-based systems and NO_x degradation capability

Considering that the particle size of TiO_2 is a significantly influential factor on the activity of photocatalytic systems, studies addressing the relationship between the particle size of TiO_2 incorporated into the cement-based systems and photocatalytic activity of such systems have been carried out. Seo and Yun (2017) used two different-size (35 and 100 nm) TiO_2 particles and obtained higher NO absorption/removal rate from mortar mixtures produced with smaller TiO_2 particles (35 nm) compared to those with larger TiO_2 particles (100 nm) (Seo and Yun, 2017). Their results were found attributable to two factors: (1) smaller-size particles mean the presence of larger number of particles and thus large surface area and high porosity beneficial for NO absorption capability, and (2) smaller-size particles provide higher amount of active surface areas. Similarly, Hunger et al. (2008), Husken et al. (2008); Chen and Poon (2009a), Folli et al. (2010) and Meng et al. (2020) found results indicating that TiO_2 particles with higher surface area exhibits better photocatalytic degradation capability compared to TiO_2 with lower surface area (Hunger et al., 2008; Husken and Brouwers, 2008; Chen and Poon, 2009; Folli et al., 2010; Meng et al., 2020). Considering the results obtained from abovementioned studies, other factors affecting the photocatalytic degradation capability of the specimens were reported such as 3D structure of the TiO_2, porosity, kinetic of the reactions in cement-based system,

dispersion of the TiO_2 particles etc. Contrary to results from above-mentioned studies, Poon and Cheung (2007) obtained better results with the use of TiO_2 particles having larger particle size, although they have made their comparison by taking three different types of commercially available TiO_2 powders and stated that their findings require further research in order to take other factors influential on the photocatalytic activity (Poon and Cheung, 2007). It was also reported in the works of Husken et al. (2008), Folli et al. (2010) and Pérez-Nicolás et al. (2017) that although smaller-size TiO_2 particles are better, they tend to exhibit more agglomeration, which may lead to the realization of certain decrements in the photocatalytic degradation capability.

2.3.3. Relationship between the amount of TiO_2 in the cement-based systems and NO_x degradation capability

The amount of irradiation-reachable photocatalyst material is an important parameter to be considered in order to obtain an optimum cementitious product that is affordable and characterized with the enhanced photocatalytic degradation capability. Many studies have addressed this issue, yet there is no consensus on the best/optimum utilization rate of TiO_2 in cement-based systems. Considering that the photocatalytic reactions can occur on the surfaces accessible to irradiation and pollutant NO_x gas, establishing a direct relationship between the amount of TiO_2 substituted and photocatalytic activity is a complex process. Considering that there are many material-, production-, target substance- and operation-related parameters that can affect the performance of cement-based photocatalytic systems, it can be anticipated that the optimum usage rate to obtain the maximum performance may vary based on the application. Furthermore, the presence of large amounts of nanomaterials can increase the tendency of agglomeration and make their distribution difficult, which can lead to a decrease in photocatalytic degradation activity (Senff et al., 2013; Xu et al., 2020a, 2020b).As also reported by, Chen and Poon (2009a), a marked increase in the utilization rate of TiO_2 cannot exhibit a proportional increase in photocatalytic degradation capability. Therefore it can be stated that there is a certain threshold for TiO_2 utilization rate/range to ensure efficient photocatalytic degradation capability (Yousefi et al., 2013; Karapati et al., 2014; Rhee et al., 2018; Xu et al. 2020a, 2020b; Şahin et al., 2021). Lucas et al. (2013) found different TiO_2 incorporation rates (0.5, 1.0, 2.5, 5.0 wt.% of cement) as optimum for NO_x degradation, which are changeable according to the utilization of different ingredients and compositions. They have found a

decreasing trend in the NO_x degradation capability of cementitious mortars with the increased utilization rate of NO_x and attributed this general outcome to the electron–hole pair deactivation in the case of excess amounts of photocatalyst. It was also stated in this work that the utilization rate of TiO_2 and the composition of the mixtures can affect the microstructural properties of the specimens and the photocatalytic degradation capability. Xu et al. (2020a, 2020b) observed that utilizing 5% TiO_2, by the weight of cement, is optimum for the best photocatalytic capability and the reaction rate of NO_x degradation decreased as the TiO_2 content was increased from 5% to 10%. Similarly, according to Seo and Yun (2017), TiO_2 utilization rate of 5%, by the weight of cement is optimum for the photocatalytic activity and there is no important increment in the NO removal rate with the increase in the TiO_2 utilization rate from 5% to 10%. Senff et al. (2013) also pointed out the optimum TiO_2 utilization rate to be 5%, by the weight of cement, considering the NO reduction levels of mixtures having TiO_2 with utilization rates ranging from 5% to 20%. Rhee et al. (2018) obtained the best photocatalytic activity from cement paste specimen prepared by using utilization rate of 10wt.% of cement among cement paste specimens prepared with utilization rates of 0, 5, 10, 20wt.% of cement and attributed this result to the increase in electron–hole recombination due to relatively large amounts of TiO_2 beyond this rate (10%) (Rhee et al., 2018). However, for mortar mixtures, the continuous increase was observed in photocatalytic degradation with increasing TiO_2 utilization rate in mortar specimens prepared at the same utilization rates with cement paste specimens (0, 5, 10, 20 wt.% of cement), most probably due to relatively less TiO_2 by volume compared to paste specimens because of presence of sand providing balance in the redox reactions (preventing excess electron-hole recombination). In some other studies, different utilization ranges of TiO_2 were also given such as 0%–10% (Pérez-Nicolás et al., 2015), 3%–10% (Hunger et al., 2008; De Melo et al., 2012), 0%–5% (Hassan et al., 2010 a, 2010b; Cárdenas et al., 2012; Guo and Poon, 2018; Janus et al., 2019) 0%–3% (Janus et al., 2020), 5%–10% (Chen and Poon, 2009a, 2009b; Chen et al., 2011), by the weight of cement; replacing 5%–10% weight of cement (Hernández-Rodríguez et al., 2019); 0.5%–2.5%, by the weight of binder (Pérez-Nicolás et al., 2017); 0%–5%, by the weight of cementitious materials (Guo et al., 2012); 0.1%–2% (Matějka et al., 2012), 0%–10% (Poon and Cheung, 2007), by the weight of the mixture without water and 2%–4%, by the volume of binder (Giosuè et al., 2018). It has been reported in these studies that increasing the utilization rate of TiO_2 within the given range increases photocatalytic degradation capability continuously.

2.3.4. Relationship between the type of TiO_2 in the cement-based systems and NO_x degradation capability

The effect of different types (phases) of TiO_2 incorporated into the photocatalytic cement-based systems is another point that drove the researchers' attention with the aim of ensuring optimum photocatalytic performance in terms of cost, producibility, and NO_x degradation activity. Numerous papers dealing with the effect of different types of TiO_2 on the photocatalytic performance of cement-based systems indicated that cement-based systems containing the combination of anatase and rutile phases of TiO_2 in the form of a commercial product named "Degussa P25" outperform those containing the different forms of TiO_2 singly in terms of photocatalytic performance (Poon and Cheung, 2007; Chen and Poon, 2009b; Rhee et al., 2018), although there are other works which state the opposite most probably due to production- and operation-related parameters effecting overall performance (Park et al., 2020). Hernández-Rodríguez et al. (2019) compared two different commercial TiO_2 products including "Kronos" [100% Anatase (7 nm)] and "Degussa P25" [82% Anatase (23 nm) +18% Rutile (44 nm)] at different utilization rates and generally obtained better photocatalytic degradation performance from Kronos-containing mortars with some exceptions due to operational and content-related factors (Hernández-Rodríguez et al., 2019). On the other hand, although it is accepted that anatase is more effective in degrading not only NO_x gas but also other pollutants (Yu and Brouwers, 2009; De Melo et al., 2012) an opposite behavior was observed in the work of Poon and Cheung (2007), who tested cement-based mortar mixtures with different types of TiO_2 for NO_x degradation capability and found better results for mixtures with rutile than mixtures with anatase. Cárdenas et al. (2013) produced cement paste mixtures containing the combination of anatase and rutile particles with different utilization rates (anatase:rutile-"0:0," "100:0," "85:15," "50:50") and achieved better NO_x degradation performance from mixtures containing anatase-rutile combination of 85:15 at early age of 65 hours. This result was found attributable to the reduction in the charge recombination due to the difference in Fermi levels (the highest energy level of an electron at absolute zero temperature) of anatase and rutile, and ease of transfer of holes/electrons due to closer contact of the anatase and rutile particles. It was also noted that as the anatase-rutile combination was changed to be 50:50, early age NO_x degradation performance similar to the case of anatase-rutile combination of 85:15 could not be obtained because of decrements in the surface active sites as a consequence of the

increments in the number of larger-size particles. On the other hand, at 28 days, mixtures containing only anatase (100:0) showed better photocatalytic degradation performance, possibly because of the fact that the microstructure got densified thanks to ongoing hydration reactions further blocking the mixtures containing the combination of anatase-rutile in terms of photocatalytic activity compared to those containing anatase solely.

2.3.5. Relationship between the combined presence of metal/non-metals and TiO_2 in the cement-based systems and NO_x degradation capability

Doping TiO_2-based cementitious systems with metallic/nonmetallic materials is a way to increase the photocatalytic degradation capability. Lucas et al. (2013) developed mortar mixtures containing Fe-doped nano-TiO_2, which outperformed the mortar mixture containing nonFe-doped nano-TiO_2 in terms of NO_x degradation. This result was associated to the narrowing of the band gap (Figure 2.5) and inhibition of the electron–hole recombination as a result of Fe doping (Moser et al., 1987; Yamashita et al., 1996).

Similarly, Hunger et al. (2008) obtained better degradation results from concretes containing carbon-doped TiO_2 than those containing noncarbon-doped TiO_2 (Hunger et al., 2008). They stated that this finding was obtained as concrete products containing carbon-doped TiO_2 use UV-A radiation more efficiently. MacPhee and Folli (2016) stated that although doping of TiO_2s (such as with tungsten and niobium) can affect the photonic efficiency negatively, doped TiO_2s have better visible light response and nitrate selectivity providing removal of NO and highly toxic NO_2 from the atmosphere, thanks to high nitrate conversion rates, which is very im- portant to improve the air quality in urban areas (MacPhee & Folli, 2016). Although the effect of different parameters was noted, results similar to the work of MacPhee and Folli (2016) were also observed in the work of Pérez-Nicolás et al. (2017), where visible light-sensitive photocatalytic performance was obtained from cement mortars through the incorporation of iron- and vanadium-doped TiO_2. Pérez-Nicolás et al. (2015) obtained the worst photocatalytic degradation results from mortars containing iron-rich calcium aluminate cement compared to those containing iron-lean cement. The reason for this finding was stated to be the generation of iron titanates (with lower band gaps and photocatalytic activity) because of the interaction between the TiO_2 and ferrite phase available in the iron-rich calcium aluminate cement.

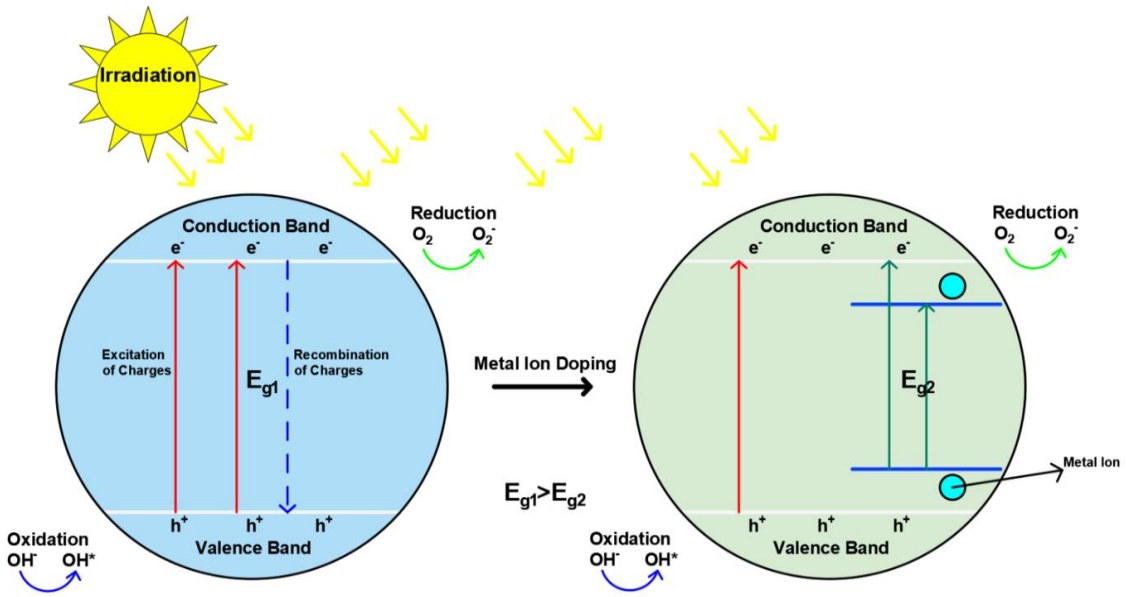

Figure 2.5. The influential mechanism of metal ion doping TiO_2/Bad gap (E_g) narrowing. (Source: Redrawn after Li et al., 2020.)

Laplaza et al. (2017) observed that incorporation of iron oxide–based pigments into cement-based systems containing TiO_2 can enhance the visible light performance of TiO_2 and is influential on the separation/occurrence of photoinduced electron–hole pairs, recombination of the photogenerated electron–hole pairs, and formation of OH*radicals, which can sabotage or enhance the photocatalytic activity (Laplaza et al., 2017). They also stated that Fe/Ti ratio and the band edge position of pigment–cement heterostructure are important parameters affecting the electron transfer between the conduction band of the pigment and the photocatalytic colored cement mortar, which are determining factors on the above-mentioned behavior.

The effect of the presence of transition metals or mixed oxides on the photocatalytic activity is a complex issue, as there are many factors influencing the phenomenon and there is possible variability potential depending on the nature/properties/proportion of the material used, the method selected and so on. Hernández-Rodríguez et al. (2019) obtained better photocatalytic degradation results from mortar mixtures manufactured with gray cement compared to white cement, and they attributed this result to the higher Fe_2O_3 content of gray cement, which is regarded as photocat- alytic activity enhancer up to a certain level. They also obtained better NO_x removal rates from mixtures containing sand compared to mixtures without sand most probably because of higher aggregation

behavior of the nano-TiO_2 particles and possibility of chemical interaction between the TiO_2 and smaller-size cement particles. However, Chen and Poon (2009a) arrived at a contrasting result and stated that the utilization of white cement is better for the increased photocatalytic degradation capability due to light absorption characteristics of white cement. The presence of transition metals (manganese and iron) in gray cement, which results in absorption or blocking a portion of incident photons usable for the photocatalytic reactions and electron–hole recombination was also stated to be responsible for the lower degradation capability of gray cement. Similarly, in the work of Guo and Poon (2018), NO_x degradation activity of white cement paste was found to be better compared to that of gray ordinary Portland cement paste. They attributed this result to the presence of higher quantities of Fe_2O_3 in the ordinary Portland cement, which led to higher light absorption ability and stronger charge transfer resistance in ordinary Portland cement resulting in higher rate of electron–hole pair recombination compared to that of electron–hole pair generation. They also incorporated different dosages of Fe_2O_3 (2, 5, and 10 wt.% of white cement) into the pastes as a replacement of white cement and observed that increase in the Fe_2O_3 dosage caused decrease in the NO_x removal rate. Park et al. (2020) also obtained better NO removal capacity from mortars with white cement compared to those with gray cement due to higher light absorption ability of the gray cement leading to fewer electron–hole pairs (Park et al., 2020).

2.3.6. Relationship between the mixture composition of cement-based systems and NO_x degradation capability

Although the properties of TiO_2 used as photocatalyst in cement-based systems have noticeable effects on the NO_x degradation capability, the mixture composition of such systems undeniably affects the activity as well, especially considering the content-specific microstructural changes. Pérez-Nicolás et al. (2017) manufactured mortars with different types of binders, namely, Portland cement, high-alumina cement, low-alumina cement, and dry slaked lime and obtained relatively higher photocatalytic degradation activity from mortars prepared by using high-alumina cement and lime separately, which contained higher amounts of pores with diameters above 0.05 μm allowing easier reach of NO molecules into more in-depth parts of the mortars in favor of further contact between the surface of photocatalytic materials and pollutants. In addition, they attributed the relatively higher photocatalytic activity of calcium aluminate cement–containing

mixtures to the sensitivity of calcium aluminates to illumination and concluded that the availability of important amounts of calcium carbonate in these mortars (both high-alumina cement and lime-based mortars) is also influential on the better photocatalytic degradation capability of these mortars. Pérez-Nicolás et al. (2015) stated that the presence of calcium aluminates in the cement-based systems is beneficial for NO_x abatement rate. Lucas et al. (2013) prepared several mortars by using different types of binders (e.g., lime, cement and gypsum) and established links between the microstructure and photocatalytic performance of these mortars. They emphasized that high porosity promotes the photocatalytic activity by facilitating gas diffusion in an effort to assist the contact between the photocatalyst and NO_x gas at the irradiated surface, and the diameter of pores should not be less than 1 μm (nanopores) to restrict the gas diffusion, as also reported by Giosuè et al. (2018). Moreover, Lucas et al. (2013) also concluded that exceedance of the optimum TiO_2 content, the presence of excessive porosity and overabundant light exposure of TiO_2 on the surface may trigger higher electron–hole recombination and thus decrease the photocatalytic degradation capability. Similarly, Sugrañez et al. (2013) stated that the formation of higher amount of hydration products provides a denser microstructure through the filling of the pores, while lower amount of hydration products and the amount of adsorbed water filling the space between the cement grains provide a more porous structure, which is beneficial for higher photocatalytic activity (Sugrañez et al., 2013). They also concluded that photocatalytic activity is enhanced as the total porosity increases because of higher possibility of having larger number of active sites accessible to the molecules needed for the photocatalytic reactions and increasing in the generation/amount of hydroxyl radicals to react with NO_x, and they proposed that poor packaging of aggregate particles (through modification of particle size distribution) is a method that can be used to create a macroporosity structure. In order to achieve improved photocatalytic activity through altering the porosity of cementitious materials, Chen and Poon (2009a, 2009b) and Poon and Cheung (2007) recommended changing the particle-size distribution of aggregates or decreasing the cement content of the mixtures. Xu et al. (2020a, 2020b) obtained a more porous structure by using fly ash Matějka et al. (2012), Boonen and Beeldens (2014), Lee et al. (2014), Guo et al. (2015b) and Meng et al. (2020), observed increments in the NO removal rate with increased porosity as well. Chen et al. (2020) also noted the positive contribution of porosity to the photocatalytic activity, as it provides a channel for pollutants to easily flow through, more surface area for the deposition of photocatalysts, and more space for

holding/accumulation of final products, which prevents the covering of the surface of the photocatalyst (Figure 2.6).

In contrast to above-mentioned works, Giosuè et al. (2018) stated that macroporosity is not beneficial for increasing the photocatalytic capability of mortar specimens. Jin et al. (2019) stated that the presence of larger amount of micropores (<5 nm) in cement-based mortars is beneficial for NO_x uptake (Giosuè et al., 2018; Jin et al., 2019). In addition, Jimenez-Relinque et al. (2015) achieved a more effective NO_x reduction process in a given porosity range (which was below a speci- fied limit value of 1 μm as reported by Lucas et al. (2013) for the enhanced photocatalytic performance), and stated that excessive porosity reduced the photocatalytic activity by letting the pollutant gas into the nonirradiated regions of the cement-based matrix (Jimenez-Relinque et al., 2015). In addition to the effect of the cement-based system's microstructure formed depending on the mixture composition on the photocatalytic activity, Jimenez-Relinque et al. (2015) stated that difference in mixture composition (e.g., utilization of different binder materials) can also affect the photocatalytic activity by causing chemically mixture-specific/different photocatalytic reaction mediums (e.g., chemically different aqueous phases in the pores and different photoabsorption energies resulting different oxidation-reduction potentials). Poon and Cheung (2007) and Chen et al. (2020) observed that utilization of ag gregates with higher porosity and low specific density provides an increase in the NO removal capability of the final cementitious products. Additionally, they demonstrated that, due to the high light transmittance of recycled crushed glass cullet, incorporating it as aggregates in cement-based systems allows photocatalytic reaction-provocative light to reach deeper TiO_2 particles, activate them, and result in an enhanced photocatalytic degradation process (Fig. 2.6).

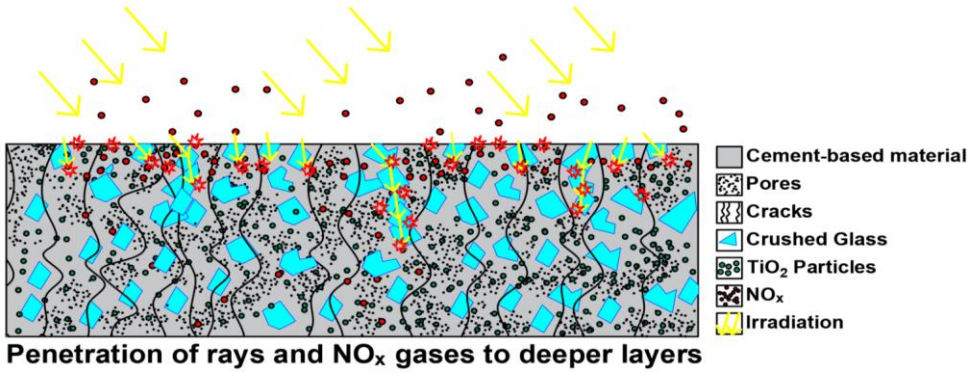

Figure 2.6. Penetration of rays and NO_x gases into deeper layers of cement-based systems with pores and crushed glass. (*Source*: Redrawn after Chen and Poon, 2009b).

Chen and Poon (2009b), Guo et al. (2012), and Guo and Poon (2013) observed similar results that utilization of glass cullet as aggregates promises better NO removal performance for the cement-based systems. They also indicated that light-tinted glasses are more effective in increasing the photocatalytic activity thanks to their low UV absorbance and the light-transmitting property of glass aggregates has significant impact on the photocatalytic performance of cement-based systems. In their work, Guo and Poon (2013) also used pigments with different colors and observed that the utilization of different-colored pigments in cement-based systems reduces the NO removal rate of photocatalytic products most probably due to increase in the light absorption capability, covering of TiO_2 particles and filling of the pores with the pigments. They further concluded that pigments with lighter colors lower the photocatalytic performance less than those with darker colors having higher light absorption capability. Giosuè et al. (2020) used aggregates with different colors and obtained the lowest NO removal activity from the mortar mixtures containing activated carbon (Giosuè et al., 2020). This was found attributable to the dark color of the activated carbon, which results in lower reflectance of radiation. Chen et al. (2018) prepared separate mortar mixtures by using two different types of aggregates and found that the mortar mixture containing aggregates with the rough surface, high water absorption, many cracks and high porosity had higher photocatalytic activity, most probably because of the higher potential of this type of aggregate to accommodate more TiO_2 particles in their pores and cracks. Similarly, Giosuè et al. (2020) obtained better NO removal rate and selectivity (low) from mortars containing ag- gregates with higher water absorption due to increased availability of absorbed water providing enhancement in the production of OH* radicals.

2.3.7. Relationship between the abrasion/wearing/weathering of the surface of cement-based systems and NO_x degradation capability

Abrasion/wearing of the photocatalytic surface is an important issue considering the real-time exposure conditions of the photocatalytic cement-based systems. In this route, some researchers performed studies positioned on the assessment of abrasion/ wearing/weathering effects on the photocatalytic activity of the cement-based systems. Hassan et al. (2010b) performed a study to evaluate wear and abrasion resistance of the TiO2 incorporated cement-based systems by using an accelerated loading test and rotary abrasion (Hassan et al., 2010a, 2010b). Although they observed a little reduce in the NO removal performance for the cement-based mixtures with high amount of TiO_2 substitution (5%) after abrasion and wearing, they obtained better NO removal performance from mixtures with low amount of substitution (3%) after the same processes. They also observed from the energy-dispersive X-ray spectroscopy analysis that the relative concentration of Ti on the worn specimens, which under-went the abrasion and wearing process, did not essentially change in comparison to the original samples. It was observed in the work of Chen et al. (2020) that the photocatalytic cement-based specimens can show some loss of photocatalytic activity after abrasion. They stated that increase in the rough and porous material content can reduce the loss potential of photocatalytic activity of the specimens after abrasion, namely a more preferable antiabrasion performance since the rough surfaces can enable photocatalysts to clamp and photocatalysts accommodating in deeper pores/spaces can become available to receive UV rays after the abrasion. Guo and Poon (2013) observed not-so-evident fluctuations in the NO removal rates at the end of abrasion applied to concrete specimens for different periods of time most probably due to the scattered distribution of TiO_2 particles throughout the photocatalytic specimens and stated that the incorporation of TiO_2 into cement-based systems is a robust and good option to prevent loss of photocatalytic performance caused by abrasion when compared to coating/spraying applications (Figure. 2.7). Boonen and Beeldens (2014) also stated that incorporation of TiO_2 into cement-based systems provides more stable photocatalytic performance under wearing action although only the TiO_2 at the irradiation-reached surface can be stimulated for the degradation process. Guo et al. (2015a) tried to simulate weathering actions on the air cleaning properties of cement-based systems by using “Rain/dry” and “day/night” cycles. They observed reduction in the photocatalytic activity of the TiO_2-incorporated

specimens after weathering which was attributed to the reduction in the blocked pores by the deposition of impurities moved due to repeated raining process reducing NO_x removal ability by preventing penetration of light and NO gas to deeper to contact with the TiO_2 particles.

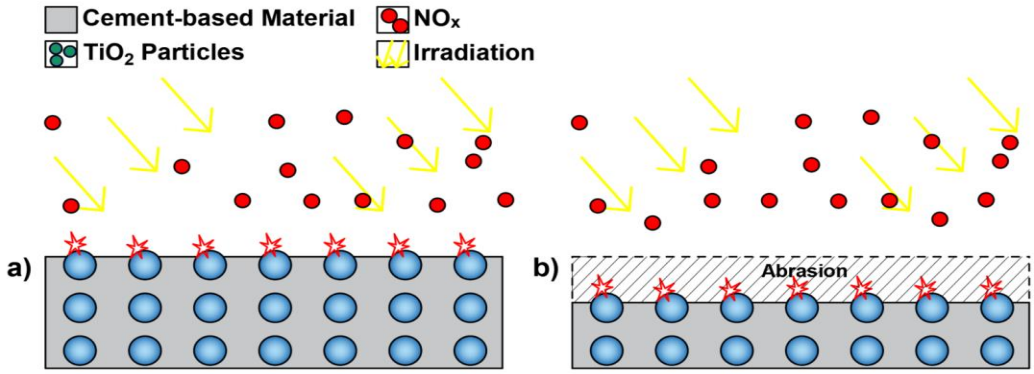

Figure 2.7. TiO_2-incorporated cement-based systems (a) new material, (a) after abrasion.

2.3.8. Relationship between the curing age/condition of cement-based systems and NO_x degradation capability

Curing age/condition applied to photocatalytic cement-based specimens/products have direct influence on the development of microstructure, therefore can be considered as critical factors affecting the NO_x degradation capability. In general, NO_x degradation capability of cement-based systems shows a decreasing trend with the prolonged curing due to time-dependent changes in the microstructure of the cement-based systems (Poon and Cheung, 2007; Chen and Poon, 2009a, 2009b; Sugrañez et al., 2013; García et al., 2017; Guo & Poon, 2018; Chen et al., 2020; Şahin et al., 2021). One of the main reasons for the observed decrease in the photocatalytic activity with prolonged curing is ongoing hydration reactions affecting pore structure and ion concentration by reducing the size/volume/connectivity of the pores together with the ion concentration of the pore solution. Ongoing hydration also changes the microstructure making the cementitious matrix denser, coating TiO_2 particles with the ongoing hydration products and lowering the adsorption capacity of the photons and target pollutants (Figure 2.8). Another possible reason for the lower photocatalytic performance with the extended curing periods is the formation of carbonation products on the surface of cement-based specimens causing the surface to be coated. Carbonation is an influential mechanism on the pore characteristics of cement-based systems; therefore it can manipulate/affect the overall photocatalytic degradation capability of the cement-based systems. In the work of Chen and Poon

(2009a), cement-based specimens were subjected to accelerated carbonation, which caused decrements in the NO_x removal performance. This finding was attributed to the increased volume of carbonation products as a result of the conversion of $Ca(OH)_2$ into $CaCO_3$, filling the pores, reduction the total porosity, thereby blocking the diffusivity of NO_x into the cement-based matrix.

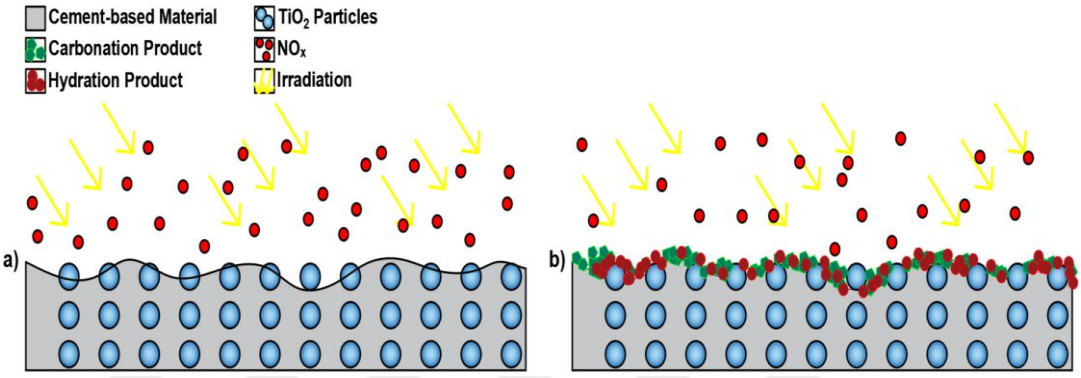

Figure 2.8. Representative scheme showing the blockage of photocatalytic reactions due to ageing (a) new material, (b) aged material. (Source: Redrawn after Vittoriadiamanti and Pedeferri, 2013.)

2.3.9. Relationship between the final surface texture of cement-based systems and NO_x degradation capability

Numerous research have established that the design of cement-based materials/products with a rougher surface (more open roughness) provides higher photocatalytic activity because of the availability of higher active surface areas for the photocatalytic reactions and exposure of larger amounts of TiO_2 particles to lights and pollutants (De Melo et al., 2012; Sugrañez et al., 2013; Jimenez-Relinque et al., 2015; Laplaza et al., 2017; Rhee et al., 2018; Jin et al., 2019). However, photocatalytic materials with high surface roughness are likely to accumulate dirt, dust, or any blocking materials on their surface that will prevent photocatalytic reactions (Figure 5.9) (Rhee et al., 2018).

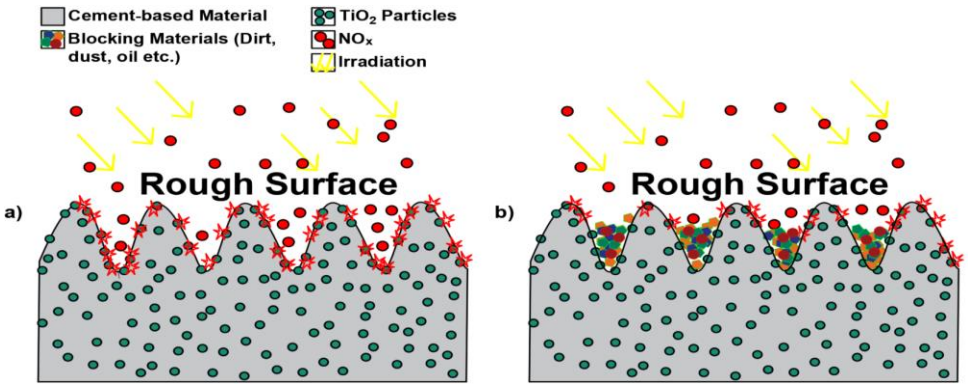

Figure 2.9 Blocking the interaction between TiO_2 particles and irradiation/pollutants because of the accumulation of blocking materials on rough concrete surface, (a) new material (b) old material (under service).

Poon and Cheung (2006) also reported that because of low possibility of accumulation of dust, dirt, oil, and grease on the surface, a product with dense surface texture provides much more stable photocatalytic degradation activity over time, (i.e., lower decrease in degradation capability with prolonged time).

2.3.10. Relationship between the operation-related parameters and NO_x degradation capability

In addition to the material- and production-related parameters detailed above, environment- and operation-related parameters including humidity, pollutant concentration, and irradiation to be exposed may affect the photocatalytic activity of cement-based materials. In terms of pollutant concentration (amount), although there are contradicting results in the literature, there is a general consensus that increased pollutant concentration decreases the rate of photocatalytic degradation. In the work of Lucas et al. (2013), it was observed that the decrease in the pollutant (NO_x) concentration (from 0.7 to 0.5 ppmv and from 0.5 to 0.3 ppmv) increased the photocatalytic activity of specimens. They also reported that for pollutant concentration beyond a certain level, in which all active sites can be used in the NO_x degradation process, an excessive amount of intermediate reaction products is formed, which sabotage the degradation process. It was observed in different studies that the increase in the inlet NO concentration (Hunger et al., 2008, Bolte, 2009; Ballari et al., 2010, 2011) and flow rate (Hunger et al., 2008; Bolte, 2009; Ballari et al., 2010; Folli et al., 2010) decrease the photocatalytic degradation rate. Contrary to these results, Yang et al. (2019) found results indicating that the increase in NO flow rate (L/min) and initial NO concentration (ppb) cause increase in the

photocatalytic activity of mortars. It was also noted that the increased blockage of the photocatalyst surface with NO molecules can increase the rate of photocatalytic reaction between photocatalyst particles and NO molecules.

There are studies that have been performed to appraise the effect of irradiation to be exposed on the photocatalytic activity of cement-based systems. Yang et al. (2019) indicated that the utilization efficiency of incident photons from light source is reduced with the increase in incident UV-A light intensity, causing decrement in the photocatalytic activity of photocatalytic products. In contrast to the results found in Yang et al. (2009), Ballari et al. (2011) stated that better NO_x conversion rates are obtained when the irradiance is increased, and they attributed this result to the increment in the production of electrons/holes leading to the generation of higher amount of hydroxyl radicals. Similarly, Hunger et al. (2008) and Bolte (2009) observed increments in the NO_x degradation rates with the increments in UV-A intensity. In addition to light intensity, type of irradiation and light source are influential on the photocatalytic degradation capability of cement-based systems as well. In this regard, Guo et al. (2015b) obtained lower NO conversion results under sunlight irra- diation compared to those under UV-A irradiation. Hunger et al. (2008) and Guo et al. (2015a) obtained better photocatalytic degradation results under UV-A irradiation compared to visible light. Pérez-Nicolás et al. (2017) used three different light sources including UV light, solar light and visible light. They obtained the highest NO removal results from the specimens irradiated by UV light regardless of other factors. The NO removal capability of identical specimens under two other light sources (solar and visible) varied depending on the mixture content and curing condition.

Relative humidity is another influential parameter on the photocatalytic degradation capability of the cement-based systems. Hunger et al. (2008), Husken et al. (2008), Ballari et al. (2011), Seo and Yun (2017) and Hernández-Rodríguez et al. (2019), obtained higher NO degradation rates under lower relative humidity conditions, which was associated to the competition between excess water molecules at high humidity and pollutant molecules to occupy the active TiO_2 sites. Presence of excessive water can prevent further interaction between the pollutant and TiO_2 particles because of the blocking effect of absorbed relative humidity on the penetration of pollutant gases to places where TiO_2 particles are.

3. EXPERIMENTAL STUDIES

In this section, detailed information about the materials including their physical and chemical characteristics used in the experimental studies of the thesis is given. In addition to this, experimental procedures including mixture and specimen preparations, curing of the specimens and testing procedures are presented under this section in detail.

3.1. Materials

3.1.1. Binding Source Material (Cement)

Considering its lower light absorption ability compared to that of Ordinary Portland Cement (OPC), CEM I 52.5R type White Portland Cement (WPC) conforming to the EN 197-1 cement standard was used as the main binder material in all mixtures. The specific gravity of WPC was determined as 3.15 g/cm^3. The physical and chemical characteristics of WPC were investigated using a variety of characterization methods. Laser diffraction analysis and X-ray fluorescence analysis (XRF) were used to determine particle size distribution and chemical composition of WPC, respectively. Furthermore, X-ray diffraction analysis (XRD) was used to determine the crystalline phases of WPC and scanning electron microscopy (SEM) was used to assess its morphological features. To prevent any error in results, a representative sample of powder was obtained from the inside of the premixed powder batch of WPC. Figure 3.1 shows a digital camera picture and a SEM image of WPC, and Table 3.1 shows the chemical composition and some physical properties of WPC.

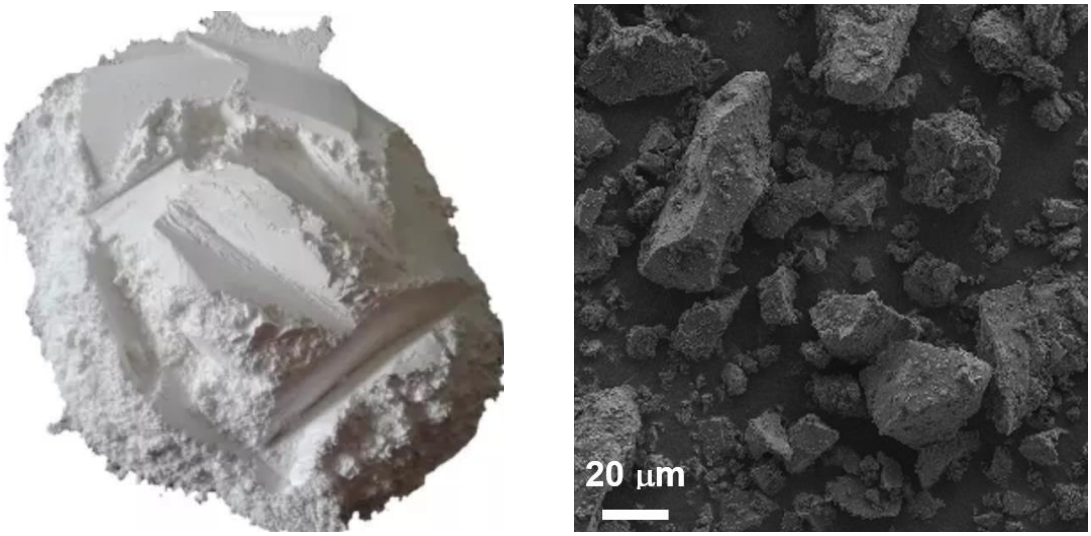

Figure 3.1. Images of WPC under digital camera and SEM.

Table 3.1. CEM I 52.5 R WPC chemical composition and physical attributes.

Chemical Composition, %						Physical Properties		
SiO_2	Al_2O_3	Fe_2O_3	CaO	MgO	SO_3	Loss on ignition	Density (g/cm^3)	Specific surface, Blaine (cm^2/g)
21.39	3.37	0.89	62.6	2.39	4.55	3.1	3.15	4650

Figure 3.2 shows the particle size distribution of WPC and Table 3.2 presents the particle size properties of WPC. XRD pattern of WPC is presented in Figure 3.3.

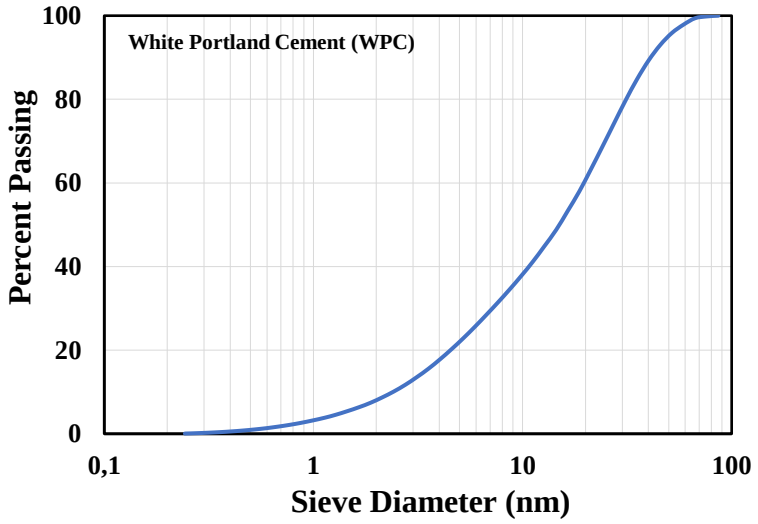

Figure 3.2. Particle size distribution of WPC.

Table 3.2. Particle size properties of WPC.

Type of Binding Source Material	Surface-weighted average size D[3,2] (µm)	Volume-weighted average size D[4,3] (µm)	d(0,1) (µm)	d(0,5) (µm)	d(0,9) (µm)
WPC	4,7	16,5	2,1	13,2	36,2

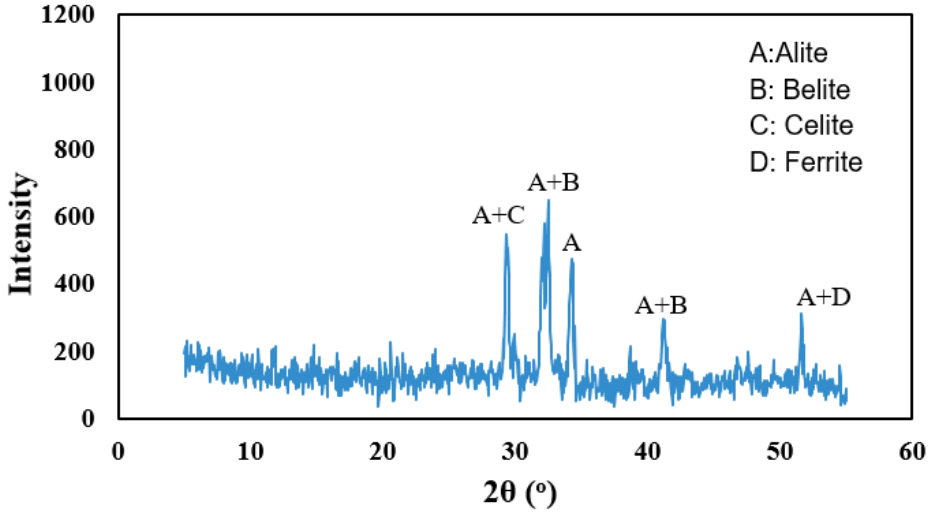

Figure 3.3. Crystal structure of WPC.

3.1.2. Titanium Dioxide (TiO_2)

A total of 6 different types (in terms of size and crystal phase) of TiO_2 was used used as photocatalysts to degrade the NO_x in the presence of UV light. These were nano-sized (10-20 nm), submicron-sized (~200 nm) and micron-sized (approximately 1.40-1.50 μm) anatase- and rutile-phase TiO_2 powders. Additionally, Degussa Evonik P25 brand TiO_2 as a commercial product, which has a proven photocatalytic performance, was used to compare its photocatalytic performance with developed cement-based composites. SEM and XRD analyses were utilized to analyze the different-sized TiO_2 powders employed as photocatalyst materials in this investigation. To rule out the possibility of error in the results, a representative sample of powder was collected from the inside of the premixed TiO2 powder batch and dried overnight in an oven prior to analysis. XRD patterns of the different-sized anatase and rutile TiO_2 powders and Degussa Evonik P25 TiO_2 particles used in experimental studies are shown in Figures 3.4, 3.5 and 3.6, respectively.

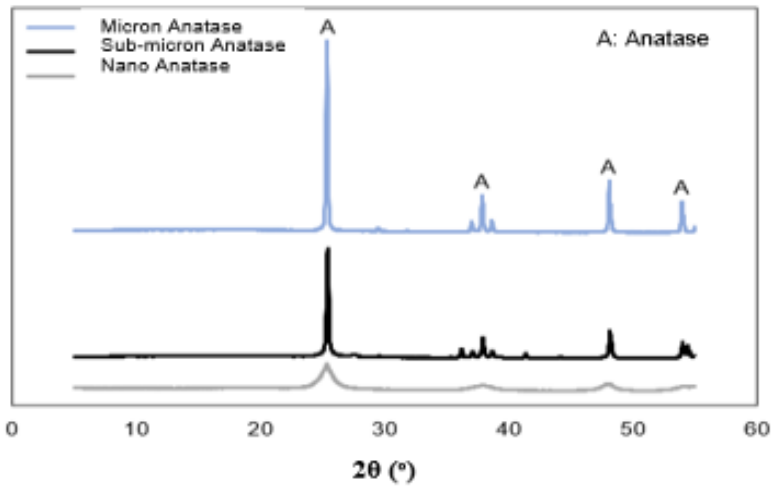

Figure 3.4. XRD analysis of TiO_2 in anatase phase.

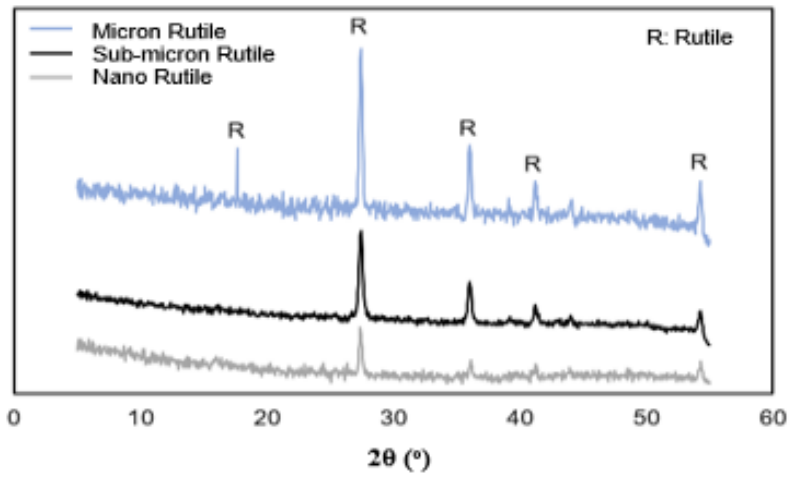

Figure 3.5. XRD analysis of TiO_2 in the rutile phase.

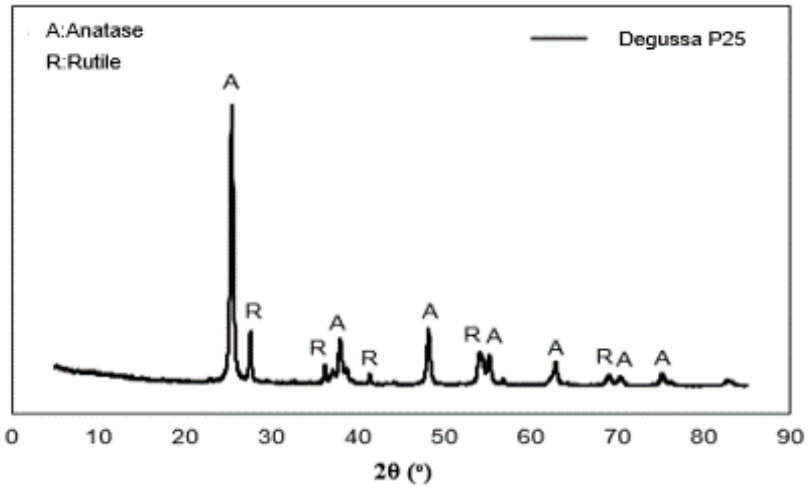

Figure 3.6. XRD analysis of Degussa Evonik P25 TiO_2.

As can be seen from the XRD analysis of TiO_2 particles, anatase-phase TiO_2s have a single peak at the same angle, while in the rutile phase, multiple peak values are observed at different angles. Degussa Evonik P25 TiO_2, which is a commercial product, contains 80% anatase and 20% rutile phase and this situation can be clearly seen from the the XRD analysis (Figure 3.6) considering that crystalline phases detected for Degussa Evonik P25 TiO_2 point out both anatase and rutile phases. Images taken by a digital camera and SEM micrographs of TiO_2s used in this study are shown in between Figure 3.7 and Figure 3.13.

Figure 3.7. Micron anatase TiO_2: General view (left figure) and SEM micrograph (right figure).

Figure 3.8. Sub-micron anatase TiO_2: General view (left figure) and SEM micrograph (right figure).

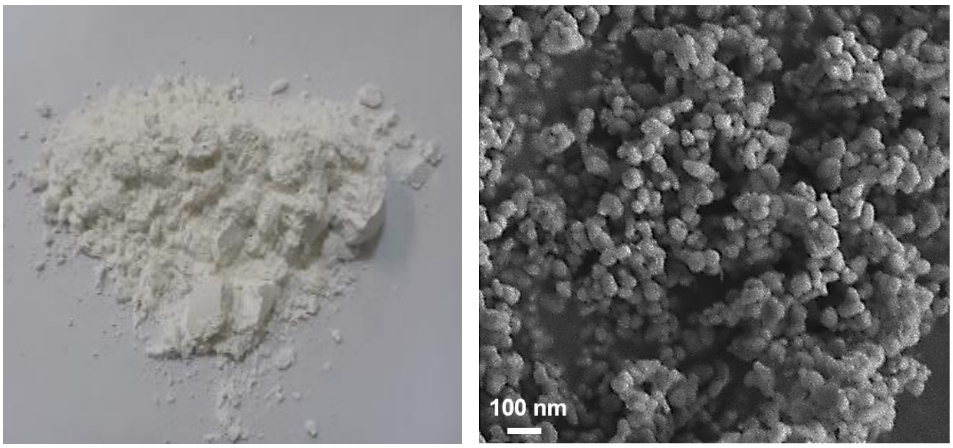

Figure 3.9. Nano anatase TiO_2: General view (left figure) and SEM micrograph (right figure).

Figure 3.10. Micron rutile TiO_2: General view (left figure) and SEM micrograph (right figure).

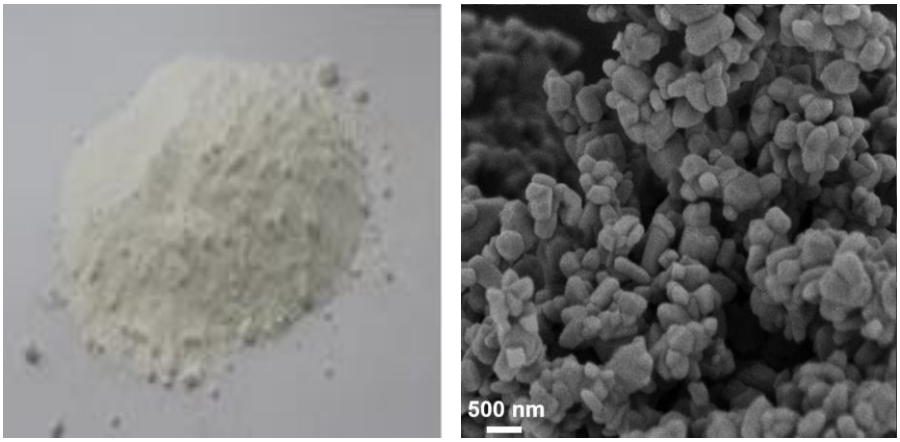

Figure 3.11. Sub-micron rutile TiO_2: General view (left figure) and SEM micrograph (right figure).

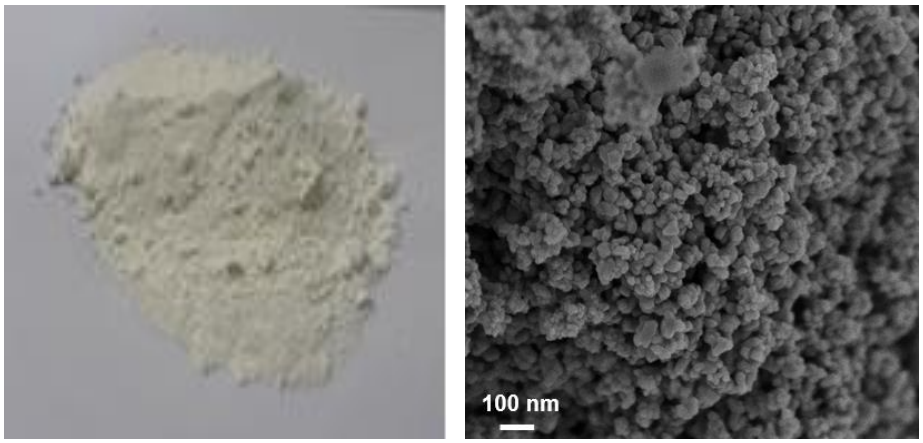

Figure 3.12. Nano rutile TiO_2: General view (left figure) and SEM micrograph (right figure).

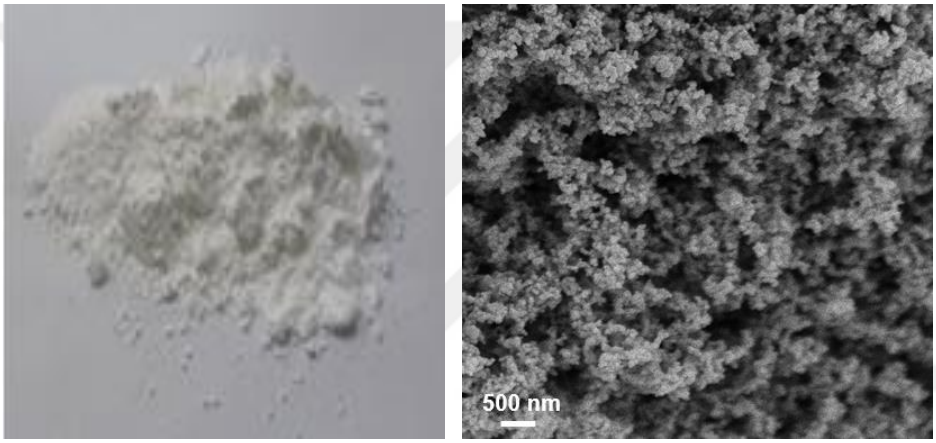

Figure 3.13. Degussa P25 TiO_2: General view (left figure) and SEM micrograph (right figure).

Particle size distribution of nano- and submicron-sized TiO_2 particles were determined by using a nanosizer. On the other hand, laser diffraction analysis was used to determine particle size distribution of micron-sized TiO_2 particles. In addition, the surface areas and chemical compositions (purities) of the TiO_2 particles were determined by using Brunauer–Emmett–Teller (BET) surface area analysis and XRF, respectively. The particle size distributions and some physical and chemical properties of TiO_2 particles are presented in Figure 3.14 and Table 3.3, respectively.

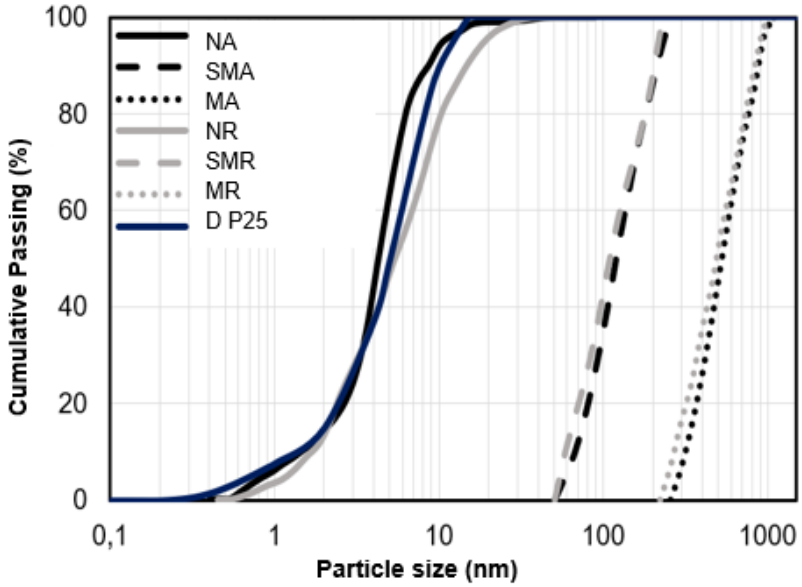

Figure 3.14. Particle size distributions of TiO_2 particles used in the studies.

Table 3.3. Some physical and chemical properties of Anatase, Rutile and Degussa P25 TiO_2 particles.

Type of TiO_2	**Label**	**Purity (%)**	**BET (m^2/g)**	**Density (gr/cm^3)**	**Maximum Particle Size (nm)**	**Minimum Particle Size (nm)**
Anatase-micron	MA	99.8	52.9	3.60	1100	250
Anatase-sub micron	SMA	99.8	74.3	3.55	250	50
Anatase-nano	NA	99.8	79.6	3.55	50	10
Rutile-micron	MR	95.6	54.8	3.81	1100	250
Rutile-sub micron	SMR	99.7	74.8	3.72	250	50
Rutil-nano	NR	99.9	82.7	3.72	50	10
Degussa Evonik P25	D P25	99.9	79.8	3.35	40	10

3.1.3. Surfactant Materials

In order for homogeneously incorporating TiO_2 particles into the cement-based systems, two different surfactants were used in experimental studies of thesis, namely polycarboxylic ether-based superplasticizer (PCE) and polyphosphates and aminocarboxylate-based liquid polyacrylic acid (PAA). The PCE (produced by BASF Construction Chemicals company and marketed under the trade name MasterGlenium 51) was liquid, conforming with ASTM-C494/C494M standard (1999), with 40% solid material content and a specific gravity of 1.1. The PAA (produced by Acar Kimya A.Ş.)

consisting of polyphosphate and aminocarboxylate was used to provide particle surface charges with its polyelectrolyte dispersant ability (Şahin et al., 2021). White, milky liquid PAA contained 48% solid material, with a density of 1.22 kg/l and pH value of in the range of 3-4.5. The dispersive effect of the surfactant materials on small-sized particles is schematized in Figure 3.15.

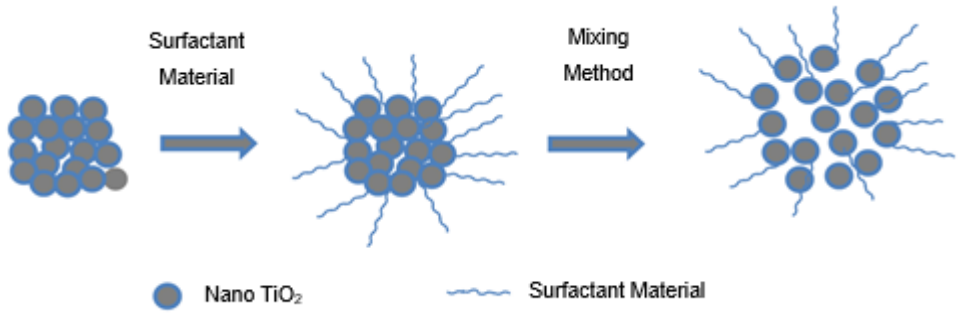

Figure 3.15. Effect of surfactants on dispersion.

3.2. Methodology

Experimental procedures including the preparation of mixtures and specimens, and their testings are detailed under this section.

3.2.1. Mixture and Specimen Preparation Procedure

Considering that higher water/binder ratio (w/b) can cause segregation/bleeding and lower mechanical properties, and surfactant materials are used, all mixtures were prepared at a constant water to powder ratio of 0.35, by weight. Firstly, mixtures were prepared using the relevant mixing method (detailed in Section 4.1.3.4). Immediately after the mixtures were prepared, they were placed into the pre-oiled molds so that each section was filled in two parts. The poured mixture was spread evenly with a large spreader by moving it back and forth once in each section of the mold. The mold and mold head were firmly placed on the mold casting vibration table, and the first layer was compacted/placed with 60 jolts. Then, the second layer was filled into the mold and smoothed with a small spreader and compacted/placed with 60 jolts. Finally, the mold was removed from the mold casting vibration tableand its surface was smoothed with a metal plate. All specimens were then demolded after curing for 24 hours in the laboratory environment and moisture cured in plastic bags at 95 ± 5% RH, 23 °C until testing age. This molding/demolding procedure was same for all mold types.

Within the scope of the thesis studies, 50x50x50 mm cube specimens and 50x50x100 (heightxwidthxlength) mm prismatic specimens were produced for compressive strength tests and photocatalytic tests, respectively. Additionally, cylindrical specimens with a diameter of 100 mm and a height of 50 mm (Ø100×50 mm) were made to determine the mixes' electrical impedance. The molds used in the mixtures and the specimens produced are presented in Figure 3.16.

Figure 3.16. The molds used in the mixtures and the specimens produced.

3.2.2. Test Procedures

3.2.2.1. Compressive Strength Test

The compressive strength of all mixtures was evaluated according to the ASTM C109 (2003) standard. 50 mm cubic specimens were prepared to determine uniaxial compressive strength. A 100 ton capacity test device (Figure 3.17) was used compressive strength tests and tests were conducted using a loading rate of 0.9 kN/s. The average compressive strength value of three cubic specimens was reported for each curing age of 2, 7, 28 and 90 days. The compressive strength test setup is shown schematically in Figure 3.18.

Figure 3.17. Compressive strength measuring device.

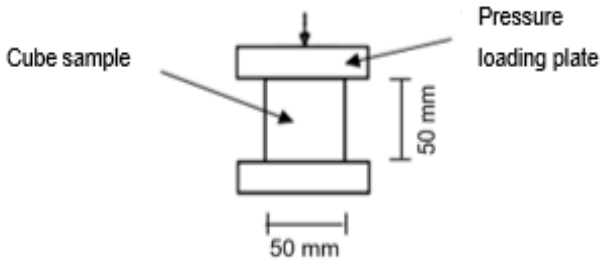

Figure 3.18. Schematic representation of the compressive strength test.

3.2.2.2. Photocatalytic Performance Measurement Experiment

The dynamic test method was used as in study of (Şahin et al., 2021) to obtain the NO_x degradation capability of the specimens. In this method, gas passes continuously throughout a test unit at a constant flow rate by interacting with the surface of specimen and the difference in gas concentration between the system inlet and outlet, which is directly related to photocatalytic efficiency is monitored by measuring simultaneously in real time. The comparison of some parameters used in the experimental studies with the those of methods applied in ISO 22197-1, JIS 1701-1 and UNI 11247 standards is shown in Table 3.4. As evidenced by the table, photocatalytic tests were carried out in accordance with the parameters specified in ISO 22197-1 and JIS 1701-1 standards, while keeping the test time less.

Table 3.4. Comparison of NO_x test standards and parameters used in the thesis study.

Test Parameters	ISO 22197-1	JIS R 1701-1	UNI 11247	Parameters Used in the Study
Gas Type	NO	NO	NO and NO_2	NO
Gas Concentration	1000 ppb	1000 ppb	400 ppb NO + 150 ppb NO_2	1000±50 ppb
Gas Flow Rate (L/min)	3	3	3	3
Test Period	5 hours	5 hours	1 hour	30 min
UV Light Intensity (W/m^2)	10	10	20	10
Sample Surface Area (cm^2)	49,25	49,25	65	50±1
Analysis Parameters	Absorbed pollutant gas	Absorbed pollutant gas	NO_x reduction percentage	NO_x reduction percentage
*: During the pre-experimental studies, the experiments were completed in 30 minutes, since there was a negligible difference between the measurements made at the end of 30 minutes and the measurements made at the end of 5 hours.				

50×100×100 mm prismatic specimens were prepared separately for each curing age of 7, 28, and 90 days to determine photocatalytic efficiency of the mixture. NO gas at a concentration of 1000±50 ppb was supplied at a rate of 3.0 l/min into the reaction chamber via a 5 mm gap between the 50±1 cm^2 specimen surface and a UV permeable quartz glass window above the closed reaction cabinet. UV light with an intensity of 10 W/m^2 was dropped on the specimen surface with two 18W UV-A blue lamps and one 36W (UVA-1) white lamp. The wavelength ranges of these lamps are presented in Figure 3.19. Photographs taken while the light sources are active on the system are shown in Figure 3.20.

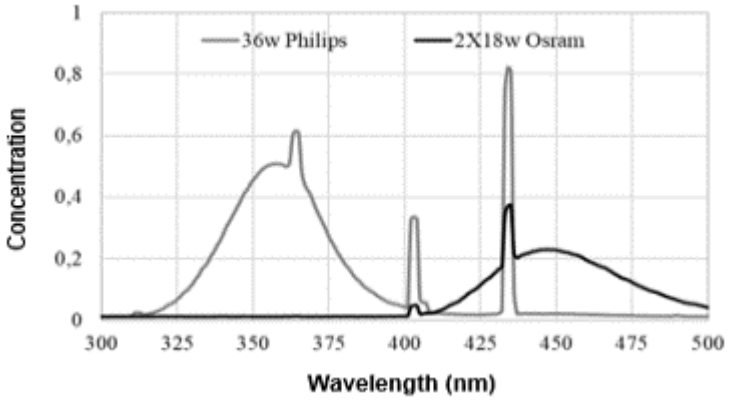

Figure 3.19. Wavelength changes of lamps used in thesis studies.

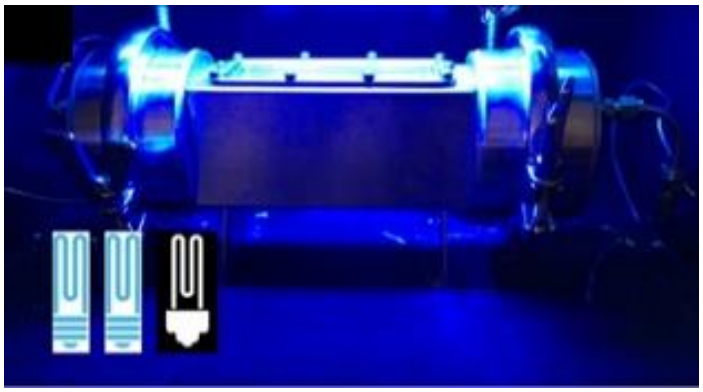

Figure 3.20. Two Osram brand and 1 Philips brand lamps (blue + white color).

NO gas entering the system was moistened with a humidifying bottle to reach 50-60% humidity level. Dry air was used to dilute NO gas from 100 ppm to 1 ppm in the system, which ensured a suitable flow rate. Thermo Scientific Model 42i NO_x analyzer (Figure 3.21) was used continuously to measure change in NO concentration.

Figure 3.21. Thermo brand 42i model NO_x analyzer.

To ensure reliable testing under consistent conditions and to prevent the manipulative effects of humidity on photocatalytic efficiency reported by Cassar et al. (2007), Dylla et al. (2010), and Seo and Yun (2017), prior to testing, all specimens were dried at 45°C for 48 hours in an oven. The testing surface of the specimen was then sanded and cleaned, and the specimen was placed in the reaction cabinet, where its upper surface could be illuminated with UV light. To adapt the specimen to the test environment, it was kept under active UV-light sources for four hours without any gas flow through the system. After this process, UV light sources were switched off and pre-adjusted gas flow was introduced to the system. After the gas concentration stayed stable for at least 10 minutes,

the UV light sources were switched on. Under the influence of UV irradiation, photocatalytic specimens started to reduce the NO_x concentration of flow. The test was performed until the lowest point at which NO_x concentration remained constant as a result of photocatalytic degradation reactions on the specimen. After that point, UV lights were turned off and gas flow was continued until NO_x concentration reached its initial level again. Details of the equipment used to measure NO_x reduction capability can be found in Figure 3.22 and 3.23. Figure 3.22 depicts a schematic depiction of the experimental setup constructed and employed within the scope of the thesis to identify the photocatalytic degradation capability of the cement-based mixtures, whereas Figure 3.23 depicts the actual experimental setup used to determine the photocatalytic property.

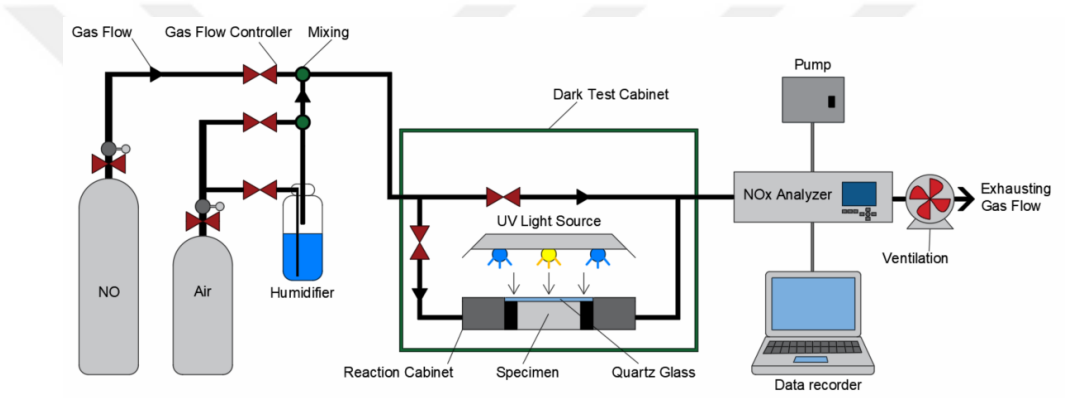

Figure 3.22. Schematic representation of the photocatalytic performance measurement experimental setup.

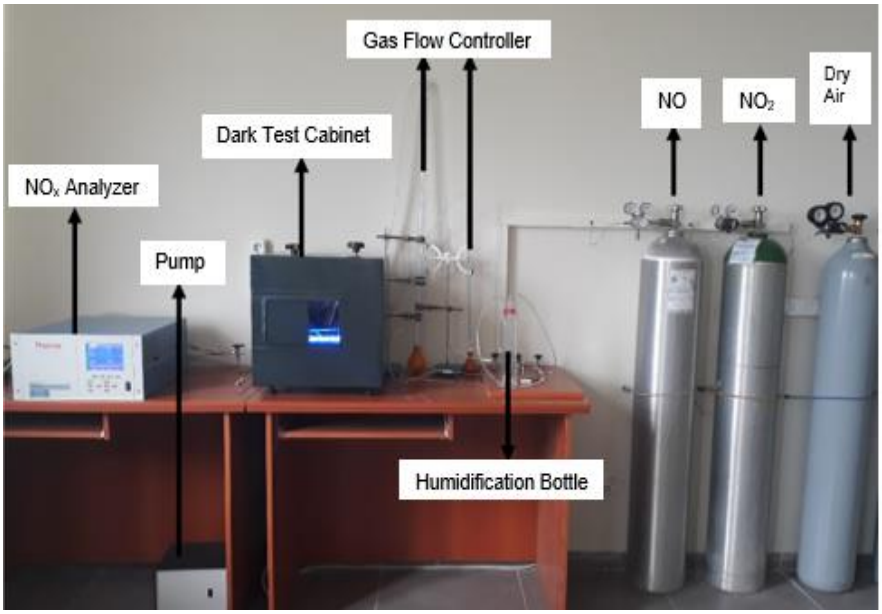

Figure 3.23. Photocatalytic performance measurement experimental setup.

At the end of the tests, in order to determine the photocatalytic performance of the cementitious systems, the NO_x and NO reduction, and NO_2 formation (%) values, which were calculated according to Equations (3.1), (3.2), and (3.3), respectively, were obtained. Furthermore, for the purpose of assessing the photocatalytic effectiveness of the system, selectivity, which represents the ratio of degraded NO that ends up as harmless nitrate rather than harmful nitrogen dioxide, is utilized and is calculated using Equation (3.4) (Balbuena et al., 2018; Si et al., 2021).

$$NO_{xred}(\%) = \frac{NO_{xi} - NO_{xf}}{NO_{xi}} \times 100, (3.1)$$

$$NO_{red}(\%) = \frac{NO_i - NO_f}{NO_i} \times 100, (3.2)$$

$$NO_{2for}(\%) = \frac{NO_{2f} - NO_{2i}}{NO_i} \times 100, (3.3)$$

$$S\ (\%) = \frac{NO_{xred(\%)}}{NO_{red(\%)}} \times 100, (3.4)$$

where NO_{xred} (%), NO_{red} (%), and NO_{2for} (%) are NO_x reduction, NO reduction and NO_2 formation, respectively; NO_{xi}, NO_i, and NO_{2i} are of the initial concentrations in order of NO_x, NO, and NO_2; and NO_{xf}, NO_f, and NO_{2f} are the final concentrations of the NO_x, NO, and NO_2, respectively; finally, S (%) is the system selectivity.

3.2.2.3. Electrical Impedance Test

Electrical impedance measurement is a non-destructive testing method used to quickly and practically evaluate the electrical resistance of cement-based systems. Electrical impedance testing is frequently used by researchers on concrete samples. Electrical impedance testing was utilized to assess the performance of composites as part of the research. A typical RCON concrete resistivity meter with axial unidirectional design was used to test electrical impedance. Details of configuration and typical test setup for this type of resistivity meter can be found in the work of Spragg et al. (2013). To be used in electrical impedance tests, three Ø100×50 mm (50 mm thickness, 100 mm diameter) cylinder specimens from each mixture were prepared. Ø100×50 mm cylindrical samples

were placed between two parallel plate electrodes with their 100 mm surface parallel to the plate electrodes. It is essential to have a conductive medium between the electrodes and the test sample (Newlands et al., 2008). Therefore, wet cylindrical sponges with a thickness of 5 mm and a diameter of 150 mm (Ø150×10 mm) were used to ensure sufficient electrical contact between the plate electrodes and the specimen. This sufficient conductive contact can also be achieved with a conductive gel or wet paper towels instead of wet sponges (Spragg et al., 2012). Before each measurement, the weight of the wet sponges used was measured to ensure that they were saturated with the same amount of water. Before starting the electrical impedance measurements, electrical impedance measurements of the sponges were made in the saturated state of water and no results were obtained. For this reason, the electrical impedance measurements of the specimens were used as they were recorded from the device, without any correction. In order to perform electrical impedance measurements more precisely, special attention was paid to select to select the contact surface of all test samples with the sponge with similar properties (without large gaps and microcracks). The concrete resistance meter device used throughout the experimental studies provides characterization by means of an alternating current impedance technique. The device can operate in a wide range of frequency values (1 Hz to 30 kHz) and can detect phase angle values between 0^o and 180^o. In addition, the device performs electrical impedance measurements in less than 5 seconds. Although the device can operate in a wide range of frequency values, the frequency value was chosen in line with the suggestion made by Hou (2008). Hou stated that the polarization effect in the material can be eliminated by applying an alternating current with a frequency of 1 kHz. As a result, electrical impedance measurements were performed at a constant frequency level of 1 kHz throughout the experimental studies. During the electrical impedance test, a line was drawn in the middle of the cut surfaces of the Ø100×50 mm cylinder samples in order to carry out repeated measurements on the same sample from the same point for each test, and the measurements were carried out in the direction of the line by accepting the drawn lines as reference. At the same time, it is aimed to easily observe the changes in electrical impedance measurements in this way. During electrical impedance measurements, the humidity level of the specimens is an important parameter, and it is known that the humidity can directly affect the results. Therefore, after curing, the specimens were kept in laboratory environment (50±5% relative humidity, 23±2 °C temperature) for one day, after being removed from the water, and then left to dry in an oven at 50 °C for two days. After that, the specimens, which

were left to dry, were removed from the oven and kept in laboratory environment for 6 hours, and the experiment was carried out. In addition, the test was carried out quickly in order to prevent the water from the wet sponges entering the pores and/or micro-cracks, so that the electrical impedance measurements could be more sensitive. The electrical impedance measuring device with two probes gives impedance and phase angle results and these values can be converted to resistance values using Equation 3.5. However, in this study, the impedance values measured by using the test specimens with same geometrical properties are considered as an indicator of resistance values.

$$\rho = Z\,x\,\cos(\phi)\,\mathrm{x}\,\frac{A}{L} \times 100, (3.5)$$

Here, ρ, Z, ϕ, A and L values represent resistance (Ω), electrical impedance (Ω), phase angle (°), cross-sectional area (m^2) and length (m), respectively. The electrical impedance test is shown schematically in Figure 3.24.

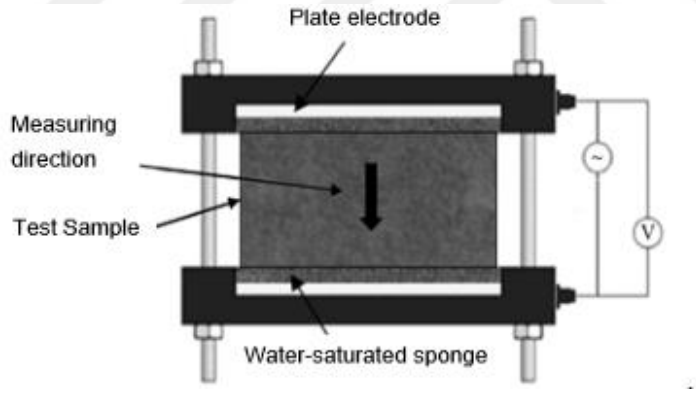

Figure 3.24. Schematic representation of the electrical impedance test setup.

3.2.2.4. Mercury Intrusion Porosimetry (MIP) Test

The mercury intrusion porosimetry (MIP) test can be used on powder or bulk samples to determine the size of the pores in the sample, the pore size distribution, surface area, and the mass density. Mercury is used in the experiment due to its non-reactive and non-wetting properties and its properties such as not penetrating fine pores if sufficient pressure is not applied. By means of the device used in the experiment, the amount of mercury that decreases in the cell depending on the applied pressure is determined from the change in capacitance between the cell ends. The Washburn equation indicates the

link between applied pressure and pore diameter, and the equation that discloses this scenario is illustrated in Equation 3.6.

$$D= (-4\gamma \cos\theta)/P \text{ , } (3.6)$$

Here P: represents the applied pressure, D: the pore diameter, γ: the surface tension of the mercury (480 dyne/cm), and θ: the contact angle between the mercury and the pore wall (usually 140^{o}). Pore size/volume distributions are generated using mercury porosimetry data. MIP can be performed on a wide range of materials, including catalysts, ceramics, minerals and mineral products, sintered material, and building materials, etc. Figure 3.25 shows the MIP test device.

Figure 3.25. MIP test device.

The mercury porosimeter includes two sample chambers: one for low pressure (up to 50 psi) and one for high pressure (up to 55,000 psi). It is possible to use penetrometers (sample cells) of various lengths and diameters for measurements. Pore diameters between 200 μm and 0.004 μm can be measured in the device. The porosimeter is computer controlled. While low pressure analysis is used for samples with pores between 4 and 200 μm, high pressure analysis is used for samples with pores between 0.004 μm and 10 μm.

In this thesis, MIP testing technique was used to characterize porosity and pore size distribution of TiO_2-based cementitious systems. First, 28-day-old prismatic specimens used for photocatalytic degradation tests were broken into small pieces, with sizes between 7-10 mm. The specimens were then dried in an oven at 50 °C for 1 day and the MIP test was conducted on the dry specimens. The instrument used for MIP testing

(Figure 2.25) (Quantachrome Corporation, Poremaster 60) had a pressure capacity of 380 MPa (55000 psia) with a contact angle of 140°.

3.2.2.5. X-Ray Diffraction Analysis (XRD)

The premise behind X-Ray Diffraction (XRD) Analysis is that each crystal refracts X-rays in a unique manner depending on the phase's atomic arrangement. These diffraction profiles for each crystal phase serve as a fingerprint for that crystal. The XRD technique does not cause damage on the tested material and may be used to analyze even extremely tiny samples. The XRD equipment can be used to investigate rocks, crystalline minerals, thin films, and polymers.

Within the scope of this thesis investigation, the Rigaku Ultima IV X-Ray Diffractometer (Figure 3.26) was used. The crystal structures of TiO_2-based cementitious systems produced within the scope of the thesis were determined using XRD Analysis. First, the samples used for photocatalytic activity (degradation) tests were powdered. The samples (approximately 30 mg) were then dried in an oven at 50 °C for 1 day and XRD tests were performed on these dried samples.

Figure 3.26. XRD Analysis

3.2.2.6. Scanning Electron Microscopy (SEM) and Energy Dispersive X-ray Analysis (EDX)

Microstructural characterization of TiO_2-based cementitious systems were investigated with scanning electron microscopy observations coupled with energy-dispersive X-ray spectroscopy (SEM/EDX) [Tescan- GAIA3+Oxford XMax 150 EDS (Figure 3.27)] to clarify their morphologies and elemental compositions. For this purpose, specimens were obtained from 28-day-old prismatic specimens used for photocatalytic degradation tests. To do that, tested surface of the photocatalytic specimen was firstly sanded and cleaned. After that, the specimen was broken into small pieces and samples were randomly

selected from among the broken pieces. SEM/EDX analyses were conducted on these specimens after being oven-dried overnight. SEM micrographs were captured, and the elemental compositions of the sections viewed were analyzed by SEM-EDX mapping.

Figure 3.27. Scanning Electron Microscopy (SEM) and Energy Dispersive X-ray Analysis (EDX).

3.2.2.7. Hydration Kinetics

Hydration kinetics of TiO_2-based cementitious mixtures were examined using a TAM Air Microcalorimeter in isothermal conditions at 25 ^{o}C, in accordance with the practice of ASTM C 1679-17. The freshly prepared pastes were immediately put in plastic containers with tight-fitting lids, and the ampoules were taken to the calorimeter for testing. Ampoules were placed into the calorimeter within 2 minutes of the end of mixing. Thermal power (measured as mW/g of total powder in the cement paste) was measured for 72 hours to determine the rate of hydration (rate of heat evolution). Using the area under the rate of hydration vs. time curves, cumulative heat of hydration curves of cementitious pastes were also generated.

4. RESULTS AND DISCUSSION

Experimental studies consist of four different parts. The first is placed on the determination of the most appropriate mixing method. The second is related to the determination of the optimum substitution ratio for different phases (anatase and rutile). Third is focused on determination of the most suitable dispersion modulus using different dispersion modules. Final part includes the determination of the most appropriate anatase and rutile combination using the data obtained. In this regard, in this section, experimental studies are detailed step by step. In this regard, specific experimental details and experimental results and discussions are presented in the following sections.

4.1. Determination of the Best Mixing Method in Cement Binder Systems with No_x Reduction Capability

4.1.1. Introduction

At this stage of the thesis, by using a multi-scale design approach, it is aimed to determine the best mixing method to develop TiO_2-substituted new generation cement-based systems without endangering engineering properties. The presence of non-homogeneous zones in the cement-based systems incorporating photocatalysts is one of the most critical factors which causes poor photocatalytic efficiency (low degradation level, unpredictable performance characteristics, low reproducibility etc.). In this context, it is important to determine practical new mixing methods for the homogeneous dispersion of nano-sized TiO_2 particles into the cement-based matrix. Here, it was investigated in which case the mixtures be prepared with different mixing methods can make more positive contributions to the photocatalytic activity and best mixing method to be used in the following stages of the experimental studies was determined.

4.1.2. Experimental Studies

At this stage of the experimental studies, with the purpose of determining a suitable mixing method to disperse TiO_2 particles throughout the cement-based matrix, in addition to the different mixing methods used in the literature (Kim et al., 2001; Musso et al., 2009; Al- Dahawi et al., 2016), different mixing methods (as detailed after) were applied using basically three different mixing tools (a conventional mortar mixer, high-speed hand blender, and ultrasonic mixer) (Figure 4.1). The ultrasonic mixer (Vibra-Cell) has a

probe diameter of 25 mm and may work at various amplitudes (0-100%) and energy levels (0-9999 Joules).

Figure 4.1. Mixing of TiO_2 particles with (a) conventional mortar mixer, (b) ultrasonic mixer and (c) high-speed hand blender.

First, optimum parameters related with ultrasonication (optimum amplitude and energy value) and surfactant materials (optimum utilization rates and combination) were determined by performing preliminary studies (zeta potential measurement of TiO_2-incorporated suspension and determination of the suspended period of TiO_2 particles in suspensions). By considering these parameters, five different mixing methods were determined (detailed in Section 4.1.3.4) and TiO_2-incorporated cement-based mixtures were produced by using these mixing methods. All mixtures were prepared at a constant water to powder ratio of 0.35, by weight. For all mixes, the utilization rate of TiO_2 particles was maintained constant at 5% of the total weight of powder material. Degussa P25 and nano-sized anatase and rutile TiO_2 powders were employed individually in the experimental trials to identify the optimal mixing procedure. Compressive strength values, electrical properties and photocatalytic activities of the specimens prepared by using each mixing method were determined at different ages. Tomography imaging and SEM characterisation were used to assess the dispersion level of the TiO_2 particles throughout the cement-based matrix. In addition, the effects of different surfactants on hydration kinetics were determined by using an isothermal calorimeter device.

4.1.3. Experimental Study Results and Discussion

4.1.3.1. Effect of Ultrasonic Mixer on the Dispersion of Nanoparticles

Solutions (water and nano-sized anatase TiO_2 powder) were created to find the optimal amplitude and energy values of the ultrasonication process in order to achieve the most

homogenous dispersion of nano TiO_2 particles. The solutions prepared was adjusted to have a water/binder ratio of 0.35 and 5% TiO_2 substitution ratio as in the cement paste. Hence, 140 ml of water and 20 g of nano anatase TiO_2 were used in the solutions. It was discovered that changing the amplitude value of the ultrasonic mixer had an influence on the zeta potential values of the suspension, therefore this was explored first. Ultrasonic mixing was done for 10 minutes at different amplitudes and 1000 J energy levels, and the zeta potentials of the suspensions were found out after that time. The zeta potential values of suspensions are presented in Figure 4.2.

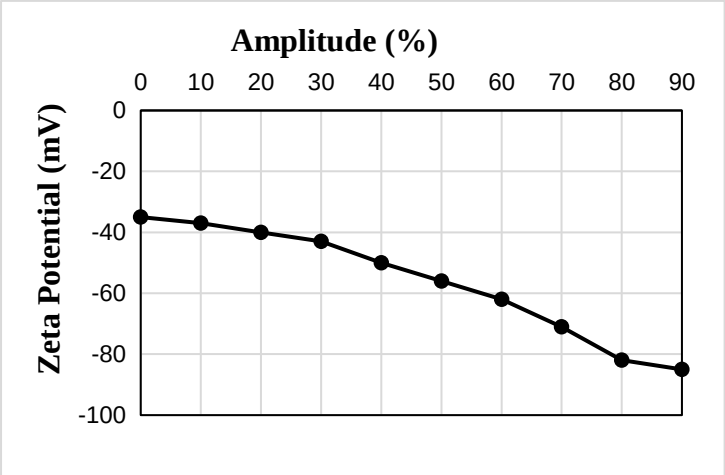

Figure 4.2. Effects of sonication amplitude variation on zeta potential (mV) of suspensions.

It is discovered that increasing the amplitude value of the ultrasonic mixer leads in a negative rise in the zeta potential values of the suspensions. This means that the particles are better dispersed with increased amplitude, and the suspension stability of the particles increases, as the increase in amplitude value allows the nanoparticles to apply more repulsive force to each other. Following an assessment of the impact of ultrasonication amplitude on the zeta potential of the suspensions, a series of experiments was conducted to determine the effect of varying the amplitude and energy values on the suspension stability of nano TiO_2-incorporated solutions. The mixture content and mixing time was same with the previous stage. The amplitude and energy values used for the experiments are presented in Table 4.1.

Table 4.1. Ultrasonic mixer amplitude and energy input values.

Suspension Name	Amplitude (%)	Energy (J)
D_1	40	1000 J
D_2	80	1000 J
D_3	40	1900 J
D_4	80	1900 J
D_5	40	4000 J
D_6	80	4000 J

The suspensions prepared with the above-mentioned amplitude and energy input values were left to stand in the same environment and the suspension duration of nano-TiO_2 particles are compared with each other. The changes in dispersion state of the TiO_2 particles throughout the suspension over time are presented in Figure 4.3.

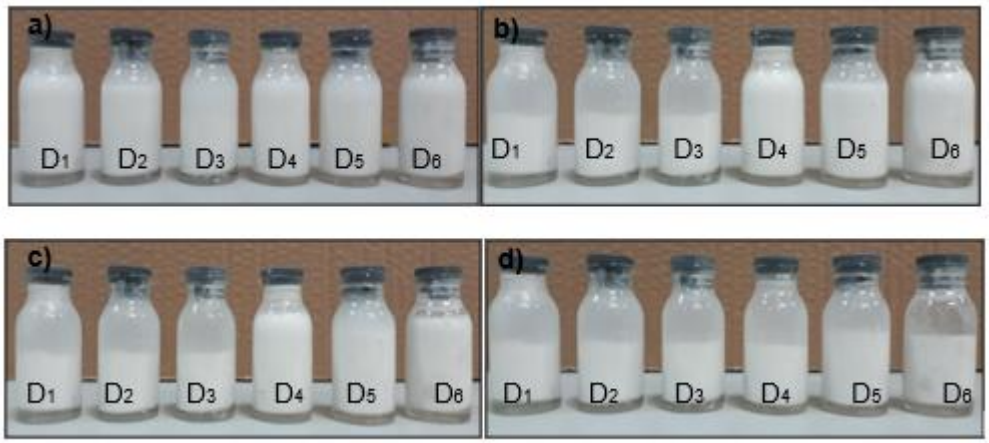

Figure 4.3. Dispersion states of nano TiO_2 particles after a) 15 minutes, b) 30 minutes, c) 1 hour, d) 2 hours from ultrasonication.

When the suspension stabilities of nano TiO_2-incorporated solutions prepared with various amplitude values and energy input levels depending on time are compared, it can be clearly seen that the increment in amplitude value and energy levels increase proportionally the suspended duration of TiO_2 particles. The nano TiO_2 particles collapsed completely within the first 30 minutes for the mixtures prepared with an amplitude value of 40% and energy values of 1000 J and 1900 J (D_1 and D_3). It was observed that the suspension, which was prepared with same amplitude value (40%) but an energy level of 4000 J, did not completely collapse even after 1 hour. Although complete collapse was observed within 30 minutes in the suspension with an amplitude

value of 80% and an energy level of 1000 J, almost no collapse was observed for other energy levels with the same amplitude value (%80) in 1 hour. In line with all these results, it was determined that the ultrasonic mixer should be used at 80% amplitude and 1900 J energy level in order to obtain the optimum performance from the ultrasonic mixing process.

4.1.3.2. The Effect of Surfactant Materials on the Dispersion of Nanoparticles

In addition to the investigation on the effect of the ultrasonication-related parameters on the zeta potential of the suspension, the effect of usage rates/combination of surfactant materials was also determined. At this point, an ultrasonication mixing with a 40% amplitude and a 1000 J energy input level was utilized to examine the influence of surfactants alone on the zeta potential of the solutions. The utilization rates were renged between 0%-2% (by total weight of binder material) for PCE, 0%-4% for PAA, and 0%-3% for PCE+PAA (equal amount). The mixture content (in terms of water and TiO_2) and mixing time was same with the previous stage. The zeta potential measurements are graphed in Figure 4.4.

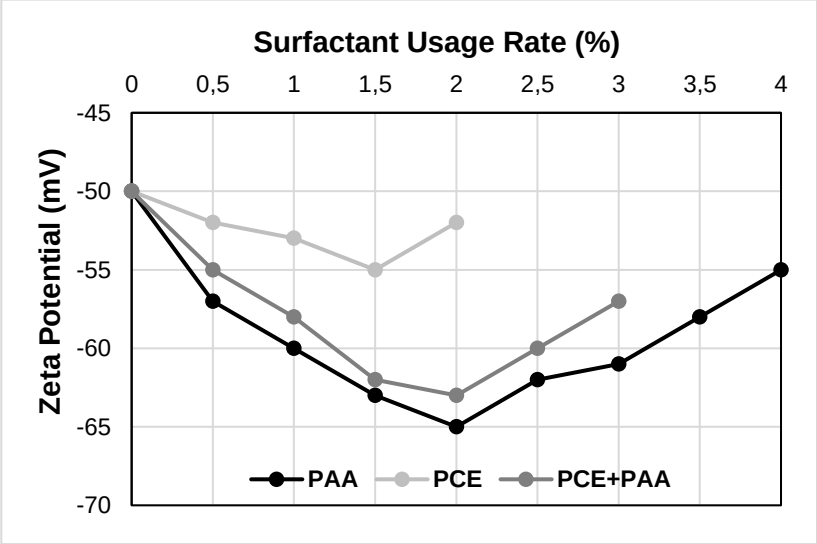

Figure 4.4. Effect of surfactant materials on zeta potential of solutions.

First, the effects of PCE on the zeta potential value of the suspensions were investigated. Using just PCE, the zeta potential values increased in a negative manner up to 1.5% utilization rate and reached a maximum value of -55 mV. A negative drop in the zeta potential value occurs when the PCE is used in excess of 1.5% utilization rate. Secondly,

the effects of using PAA on the zeta potential values of the suspensions were investigated. The zeta potential values of the suspensions prepared using only PAA increased negatively up to a 2% utilization rate and reached the highest value of -65 mV. After 2% utilization rate, the increase in the utilization rate of PAA caused a negative reduce in the zeta potential values. Finally, the changes in zeta potential values of the suspensions were observed when PAA and PCE were used together in equal proportions. In this case, the zeta potential values of the suspensions containing both PAA and PCE incremented up to total usage rate of 2% in the negative direction and reached a value of -62 mV. When the total usage rate of PAA and PCE was more than 2%, negative decreases in the zeta potential value were observed. In addition to the zeta potential measurements, in order to compare the effects of surfactant materials on the suspension stability of nano TiO_2-incorporated solutions, suspensions containing surfactant materials were prepared. The mixture content (in terms of water and TiO_2) and mixing time was same with the previous stages. The usage rates of the surfactant materials in the mixtures (by weight of binder content) are presented in Table 4.2.

Table 4.2. Different surfactant ratios of the mixture.

Suspension Name	**PCE (%)**	**PAA (%)**
S_1	-	-
S_2	0,5	-
S_3	0,5	0,5
S_4	-	0,5
S_5	1	-
S_6	-	1
S_7	1	1

The suspensions prepared with the above-mentioned usage rates of surfactant materials were left to stand in the same environment and the suspension duration of nano-TiO_2 particles are compared with each other. The changes in dispersion state of the TiO_2 particles throughout the suspension over time are presented in Figure 4.5.

Figure 4.5. Dispersion states of nano TiO_2 particles after a) 2 hours, b) 1 month, c) 3 months, d) 6 months from the ultrasonication.

For the suspension prepared without the use of surfactant materials, complete precipitation of TiO_2 particles was observed after approximately 2 hours. When both surfactant materials (PAA+PCE) were used at the utilization rate of 1% (0.5+0.5) (S_3), it was observed that there was no complete precipitation of TiO_2 particles even after 6 months. Considering the suspended period of TiO_2 particles, it can be stated that the single use of PAA provides better dispersion and suspension stability than that of PCE at the same utilization rate. Accordingly, considering the zeta potential values and suspension stability properties obtained according to the utilization rates of the surfactant materials, it can be stated that the ideal utilization rates for singly-utilized PCE and PAA are 1% and among 0.5-1%, respectively. In the case of co-utilization of PCE and PAA, it was observed that the suspension is more stable when the total utilization rate is 1-1.5%. In line with these results, it can be stated that the co-utilization of PAA and PCE at the utilization rate of 1% (0.5+0.5) resulted that the nanoparticles remain suspended for a very long time. At this point, it should be kept in mind that the effect of surfactant materials on hydration process is an important parameter that should be considered when designing mixtures. As a result, considering the preliminary studies detailed above, five different mixing methods given in Section 4.1.3.4 were designed and mixtures were prepared using these mixing methods. The feasible and effective mixing method was determined by evaluating the performance of the prepared mixtures. Details of all this evaluation process are presented in the following sections.

4.1.3.3. Hydration Kinetics

The effects of different surfactant materials on hydration kinetics of the cement-based systems were examined by using an isothermal calorimeter device. In this context, mixtures were prepared by singly using PCE and PAA at the rates of 1% and 0.5% by weight of the total binder, respectively. In case of concomitant utilization of PCE and PAA, mixtures were prepared by using them at utilization rate of 1% by weight of the total binder (0.5% PCE and 0.5% PAA) and their effects on hydration kinetics were evaluated. For comparison, a reference mixture (non-containing surfactant materials) was also produced. The hydration rate and cumulative heat of hydration of cementitious pastes are presented in Figure 4.6.

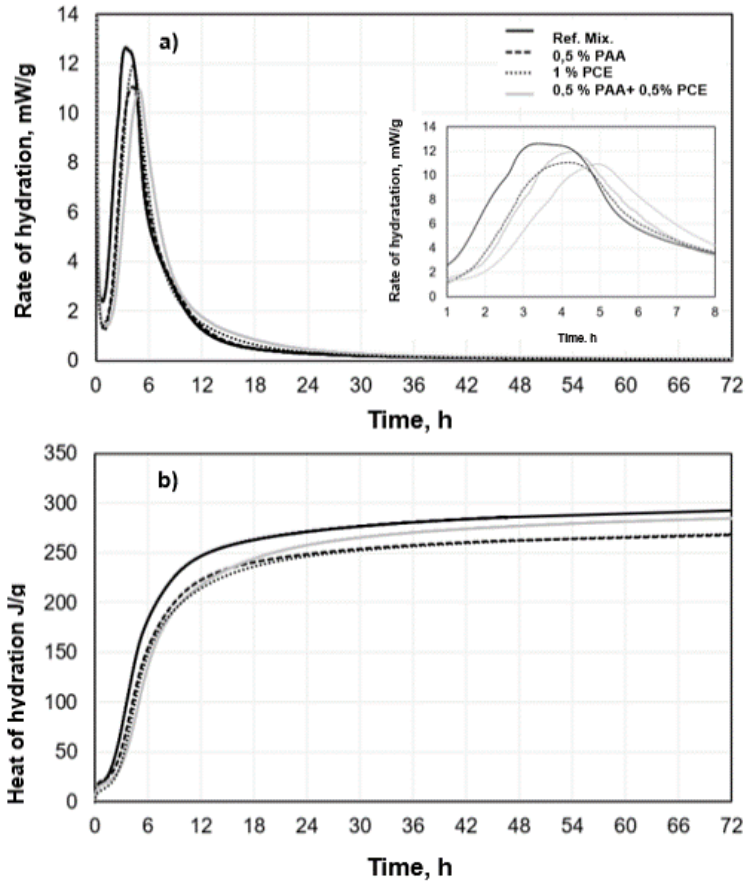

Figure 4.6. a) Rate of hydration and b) heat of hydration of cementitious systems with variable surfactant materials content.

As can be followed from Figure 4.6, the reference mixture (without surfactant materials) reached the hydration peak first and had the highest rate of hydration. The singly utilization of surfactant materials (1% PCE or 0.5% PAA) in the mixture, especially in

the early hydration period, delayed the occurrence of peak of the rate of hydration and caused a reduction in the cumulative heat of hydration released (Cheung et al., 2011). However, this effect reduced over time. The binary utilization of PCE and PAA (0.5%+0.5%=1%) caused significant delay in the hydration reactions, although the amount of heat released stabilized over time.

4.1.3.4. Mixing Methods Used

4.1.3.4.1. First mixing method (reference)

This mixing process for the paste phase was designed by modifying the standard mortar mixing procedure given in TS EN 196-1. For 10 minutes, the mortar mixer was running at 100 rpm (revolutions per minute) with dry TiO_2 and cement. After 10 minutes, all the mixing water was added to the dry powder ingredients in roughly 30 seconds, while the mixer was running at 100 rpm. After that, the mixer rotation speed was raised to 300 rpm, and the PCE (1% by total weight of binder) was added to the mixer in less than 30 seconds. Finally, at this pace (300 rpm), all ingredients were mixed for an additional 10 minutes, and the mixing process was completed (Musso et al., 2009).

4.1.3.4.2. Second Mixing Method

Ultrasonic mixing was used to mix TiO_2 powder, PCE (1%) powder, and all the mixing water for 10 minutes. With an amplitude of 80% and energy input of 1900 Joules, an ultrasonic mixer was employed. In about 30 seconds, the suspension made after 10 minutes of ultrasonication was gently added to the cement in a mixer that was moving at 100 rpm. Then, all ingredients (cement, TiO_2 powder, water, and PCE) were mixed in mixer for 10 minutes at 300 rpm (Moore et al., 2003; Sobolkina et al., 2012; Saafi et al., 2013).

4.1.3.4.3. Third Mixing Method

A hand blender was used to mix TiO_2 powder, PCE (1%) powder, and all of the mixing water at high speed (3000 rpm) for 10 minutes. After mixing at high speed for about 30 seconds, the resulting suspension was gently added to the cement in the mixer operating at 100 rpm. Finally, all ingredients (cement, TiO_2 powder, water, and PCE) were mixed in mixer for 10 minutes at 300 rpm.

4.1.3.4.4. Fourth Mixing Method

This mixing technique was primarily used to determine the influence of PAA on the dispersion of TiO_2 particles in cement-based systems. In this mixing method, PAA (0.5%) was utilized singly as surfactant material. First, an ultrasonic mixer was used to mix TiO_2 powder and all mixing water for 10 minutes at 80% amplitude and 1900 Joules energy input. PAA was added to the solution slowly and steadily during ultrasonication process. After the ultrasonication procedure, the resulting suspension was mixed with the cement for 30 seconds in a mixer spinning at 100 rpm. Finally, all ingredients (cement, TiO_2 powder, water, and PCE) were mixed in mixer for 10 minutes at 300 rpm.

4.1.3.4.5. Fifth Mixing Method

Using binary surfactant materials PAA and PCE (0.5 % +0.5 %) in this mixing technique, the impact of PAA and PCE on the dispersion of TiO_2 particles in cementitious systems was investigated. The goal was to enhance the homogeneous distribution of TiO_2 powder along cement-based systems. For 10 minutes at an amplitude of 80% and an energy input of 1900 Joules, an ultrasonic mixer was used to mix TiO_2 powder with water, PCE, and PAA. The resulting suspension was added to the cement in a mixer spinning at 100 rpm for 30 seconds after the ultrasonication procedure. Finally, all ingredients (cement, TiO_2 powder, water, PAA and PCE) were mixed in mixer for 10 minutes at 300 rpm.

4.1.4.4. Compressive Strength

The compressive strength of 5% (by weight of cement) anatase-phase, rutil-phase and Degussa P25 TiO_2-substituted cementitious systems for different curing ages was determined. The compressive strength results are presented in Figure 4.7 (anatase-phase TiO_2-substituted cementitious systems), Figure 4.8 (rutil-phase TiO_2-substituted cementitious systems), and Figure 4.9 (Degussa P25 TiO_2-substituted cementitious systems).

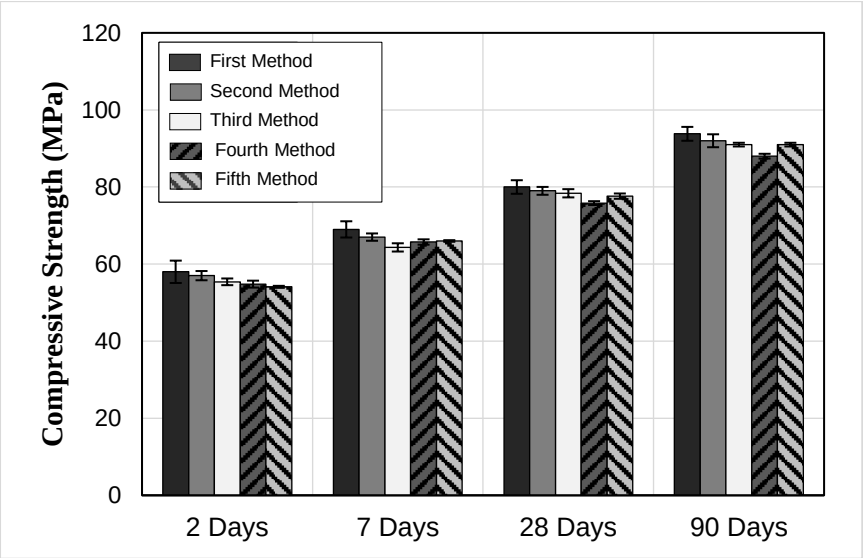

Figure 4.7. Compressive strength results of nano-anatase TiO_2-substituted cementitious composites prepared with different mixing methods.

As seen in Figure 4.7, the compressive strength values of the nano-anatase TiO_2-substituted cementitious composites varied between approximately 54.1 MPa (for 2-day) and 93.8 MPa (for 90-day). When the compressive strength values were examined, although some natural variations were observable, the lowest 2-day strength values were obtained from the specimens prepared with fourth and fifth mixing methods (54.8 MPa and 54.10 MPa, respectively). The highest 2-day compressive strength was recorded from the mixtures prepared by using first mixing method as 58.0 MPa. Although some natural variations were observable, the lowest 90-day strength values were obtained from the specimens prepared with third, fourth and fifth mixing methods (91.0 MPa, 88.0 MPa and 91.0 MPa, respectively). The highest 90-day compressive strength was recorded from the mixtures prepared by using first mixing method as 93.8 MPa. Although there are some natural variations when the whole curing ages are taken into account, the highest compressive strength values were obtained from the mixtures prepared with first mixing method while the lowest ones were obtained from those prepared with fourth mixing method.

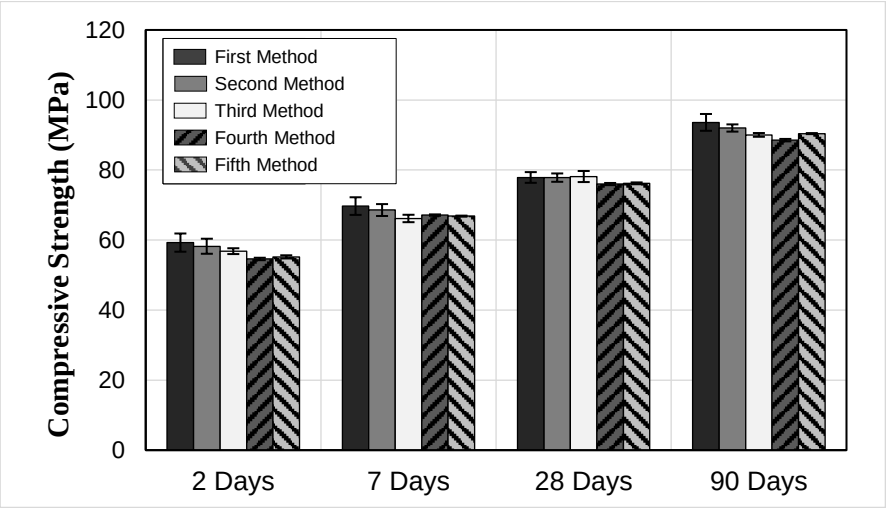

Figure 4.8. Compressive strength results of nano-rutile TiO_2-substituted cementitious composites prepared with different mixing methods.

As seen in Figure 4.8, the compressive strength values of the nano-rutile TiO_2-substituted cementitious composites varied between approximately 54.6 MPa (for 2-day) and 93.6 MPa (for 90-day). When the compressive strength values were examined, although some natural variations were observable, the lowest 2-day strength values were obtained from the specimens prepared with fourth and fifth mixing methods (54.6 MPa and 55.2 MPa, respectively). The highest 2-day compressive strength was recorded from the mixtures prepared by using first mixing method as 59.3 MPa. Although some natural variations were observable, the lowest 90-day strength values were obtained from the specimens prepared with third and fourth mixing methods (90.0 MPa and 88.5 MPa, respectively). The highest 90-day compressive strength was recorded from the mixtures prepared by using first mixing method as 93.6 MPa. Although there are some natural variations when the whole curing ages are taken into account, the highest compressive strength values were obtained from the mixtures prepared with first mixing method while the lowest ones were obtained from those prepared with fourth mixing method.

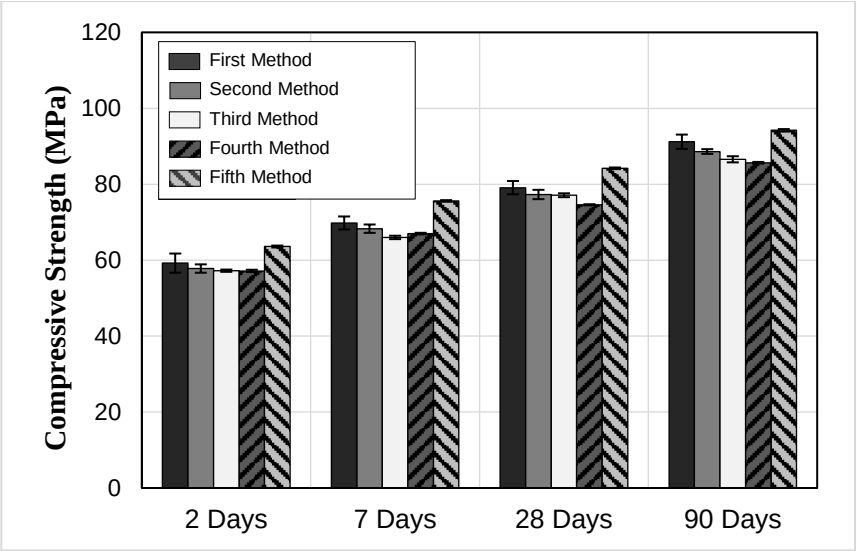

Figure 4.9. Compressive strength results of Degussa P25 TiO_2-substituted cementitious composites prepared with different mixing methods

As seen in Figure 4.9, the compressive strength values of the Degussa P25 TiO_2-substituted cementitious composites varied between approximately 57.2 MPa (for 2-day) and 94.2 MPa (for 90-day). When the compressive strength values were examined, although some natural variations were observable, the lowest 2-day strength values were obtained from the specimens prepared with third and fourth mixing methods (both 57.2 MPa). The highest 2-day compressive strength was recorded from the mixtures prepared by using fifth mixing method as 63.6 MPa. Although some natural variations were observable, the lowest 90-day strength values were obtained from the specimens prepared with third and fourth mixing methods (86.6 MPa and 85.7 MPa, respectively). The highest 90-day compressive strength was recorded from the mixtures prepared by using fifth mixing method as 94.2 MPa. Unlike the anatase- and rutile-phase TiO_2-substituted composites, as a striking point, although there are some natural variations when the whole curing ages are taken into account, the highest compressive strength values were obtained from the mixtures prepared with fifth mixing method while the lowest ones were obtained from those prepared with fourth mixing method.

When the compressive strength results are evaluated in general, the compressive strength values of the cementitious composites produced with anatase- and rutile-phase exhibited close results. This was an expected result when considering their similar particle size distributions and chemical inertness structures, mutually. Considerably lower

compressive strength values obtained from the mixtures prepared by using third mixing method (high-speed mixing with hand blender) are attributable to the reduction in the thickness of electrical double layers as a consequence of increased ionic concentration during the mixing process, resulting inrements in agglomeration (Han and Ferron, 2016). The reduced compressive strength of mixes created using the fourth and fifth mixing procedures might be attributable to the presence of a large number of voids caused by the use of PAA in these methods (Tian et al., 2013; Negim et al., 2017). In the available literature, there are many studies showing that the use of PAA beyond a certain level adversely affects the compressive strength (Ma et al., 2011; Ma and Li, 2013; Tian et al., 2013; Alqedra et al., 2014). The influence of different PAA concentrations on the mechanical parameters of concrete was investigated by Alqedra et al. (2014). The compressive strength of 3-day and 28-day old concrete specimens increased up to a 1% PAA use rate, after which the strength results decreased. Although a lower dosage of PAA was used within the scope of the thesis, it can be thought that the compressive strength values obtained from the fourth and fifth mixing methods are affected by the addition of PAA. However, when evaluating the mixing methods' performance in dispersing nano-sized TiO_2, not only compressive strength should be considered, but also photocatalytic activity, electrical properties, and, most importantly, the microstructural characteristics of the samples prepared using the various mixing methods, as this will help determine the best mixing method.

4.1.4.5. Electrical Impedance

The electrical impedance values of 5% (by weight of cement) anatase-phase, rutil-phase and Degussa P25 TiO_2-substituted cementitious systems for different curing ages was determined. The electrical impedance results are presented in Figure 4.10 (anatase-phase TiO_2-substituted cementitious systems), Figure 4.11 (rutil-phase TiO_2-substituted cementitious systems), and Figure 4.12 (Degussa P25 TiO_2-substituted cementitious systems). Considering the differences in electrical impedance results depending on mixing methods, the dispersion quality of the TiO_2 particles throughout the cement-based systems prepared with five different mixing methods were evaluated. Homogeneously dispersed TiO_2 particles can improve electrical conductivity of the cementitious systems, since they will create much more surface area than agglomerated TiO_2 particles, and conductive paths throughout the matrix. In this way, the electrical conductivity/resistivity can give an idea about the general distribution of TiO_2 particles in the matrix. The most

stable and lowest electrical resistance value means that the mixture is mixed more homogeneously.

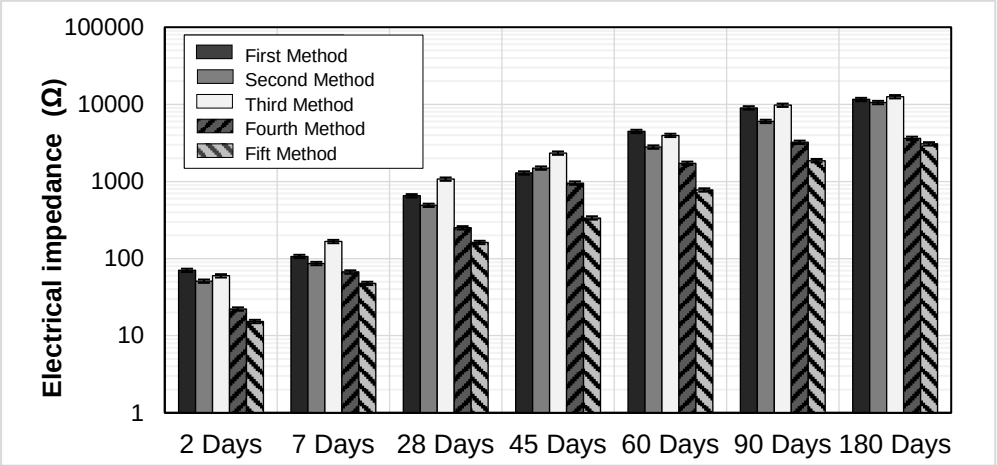

Figure 4.10. Electrical impedance results of nano-anatase TiO_2-substituted cementitious composites prepared with different mixing methods

When the electrical impedance results of 5% (by weight of cement) nano-anatase TiO_2-substituted cementitious composites prepared with different mixing methods are evaluated from Figure 4.10, it can be observed that, regardless of the mixing method used for mixture preparation, the electrical impedance values of all specimens increase with the prolonged curing age. However, the increase rate varied depending on the mixing method. The electrical impendance values of 180-day-old specimens produced by using the first, second and third mixing methods were considerably higher than those produced using the fourth and fifth mixing methods. At the end of 180-day curing age, the electrical impedance values of nano-anatase TiO_2-substituted cementitious composites prepared by using the first, second and third mixing methods ranged between 10570 Ω and 12567 Ω, while those prepared by using fourth and fifth mixing methods were 3630 Ω and 3075 Ω, respectively (Figure 4.10).

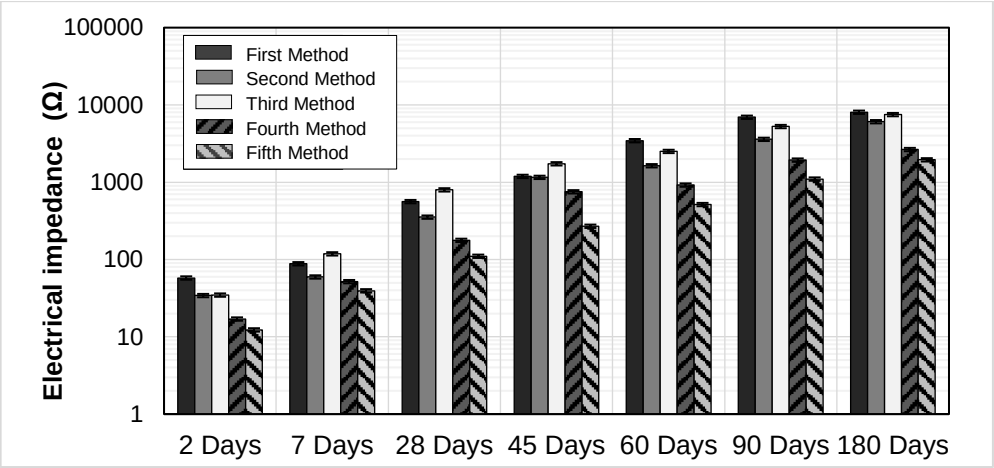

Figure 4.11. Electrical impedance results of nano-rutile TiO_2-substituted cementitious composites prepared with different mixing methods

When the electrical impedance results of 5% (by weight of cement) nano-rutile TiO_2-substituted cementitious composites prepared with different mixing methods are evaluated from Figure 4.11, as in the nano-anatase TiO_2-substituted cementitious composites, it can be observed that, regardless of the mixing method used for mixture preparation, the electrical impedance values of all specimens increase with the prolonged curing age. However, when the results are compared with those of nano-anatase TiO_2-substituted cementitious composites, it is observed that lower electrical impedance values are obtained from nano-rutile TiO_2-substituted cementitious composites. While the electrical impendance values of 180-day-old specimens prepared with nano-anatase TiO_2-substituted cementitious composites were more than 10000 Ω for the first, second and third mixing methods, the electrical impedance values for the the first, second and third mixing methods in nano-rutile TiO_2-substituted cementitious composites were recorded as 8050 Ω, 6071 Ω and 7500 Ω, respectively. The 180-day electrical impedance values of the nano-rutile TiO_2-substituted cementitious composites prepared by using fourth and fifth methods were recorded as 2650 Ω and 1950 Ω, respectively (Figure 4.11). Obtaining considerably lower electrical impedance values from the nano-rutile TiO_2-substituted cementitious composites was an expected result when considering the fact that the electrical properties of the materials are closely related to the electronic band structure and the rutile-phase TiO_2 shows better conductivity than the anatase-phase TiO_2 because of its lower band gap (Sayılkan, 2007).

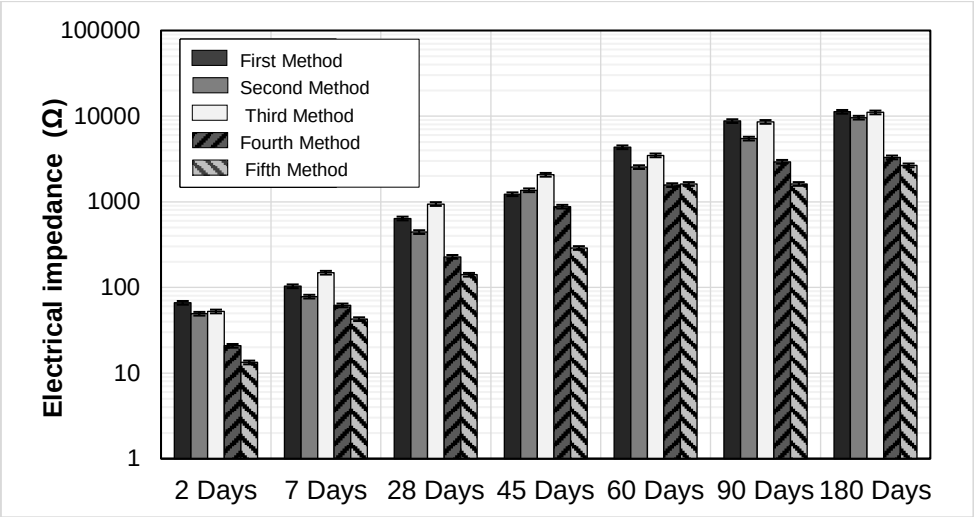

Figure 4.12. Electrical impedance results of Degussa P25 TiO_2-substituted cementitious composites prepared with different mixing methods

When the electrical impedance results of 5% (by weight of cement) Degussa P25 TiO_2-substituted cementitious composites prepared with different mixing methods are evaluated from Figure 4.12, as in the nano-anatase and nano-rutile TiO_2-substituted cementitious composites, it can be observed that, regardless of the mixing method used for mixture preparation, the electrical impedance values of all specimens increase with the prolonged curing age. When the electrical impedance results are evaluated in general, it can be seen that the electrical impedance values increase over time, regardless of the mixing method and the type of TiO_2 used. The electrical impedance values of concrete are highly dependent on the microstructure-related parameter such as pore structure, pore solution, etc. (Spragg et al., 2013). It is well established that one of the primary causes for the increment in electrical impedance over time is the composite's time-varying microstructure. Ongoing hydration reactions, reduction in the size, volume, and connectivity of the pores, decrease in pore solutions effective on transporting the conductive ions, and more condensation of the matrix over time affect the electrical properties. When the electrical impedance values of the composites prepared by using anatase-phase, rutile-phase and Degussa P25 TiO_2 at the same utilization rate are examined, it can be seen that the increase in the impedance values of the composites decreased with the increased curing age. This reduction was greater for the mixtures prepared by using fourth and fifth mixing methods, which means a more stable electrical performance over time. Therefore, it can be said that composites prepared using these two

methods are more regular and nano-sized TiO_2 particles are more homogeneously dispersed in composites prepared by using these mixing methods. When the foregoing findings are taken into consideration, it is evident that the fifth mixing method is the most effective in terms of decreasing the electrical impedance of TiO_2-substituted composites.

The electrical impedance values of nano-rutile TiO_2-substituted specimens were lower than those of nano-anatase- and Degussa P25 (containing approximately 80% anatase- and 20% rutile-phase TiO_2)-substituted specimens. As mentioned before, this is because of that the conduction band of anatase phase is (0.2 eV) more than that of rutile phase (the band gaps of rutile and anatase TiO_2 are 3.00 and 3.20 eV, respectively) (Daude et al., 1977; Kavan et al., 1996; Reddy et al., 2003; Beltran et al., 2006; Serpone, 2006; Hanaor and Sorrell, 2011). Because, as the band energy increases, the materials show more insulating properties.

As previously stated, the electrical conductivity of cementitious composites is very reliant on the pore structure and the pore solution. Additionally, the incorporation of nanoparticles affects the matrix's compactness, porosity, and microstructure. Moreover, incorporating nano-sized TiO2 as a semiconductor, on the other hand, increases electrical conductivity of cement-based systems by generating conductive channels (Xiong et al., 2006; D'Alessandro et al., 2017; Li et al., 2017; Jiang et al., 2018). In addition, it should be stated that both PCE and PAA can enhance the electrical conductivity of cement-based systems (Li et al., 2018; Ismail et al., 2019; LeonaviČIus et al., 2019). This circumstance was true for all mixes generated in this investigation, however, and the surfactant materials were used at a modest rate. As a consequence, it is plausible to conclude that surfactant materials have a minimal influence on electrical conductivity and hence have no effect on the findings.

As a consequence of all of these assertions, it is clear that nano-sized TiO_2 particles are more uniformly dispersed throughout the composites prepared by using fifth mixing method. Because this mixing method resulted in an increase in the electrical conductivity by forming additional conductive paths with semiconductor TiO_2 particles via homogenous dispersion of them along the matrix. The results of the microstructural study reported in the next sections corroborate these findings.

4.1.4.6. Photocatalytic Performance

The photocatalytic performance of 5% (by weight of cement) anatase-phase, rutil-phase and Degussa P25 TiO_2-substituted cementitious systems for different curing ages was determined. The NO_x, NO, and NO_2 concentration profiles obtained during the NO_x degradation tests under illumination are presented in Figure 4.13 (anatase-phase TiO_2-substituted cementitious systems), Figure 4.15 (rutil-phase TiO_2-substituted cementitious systems), and Figure 4.17 (Degussa P25 TiO_2-substituted cementitious systems). In addition, NO_x and NO degradation and NO_2 formation rates (in percentage) of the developed systems together with the system selectivity values are summarized in Figure 4.14 (anatase-phase TiO_2-substituted cementitious systems), Figure 4.16 (rutil-phase TiO_2-substituted cementitious systems), and Figure 4.18 (Degussa P25 TiO_2-substituted cementitious systems) for easy comparison of photocatalytic performances of the specimens. Considering the differences in NO_x and NO degradation and NO_2 formation rates depending on mixing methods, the dispersion quality of the TiO_2 particles throughout the cement-based systems prepared with five different mixing methods were evaluated.

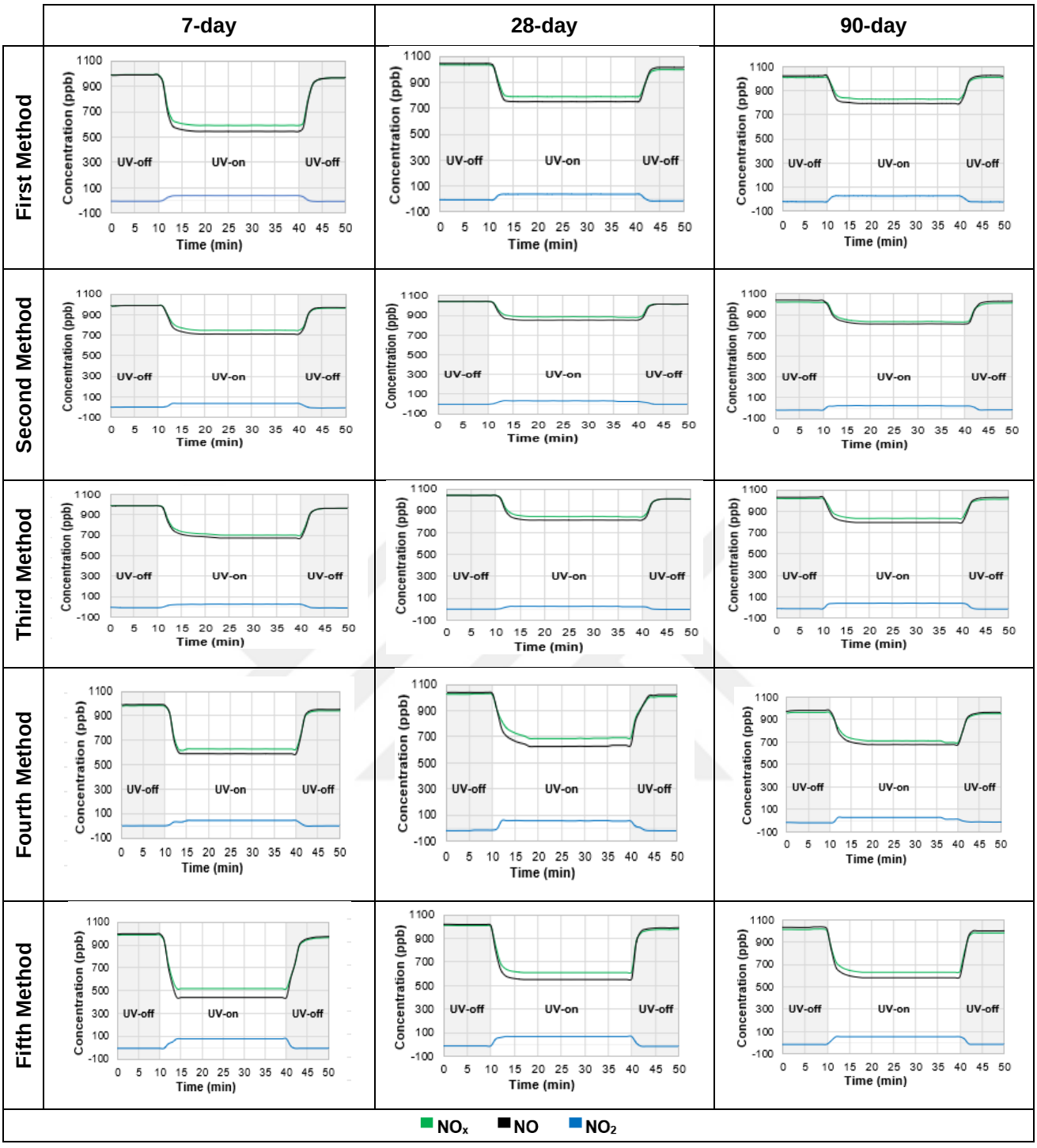

Figure 4.13. Variation of NO_x, NO, and NO_2 concentrations during each test for 7, 28, and 90-day-old samples of nano-anatase TiO_2-substituted composites prepared with different mixing methods.

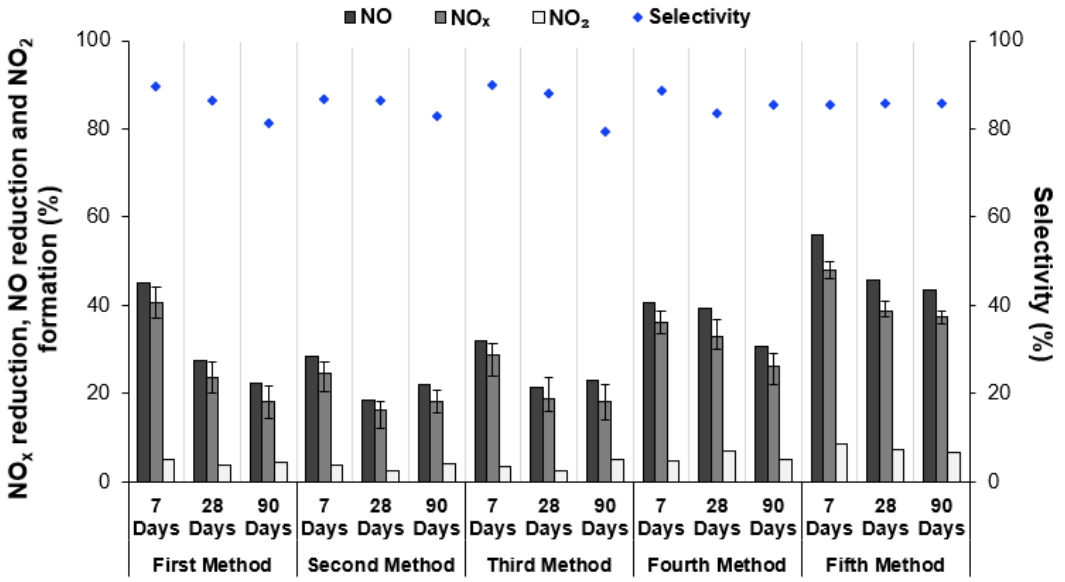

Figure 4.14. The rate of NO_x reduction, NO reduction, and NO_2 conversion and system selectivity (%) in each test for 7, 28, and 90-day-old specimens of nano-anatase TiO_2-substituted composites prepared with different mixing methods.

When the degradation rates of 7-day, 28-day and 90-day-old nano-anatase TiO_2-substituted specimens are evaluated from Figure 4.13 and Figure 4.14, it can be seen that NO_x and NO reduction rates reduced with the prolonged curing ages, irrespective of mixure design parameters and mixing method used. This time-dependent trend may have come from the ongoing hydration reactions, leading to the coating of TiO_2 particles with further hydration product and thereby reducing the presence of TiO_2 materials on specimen surfaces reached by UV irradiation. A more likely reason is that carbonation products, produced by binding carbon dioxide (CO_2) into solid carbonates on the specimen surface or another possible process, cause the specimen surface to be coated (Lackhoff et al., 2003; Poon and Cheung, 2007; Chen and Poon, 2009; Matějka et al., 2012,). As shown in Figure 4.14, the nano-anatase TiO_2-substituted composites prepared by using fifth mixing method had the largest NO_x reduction rates for each curing age. NO_x reduction rates of the 7-, 28-, and 90-day-old nano-anatase TiO_2-substituted composites prepared by using fifth mixing method were obtained as 47.9%, 38.8%, and 37.3%, respectively. The reason of obtaining higher NO_x reduction rates from fifth mixing method compared to other mixing methods can be related to that this mixing method distributes TiO_2 particles more homogeneously thoroughout the matrix, preventing TiO_2 particles from agglomeration and staying deep dark zones of the composites and

providing the presence of relatively higher TiO_2 particles on the irradiation-reached specimen surface. As followed from Figure 4.14, different NO_2 formation levels were obtained from the specimens at the end of the photocatalytic reactions. The formation of NO_2 in photocatalytic reactions can be related to the HNO_3 and NO_3^- accumulation on the TiO_2 surface over time, reacting with NO, beyond a threshold value, to form NO_2 (Wang et al., 2007; Mills and Elouali, 2015). Besides, the reactions between NO and O_2 and/or HNO_2 and OH* could be another possible reason of the formation of NO_2 (Wang et al., 2007; Mills and Elouali, 2015; Han et al., 2021). Considering the fact that the toxicity of NO_2 is significantly higher than the primary pollutant NO (Yang et al., 2018), it was critical to monitor the change of NO_2 levels throughout the photocatalytic reactions, and the system selectivity. When the system selectivity of the cementitious systems is evaluated, it was clearly observed that the system selectivity of almost all specimens exhibited a decremental trend starting from 7 to 90 days whereas the reverse was true for composites prepared by using fifth mixing method. Furthermore, the composites made utilizing the fifth mixing procedure had the greatest system selectivity value (85.8%) at the conclusion of the 90-day curing period. As a result, among nano-anatase TiO_2-substituted specimens, the highest photocatalytic performance and efficiency values were obtained from those prepared by using fifth mixing method. Therefore, it is thought that the fifth mixing method among all mixing methods provides a more homogeneous distribution of TiO_2 particles thoroughout TiO_2-substituted composites.

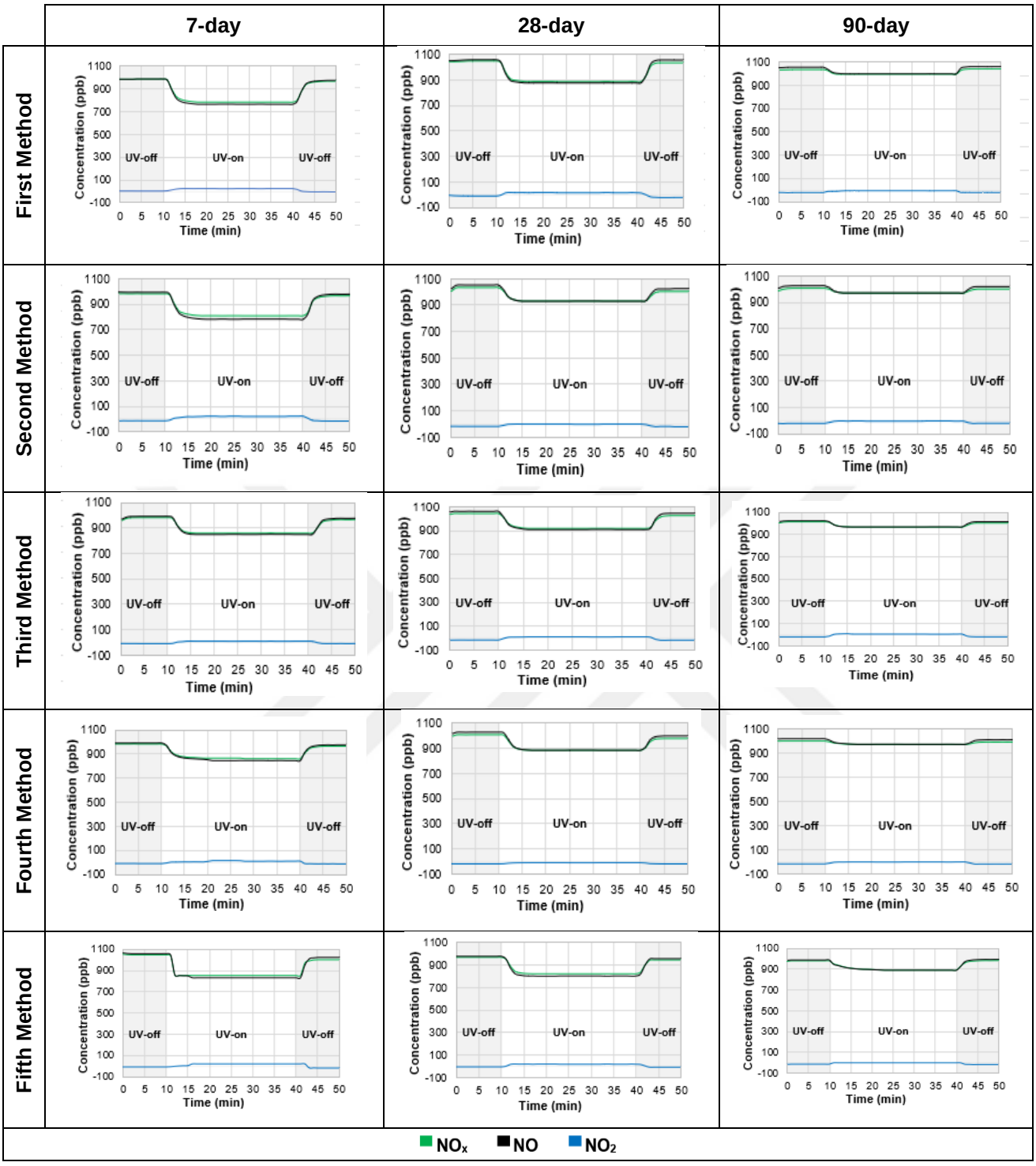

Figure 4.15. Variation of NO_x, NO, and NO_2 concentrations during each test for 7, 28, and 90-day-old samples of nano-rutile TiO_2-substituted composites prepared with different mixing methods.

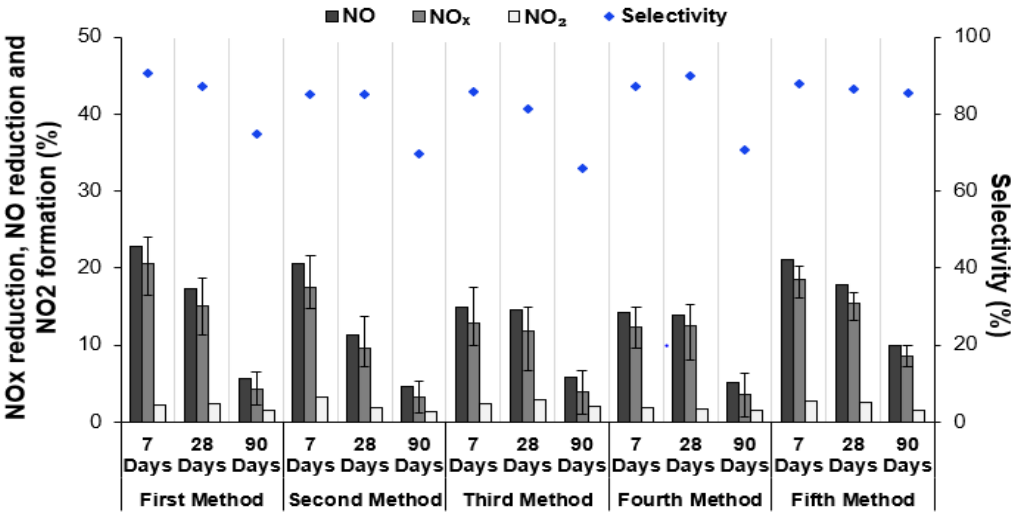

Figure 4.16. The rate of NO_x reduction, NO reduction, and NO_2 conversion and system selectivity (%) in each test for 7, 28, and 90-day-old samples of nano-rutile TiO_2-substituted composites prepared with different mixing methods.

When the degradation rates of 7-day, 28-day and 90-day-old nano-rutile TiO_2-substituted specimens are evaluated from Figure 4.15 and Figure 4.16, as in the nano-anatase TiO_2-substituted specimens, it can be seen that NO_x and NO reduction rates decreased with the prolonged curing age, irrespective of mixure design parameters and mixing method used. However, this decrease was much lower in composites prepared by using fifth mixing method. This is due to the fifth mixing method's better TiO_2 distribution capacity, which results in more homogenous composites. As can be seen from Figure 4.16, the composites prepared by using fifth mixing method achieved the highest NO_x reduction rates for each curing age. The 7, 28, and 90-day NO_x reduction rates of the composites prepared by using fifth mixing method were recorded as 18.5%, 15.4%, and 8.6%, respectively. When the system selectivity of the cementitious systems is evaluated from Figure 4.16, It was readily seen that the system selectivity of all specimens exhibited a decremental trend starting from 7 to 90 days. The composites generated utilizing the fifth mixing procedure had the greatest system selectivity value (85.6 %) at the conclusion of the 90-day curing age. In addition, on contrary to the composites prepared by using fifth mixing method, it was determined that the system selectivity values of the composites prepared using first, second, third and fourth mixing methods showed a sudden decrease at the 90-day curing age. This situation can be accepted as an indication that the composites prepared using the fifth mixing method behave more time-dependent stable. As a result, among nano-

rutile TiO_2-substituted specimens, the highest photocatalytic performance and efficiency values were obtained from those prepared by using fifth mixing method. Therefore, it is thought that the fifth mixing method among all mixing methods provides a more homogeneous distribution of TiO_2 particles thoroughout TiO_2-substituted composites.

Another remarkable point was that the composites prepared by using nano-rutile TiO_2 powder showed considerably lower NO_x reduction performance compared to those prepared by using nano-anatase one, as expected. Recent studies have shown that rutile-phase TiO_2 particles have better photocatalytic activity than anatase-phase ones (Hanson and Tikalsky, 2013). One of the primary reasons for the anatase-phase's superior photocatalytic activity is that it has a lower density than rutile-phase, resulting wider TiO_2 surface area in the TiO_2-incorporated (by weight) cement-based systems (Melo et al., 2012). Furthermore, the crystal structural problems in rutile-phase TiO_2 are much greater than in anatase-phase TiO_2. Because of an excited electron being in the conduction band for a little period of time, the rutile phase is not favoured as an efficient photocatalytic material (Schindler and Kunst, 1990). In addition, another reason for the lower photocatalytic degradation performance of rutile-phase compared to the anatase-phase is the presence of defects in the crystal structure of the rutile-phase TiO_2, resulting decrease in the amount of adsorption on the surface of the rutile-phase TiO_2 and thereby a decrease in photocatalytic efficiency (Lewis and Rosenbluth, 1989).

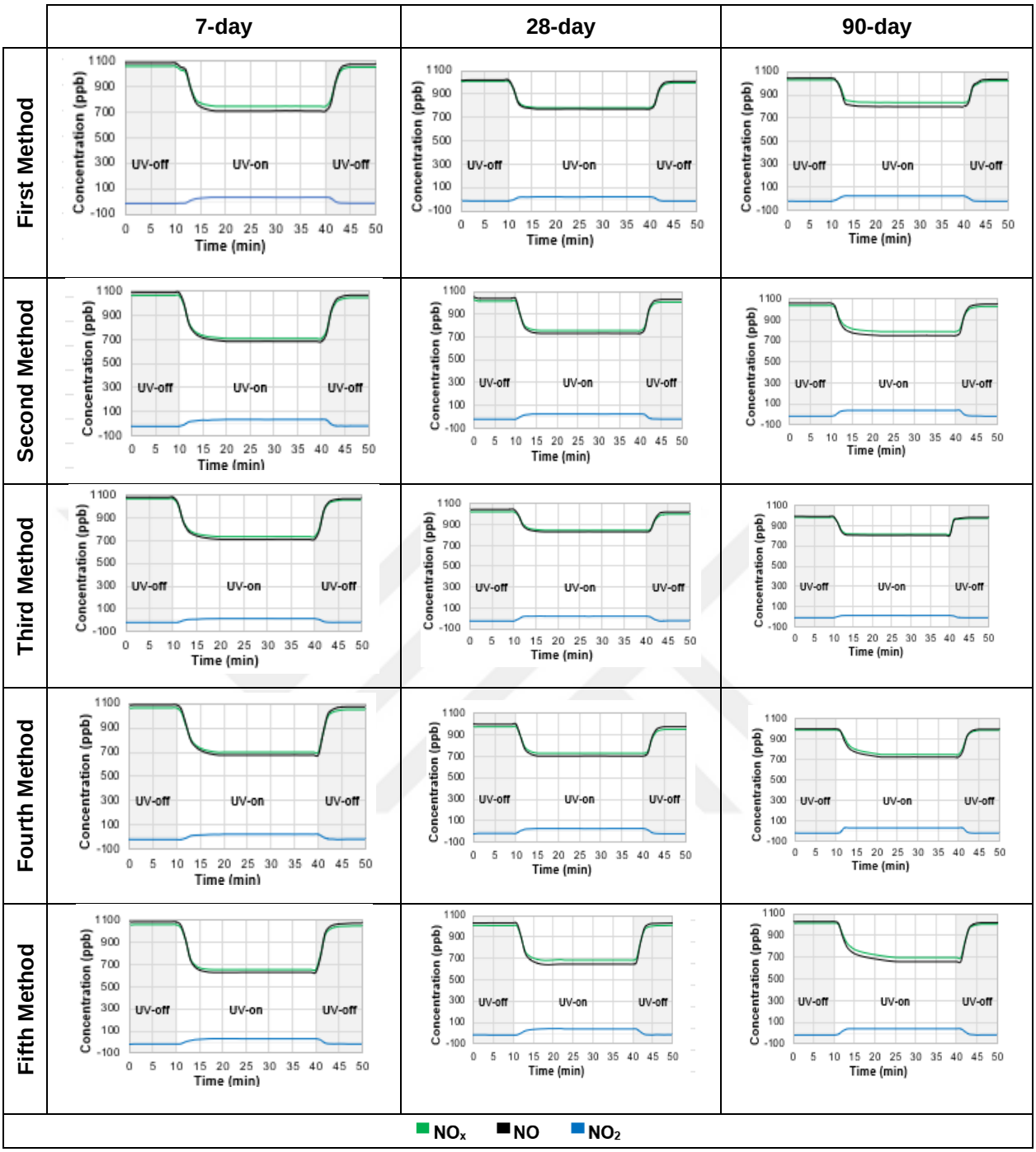

Figure 4.17. Variation of NO_x, NO, and NO_2 concentrations during each test for 7, 28, and 90-day-old samples of Degussa P25 TiO_2-substituted composites prepared with different mixing methods.

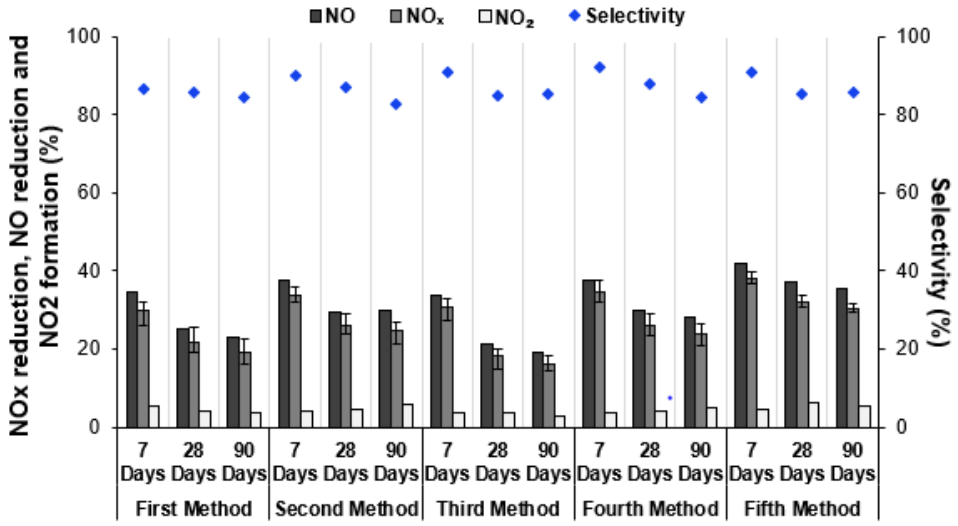

Figure 4.18. The rate of NO_x reduction, NO reduction, and NO_2 conversion and system selectivity (%) in each test for 7, 28, and 90-day samples of Degussa P25 TiO_2-substituted composites prepared with different mixing methods.

When the degradation rates of 7-day, 28-day and 90-day-old Degussa P25 TiO_2-substituted specimens are evaluated from Figure 4.17 and Figure 4.18, as in the nano-rutile and nano-anatase TiO_2-substituted specimens, the specimens prepared by using fifth mixing method achieved the highest NO_x reduction rates for each curing age. The 7, 28, and 90-day NO_x reduction rates of the composites prepared by using fifth mixing method were recorded as 38.1%, 31.9%, and 30.5%, respectively. When the system selectivity of the cementitious systems is examined from Figure 4.18, the composites created using the fifth mixing technique have the greatest system selectivity value (85.9%) at the conclusion of the 90-day curing age. These findings may be ascribed to the fifth mixing method's increased TiO_2 dispersion capability, which results in more homogenous composites. As a result, it can be possible to state that the fifth mixing method among all mixing methods provides a more homogeneous distribution of TiO_2 particles thoroughout TiO_2-substituted composites.

4.1.3.7. Image Analysis with Computed Tomography Device

Considering the compressive strength values, electrical properties, and photocatalytic performances of the specimens prepared by using five different methods, the fifth mixing method was the best method providing more homogeneous dispersion of TiO_2 particles. At this point in the study, a computed tomography device was used to figure out how well

the TiO_2 particles were spread out in the cement-based matrix. Tomographic imaging was performed on the nano-anatase TiO_2-substituted specimens. The data generated via this approach is intended to be used to examine the dispersion level of nano-TiO_2 particles along the cement-based matrix with an image processing method. A representative computed tomography image of the sample (with 18 mm diameter and 20 mm height) is shown in Figure 4.19.

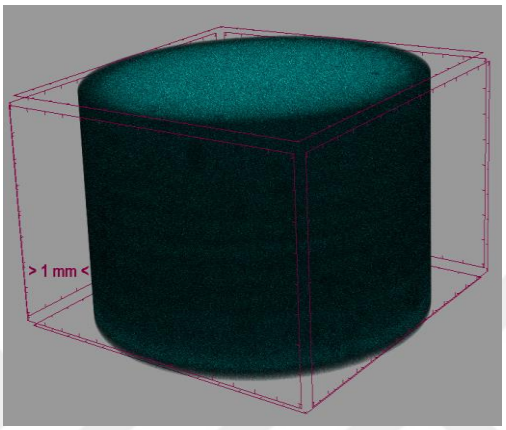

Figure 4.19. Computed tomography image of nano-anatase TiO_2-substituted composite.

Figure 4.20 depicts cross-section views of the computed tomography scans of the specimens. TiO_2 particles are shown as yellow dots. There are no traces of aggregation along the cross-section of the matrix in the mixtures made using the fourth and fifth mixing procedures, as shown in Figures 4.20-d and 4.20-e. As a result, the time-dependent stability of photocatalytic performance in these samples may be a result of the uniform distribution of nano-sized TiO_2 particles. Because of the optimal distribution of nano-sized TiO_2 particles, which provides a relatively high TiO_2 particle concentration on the sample surface exposed to UV radiation, the specimen prepared utilizing the fifth mixing procedure exhibited the largest photocatalytic degradation capability. Using third mixing method for mixture preparation, on the other hand, resulted in relatively lower photocatalytic degradation capability because of agglomeration issues with nano-sized TiO_2 particles and generated instability along the matrix, as seen in Figure 4.20-c. Due to the agglomeration issue induced by the surface charge of the TiO_2 particles, the vast majority of TiO_2 particles may remain in the dark depths of composites, preventing them from coming into touch with UV irradiation (inhomogeneous dispersion). As a result, this

inhibits photocatalytic reactions from occurring. While this is true for the first and second mixing procedures, it is more pronounced for the third one, as seen in Figure 4.20-c.

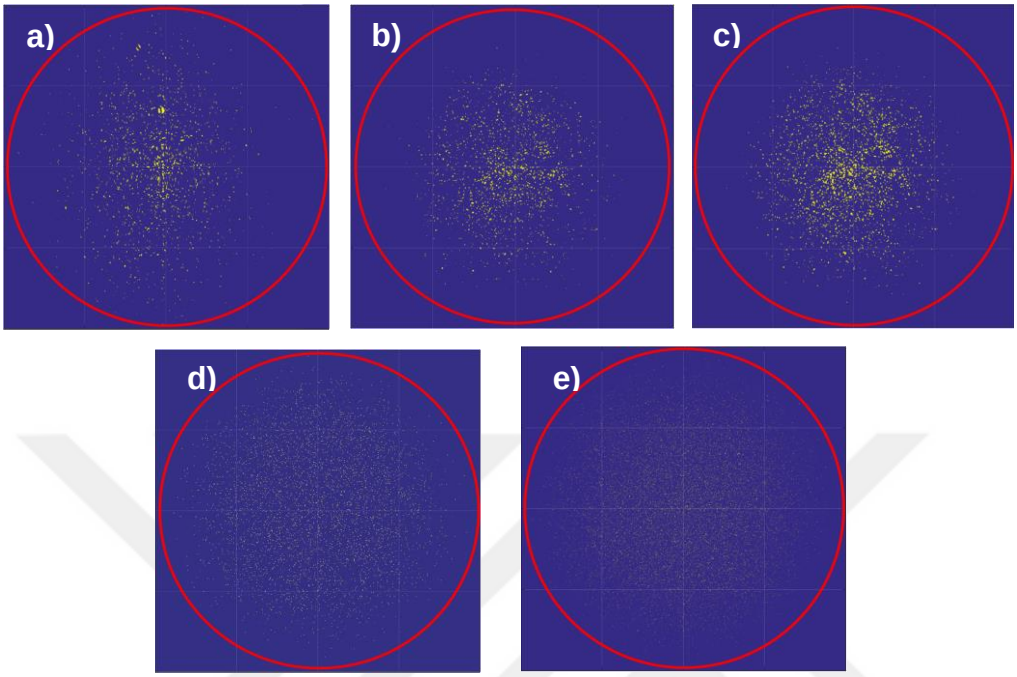

Figure 4.20. Image analysis of nano-anatase-substituted composites prepared with different mixing methods with a computed tomography device; a) first, b) second, c) third, d) fourth and e) fifth mixing method.

4.1.3.8. Scanning Electron Microscopy (SEM) Analysis

At this stage of the study, microstructural imaging of nano-anatase TiO_2-substituted composites prepared by using different mixing methods was performed by scanning electron microscopy analysis (SEM). Figure 4.21 shows the distribution of Ti elements thoroughout the cement-based specimens prepared by using various mixing procedures. Ti particles (red) were found to be evenly distributed in the cross-section of the composite prepared by using fifth mixing method (Figure 4.21-e). This can be shown as an indication that the fifth mixing method has a very good nano-sized TiO_2 dispersion capability. The specimens prepared by using fourth and fifth mixing methods exhibited much higher photocatalytic degradation capability than the others. As a result, PAA greatly contributes to the homogenous dispersion of nano-sized TiO_2 particles throughout the matrix. In a number of studies, it was stated that the fluidity of the mixtures has an effect on their homogeneity (Jimenez-Relinque et al., 2015). Thus, it is highly likely that the increased

fluidity of the mixture prepared using the fifth mixing method (as a result of the presence of PCE and PAA) will result in a more homogeneous matrix, further enhancing the mixture's microstructural characteristics in favor of photocatalytic degradation capability. As for the mixture prepared by using third mixing method, it can be seen from Figure 4.21-c that, the third mixing method results in a significant degree of agglomeration. Figures 4.21-a and 4.21-b illustrate the occurrence of agglomeration zones in the TiO_2-substituted composites prepared by using first and second mixing methods.

As a result, according to the results discussed in Section 4.1, the fifth mixing method was chosen to be used for the preparation of the mixtures in the next stages of the experimental studies.

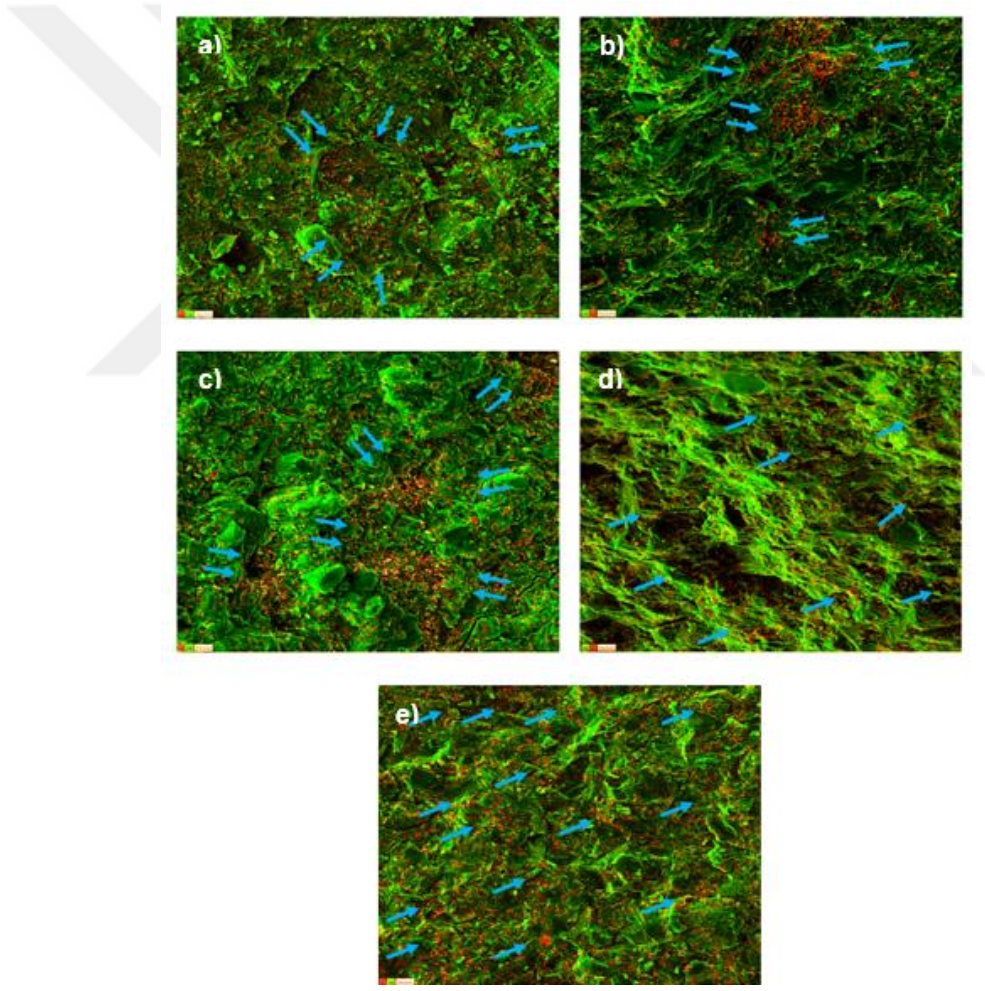

Figure 4.21. SEM images of nano-anatase TiO_2-substituted composites prepared with a) first, b) second, c) third, d) fourth and e) fifth mixing method.

4.2. Determination of Critical Utilization Rate of TiO_2 Particles in Cement-Based Systems with NO_x Reduction Capability

4.2.1. Introduction

Developing technology allows materials to be produced in much smaller sizes. Applications and research mostly aim to develop new generation function-added construction materials with small-sized (nano- and micron-sized) materials. Developing environmentally friendly multi-functional construction materials with air purification capability (photocatalytic degradation capability) is one of the research interests using small-sized materials (e.g., TiO_2 as a photocatalyst). Despite having the same chemical content, materials with smaller size have physically different properties from those with larger ones. Therefore, the influence of photocatalyst particle size on the characteristics of cement-based materials must be well understood and researched. In addition to that, considering the fact that the amount of irradiation-reachable photocatalyst material available on the cement-based materials's surface is an important parameter to be considered in order to obtain an optimum cementitious product that is affordable and characterized with the enhanced photocatalytic degradation capability, optimum utilization rate of the photocatalyst materials in the cement based-materials should be studied. Therefore, in this step of the thesis, it was planned to determine the optimum utilization rates in cases where nano, sub-micron and micron-sized TiO_2 particles were used individually. By doing this, both the optimum utilization rate of TiO_2 materials in the cement-based systems was determined and the influences of particle size on the various engineering features of TiO_2-substituted cement-based materials were investigated.

4.2.2. Experimental Studies

The fifth mixing technique, which was considered to be the best mixing procedure (in Section 4.1), was used to produce mixtures at this stage of the experimental research. A constant water to powder ratio of 0.35, by weight for all mixtures and four different usage rates of TiO_2 powders (2.5%, 5%, 7.5% and 10% by total weight of powder materials) were used for the preparation of the mixtures. In the experimental studies where the optimum utilization rate of TiO_2 materials was determined, Degussa P25 and nano-, submicron-, micron-sized anatase and rutile TiO_2 powders were used separately. Compressive strength values, electrical properties and photocatalytic activities of the specimens prepared were determined at different ages. Dispersion level of the TiO_2

particles throughout the cement-based matrix was determined by using tomography imaging. In addition, the effects of TiO_2 utilization rate or particle size on the hydration kinetics of the cement-based systems were determined by using an isothermal calorimeter device.

4.2.3. Experimental Study Results and Discussion

4.2.3.1. Hydration Kinetics

The hydration kinetics of cement-based systems prepared by using nano-, submicron-, micron-sized anatase-phase TiO_2 powders (separately) at four different utilization rates (2.5%, 5%, 7.5% and 10% the total powder material weight) were determined using an isothermal calorimeter device**.** The hydration rate and cumulative heat of hydration of cementitious pastes are presented in Figure 4.22 (nano-sized anatase-phase TiO_2-substituted cementitious systems), Figure 4.23 (submicron-sized anatase-phase TiO_2-substituted cementitious systems) and Figure 4.24 (micron-sized anatase-phase TiO_2-substituted cementitious systems).

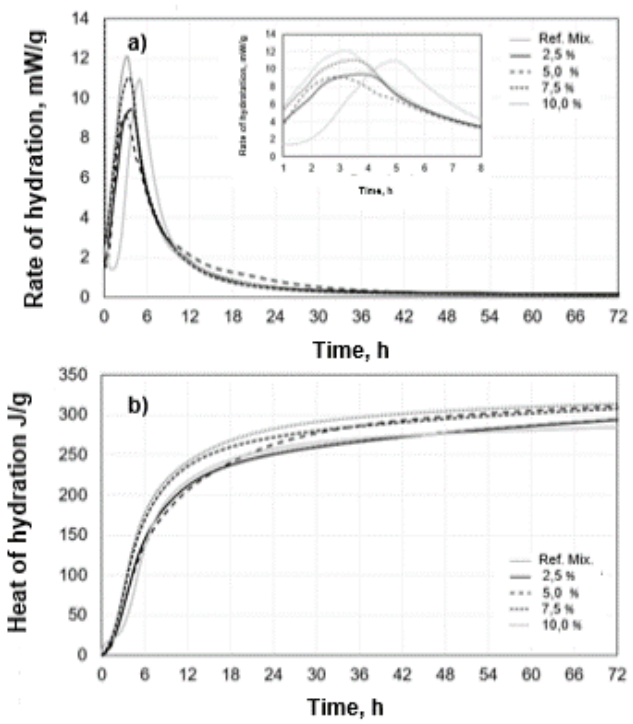

Figure 4.22. a) Rate of hydration and b) heat of hydration of nano-sized anatase-phase TiO_2-substituted (2.5%, 5%, 7.5%, and 10% by weight of the binder) cementitious systems.

When isothermal calorimetry results of the nano-sized anatase-phase TiO_2-substituted (2.5%, 5%, 7.5%, and 10% by weight of the binder) cement-based materials are evaluated from Figure 4.22, it can be noticed that the addition of nano-sized anatase-phase TiO_2 resulted in a faster rate of hydration peak. As is generally known, the use of nanoparticles in cementitious systems accelerates hydration (Mohseni et al., 2015). After a certain level of TiO_2 utilization rate, the utilization of nano-sized anatase-phase TiO_2 began to have a more noticeable influence on the hydration kinetics, and it was particularly effective on the rate of hydration, and the total heat of hydration in the early period of the reactions. As can be clearly seen from Figure 4.22, nano-sized anatase-phase TiO_2-substituted mixtures had a higher rate of hydration and reached rate of hydration peak earlier compared to the reference mixture (without TiO_2), when the utilization rate of TiO_2 exceeded the rate of 7.5%. As a striking point, although the highest rate of hydration was obtained from the mixture prepared by using 10% nano-sized anatase-phase TiO_2, the mixture prepared by substituting 2.5% nano-sized anatase-phase TiO_2 reached hydration peak earliest. Although mixtures with higher rate of hydration were obtained when the utilization rate of nano-sized anatase-phase TiO_2 exceeded 7.5%, higher compressive strength results were obtained from the reference mixture and the mixture prepared by using 2.5% nano-sized anatase-phase TiO_2 (Section 4.2.3.2). When the utilization rate of TiO_2 exceeded a certain level (especially 7.5% and 10% for this study), the amount of hydration products decreased, and lower compressive strength was obtained. This can be atrributed to the fact that there is less reactive cement (in percentage) because of substitituon (Jayapalan et al., 2013; Xu et al., 2019; Erdem et al., 2020) and the presence of nano-sized of TiO_2 particles can limit the formation of dicalcium silicate (C_2S) (Behfarnia et al., 2013).

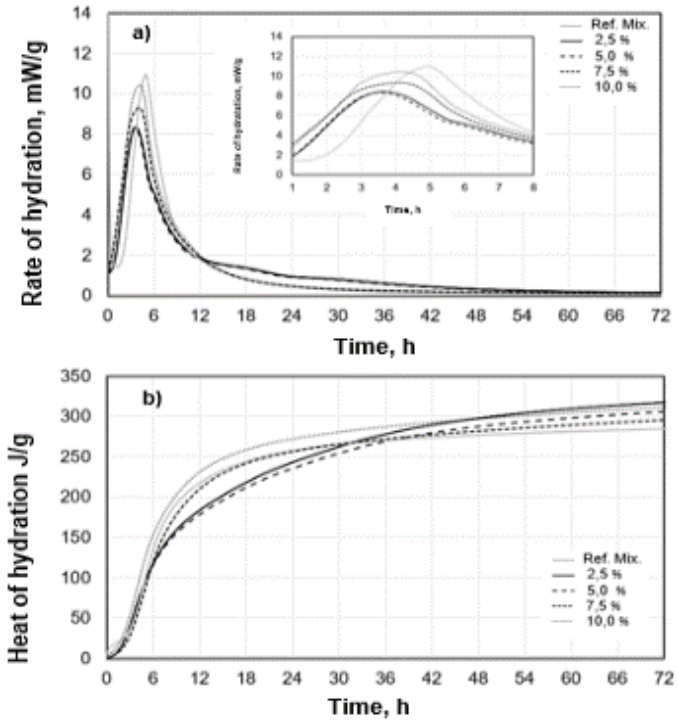

Figure 4.23. a) Rate of hydration and b) heat of hydration of submicron-sized anatase-phase TiO_2-substituted (2.5%, 5%, 7.5%, and 10% by weight of the binder) cementitious systems.

When isothermal calorimetry results of the submicron-sized anatase-phase TiO_2-substituted (2.5%, 5%, 7.5%, and 10% by weight of the binder) cement-based materials are evaluated from Figure 4.23, as in the nano-sized anatase-phase TiO_2-substituted cement-based materials, it can be seen that the addition of submicron-sized anatase-phase TiO_2 resulted in a faster rate of hydration peak. Similar to nano-sized anatase-phase TiO_2-substituted cement-based materials, when the TiO_2 usage rate rose, so did the rate of hydration peak values. As a remarkable point, the composites prepared by using submicron-sized anatase-phase TiO_2 powder exhibited lower hydration peak magnitudes compared to those prepared by using nano-sized one. This clearly shows the effects of particle size of TiO_2 incorporated on hydration. In the study of Chen et al. (2012), it was determined that nano-sized TiO_2 substitution resulted in reaching heat of hydration peak value earlier, and it was stated that the peak magnitude increased when the substitution rate increased from 5% to 10%. Although incorporation of anatase-phase TiO_2 resulted in reaching rate of hydration peak earlier and increase in the TiO_2 utilization rate resulted in increases in the rate of hydration peak values, very small differences were observed between the total heat of hydration of different mixtures in the late periods.

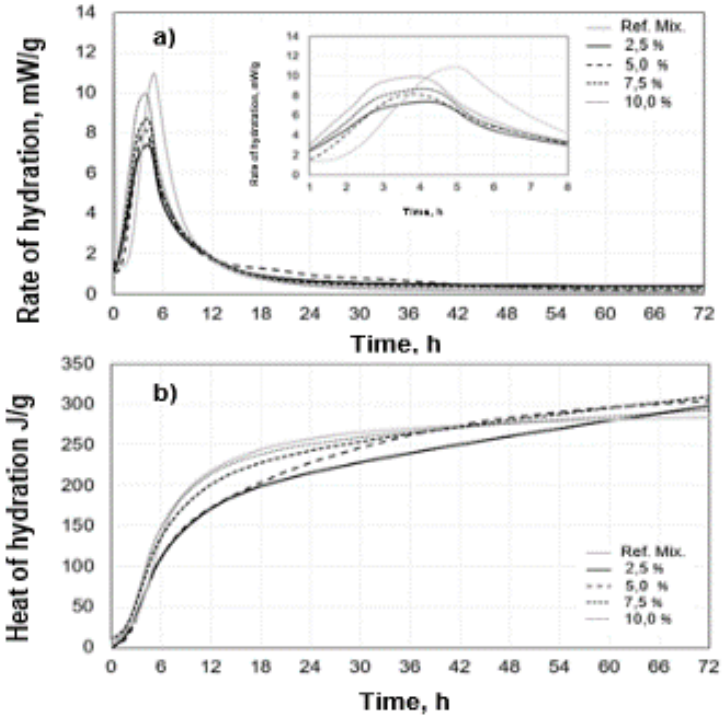

Figure 4.24 a) Rate of hydration and b) heat of hydration of micron-sized anatase-phase TiO_2-substituted (2.5%, 5%, 7.5%, and 10% by weight of the binder) cementitious systems.

When isothermal calorimetry results of the micron-sized anatase-phase TiO_2-substituted (2.5%, 5%, 7.5%, and 10% by weight of the binder) cement-based materials are evaluated from Figure 4.24, as in the nano- and submicron-sized anatase-phase TiO_2-substituted cement-based materials, it can be observed that the addition of micron-sized anatase-phase TiO_2 accelerated the rate of hydration. Similar to nano- and submicron-sized anatase-phase TiO_2-substituted cement-based materials, with the increment in the TiO_2 usage rate, rate of hydration peak values increased. However, it was determined that even at the micron-sized anatase-phase TiO_2 utilization rate of 10%, the hydration peak level obtained from the reference mixture (without TiO_2) could not be reached.

In various studies, it has been stated that when nanomaterials with finer grain size compared to cement are added to the mixture, particles act as filler and accelerate the hydration of the mixture by creating nucleation effects (Yeşilmen et al., 2015). Many fine-grained materials in question are chemically active, thus contributing to and assisting the hydration process to some extent. However, the chemically inert TiO_2 particles poses various question marks in terms of hydration development. Due to the fact that TiO_2

particles used in different sizes are both chemically inert materials and have much smaller particle size than the cement, it is very important to fully reveal their effects on hydration development. As a consequence, it was seen that TiO_2 particles with various particle size ranges added to the mixture have a significant influence on the pace of hydration and the total heat of hydration. In general, it was determined that utilization of anatase-phase TiO_2 resulted in reaching rate of hydration peak earlier compared to the reference mixture (without TiO_2). This indicates that TiO_2 substitution accelerates early age hydration. In addition, the increase in the particle size of TiO_2 particles resulted in reaching rate of hydration peak later and a lower rate of hydration.

4.2.3.2. Compressive Strength

To determine the optimum utilization rate of TiO_2 materials in the cement-based systems and the effect of the particle size/type of TiO_2 substituted on the mechanical properties of the cement-based systems, the compressive strength of anatase-phase (nano-, submicron- and micron-sized), rutil-phase (nano-, submicron- and micron-sized) and Degussa P25 TiO_2-substituted (at four different utilization rates: 2.5%, 5%, 7.5% and %10 by weight of the powder materials) cementitious systems for different curing ages was determined. From Figure 4.25 through Figure 4.31, the compressive strength results are shown. Considering the differences in compressive strength depending on utilization rate or type of TiO_2 used, the mechanical performances of the TiO_2-substituted cement-based systems were evaluated.

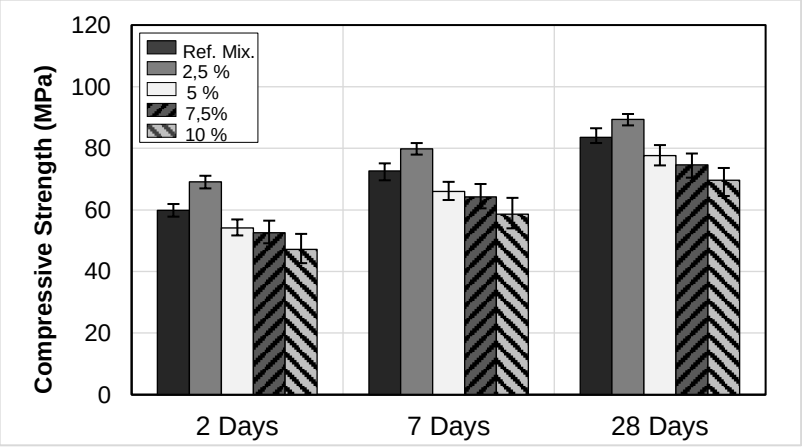

Figure 4.25. Compressive strength results of nano-anatase TiO_2-substituted composites prepared with different substitution rates.

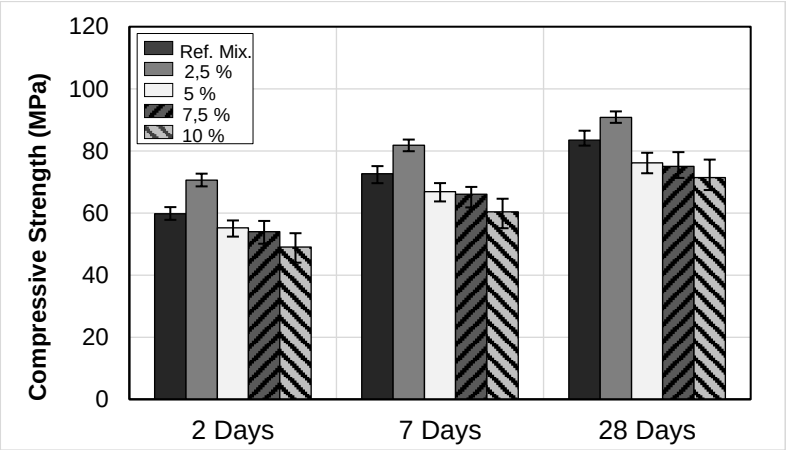

Figure 4.26. Compressive strength results of nano-rutile TiO_2-substituted composites prepared with different substitution rates.

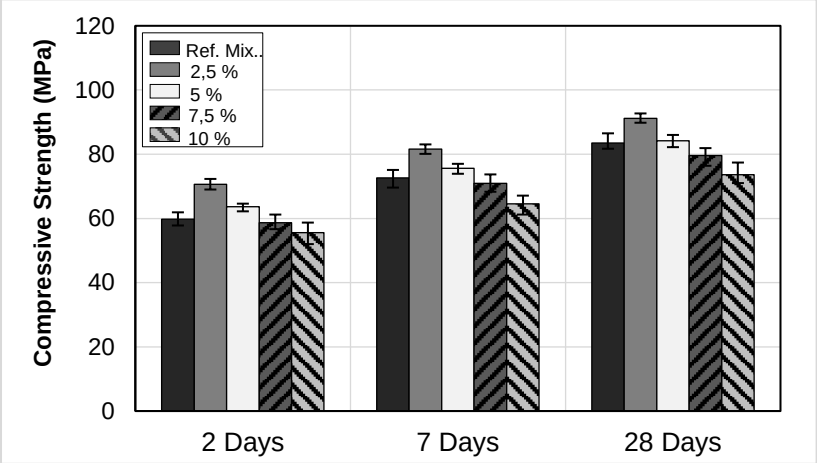

Figure 4.27. Compressive strength results of Degussa P25 TiO_2-substituted composites prepared with different substitution rates.

When the compressive strength results of the nano-sized anatase, rutile and Degussa P25 TiO_2-substituted composites are evaluated from Figure 4.25, 4.26, and 4.27, respectively, it can be seen that, owing to continued hydration processes, the protracted aging/curing resulted in constant increments in compressive strength findings, regardless of mixture parameters. The compressive strength of the nano-sized TiO_2-substituted cement-based systems, which was in an upward trend, displayed opposite trend after a certain point of diffraction, where the utilization rate was 2.5%. This means that the maximum compressive strength values were obtained from 2.5% nano-sized TiO_2-substituted cement-based systems. Besides, the incorporation of nano-sized TiO_2 up to a certain point of utilization rate resulted in higher compressive strength values compared to reference

mixture (without TiO_2). This certain point of utilization rate was 2.5% for nano-sized anatase and rutile TiO_2-substituted cement-based systems and 5% for Degussa P25 TiO_2-substituted cement-based systems. Numerous studies have reported that substituting nano-sized TiO_2 materials increases the compressive strength of cement-based composites and decreases their porosity, most probably due to the filler effect of TiO_2 particles (Feng et al., 2013; Noorvand et al., 2013; Ma et al., 2015; Yang et al., 2015; Rahim and Nair, 2016; Li et al, 2017). However, it has been reported in the current literature that the mechanical performance of cement-based systems can be improved by incorporating different nanomaterials up to a certain utilization rate, and beyond this utilization rate, decreases or negligible increases can be recorded (Xu et al., 2019; Erdem et al., 2020). According to Jimenez-Relinque et al. (2015), replacement of 2% (by weight of cement) TiO_2 decreases the compressive strength of cementitious systems. Salemi et al. (2014), moreover observed that by adding 2% (by weight of of cement) nano-sized TiO_2, compressive strength of cementitious composites was higher at 27% compared to the control mixture (without TiO_2). Additionally, it was observed that the TiO_2-added cement-based composite had a greater rate of hydration and a lower porosity (at nanoscale) than the control mixture. Similarly, Li et al. (2017) demonstrated that by adding nano-sized TiO_2, it is possible to minimize the porosity of cement-based composites, hence increasing the composite's compressive strength. Various parameters, including the TiO_2 dosage used (Turcyc and Loukili, 2003; Nazari and Riahi, 2011; Aslani, 2015; Salman et al., 2016), particle size of TiO_2 (Chen et al., 2012; Folli et al., 2012; Li et al., 2018), and the water/cement ratio (Lee et al., 2013) may influence the compressive strength of cementitious composites incorporating nano-sized TiO_2. Besides, it has been stated in the studies carried out that the optimum dosage of nano-sized TiO_2 particles is directly dependent on the degree of agglomeration of the particles (Behfarnia et al., 2013; Salemi et al., 2014). Li et al. (2018) studied the influence of 10 and 15 nm TiO_2 size on the mechanical characteristics of cement. It was observed that both sizes of TiO_2 particles increased the cement-based composite's 28-day compressive strength. However, when TiO_2 with a particle size of 10 nm was used, the number of nucleation sites was increased while the energy needed to generate each nucleation zone was decreased. Consequently, the compressive strength of the cement-based composite containing 10 nm TiO_2 enhanced higher compared to those containing 15 nm TiO_2. In addition, self-agglomeration of nano-sized TiO_2 particles can occur more when finer-sized TiO_2 particles are added, and this can affect the mechanical characteristics of

cement-based composites adversely (Sanchez et al., 2010). According to other research, nano-sized TiO_2 particles did not enhance the mechanical characteristics of cement-based composites (Noorvand et al., 2013), but rather damaged them after 28 days due to the limitation of dicalcium silicate (C_2S) hydration (Meng et al., 2012; Behfarnia et al..2013). According to Li (2019), adding 10% TiO_2 (by weight of cement) to the engineered cementitious composites (ECC) decreased the 28-day compressive strength by 12%, due to agglomeration of nano-sized TiO_2 particles resulting flaws in the cement paste. Considering all these studies detailed above, there are several parameters influential on the properties of nano-sized TiO_2-substituted cement-based systems.

As a result of the detailed studies carried out within the scope of the thesis, in general, it was seen that the compressive strength of nano-sized anatase, rutile, and Degussa P25 TiO_2-substituted composites are quite similar, apart from minor differences. However, it should be noted that the highest strength results were obtained from Degussa P25 TiO_2-substituted composites. As a result, in this study, it was revealed that the nano-sized TiO_2 substitution improves the compressive strength up to a certain substitution rate beyond which decreases was noted. The probable reason for the improvement in compressive strength, primarily at the relatively low nano TiO_2 substitution rate (2.5%) is that nano-sized powders create higher density due to the filler effect arising from comparatively smaller particle size (Al-Dahawi et al., 2016). This behavior can also be attributed to the seeding effect, which is the formation of additional area (nucleation sites) due to the extremely fine particle size of nano materials (and thereby their high surface area) that can pull unhydrated cement particles towards themselves, resulting in more suitable places for the precipitation of hydration product (Yeşilmen et al., 2015; Al Najjar et al., 2016). However, the decrease in compressive strength after a certain substitution rate can be related to the fact that the addition of inert TiO_2 powders resulted a less amount of presence of reactive cement (in percentage) in the mixtures decreasing the rate/amount of hydration products manufactured and causing lower compressive strength (Jayapalan et al., 2013; Xu et al., 2019; Erdem et al., 2020) and nano-sized TiO_2 particles can limit the formation of dicalcium silicate (C_2S) (Behfarnia et al., 2013).

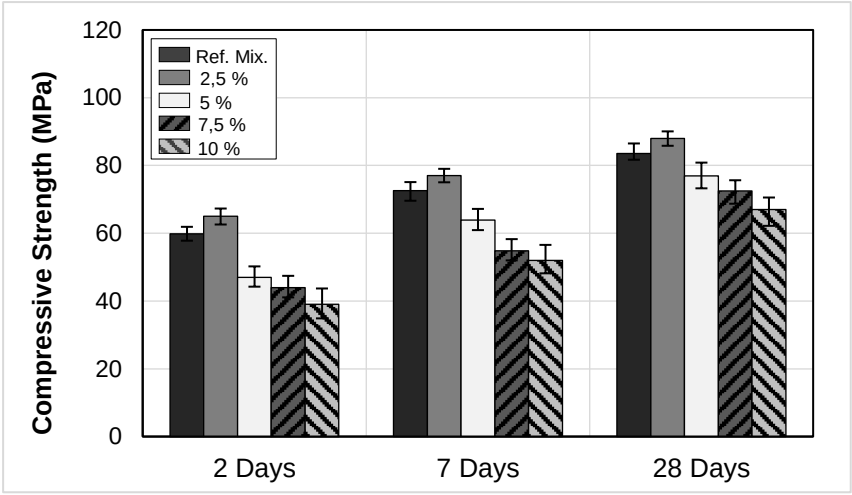

Figure 4.28. Compressive strength results of sub-micron anatase TiO_2-substituted composites prepared with different substitution rates.

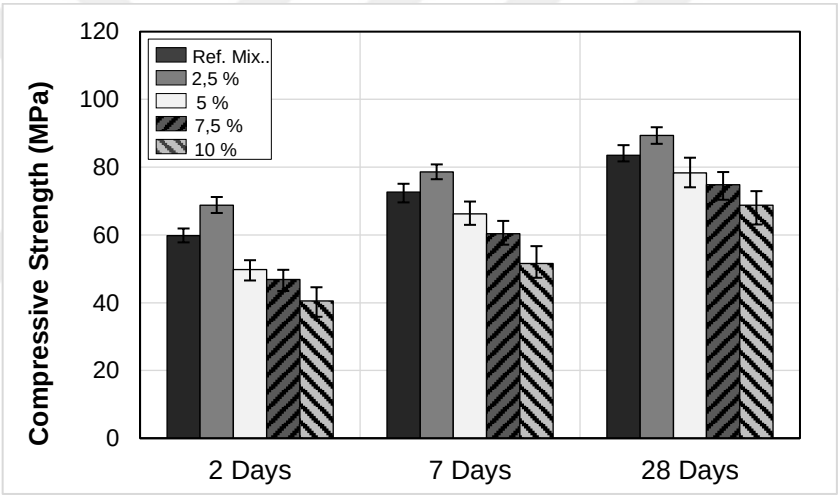

Figure 4.29. Compressive strength results of sub-micron rutile TiO_2-substituted composites prepared with different substitution rates.

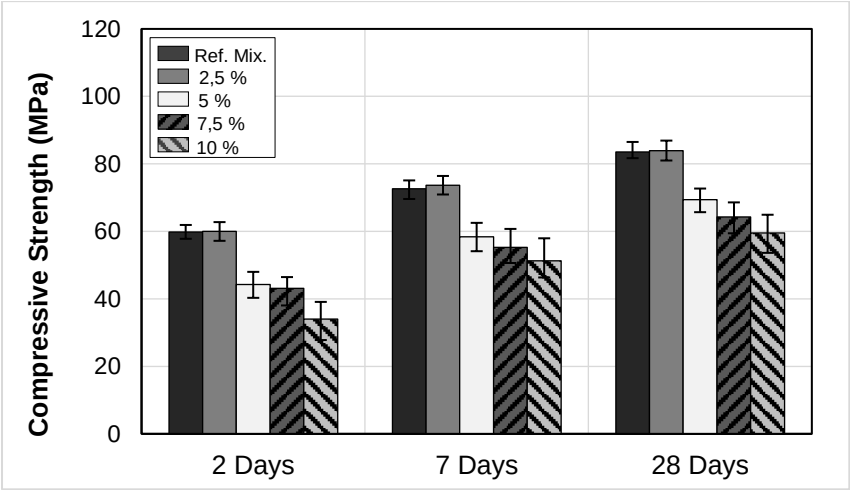

Figure 4.30. Compressive strength results of micron-anatase TiO_2-substituted composites prepared with different substitution rates.

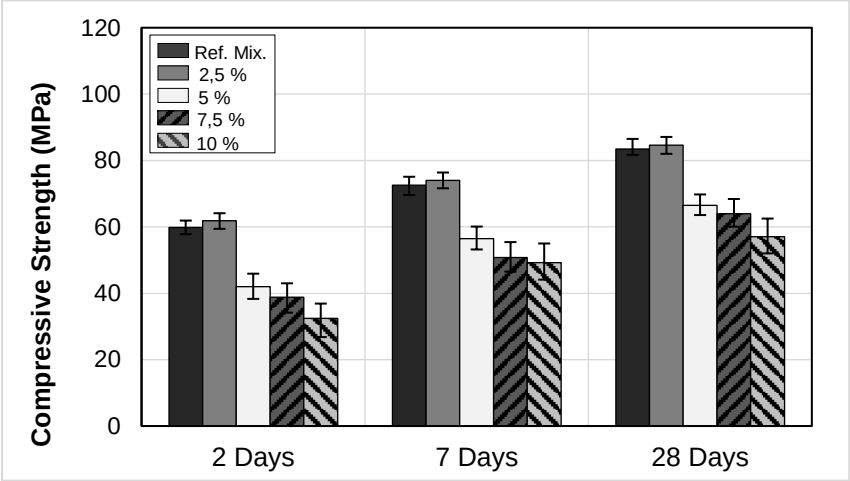

Figure 4.31. Compressive strength results of micron-rutile TiO_2-substituted composites prepared with different substitution rates.

When the compressive strength results of the submicron- and micron-sized anatase- and rutile-phase TiO_2-substituted composites are evaluated from Figure 4.28-Figure 4.31, it can be seen clearly that the lengthy aging/curing resulted in continuing increases in compressive strength findings, regardless of mixture parameters, owing to ongoing hydration processes. Like the nano-sized anatase and rutile TiO_2-substituted cement-based systems, the incorporation of submicron- and micron-sized TiO_2 up to a certain point of utilization rate resulted in higher compressive strength values compared to reference reference mixture (without TiO_2). This certain point of utilization rate where

the maximum compressive strength values were obtained from was 2.5%. As shown by the compressive strength data, the highest strength was obtained in composites using nano-sized TiO_2. Relatively less strength was obtained in the sub-micron size, and the least strength was obtained in the micron size substitution. It is expected that the beneficial effect of TiO_2 incorporation on compressive strength of cement-based systems can diminish as the TiO_2 particle size range increases, most probably because of the lower capability of the TiO_2 particles with higher particle size in terms of refinement of pore size structure in the paste due to their coarser structure and thereby lower surface areas (Chen et al., 2012).

As a result of the detailed studies carried out within the scope of the thesis, effects of different usage rates (2.5%, 5%, 7.5%, and 10% by weight of the cement) in the mixtures prepared by using TiO_2 particles in different phases with different particle size ranges (nano, sub-micron, and micron) on the compressive strength were similar, but the effect of TiO_2 particle size affected the compressive strength results in different ways.

4.2.3.3. Electrical Impedance

The electrical impedance values of anatase-phase (nano-, submicron- and micron-sized) and rutile-phase (nano-, submicron- and micron-sized) TiO_2-substituted (at four different utilization rates: 2.5%, 5%, 7.5% and %10 by weight of the powder materials) cementitious systems for different curing ages were determined. The electrical impedance results are presented in Figure 4.32 (anatase-phase TiO_2-substituted cementitious systems) and Figure 4.33 (rutile-phase TiO_2-substituted cementitious systems). Considering the differences in electrical impedance values depending on utilization rate or type of TiO_2 used, the performances of the TiO_2-substituted cement-based systems were evaluated.

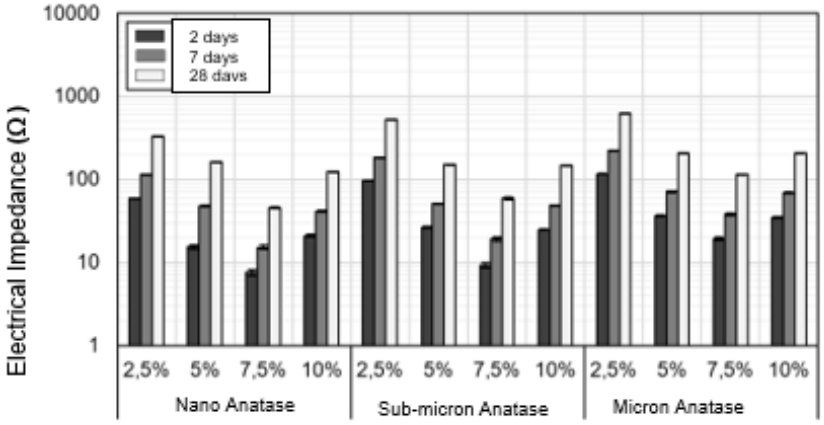

Figure 4.32. Electrical impedance results of anatase TiO_2-substituted composites prepared with different substitution rates.

When the electrical impedance results of anatase TiO_2-substituted (at four different utilization rates: 2.5%, 5%, 7.5% and %10 by weight of the powder materials) cementitious composites were evaluated from Figure 4.32, it can be seen that, irrespective of the utilization rate of TiO_2, the electrical impedance values of all specimens increase with the prolonged curing age. However, the increase rate varied depending on the utilization rate of TiO_2. Highest 28-day-old electrical impedance results were obtained from the specimens prepared with the TiO_2 utilization rate of 2.5%, regardless of the particle size range of TiO_2 used. Figure 4.32 shows that when the substitution rate rose from 2.5% to 7.5%, the electrical impedance values fall. On the other hand, there was an important increment in electrical impedance values with the increase in the utilization rate from 7.5% to 10%. This can be related to the fact that, after exceeding a certain substitution rate of TiO_2, the mixture cannot be mixed homogeneously and therefore regional agglomerations occur. Besides, with the increment in the particle size of the anatase-phase TiO_2 substituted, the electrical impedance results also increased. According to the electrical impedance results of the 28-day-old specimens, the highest values were obtained from the micron-sized anatase TiO_2-substituted composites. It is thought that the differences between the electrical impedance results of the anatase TiO_2-substituted composites can be related to the microstructural differences considering that the electrical conductivity of cementitious composites is very reliant on the pore structure and the pore solution.

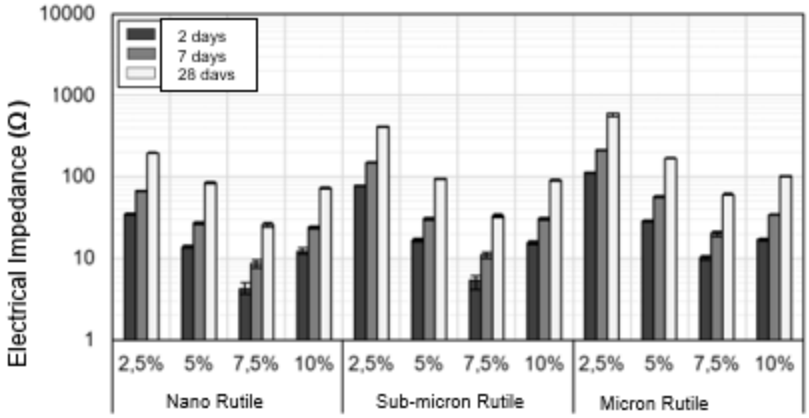

Figure 4.33. Electrical impedance results of rutile TiO_2-substituted composites prepared with different substitution rates.

When the electrical impedance results of rutile TiO_2-substituted (at four different utilization rates: 2.5%, 5%, 7.5% and %10 by weight of the powder materials) cementitious composites were examined from Figure 4.33, it can be seen that, irrespective of the utilization rate of TiO_2, the electrical impedance values of all specimens increase with the prolonged curing age. However, the increase rate varied depending on the utilization rate of TiO_2. Highest 28-day-old electrical impedance results were obtained from the specimens prepared with the TiO_2 utilization rate of 2.5%, regardless of the particle size range of TiO_2 used. The electrical impedance values decreased when the replacement rate increased from 2.5% to 7.5%, as shown in Figure 4.33. On the other hand, there was a significant increment in electrical impedance values with increase in the utilization rate from 7.5% to 10%. Besides, with the increase in the particle size of the rutile-phase TiO_2 substituted, the electrical impedance results also increased. According to the electrical impedance results of the 28-day-old specimens, the highest values were obtained from the micron-sized rutile TiO_2-substituted composites. It can be said that the electrical impedance results of anatase and rutile TiO_2-substituted cementitious composites showed a similar trend with each other based on the curing age, particle size, and substitution rate.

As defined before, the electrical impedance values of concrete are highly dependent on the microstructure-related parameter such as pore structure, connectivity of the pores, pore solution etc. (Spragg et al., 2013). For this reason, it can be stated that any factor affecting these parameters can also affect the electrical resistance of the concrete material.

It's one of the main reasons why the electrical resistance of the composite increases over time is because its microstructure changes over time. The electrical characteristics are affected by ongoing hydration processes, reductions in the volume, size, and connectivity of the pores, decreases in pore solutions efficient at transporting conductive ions, and increased matrix condensation with time. Additionally, as mentioned before, since TiO_2 is a semiconductor, it can affect the electrical properties of cement-based composites. Therefore, in addition to the effects of final hydration products such as CSH gels and CH on the porosity, particularly for specimens containing semiconductor TiO_2 materials, significant increases in electrical resistance over time can be related to limiting the interaction between conductive materials by surrounding them with hydration products (Liu et al., 2013). Homogeneously dispersed TiO_2 particles can improve electrical conductivity of the cementitious systems, since they can create much more surface area than agglomerated TiO_2 particles, and conductive paths throughout the matrix (Xiong et al., 2006; D'Alessandro et al., 2017; Li et al., 2017; Jiang et al., 2018; Kannan et al., 2018). Therefore, the decrease in electrical impedance values with the increase in the substitution rate from 2.5% to 7.5% can be attributed to the beneficial effect of the TiO_2 materials on the electrical conductivity of concrete. In contrast, as a counter-trend, a significant increase in electrical impedance values with increase in the utilization rate from 7.5% to 10% can be related to the lack of the formation of conductive paths due to agglomerations in the inhomogeneous mixture (because of higher utilization rate). In addition to that, increase in the electrical impedance results with the increment in the particle size of the TiO_2 substituted can be related to the occurrence of larger interparticle distances between larger-sized TiO_2 particles compared to smaller ones. When the results are evaluated comparatively, it can be observed that lower electrical impedance values (higher conductivity) were obtained from rutile TiO_2-substituted cementitious composites. Obtaining considerably lower electrical impedance values from the nano-rutile TiO_2-substituted cementitious composites was an expected result when considering the fact that the electrical properties of the materials are closely related to the electronic band structure and the rutile-phase TiO_2 shows better conductivity than the anatase-phase TiO_2 because of its lower band gap (Sayılkan, 2007). Since the reasons of this were discussed in detail previously, no further comments were made here.

4.2.3.4. Photocatalytic Performance

The photocatalytic performance of anatase-phase (nano-, submicron- and micron-sized), rutil-phase (nano-, submicron- and micron-sized) and Degussa P25 TiO_2-substituted (at four different utilization rates: 2.5%, 5%, 7.5% and %10 by weight of the powder materials) cementitious systems for different curing ages were determined. The NO_x, NO, and NO_2 concentration profiles obtained during the NO_x degradation tests under illumination are presented in Figure 4.34, Figure 4.36, Figure 4.38, Figure 4.40, Figure 4.42, Figure 4.44 and Figure 4.46. In addition, NO_x and NO degradation and NO_2 formation rates (in percentage) of the developed systems together with the system selectivity values are summarized in Figure 4.35, Figure 4.37, Figure 4.39, Figure 4.41, Figure 4.43, Figure 4.45 and Figure 4.47. Considering the differences in NO_x and NO degradation and NO_2 formation rates depending on utilization rate or type of TiO_2 used, the performances of the TiO_2-substituted cement-based systems were evaluated.

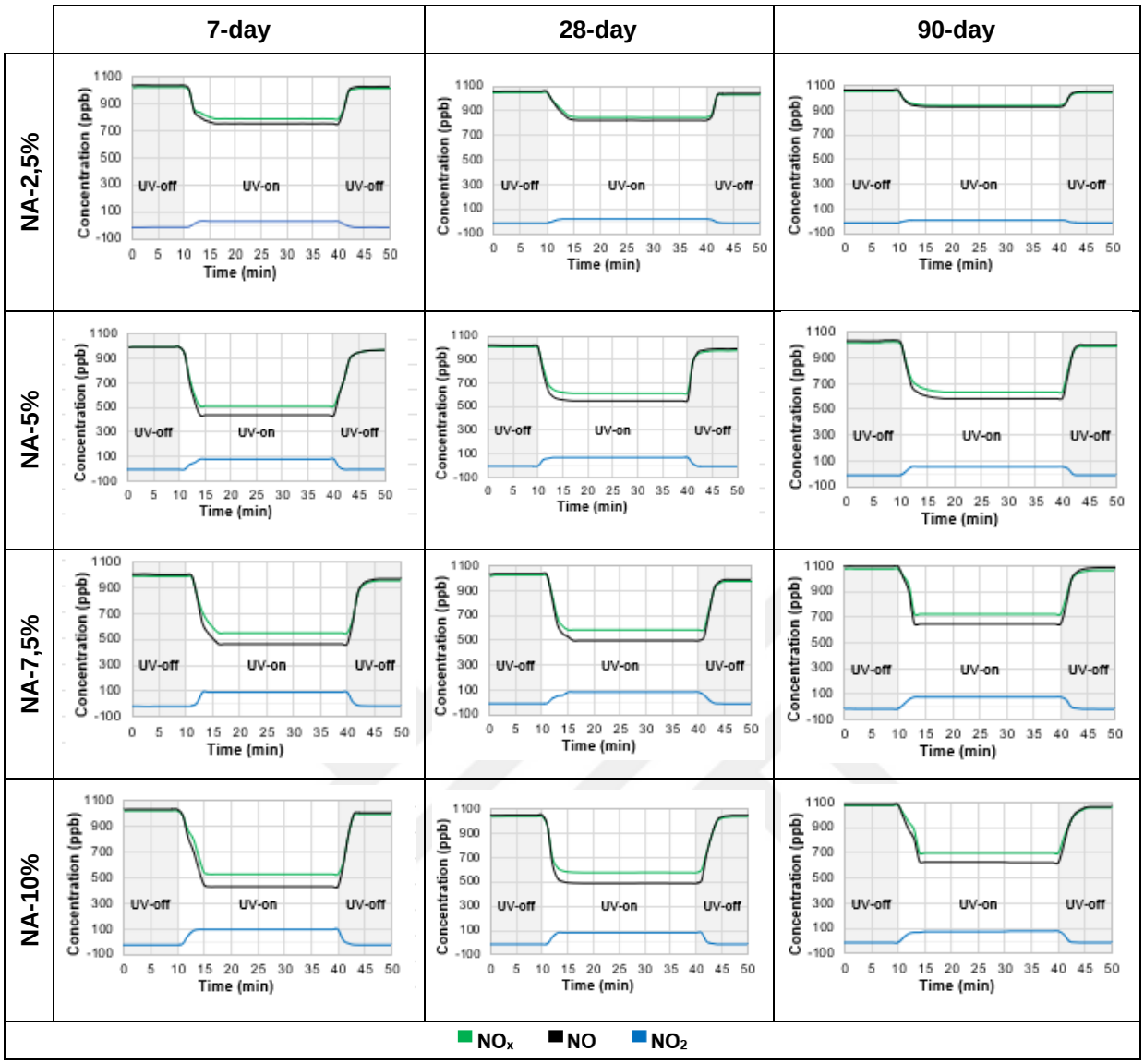

Figure 4.34. Variation of NO_x, NO, and NO_2 concentrations during each test for 7, 28, and 90-day samples of nano anatase TiO_2-substituted composites prepared with different substitution ratios.

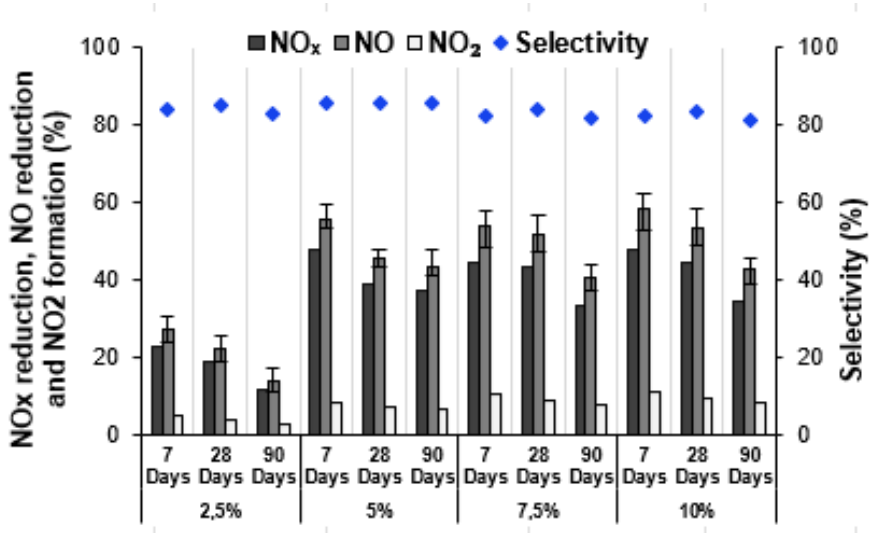

Figure 4.35. The rate of NO_x reduction, NO reduction, and NO_2 conversion and system selectivity (%) in each test for 7, 28, and 90-day samples of nano-anatase TiO_2-substituted composites prepared with different substitution ratios.

When the degradation rates of 7-day, 28-day and 90-day-old nano-anatase TiO_2-substituted specimens are evaluated from Figure 4.34 and Figure 4.35, regardless of the utilization rate of TiO_2, it can be seen that NO_x and NO reduction rates decreased with the prolonged curing ages. This time-dependent trend may have come from the ongoing hydration reaction, leading to the coating of TiO_2 particles with further hydration product and thereby reducing the presence of TiO_2 materials on specimen surfaces reached by UV irradiation. A more likely reason is that carbonation products, produced by binding carbon dioxide (CO_2) into solid carbonates on the specimen surface or another possible process, cause the specimen surface to be coated (Lackhoff et al., 2003; Poon and Cheung, 2007; Chen and Poon, 2009; Matějka et al., 2012). When the results are evaluated in terms of the effect of the TiO_2 utilization rate on the photocatalytic performances of nano-anatase TiO_2-substituted composites from Figure 4.35 and Figure 4.36, it can be seen that NO_x reduction rates (in percentage) of the nano-sized anatase TiO_2-substituted cement-based systems, which was in an upward trend, displayed opposite trend after a certain point of diffraction, where the utilization rate was 5% (irrespective of curing age). This means that there is an optimum amount of TiO_2 for the achievement of most effective photocatalytic activity. Inadequate interaction of TiO_2 particles with the irradiation and agglomeration in the case of overuse of TiO_2 can be shown as the reason for the reversal of the trend after a certain utilization rate of TiO_2 (Senff et al. 2013; Xu et al. 2020b). At the

conclusion of the 90-day curing period, the highest NO_x reduction rate (37.3%) and system selectivity value (85.6%) were obtained from 5% nano-sized TiO_2-substituted cement-based systems. This means that utilization rate of 5% for nano-sized TiO_2 provided a more effective photocatalytic degradation process.

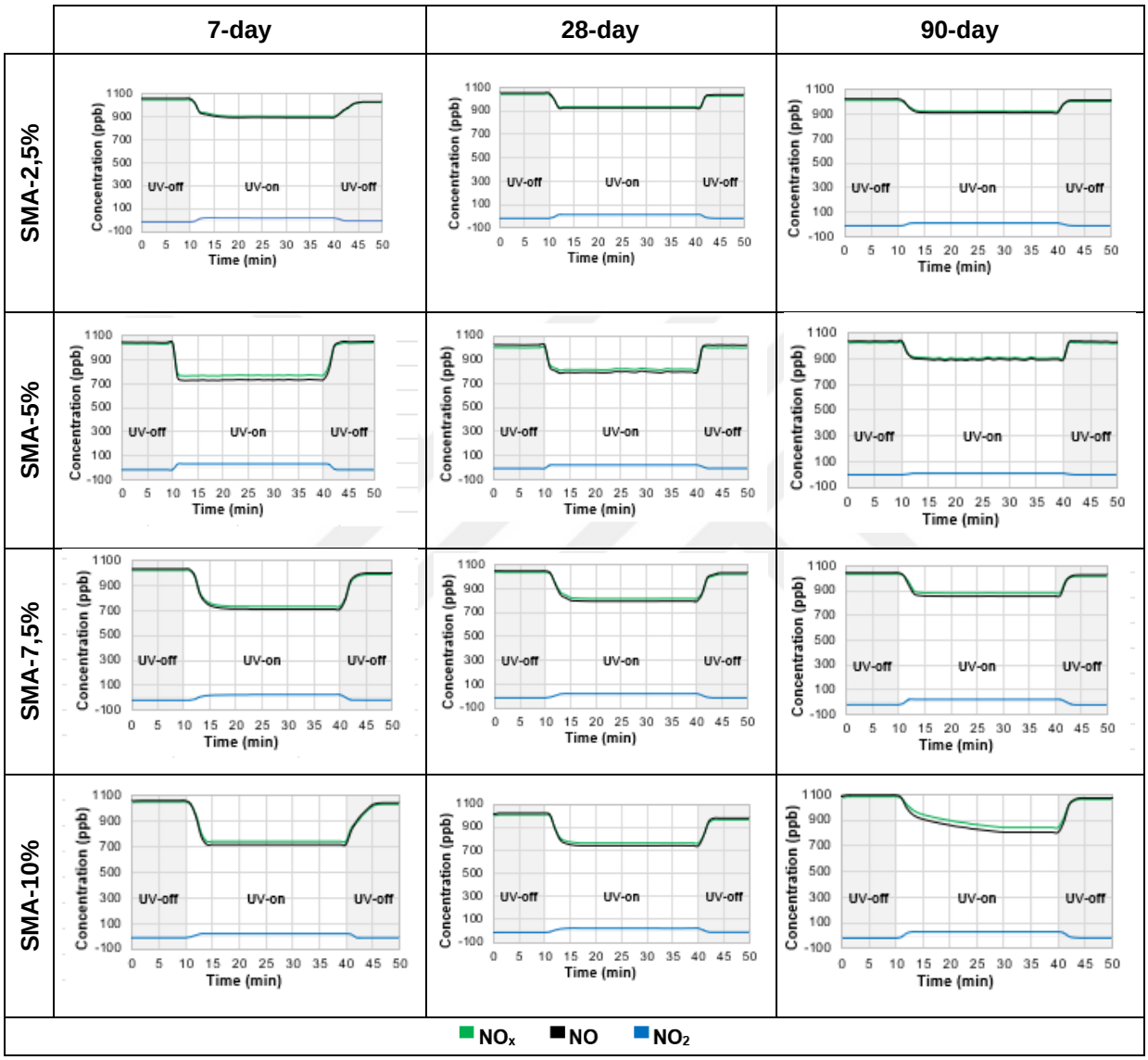

Figure 4.36. Variation of NO_x, NO, and NO_2 concentrations during each test for 7, 28, and 90-day samples of sub-micron anatase TiO_2-substituted composites prepared with different substitution ratios.

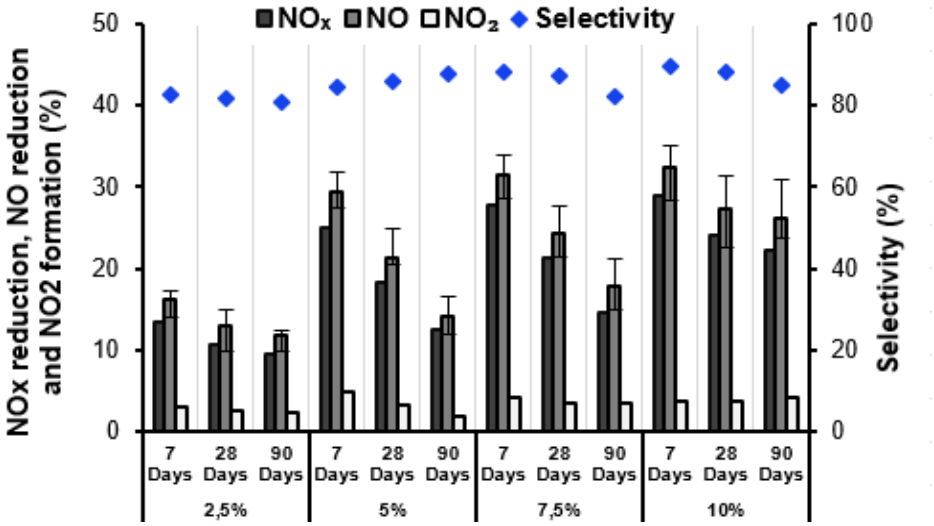

Figure 4.37. The rate of NO_x reduction, NO reduction, and NO_2 conversion and system selectivity (%) in each test for 7, 28, and 90-day samples of sub-micron anatase TiO_2-substituted composites prepared with different substitution ratios.

When the degradation rates of 7-day, 28-day and 90-day-old submicron-anatase TiO_2-substituted specimens are evaluated from Figure 4.36 and Figure 4.37, as in the the nano-anatase TiO_2-substituted specimens, regardless of the utilization rate of TiO_2, it can be seen that NO_x and NO reduction rates decreased with the prolonged curing age. In contrast to the presence of a diffraction point where the trend (increase in NO_x reduction rates with the increment in the TiO_2 usage) reversed after a certain point (at the utilization rate of 5% of the total binder weight) in nano-anatase-substituted mixtures, for the submicron-anatase TiO_2-substituted specimens, NO_x reduction rates increased continuously with the increment in the TiO_2 usage rate. At the end of 90 days, the highest NO_x reduction rate (22.3%) was obtained from 10% submicron-sized TiO_2-substituted cement-based system although the highest system selectivity value (87.8%) was obtained from the 5% TiO_2-substituted mixture. Considering the fact that the toxicity of NO_2 is significantly higher than the primary pollutant NO (Yang et al., 2018), it was critical/necessary to monitor the change of NO_2 levels throughout the photocatalytic reactions, and the system selectivity to assess the photocatalytic efficiency of the mixtures. In this regard, higher system selectivity can be an indicator to determine the mixtures as exhibiting more efficient photocatalytic degradation process. In addition, although an increase in the utilization rate from 5% to 10% resulted in an increase (relatively low) in the NO_x reduction rate of the

cement-based systems, negative effect of the increased TiO_2 content on the mechanical properties and cost-efficieny must also be considered. In the light of this information, although the highest NO_x reduction rate was obtained from 10% submicron-sized TiO_2-substituted cement-based system, considering its higher system selectivity, it can be said that 5% submicron-sized TiO_2-substituted cement-based system exhibited the optimum photocatalytic performance.

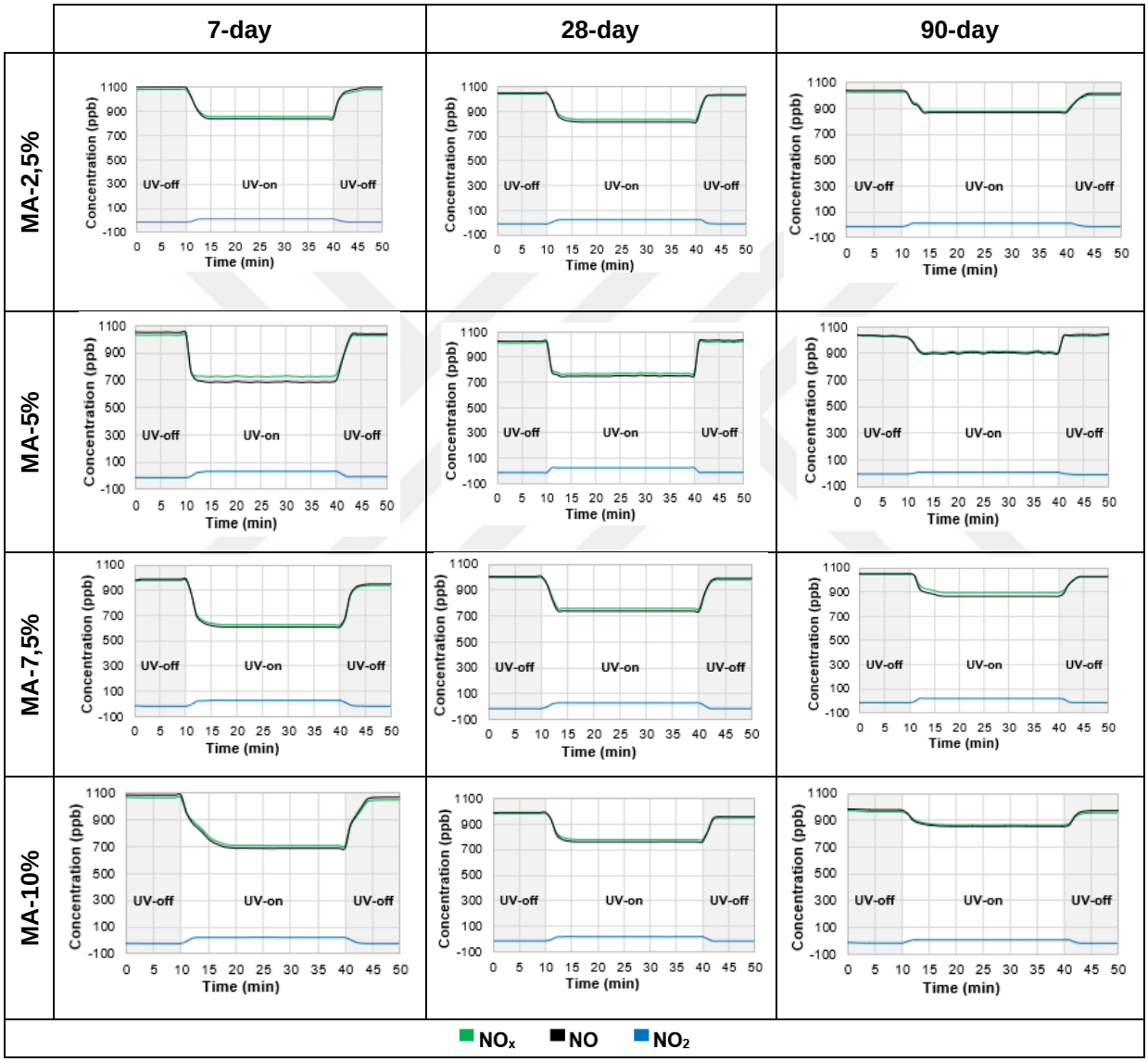

Figure 4.38. Variation of NO_x, NO, and NO_2 concentrations during each test for 7, 28, and 90-day samples of micron anatase TiO_2-substituted composites prepared with different substitution ratios.

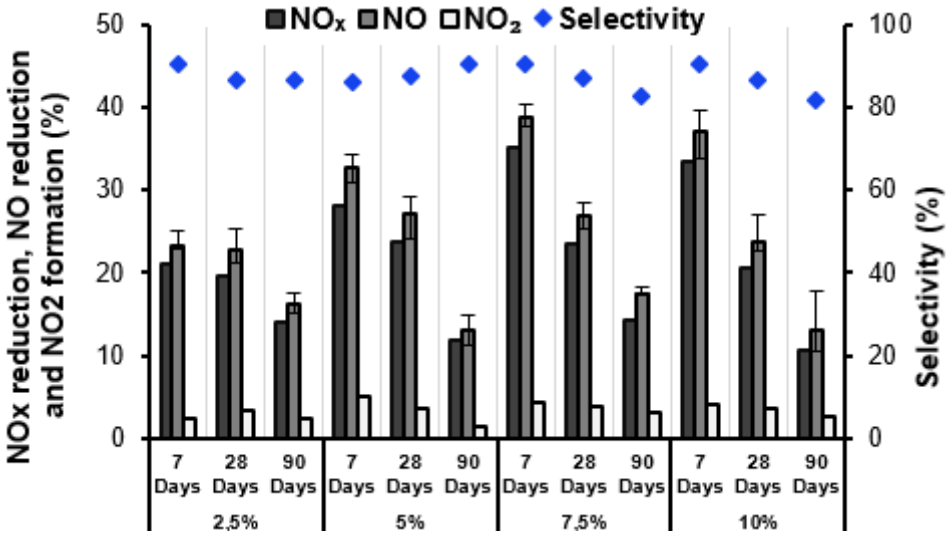

Figure 4.39. The rate of NO_x reduction, NO reduction, and NO_2 conversion and system selectivity (%) in each test for 7, 28, and 90-day samples of micron anatase TiO_2-substituted composites prepared with different substitution ratios.,

When the degradation rates of 7-day, 28-day and 90-day-old micron-anatase TiO_2-substituted specimens are evaluated from Figure 4.38 and Figure 4.39, as in the the other TiO_2-substituted specimens, regardless of the utilization rate of TiO_2, it can be seen that NO_x and NO reduction rates decreased with the prolonged curing age. In terms of the effect of the TiO_2 utilization rate on the photocatalytic performances of micron-anatase TiO_2-substituted composites that can be followed from Figure 4.38 and Figure 4.39, as in the nano-sized anatase TiO_2-substituted cement-based systems, it can be stated that there is a certain point of diffraction (at the utilization rate of 7.5% of the total binder weight) where the trend reversed. NO_x reduction rates (in percentage) of the micron-sized anatase TiO_2-substituted cement-based systems increased with the increment in TiO_2 usage rate up to 7.5% of total weight of binder and displayed opposite trend after this point. At the end of 90 days, the highest NO_x reduction rate (14.4%) was obtained from 7.5% micron-sized TiO_2-substituted cement-based system although the highest system selectivity value (90.2%) was obtained from the 5% TiO_2-substituted mixture. As a result, although the highest NO_x reduction rate was obtained from 7.5% micron-sized TiO_2-substituted cement-based system, considering its higher system selectivity, it can be said that 5% micron-sized TiO_2-substituted cement-based system exhibited the optimum photocatalytic performance.

In general, the optimum TiO_2 utilization rate in terms of NO_x reduction rates varied depending on the particle size of the anatase-phase TiO_2 substituted. This can be attributed to the easy current transfer capability of the smaller-sized TiO_2 from its surface resulting increase in reaction efficiency (namely the differences in their efficiency) (Zhao and Yang, 2003; Carp et al., 2004). This can also be related to the differences in the mixtures' workability because of the differences in the particle size of TiO_2 used. Besides, increasing the substitution rate of anatase-phase TiO_2 particles did not provide a linear increase in the NO_x reduction rates. The reason for this is that as the rate of TiO_2 substitution increases, it becomes more difficult to spread the TiO_2 particles through cement-based systems. This means that most of the TiO_2 particles can stay in the dark parts of the composites, where UV rays can not reach them. As a result, this inhibits photocatalytic reactions from occurring. When considering the results obtained from the anatase TiO_2-substituted specimens, it is thought that the TiO_2 substitution rate of 5% was ideal because of superior characteristics of 5% TiO_2-substituted mixtures in terms of cost effectivenes, mechanical properties and photocatalytic performance-related issues.

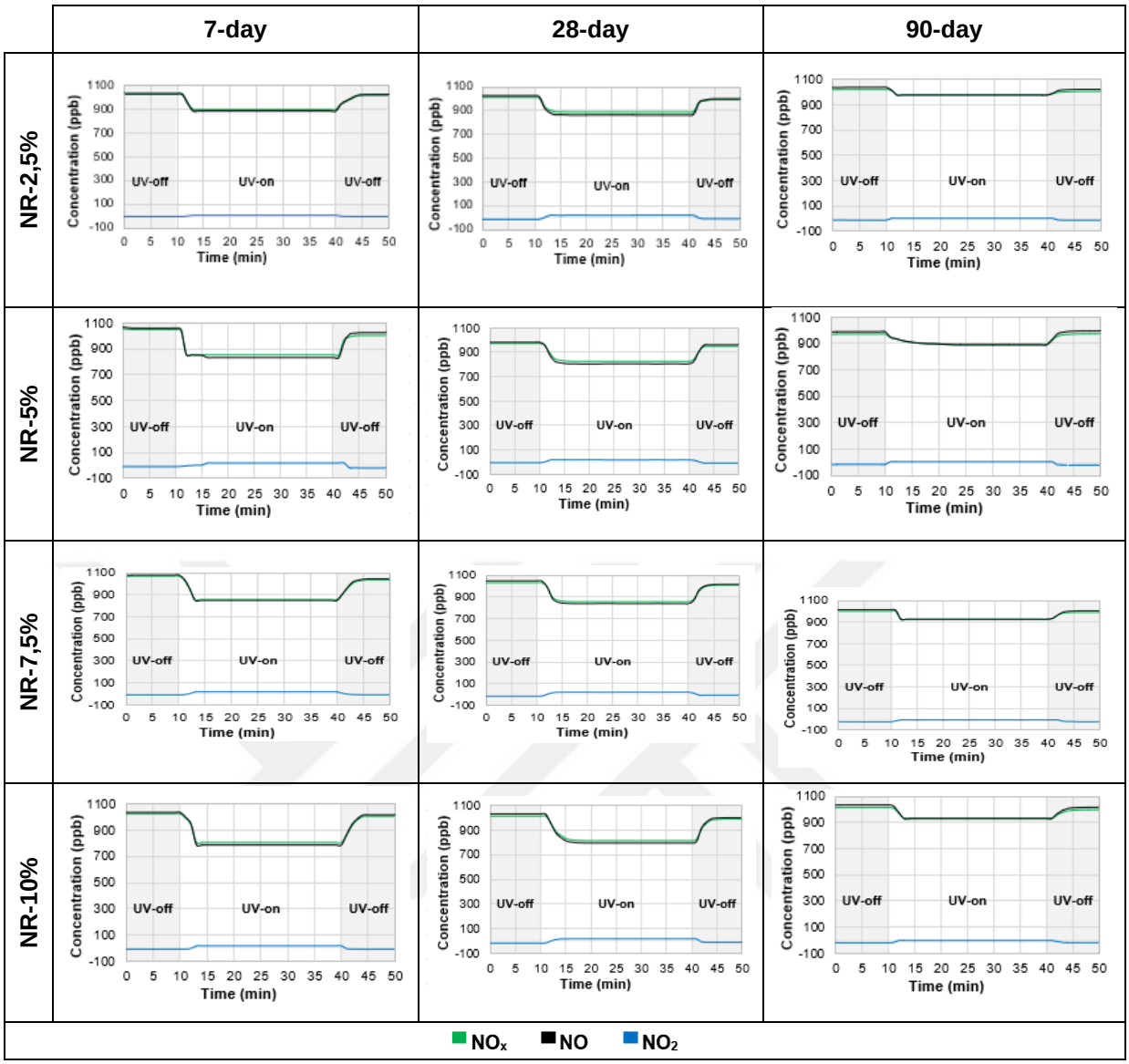

Figure 4.40. Variation of NO_x, NO, and NO_2 concentrations during each test for 7, 28, and 90-day samples of nano rutile TiO_2-substituted composites prepared with different substitution ratios.

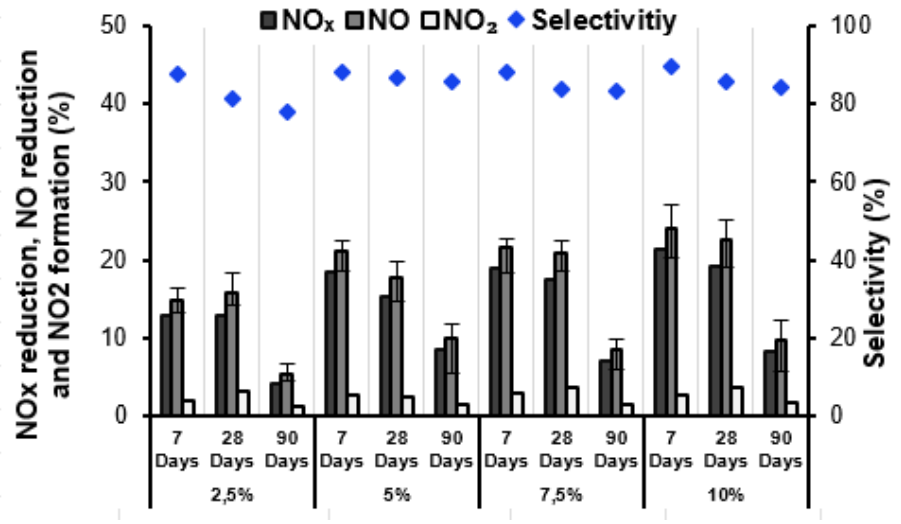

Figure 4.41. The rate of NO_x reduction, NO reduction, and NO_2 conversion and system selectivity (%) in each test for 7, 28, and 90-day samples of nano rutile TiO_2-substituted composites prepared with different substitution ratios.

When the degradation rates of 7-day, 28-day and 90-day-old nano-rutile TiO_2-substituted specimens are evaluated from Figure 4.40 and Figure 4.41, as in the anatase TiO_2-substituted specimens, regardless of the utilization rate of TiO_2, it can be seen that NO_x and NO reduction rates decreased with the prolonged curing age. This time-dependent trend can be related to the ongoing hydration reactions. In general, the photocatalytic activity of nano-rutile-containing mixtures lagged far behind nano-anatase TiO_2-containing mixtures. The differences between the photocatalytic activities of the anatase and rutile phases of TiO_2 particles are directly related to their crystal structures. Since the reasons of this were discussed in detail previously, no further comments were made here. As can be followed from from Figure 4.40 and Figure 4.41, the general trend was towards an increase in the NO_x reduction rate of nano-rutile TiO_2-substituted composites as the TiO_2 utilization rate increased in nano-rutile composites. However, when both the increase rate in the NO_x reduction rate with the increment in the usage rate of TiO_2 and its effect on system selectivity are evaluated, it can be said that increment in the TiO_2 usage rate beyond a certain point was not efficient for photocatalytic performance. The presence of large amounts of nanomaterials can increase the aggregation tendency, which can negatively affect photocatalytic efficiency and lead to a reduction in photocatalytic activity (Xu et al., 2020). At the conclusion of the 90-day curing period, the highest NO_x reduction rate (8.6%) and system selectivity value (85.6%) were obtained from 5% nano-

sized TiO_2-substituted cement-based systems. This means that the utilization rate of 5% for nano-sized TiO_2 provided a more effective photocatalytic degradation process.

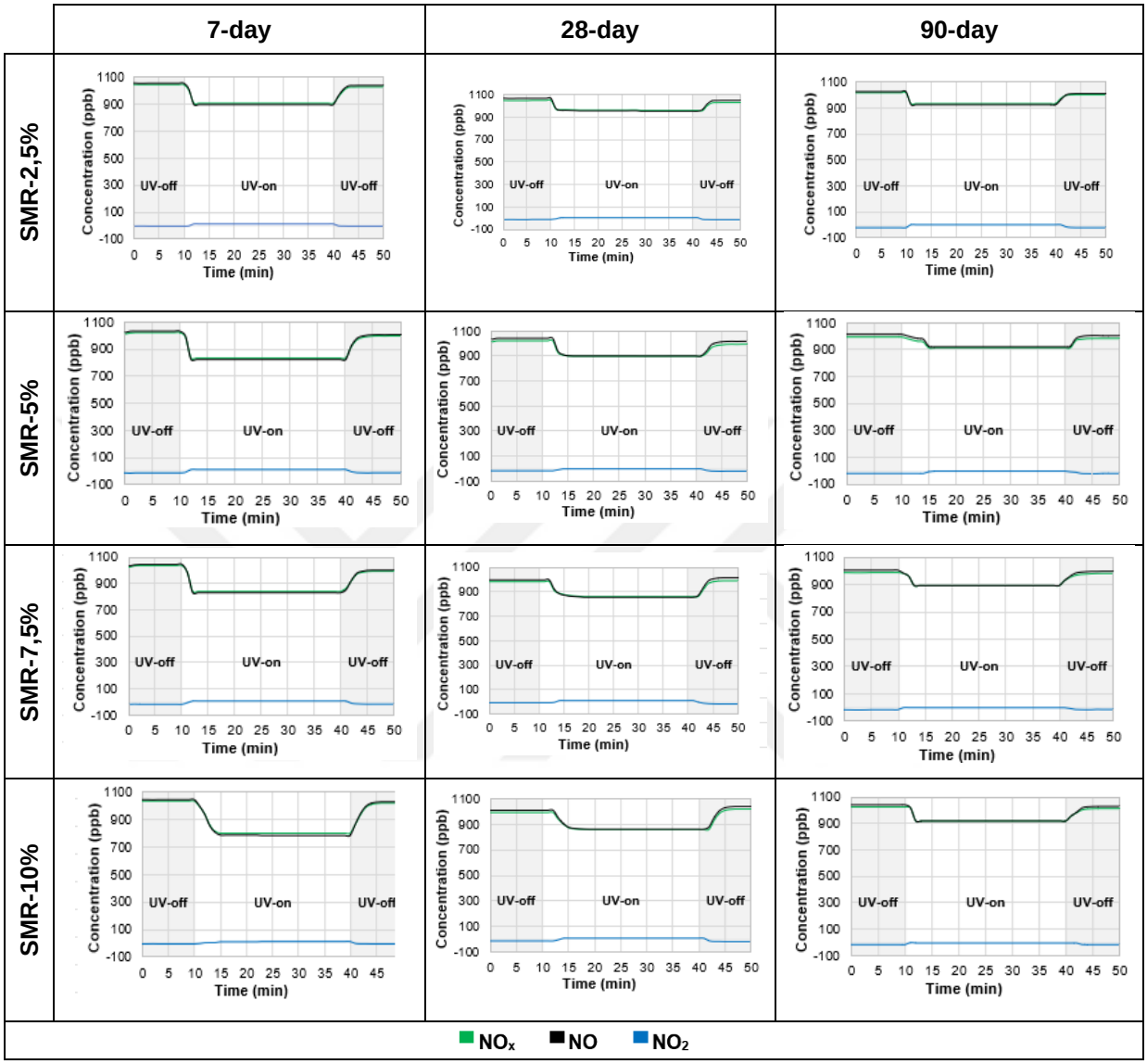

Figure 4.42. Variation of NO_x, NO, and NO_2 concentrations during each test for 7, 28, and 90-day samples of sub-micron rutile TiO_2-substituted composites prepared with different substitution ratios.

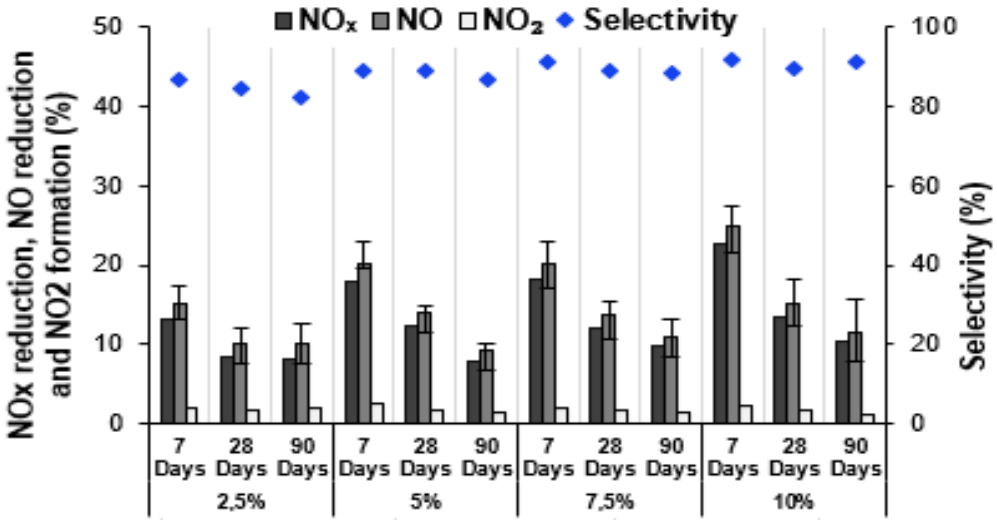

Figure 4.43. The rate of NO_x reduction, NO reduction, and NO_2 conversion and system selectivity (%) in each test for 7, 28, and 90-day samples of sub-micron rutile TiO_2-substituted composites prepared with different substitution ratios.

When the degradation rates of 7-day, 28-day and 90-day-old submicron-rutile TiO_2-substituted specimens are evaluated from Figure 4.42 and Figure 4.43, as in the other TiO_2-substituted specimens, regardless of the utilization rate of TiO_2, it can be seen that NO_x and NO reduction rates decreased with the prolonged curing age due to the ongoing hydration reactions. Similar to nano-anatase TiO_2-substituted composites, photocatalytic degradation capability of the rutile TiO_2-substituted composites decreased generally with the increment in the particle size of TiO_2 used. However, the highest photocatalytic activity results (NO_x reduction rates) obtained from the 10% TiO_2 substituted composite for each curing age. At the conclusion of the 90-day curing period, the highest NO_x reduction rate and system selectivity were recorded as 10.4% and 91.3%, respectively, which were obtained from 10% submicron-sized rutile TiO_2-substituted cement-based systems. A striking point was that the best photocatalytic performance obtained from the sub-micron rutile-substituted composites, which contain coarser particles compared to nano-rutile-substituted composites, was higher than the best photocatalytic performance obtained from the nano-rutile TiO_2-substituted composites.

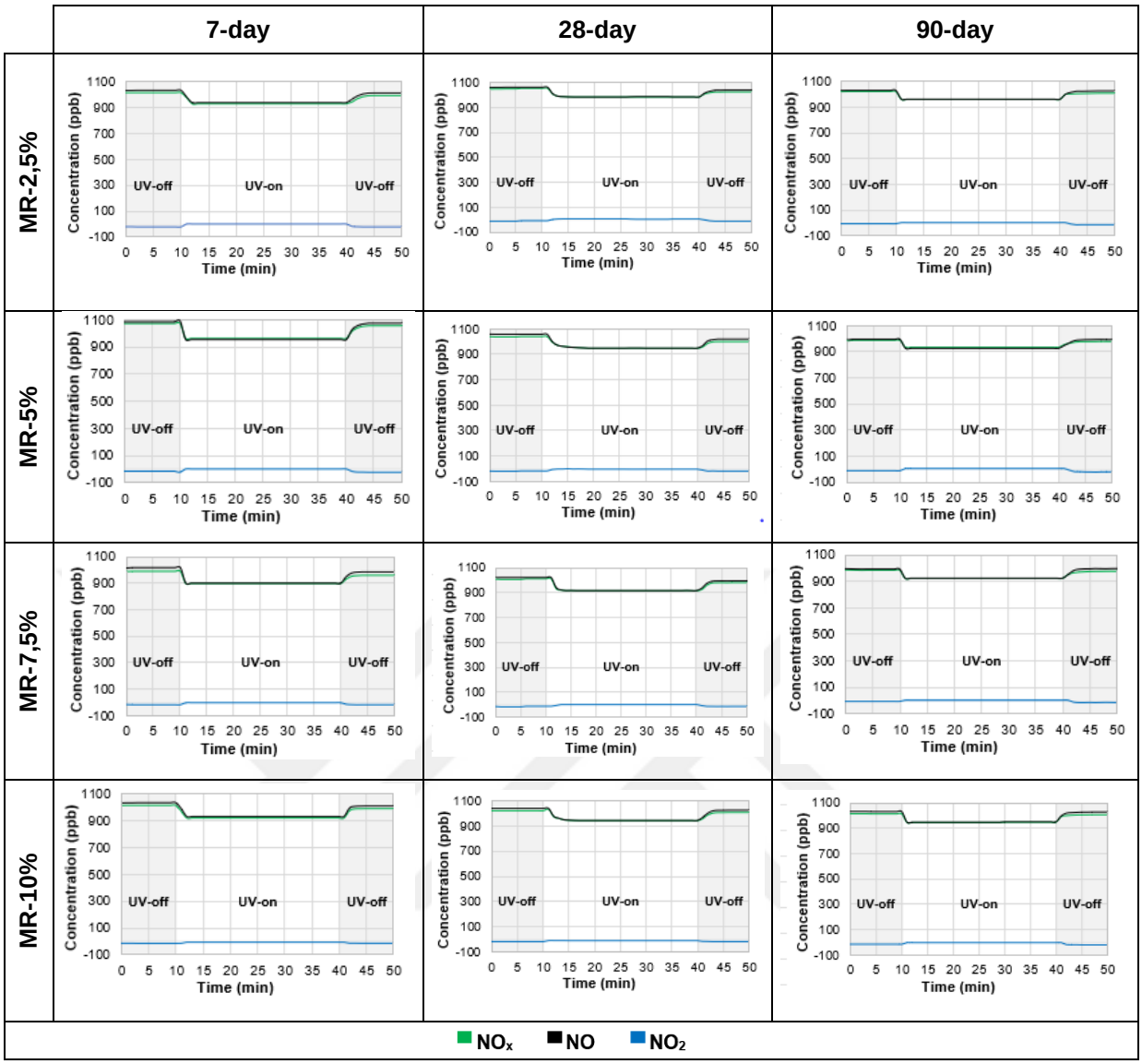

Figure 4.44. Variation of NO_x, NO, and NO_2 concentrations during each test for 7, 28, and 90-day samples of micron rutile TiO_2-substituted composites prepared with different substitution ratios.

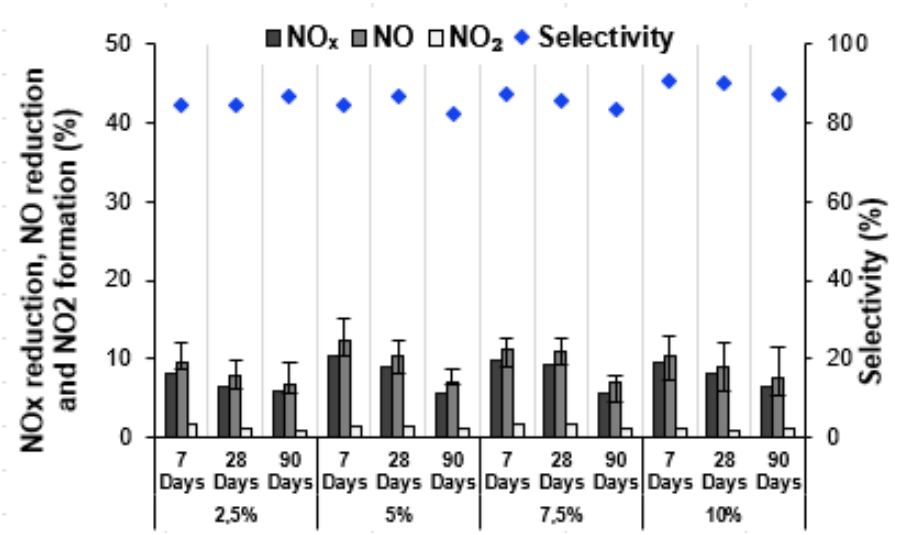

Figure 4.45. The rate of NO_x reduction, NO reduction, and NO_2 conversion and system selectivity (%) in each test for 7, 28, and 90-day samples of micron rutile TiO_2-substituted composites prepared with different substitution ratios.

When the degradation rates of 7-day, 28-day and 90-day-old micron-sized rutile TiO_2-substituted specimens are evaluated from Figure 4.44 and Figure 4.45 as in the other TiO_2-substituted specimens, regardless of the utilization rate of TiO_2, it can be seen that NO_x and NO reduction rates decreased with the prolonged curing age due to the ongoing hydration reactions. Among all rutile TiO_2-substituted cement-based composites, the lowest reduction rates were obtained from the micron-size rutile TiO_2-substituted ones. NO_x reduction rates of the micron-sized rutile TiO_2-substituted specimens generally increased with the increment in TiO_2 substitution rate up to 5% of the total binder weight. Beyond the 5% TiO_2 substitution rate, the NO_x reduction rates of the micron-sized rutile TiO_2-substituted specimens decreased. At the conclusion of the 90-day curing period, the highest NO_x reduction rate and system selectivity (recorded as 6.6% and 86.9%, respectively) were obtained from 10% micron-sized rutile TiO_2-substituted cement-based systems.

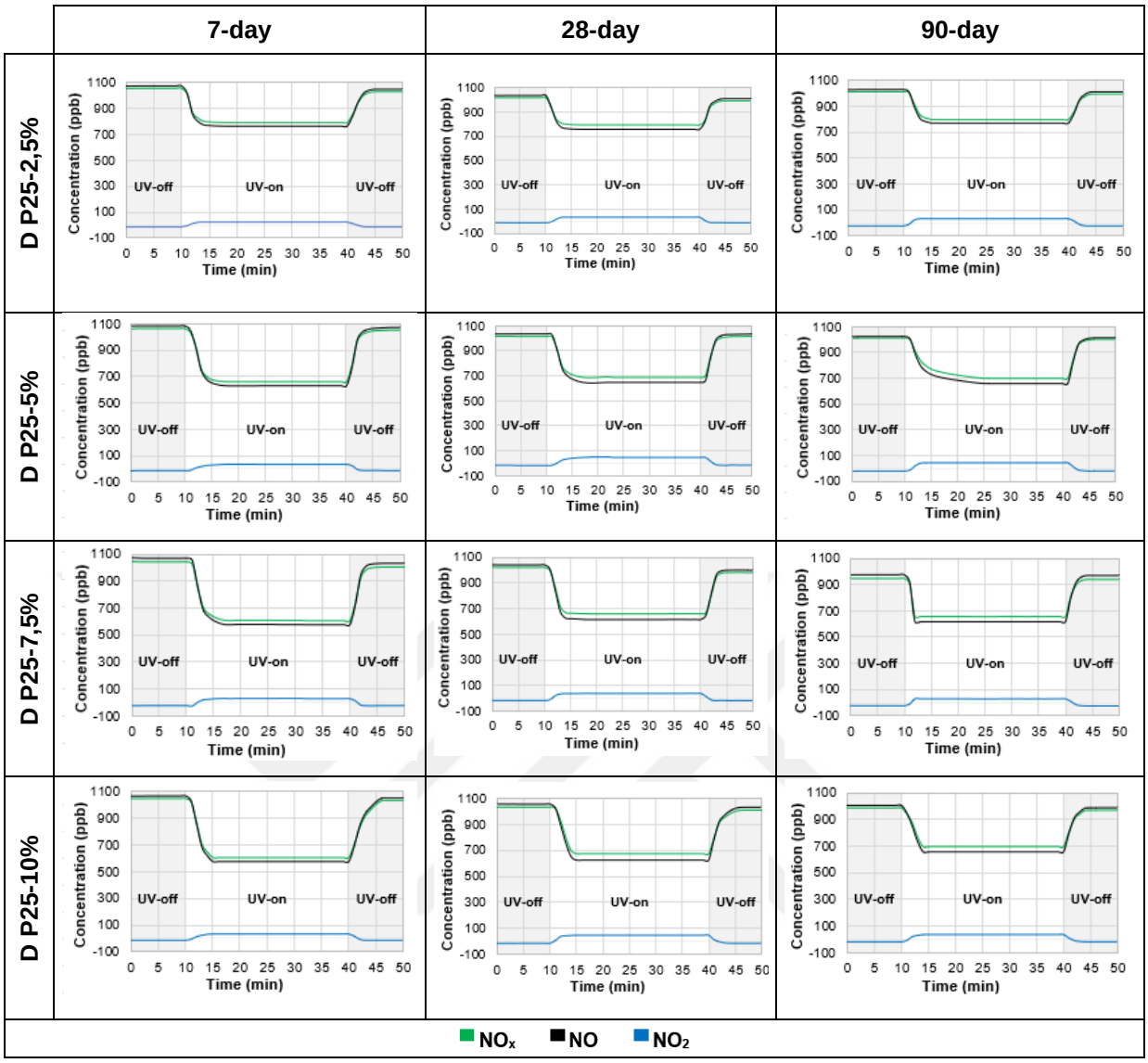

Figure 4.46. Variation of NO_x, NO, and NO_2 concentrations during each test for 7, 28, and 90-day samples of Degussa P25 TiO_2-substituted composites prepared with different substitution ratios.

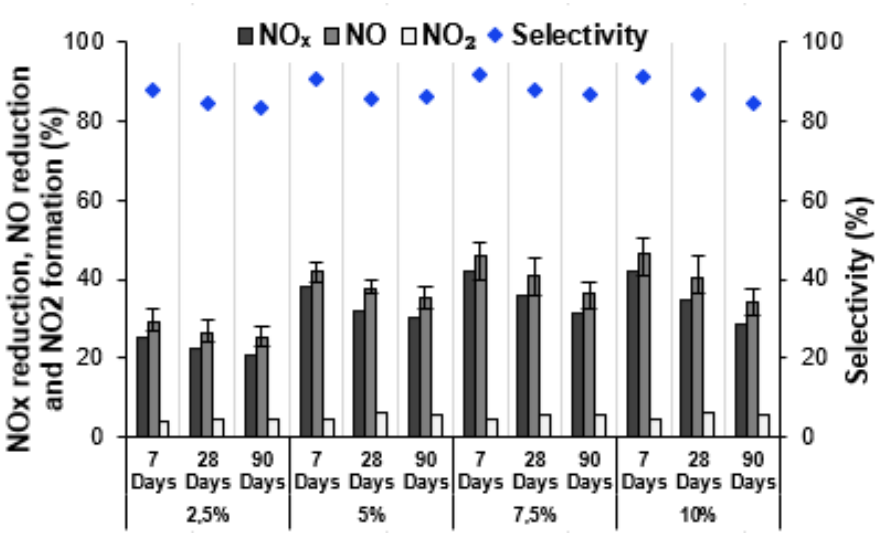

Figure 4.47. The rate of NO_x reduction, NO reduction, and NO_2 conversion and system selectivity (%) in each test for 7, 28, and 90-day samples of Degussa P25 TiO_2-substituted composites prepared with different substitution ratios.

When the degradation rates of 7-day, 28-day and 90-day-old Degussa P25 TiO_2-substituted specimens are evaluated from Figure 4.46 and Figure 4.47, as in the the other TiO_2-substituted specimens, regardless of the utilization rate of TiO_2, it can be seen that NO_x and NO reduction rates decreased with the prolonged curing age. In terms of the effect of the TiO_2 utilization rate on the photocatalytic performances of Degussa P25 TiO_2-substituted composites that can be followed from Figure 4.46 and Figure 4.47, it can be stated that there is a certain point of diffraction (at the utilization rate of 7.5% of the total binder weight) where the trend reversed. NO_x reduction rates (in percentage) of the Degussa P25 TiO_2-substituted cement-based systems increased with the increment in TiO_2 usage rate up to 7.5% of total weight of binder and displayed opposite trend after this point. At the end of 90 days, the highest NO_x reduction rate (31.3%) and system selectivity value (86.5%) were obtained from the 7.5% Degussa P25 TiO_2-substituted cement-based system. However, the NO_x reduction rate (30.5%) and system selectivity (85.9%) of the the 5% Degussa P25 TiO_2-substituted cement-based system were really close to the those of 7.5% Degussa P25 TiO_2-substituted one.

The most important requirement for efficient photocatalytic performance is the high NO_x or NO reduction levels, which is directly related to the air cleaning performance of the photocatalyst-containing cementitious composites. In photocatalytic systems, one of the

main requirements for the reaction mechanism is that the UV light reaches the photocatalyst particles. Because of this, it is vital to ensure that there is adequate photocatalyst on the surfaces exposed to UV radiation in order to promote photocatalytic reactions and obtain a high photocatalytic efficiency. To ensure an efficient photocatalytic degradation process, the presence of photocatalyst particles on the UV-illuminated surface should be maximized, while the formation/increase of embedded/agglomerated particles in the dark depths of cement-based composites should be avoided. By ensuring a homogenous distribution of TiO_2 particles in the mixtures, specimens with more stable and regular microstructures may be created, which is good for repeatability and stability. In the light of all these reasons, it is understood that there is an important relationship between the microstructure of the photocatalyst-containing cement-based composites and their photocatalytic efficiency. In addition, as followed from the results of experimental study, the utilization of TiO_2 particles above a certain level can be harmful or less beneficial than expected in terms of both electrical resistivity and photocatalytic performance. This is most probably due to the increased agglomeration of the TiO_2 particles with the increased TiO_2 content, as mentioned before, which results in remaining TiO_2 particles in the dark depths of the specimens and thereby insufficient contact with UV-light and TiO_2 particles preventing photocatalytic reactions. In the light of all the information presented above (in Section 4.2), optimum TiO_2 utilization rate was determined as 5% and this utilization rate was chosen to be used for the preparation of the mixtures in the next stages of the experimental studies.

4.2.3.5. Image Analysis with Computed Tomography Device

At this stage of the study, the dispersion level of the TiO_2 particles throughout the nano-anatase TiO_2-substituted (at four different utilization rates: 2.5%, 5%, 7.5% and %10 by weight of the powder materials) cement-based matrix was determined by using a computed tomography device. The data generated via this approach is intended to be used to examine the distribution level of nano-TiO_2 particles along the cement-based matrix through the use of an image processing method. Figure 4.48 shows the cross-section view of the computed tomography images of the specimens. Yellow dots indicate TiO_2 particles. Figures 4.48-a, 4.48-b, and 4.48-c (the mixtures prepared with prepared with the utilization rates of 2.5%, 5%, 7.5%, respectively) indicate that nano-sized TiO_2 particles are effectively disseminated and there is no evidence of aggregation along the

matrix's cross-section. Agglomeration zones (inhomogeneity in the dispersion of particles) were observed on the 10% TiO_2-substituted cement-based system (Figure 4.48-d). Figure 4.48-d shows that exceeding a certain utilization rate led to less photocatalytic degradation capability because small-sized TiO_2 particles agglomerated and caused instability in the matrix. The great majority of TiO_2 particles might stay at the dark depths of composites, preventing them from coming into touch with UV irradiation, due to an aggregation problem produced by the surface charge of the particles (inhomogeneous dispersion caused by the presence of an excessive quantity of TiO_2). As a result, this inhibits photocatalytic reactions from occurring.

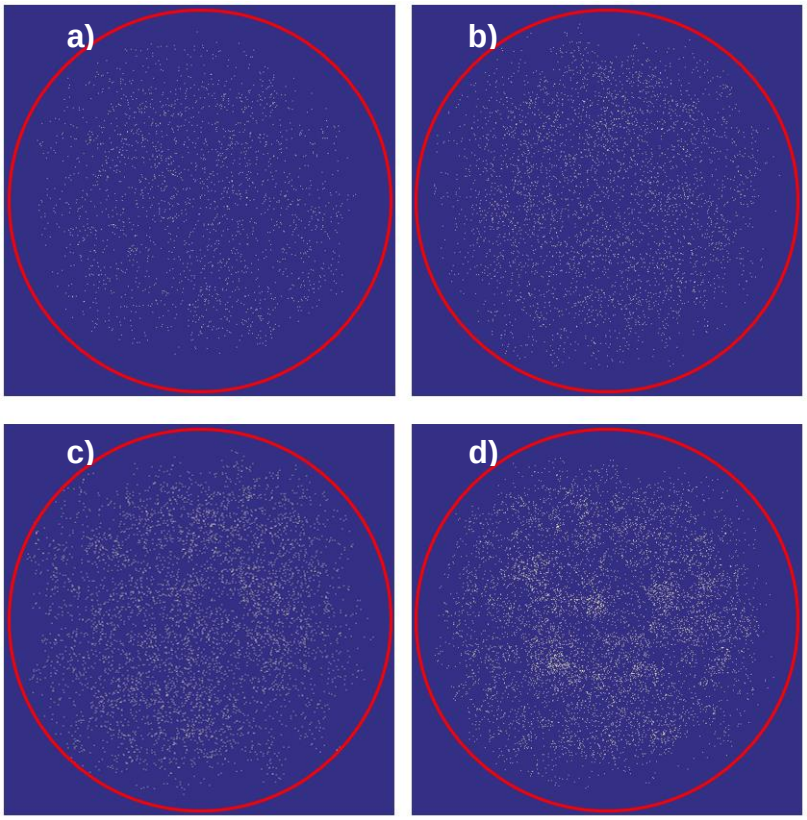

Figure 4.48. Image analysis of nano-anatase TiO_2-substituted composites prepared with different utilization rates with a computed tomography device a) 2.5%, b) 5%, c) 7.5% and d) 10% of total powder material.

4.3. Determination of Optimum TiO_2 Particle Size Distribution for Photocatalytic Cementitious Systems

4.3.1. Introduction

Photocatalytic degradation capability of the TiO_2-incorporated cementitious systems is directly related to surface morphology, specific surface area and particle size of TiO_2 utilized and the number of photocatalyst particles on UV-reached surfaces of photocatalytic cementitious systems. Considering that the particle size of TiO_2 is a significantly influential factor on the activity of photocatalytic systems, studies addressing the relationship between the particle size of TiO_2 incorporated into the cement-based systems and photocatalytic activity of such systems have been performed. In the case of co-utilization of TiO_2 particles of different sizes, optimizing particle size distribution (PSD) of all TiO_2 particles can be essential for optimum performance and/or improvement in performance of systems in several ways. Feret (1892) first studied the PSD to obtain more economical concrete mixture designs by filling in voids among particles. The Fuller and Thompson method has also been used for a long time in determining the extent to which concrete aggregates should be mixed during PSD optimization (Fuller and Thompson, 1907). In 1980, the "minimum particle diameter" technique, which considers the size of the smallest grain used as well as the largest one, was used by Funk et al. (1980) to create mixtures with the highest packing density. There have also been other methods used to ensure high compactness of aggregates (Andreasen and Andersen, 1930; Johansen and Andersen, 1991). On the other hand, in addition to PSD optimization of aggregates, proper gradation of powdery materials such as cement or mineral admixtures can fill entire voids among different particles. There are number of studies related to the effects of optimizing the PSD of some powder materials on several properties of cementitious systems. Sevim and Demir (2019a) studied the effect of optimizing the PSD of fly ash on the performance of cement-based systems in terms of mechanical and durability perspectives. They concluded that optimizing the PSD of fly ash particles in a proper manner provided much better performance for cementitious systems. Another study of Sevim and Demir (2019b) investigated changes in physical and permeability properties of cementitious mortars through optimizing the PSD of fly ash. They found that modifying the PSD of fly ash particles as a pozzolanic material has an undeniable effect on properties of cement-based systems, due to proper PSD playing a major role in filler effect and providing a good distribution of solid concentration. Lim et

al. (2019) also studied the effects of particle grading on autogenous shrinkage and strength of ultra-high-performance concrete, and they reported that PSD is reasonably influential on these concrete properties.

As results of several literature studies show, the PSD of powder materials has a significant influence on several properties of cementitious systems. However, until now, there have been no specific studies on using different-sized TiO_2 materials with optimized PSD in cementitious systems to improve microstructures in favor of optimum photocatalytic efficiency. In this instance, optimization of the PSD of TiO_2 particles in a wide range of sizes (inert ingredients that can be considered filling materials along with their photocatalytic efficiency) is necessary to improve the engineering properties of cementitious systems and/or the degree of photocatalytic reactions in favor of NO_x degradation capability. Therefore, due to the absence of relevant studies, at this stage of the thesis, the effects of PSD of TiO_2 with ternary use of nano-sized, sub-micron-sized, and micron-sized TiO_2 particles on photocatalytic performance and mechanical properties of cementitious systems were investigated. The goal of this step of the thesis research is to determine optimum PSD when the nano, sub-micron, and micron-sized TiO_2s are used together.

4.3.2. Experimental Studies

At this step of the experiment, mixes were made using the fifth mixing procedure (in Section 4.1), which was judged to be the best. A constant water to powder ratio of 0.35, by weight for all mixtures and TiO_2 utilization rate of %5 (by total weight of powder materials) (determined as optimum utilization rate in Section 4.2) were used for the preparation of the mixtures. Six different types of TiO_2 (nano-, submicron-, micron-sized anatase and rutile TiO_2 powders) were used. Nano-, submicron-, micron-sized TiO_2 powders were used as ternary and their incorporation rates were determined in accordance with the PSD equation proposed by Funk et al. (1980). Various PSD moduli (0.1, 0.5, 0.9) representative of a wide region were used.

To study the influence of optimizing the PSD of TiO_2 particles in co-utilization of different-sized TiO_2 particles on the mechanical properties and photocatalytic efficiency of the cementitious systems, the PSD Equation (6.1) proposed by Funk et al. (1980), was adapted to this study. When using this equation to calculate incorporation rates of TiO_2 powders with different particle size fractions, three sieve diameters of 50 nm, 255 nm and 1110 nm were considered: the maximum grain sizes of each TiO_2 powder batch classified by particle size (nano-, submicron-, micron-sized; respectively) and the limit values separating the TiO_2 materials from each other in accordance with particle size.

$$P(D) = \frac{D^q - D_{min}^q}{D_{max}^q - D_{min}^q}, (6.1)$$

where P(D) is the passing percentage of TiO_2 particles passing through relevant sieve, D is the diameter of relevant sieve opening, D_{min} is the minimum particle diameter in all TiO_2 powders and D_{max} is the maximum, and q is the PSD modulus. Three different PSD moduli of 0.1, 0.5 and 0.9 were used. It should be noted that mixtures containing relatively higher proportion of particles with larger grain size were obtained when the numerical value of the PSD modulus increased. Nano-, submicron-, micron-sized anatase or rutile TiO_2 powders were also used solely to observe their individual influences on the performance of cementitious systems. In addition, a reference mixture was manufactured without TiO_2 powder content for comparison. PSD curves were plotted using the equation above for values of q: 0.1, q: 0.5 and q: 0.9. These PSD curves and those of nano-, submicron-, micron-sized anatase and rutile TiO_2 powders TiO_2 powders are displayed in Figure 4.49 and Figure 4.50

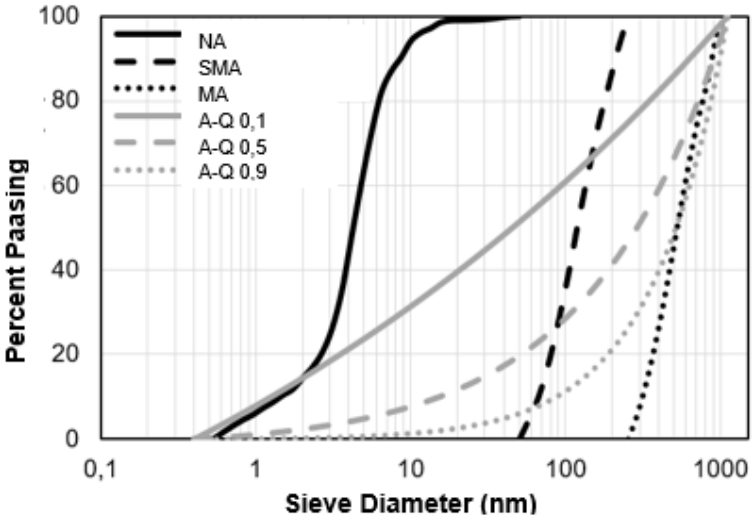

Figure 4.49. PSD curves of nano-, submicron-, micron-sized anatase TiO_2 powders and TiO_2 powders with varying PSD moduli

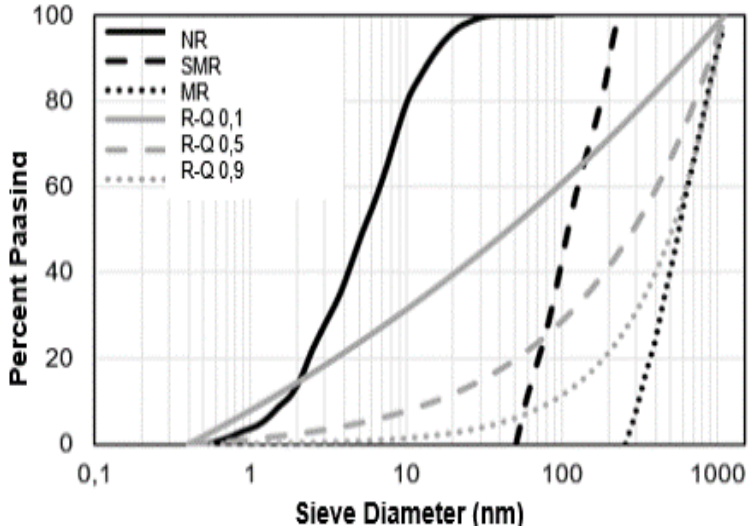

Figure 4.50. PSD curves of nano-, submicron-, micron-sized rutile TiO_2 powders and TiO_2 powders with varying PSD moduli

The effects of PSD optimization on the mechanical properties (compressive strength), physical properties (pore volume and pore size distribution-by using MIP), hydration kinetics, and NO_x degradation capability were investigated using different dispersion moduli. In addition, microstructural features of specimens were examined by microstructural characterization analyses including scanning electron microscopy with energy-dispersive X-ray spectroscopy (SEM/EDX).

4.3.3. Experimental Study Results and Discussion

4.3.3.1. Hydration Kinetics

Isothermal calorimetry was used to examine the hydration of cementitious pastes, using 0.35 water-to-powder ratio at 25°C to observe the influence of the PSD of anatase-phase TiO_2 on hydration kinetics. Since the anatase-phase TiO_2-incorporated cement-based systems exhibited higher photocatalytic degradation performances, the effect of the PSD optimization on the hydration kinetics was evaluated by using anatase-phase TiO_2 incorporated systems. Figures 4.51 and 4.52 show the hydration rate and cumulative heat of hydration of cementitious pastes, respectively.

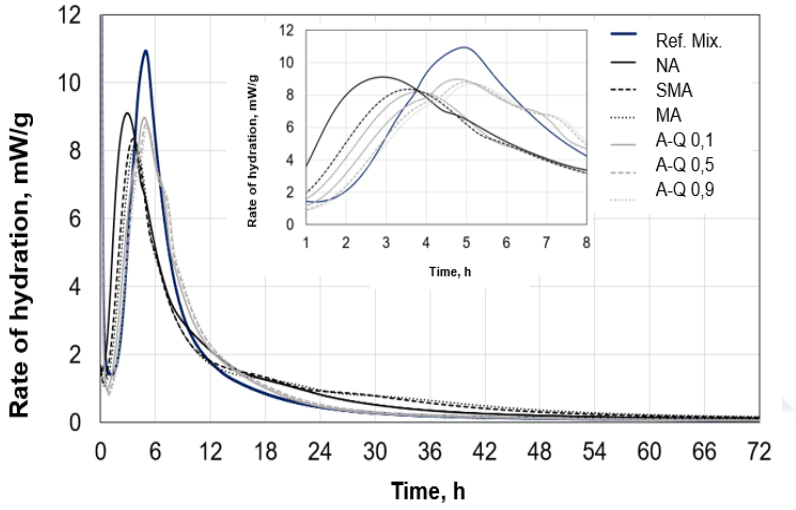

Figure 4.51. Rate of hydration of cementitious systems with variable PSD of anatase TiO_2

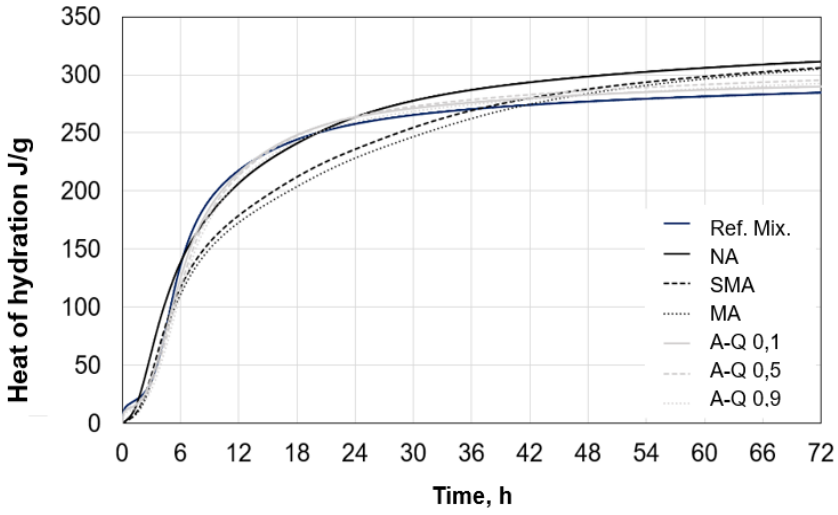

Figure 4.52. Heat of hydration of cementitious systems with variable PSD of anatase TiO_2

As seen from Figure 4.51, although reference specimen non-containing TiO_2 was not the specimen which reached rate of hydration peak earliest, the highest rate of hydration peak value was obtained from this specimen. This result can be attributable to the relatively higher cement content of reference specimen compared to those of TiO_2-substituted specimens, which is detailed in compressive strength results section (Section 4.3.3.2.).

Among the non-optimized specimens (specimens prepared by using nano-, submicron-, micron-sized anatase TiO_2 powders, solely), nano-sized anatase TiO_2 addition resulted in an earlier and higher rate of hydration peak compared to submicron- and micron-sized anatase TiO_2s, probably due to more effective nucleation effects provided by significantly smaller particles of nano-sized anatase TiO_2. Incorporating nano materials with extremely small particle size has a hydration agitation and acceleration effect (Chen et al., 2012; Mohseni et al., 2015; Han et al., 2017; Li et al., 2017). This caused higher heat of hydration for the cementitious system containing nano-sized anatase TiO_2 than for the pastes with submicron- and micron-sized anatase TiO_2s, especially between 8-48 hours of hydration (Figure 4.52). However, the heat of hydration values of nano-, submicron-, micron-sized anatase TiO_2-substituted mixtures were similar at the end of 72 hours of hydration. On the other hand, cementitious systems containing a combination of nano-, submicron-, micron-sized anatase TiO_2 powders with varying PSD moduli exhibited a maximum rate of hydration comparable to that of the paste with only nano-sized anatase TiO_2 indicating similar seeding/nucleation effects. However, the apparent initial retardation effect-where a longer induction period is observed but without a reduction rate of peak heights for the mixtures prepared by using three different PSD moduli of 0.1, 0.5 and 0.9 may be attributed to retardation of cement grains dissolution because of residual inorganic substances. Knowing that some inorganic materials (SO_4^{2-}, CO_3^{2-}, PO_4^{3-}, and F^-) have an adverse effect on early dissolution rate (Taylor, 1997). In this regard, sulfate ions, coming from extracting and purifying process, on TiO_2's surface may be dissolved into C_3S particles, causing dissolution to be delayed (Chernet, 1999;Lee and Kurtis, 2010). The reason why shifted peak observed by the mixtures prepared by using three different PSD moduli of 0.1, 0.5 and 0.9 were related with the retardation effects of residual inorganic materials. However, these retardations were not effective on non-optimized TiO_2 used paste mixtures. This could be attributed to the effects of PSD which

lead more densify structure and covering more cement grain in fresh stages, hence results more retardation effects and less dissolution of particles in initial duration.

When comparing the influence of PSD modulus on the rate and heat of hydration, increasing PSD modulus of TiO_2 particles from 0.1 to 0.9 made no considerable difference. Besides, TiO_2 addition with varying PSD moduli resulted in a higher heat of hydration than submicron- and micron-sized anatase TiO_2 for hydration time of up to 48 hours. However, the reverse was true thereafter. This finding indicates that using nano-, submicron- and micron-size particles, mixed to provide varying PSD moduli, is highly effective on the rate and total heat of hydration at early periods before 48 hours. Furthermore, anatase-TiO_2 with varying PSD moduli caused a small shoulder formation in the rate of hydration curves at around 8 hours. This kind of shoulder formation in the deceleration stage of the main hydration peak is generally associated with conversion of AFt to AFm (Aitcin and Flatt, 2016). Earlier conversion of AFt to AFm, in the case of anatase-TiO_2 with varying PSD moduli, could be attributed to the specific influence of PSD on the hydration of calcium aluminates, which cause earlier conversion of AFt to AFm.

The hydration kinetics results of cementitious pastes shown in Figure 4.51 and 4.52 show that using nano-sized TiO_2 (NA) caused an enhanced/accelerated degree of hydration reaction (kinetics) of the cementitious paste (larger peak magnitude and earlier time of peak occurrence) owing to its considerably fine structure providing significant surface energy. This acceleration confirms that using nanoparticles (NA) provides higher early-age strength. As the particle size of the TiO_2 in cementitious systems increased (among specimens characterized by single use of TiO_2 particles), the peak occurrence time increased and the peak magnitude decreased. This circumstance is consistent with compressive strength findings, which show that increasing particle size reduces strength.

When the hydration kinetics results shown in Figure 4.51 and 4.52 are evaluated, it can be clearly seen that using TiO_2 with varying PSD moduli resulted in a retardation of peak occurrence compared to the single-sized TiO_2 (longer time of peak occurrence) due to retardation of early dissolution as a result of residual inorganic chemicals (Lee and Kurtis, 2010) and better-covering capability of PSD-optimized TiO_2 particles. As the PSD

modulus increased, the peak occurrence time increased and also its magnitude decreased due to decrement in seeding and nucleation capability with increased coarser TiO_2 particles.

4.3.3.2. Compressive Strength

Compressive strength of TiO_2-substituted (at a usage rate of 5% by weight of the powder materials) cementitious systems for various curing ages was evaluated to better understand the impacts of PSD optimization of TiO_2 particles on the mechanical characteristics of TiO_2-substituted systems. The compressive strength results are presented in Figure 4.53 to 4.54. Considering the differences in compressive strength depending on PSD of TiO_2 used, the mechanical performances of the TiO_2-substituted cement-based systems were evaluated.

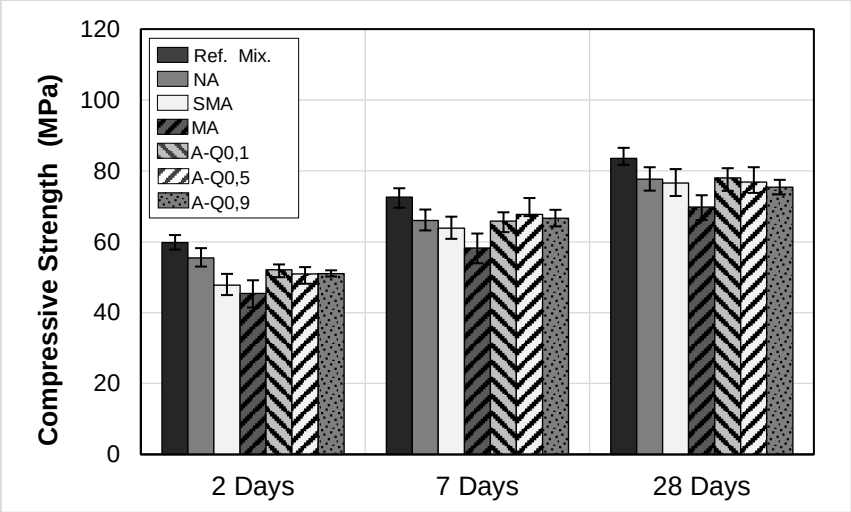

Figure 4.53. Compressive strength results of anatase TiO_2-substituted cement-based composites

The compressive strength test results of each anatase TiO_2-substituted mixture for various curing ages are shown in Figure 4.53. Because of continued hydration processes, the protracted aging/curing resulted in constant increases in compressive strength findings, regardless of mixture characteristics. Submicron-sized anatase-phase TiO_2-incorporated specimen showed the highest strength increase at 33.7%, from 2-day to 7-day curing age. Between 7-day and 28-day curing ages, strength increases slowed for all mixtures. The highest compressive strength test results were recorded from reference specimen (non-containing TiO_2) for each curing age with the values reaching 59.32 MPa for 2-day-old

specimens, 71.33 MPa for 7-day-old specimens and 85.30 MPa for 28-day-old specimen. In the available literature, it was reported that the mechanical performance of cementitious systems can be improved with the incorporation of different nano materials up to a certain nano-material utilization rate beyond which decrements or negligible increments can be noted (Xu et al., 2019; Erdem et al., 2020). In the study of Jimenez-Relinque et al. (2015), incorporation of 2% TiO_2 (by mass of cement) reduced the compressive strength of the cementitious systems. In this regard, considering relatively higher incorporation rate of TiO_2 powder in this study (5% of total weight of powder material), the relatively lower compressive strength results of the TiO_2-incorporated systems (especially of nano-sized anatase-phase TiO_2-incorporated specimen) compared to that of reference specimen can be attributed to the dilution effect (diminution of cement). The addition of inert TiO_2 powders resulted a less amount of presence of reactive cement (in percentage) in the mixtures decreasing the rate/amount of hydration products manufactured and causing lower compressive strength (Jayapalan et al., 2013; Xu et al., 2019; Erdem et al., 2020).

Among the non-optimized specimens (specimens prepared by using nano-, submicron-, micron-sized anatase TiO_2 powders, solely), it was evident that those containing nano-sized anatase TiO_2 showed the highest compressive strength results for each curing age. The compressive strength values of nano-sized anatase-phase TiO_2-incorporated specimen for 2-day, 7-day and 28-day curing ages were 55.40, 66.00 and 77.63 MPa, respectively. The probable reason for this behavior is that nano-sized powders create higher density due to the filler effect arising from comparatively smaller particle size (Al-Dahawi et al., 2016). This behavior can also be attributed to the seeding effect, which is the formation of additional area (nucleation sites) due to the extremely fine particle size of nano materials (and thereby their high surface area) that can pull unhydrated cement particles towards themselves, resulting in more suitable places for the precipitation of hydration product (Yeşilmen et al., 2015; Al Najjar et al., 2016).

Although the NA showed highest compressive strength performances among non-optimized specimens for each curing age, the incorporation of nano-sized TiO_2 reduced the compressive strength results of the cementitious system considering relatively higher compressive strength performance of the TiO_2 non-containing specimen (Ref. Mix). In

this regard, it is possible to state that the decremental effect of the decrease in the reactive cement content of NA, because of replacement of cement with inert TiO_2, on mechanical performance was more dominant than the enhancing effects of the nano materials incorporation into cementitious systems. It should be also stated that although, at the end of the 48 hours, heat of hydration released from NA was higher than the reference mixture (detailed in previous section), the compressive strength results were inconsistent with this case. The possible reason of this situation can be related with (i) differences in the consistency of the mixtures due to the different sized TiO_2 content, (ii) formation of heterogenous reaction product for faster hydration at the early age and (iii) differences in the hydration products because the possible effects of TiO_2 existence.

Micron-sized anatase-phase TiO_2-incorporated specimen showed the lowest compressive strength performance among all tested mixtures for each curing age, most probably because of the lower capability of the micron-sized TiO_2 particles in terms of refinement of pore size structure in the paste due to their coarser structure and thereby lower surface areas.

In the PSD-optimized specimens (the mixtures prepared by using three different PSD moduli of 0.1, 0.5 and 0.9), although there was no important difference in their compressive strength values, the mixture prepared by using PSD moduli of 0.1 had the highest compressive strength values at approximately 52.10 (2-day), 65.82 (7-day) and 78.01 MPa (28-day), for almost all curing ages except for 7 days. After 28 days of curing, the lowest compressive strength achieved among PSD-optimized specimens was 75.37 MPa for the combination created with PSD moduli of 0.9. When all results (obtained from TiO_2-incorporated mixtures) are evaluated together and micron-sized anatase-phase TiO_2-incorporated specimen results are excluded, the differences in compressive strength results of mixtures at 28 days was not significantly evident, and compressive strength test results were 76-79 MPa for tests carried out on all TiO_2-incorporated mixtures after 28 days. It is especially noteworthy that the compressive strength of A-Q0.1 is higher than that of NA, which can be attributed to its well-graded PSD achieving high particle packing density. Peak magnitude values (maximum rate of hydration) of cementitious systems containing a combination of NA, SMA, and MA TiO_2 particles with varying PSD moduli were higher than those in systems containing SMA or MA TiO_2, and lower than in those

containing NA TiO_2. As a result, considering the higher peak magnitude value, the earlier peak occurrence and the higher cumulative heat of hydration of cementitious system containing NA TiO_2 at the end of 72 hours of hydration, it can be clearly stated that A-Q0.1's relatively high compressive strength compared to NA was geometry-related (physical) rather than chemistry-related (chemical), and PSD optimization with PSD modulus of 0.1 provided the highest particle packing density.

Considering all of these results, it can be clearly stated that although the difference between compressive strength results was not significantly prominent, meaningful differences were noted for 28-day-old specimens. Less pronounced effect of the modification/optimization of the PSD of TiO_2 powders on the compressive strength of specimens containing PSD-optimized powders can be attributed to the relatively wide range of particle sizes of NA and SMA TiO_2 batches, resulting in naturally good particle grading, thereby positively affecting the mechanical properties of specimens. Although it was minimally effective in increasing compressive strength for this study, the advantages of PSD-optimization of TiO_2 powders in tailoring microstructural properties are also likely to improve compressive strength results of mixtures with PSD-optimized powders over those containing TiO_2 powders with a narrower range of particle sizes.

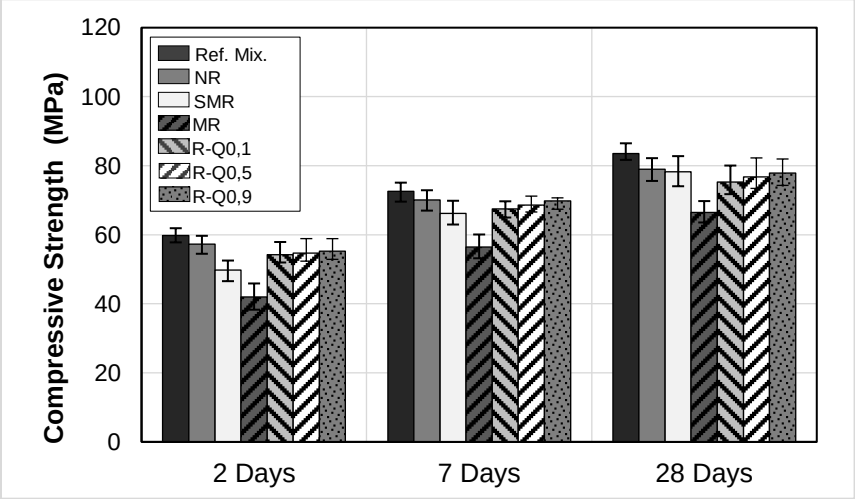

Figure 4.54. Compressive strength results of rutile TiO_2-substituted composites

When the compressive strength results of the rutile-phase TiO_2-substituted composites are evaluated from Figure 4.56, it can be seen that the extended aging/curing resulted in continuous increments in the compressive strength results, regardless of mixture

parameters, due to ongoing hydration reactions. According to the compressive strength results, in general, the compressive strength of nano-anatase and nano-rutile TiO_2-substituted composites are quite similar, apart from minor differences. The compressive strength values of the mixture containing nano-sized rutile TiO_2 were recorded as 57.3, 70.10 and 79.0 MPa for the curing ages of 2 days, 7 days and 28 days, respectively. This can be attributed to the fact that the rutile phase TiO_2 contributes relatively more to the strength than the anatase phase TiO_2 for each curing age. Apart from nano size, it was observed that composites using PSD modulus provide better compressive strength compared to single size uses (submicron and micron). This shows that PSD optimization has a positive effect on compressive strength. At the end of 28 days, the compressive strengths of the samples produced with PSD optimization (q 0.1, 0.5 and 0.9) were determined as 75.27, 76.74 and 77.90 MPa, respectively. In other words, higher compressive strength was obtained in the composite containing less nano-sized material. The compressive strength of the reference mixture without TiO_2 (Ref. Mix.) was the highest among all mixtures, regardless of the curing age. Among the TiO_2-incorporated mixtures, modification/optimization of the PSD of TiO_2 powders with a proper PSD modulus provided relatively better mechanical performance by ensuring high compactness. Specimens prepared by using TiO_2 powder optimized with the PSD modulus of 0.9 performed comparatively better under compressive strength test than other non-optimized and PSD-optimized specimens at the end of 28 days.

4.3.3.3. Photocatalytic Performance

The photocatalytic performance of anatase-phase and rutil-phase TiO_2-substituted cementitious systems for different curing ages were determined. The NO_x, NO, and NO_2 concentration profiles obtained during the NO_x degradation tests under illumination are presented in Figure 4.55 and Figure 4.57. In addition, NO_x and NO degradation and NO_2 formation rates (in percentage) of the developed systems together with the system selectivity values are summarized in Figure 4.56 and Figure 4.58. Considering the differences in NO_x and NO degradation and NO_2 formation rates depending on PSD of TiO_2 used, the performances of the TiO_2-substituted cement-based systems were evaluated.

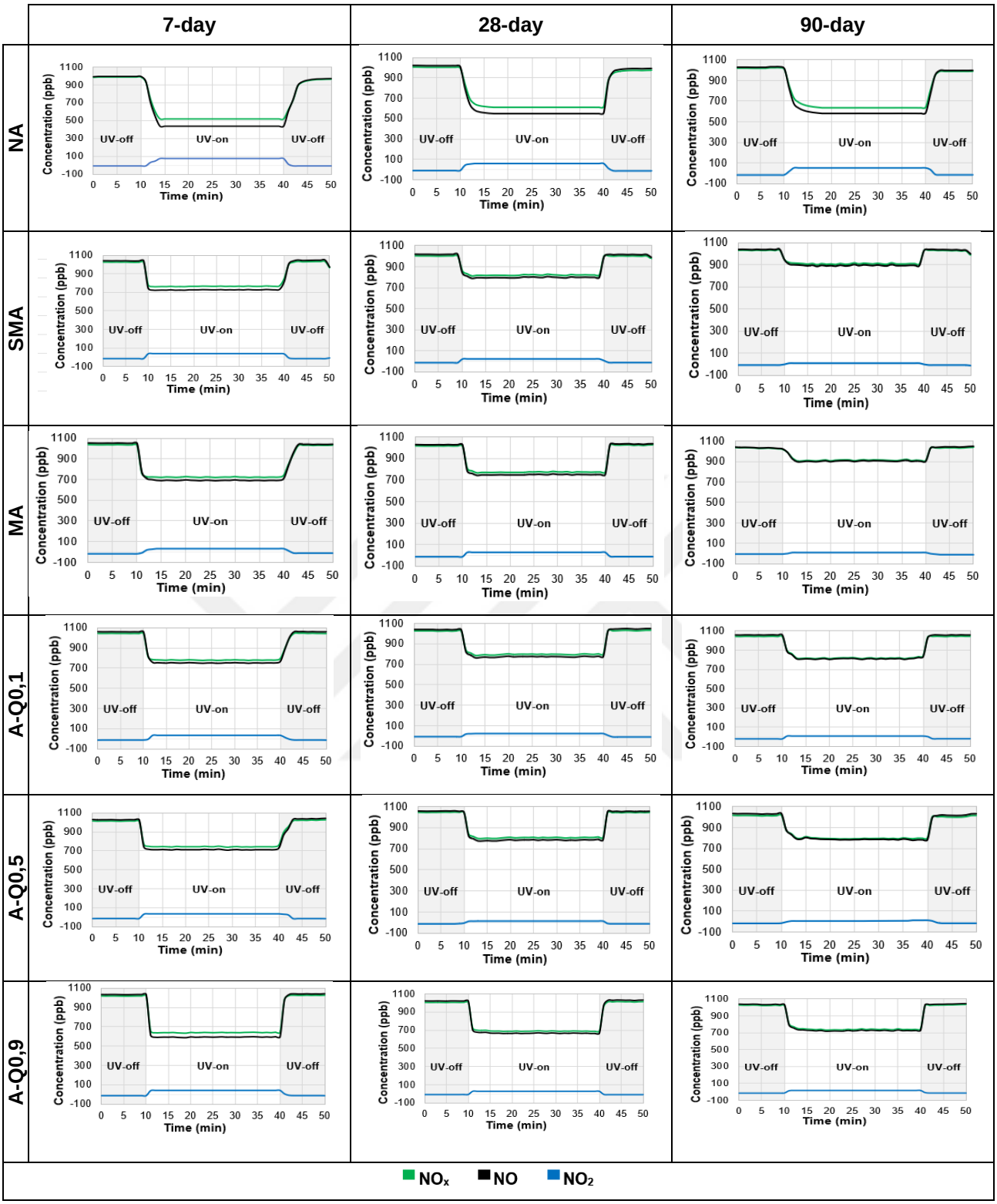

Figure 4.55. Variation of NO_x, NO, and NO_2 concentrations during each test for 7, 28, and 90-day specimens of anatase TiO2-substituted composites

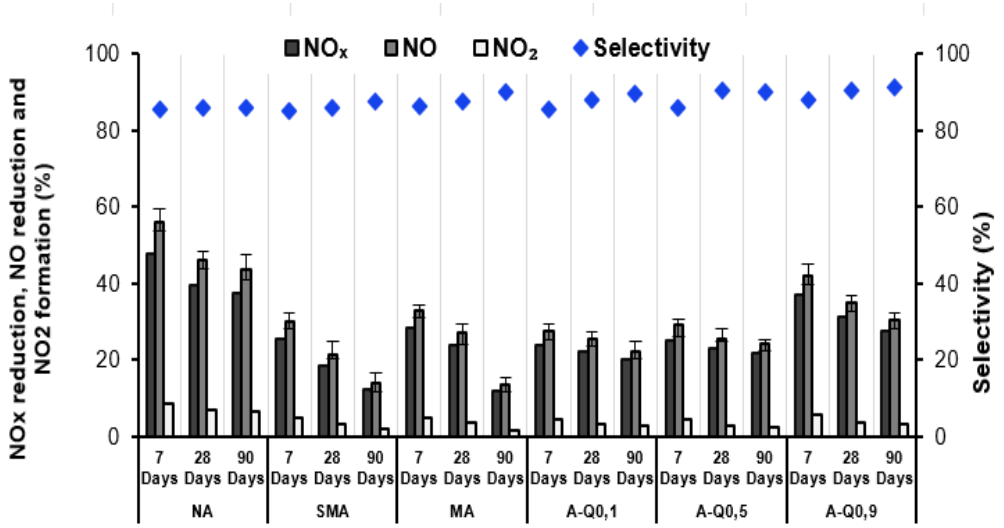

Figure 4.56. The rate and system selectivity (%) of NO_x reduction, NO reduction, and NO_2 conversion in each test for 7, 28, and 90-day specimens of anatase TiO_2-substituted composites

When the degradation rates of 7-day, 28-day and 90-day-old anatase TiO_2-substituted specimens are evaluated from Figure 4.55 and Figure 4.56, it can be clearly seen that the NO_x degradation rates of nano-sized anatase-phase TiO_2-substituted composite were the highest for each curing age. Although utilizing nano-sized materials in cementitious systems causes agglomeration issues because to the particles' large surface area and energy (Kawashima et al., 2013), specimens using nano-sized anatase TiO_2 powder demonstrated comparably strong photocatalytic degradation capacity. This can be attributed to the easy current transfer capability of the nano-sized TiO_2 from its surface, especially when uniform distribution was guaranteed (Almquist and Biswas, 2002; Zhao and Yang, 2003; Carp et al., 2004).

Due to the fact that photocatalytic reactions occur at the surface of the photocatalyst and photons are captured from the surface of materials (Minero et al., 1992), it is also possible to state that the photocatalytic activity directly depends on the total surface area of the photocatalyst where UV irradiation is reached and on the grain size of the photocatalyst affecting this area, and therefore nano particles can provide maximal photocatalytic surface area accessible to polluting substances. However, the microstructure of cementitious systems incorporating TiO_2 particles is significantly influential on the dispersion of TiO_2 particles throughout the surface where the photocatalytic reactions

occur and thereby on the performance of these systems. On the other hand, submicron- and micron-sized anatase-phase TiO_2-substituted composites showed considerably lower photocatalytic degradation performance than nano-sized anatase-phase TiO_2-substituted one, with the differences in degradation results becoming significantly more pronounced with longer curing periods. Among the PSD-optimized specimens, photocatalytic degradation rates of the mixture prepared by using PSD moduli of 0.9 were the highest for all curing ages and after that, in decreasing order, those of for the mixture prepared by using PSD moduli of 0.5 and for the mixture prepared by using PSD moduli of 0.1. Photocatalytic degradation rates of all specimens exhibited a decremental trend starting from 7 to 90 days. This time-dependent trend may have come from the ongoing hydration reaction, leading to the coating of TiO_2 particles with further hydration product and thereby reducing the presence of TiO_2 materials on specimen surfaces reached by UV irradiation. A more likely reason is that carbonation products, produced by binding carbon dioxide (CO_2) into solid carbonates on the specimen surface or another possible process, cause the specimen surface to be coated (Poon and Cheugn, 2007; Chen and Poon, 2009; Matějka et al., 2012). The rate of decrement in photocatalytic degradation results of non-optimized specimens from 7 to 28 days was more evident than in PSD-optimized specimens. With further aging of specimens beyond 28 days, the rate of decrement in photocatalytic degradation results of submicron- and micron-sized anatase-phase TiO_2-substituted composites was significantly higher than in other specimens.

As followed from Figure 4.58, different NO_2 formation levels were obtained from the specimens at the end of the photocatalytic reactions. The formation of NO_2 in photocatalytic reactions can be related to the HNO_3 and NO_3^- accumulation on the TiO_2 surface over time, reacting with NO, beyond a threshold value, to form NO_2 (Mills and Elouali 2015 ; Wang et al., 2007). Besides, the reactions between NO and O_2 and/or HNO_2 and OH* could be another possible reason of the formation of NO_2 (Wang et al., 2007; Mills and Elouali 2015; Han et al., 2021;). Considering the fact that the toxicity of NO_2 is significantly higher than the primary pollutant NO (Yang et al., 2018), it was critical to monitor the change of NO_2 levels throughout the photocatalytic reactions, and the system selectivity. When evaluating the system selectivity of the cementitious systems, it was clearly observed that the system selectivity of all specimens exhibited an incremental trend starting from 7 to 90 days. In terms of NO_x and NO reduction, although the nano-

sized anatase-phase TiO_2-substituted specimen was exhibited better performances, the higher selectivity values were obtained from the PSD-optimized specimens. Therefore, it is possible to state that PSD optimization significantly contributed to enhancement in the photocatalytic efficiency of the cementitious systems by increasing the system selectivity. In the PSD-optimized specimens (the mixtures prepared by using PSD moduli of 0.1, 0.5 and 0.9), although there was no significant difference in their system selectivity values, the mixture prepared by using PSD moduli of 0.9 had the highest one (91.1%) at the conclusion of the 90-day cure period. Relatively higher system selectivity of A-Q0.9 means a more efficient NO_x degradation capability. Although a refined pore structure due to good particle grading caused relatively greater compressive strength, this negatively affected the photocatalytic activity of the mixtures, thereby causing NO_x degradation with low efficiency. This situation was also valid for PSD-optimized specimens. Although A-Q0.1 contains higher amounts of more active nano-sized TiO_2, its dense structure resulted in lower photocatalytic efficiency compared to other PSD-optimized specimens. On the other hand, A-Q0.9 showed superior photocatalytic efficiency among all PSD-optimized specimens, despite having a small amount of nano-TiO_2. Therefore, it is plausible that the NO_x degradation capability of the mixtures is strongly related to the microstructure characteristics of matrix (as mentioned earlier) although their relationship is quite different than the relationship between microstructure and compressive strength. Namely, the optimal TiO_2 quantities from different-sized TiO_2 batches sufficient for efficient photocatalytic activity were different than those sufficient for mechanical property. In this regard, the most favorable particle packing was provided at a PSD modulus of 0.1 with well-graded TiO_2 particles (A-Q0.1), which achieved higher strength results than the other PSD-optimized mixtures, although some natural variations were observed. This can be attributed to the improvement/optimization of the PSD of powder materials in a proper manner, which promoted pore refinement of the microstructure of the cementitious systems, thereby obtaining a relatively denser matrix.

Higher photocatalytic degradation capability of the A-Q0.9 compared to the other PSD-optimized specimens may stem from the larger number of pores limiting coverage of the TiO_2 particles with hydration product. Another possible reason for the better photocatalytic efficiency of A-Q0.9 is due to the multiple pore-structure of A-Q0.9 homogeneously spread throughout the surface morphology, which causes a large number of TiO_2 particles to be dispersed throughout pore walls for maximum photocatalytic

surface area. In addition, larger pores can allow pollutant gas (NO_x gas) to diffuse into the cementitious matrix more easily, thereby more pollutants participate in the photocatalytic reactions and provide easily reaching of photons to the TiO_2-containing inner parts of the specimens in favor of further contact between the surface of photocatalytic materials and UV irradiation. This situation also evident for MA and SMA. Although SMA contained submicron-sized TiO_2 particles with photocatalytic efficiency that is expected to be higher than in micron-sized TiO_2, the NO_x degradation capability of MA at 7 and 28 days was higher than that of SMA. This may also be attributable to the fact that MA had a greater volume of holes, the vast majority of which were pores larger than 50 nm.

Although specimens containing nano-sized TiO_2 particles showed the highest photocatalytic activity, a comparatively high efficiency cementitious system in terms of NO_x degradation capability was obtained with PSD optimization of TiO_2 powders, probably due to the pore structure. High photocatalytic efficiency was obtained by using a considerably smaller number of nano TiO_2 particles, which have higher photocatalytic activity than larger ones. By optimizing the PSD of TiO_2 particles, lower decrements in NO_x degradation of mixtures over curing time were also achieved. Furthermore, PSD optimization increased the system selectivity, which proves that PSD optimization contributes to the enhancement in photocatalytic efficiency of the TiO_2-incorporated cementitious systems.

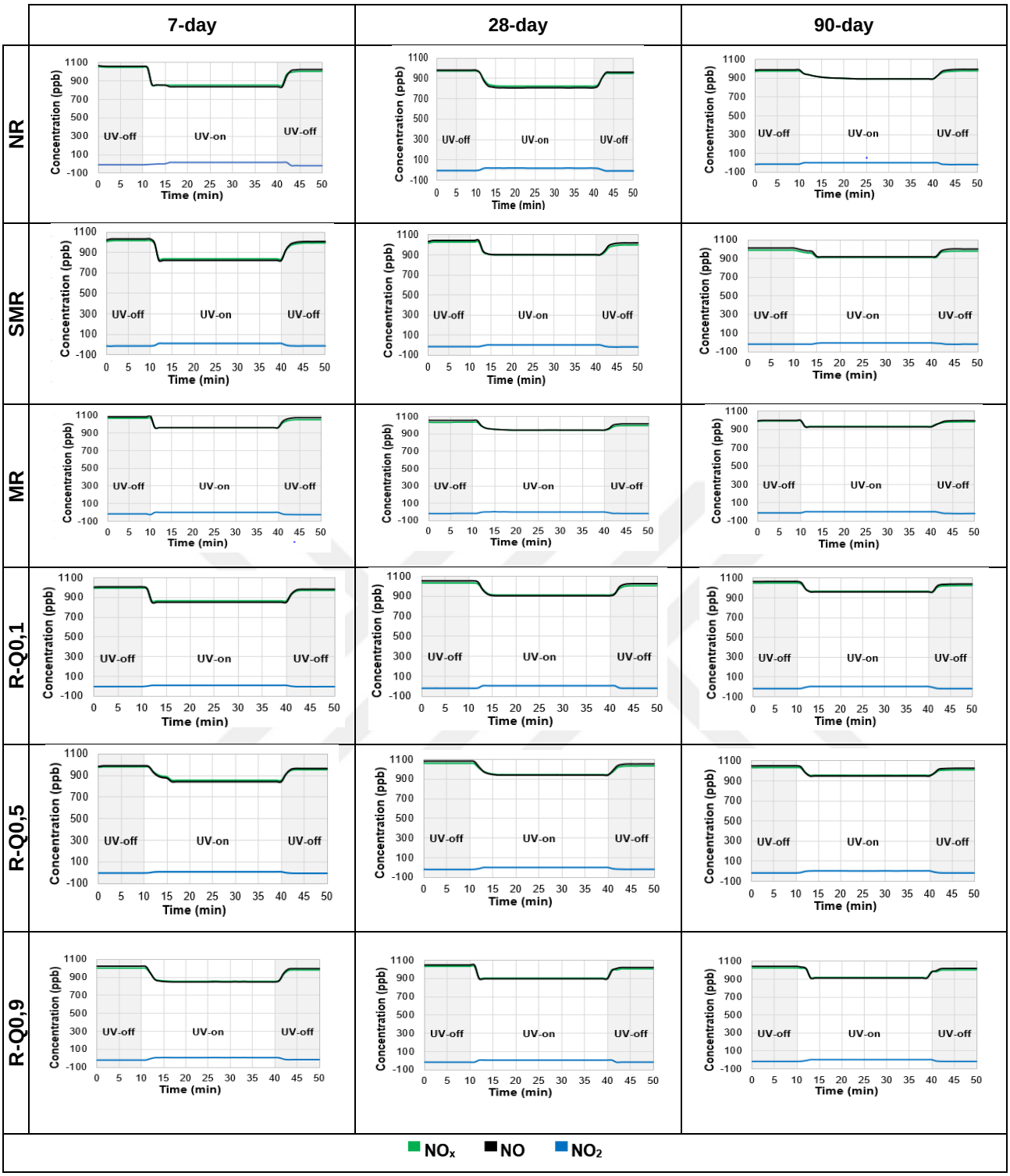

Figure 4.57. Variation of NO_x, NO, and NO_2 concentrations during each test for 7, 28, and 90-day specimens of rutile TiO_2-substituted composites

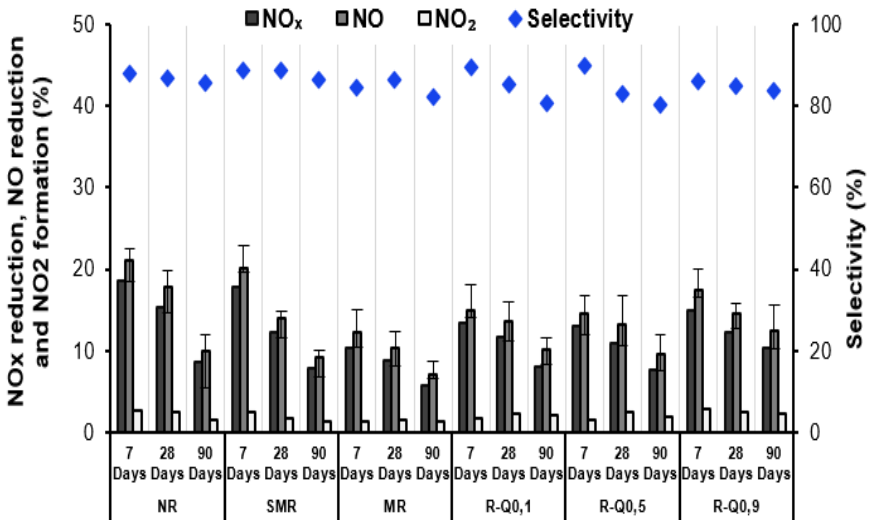

Figure 4.58. The rate and system selectivity (%) of NO_x reduction, NO reduction, and NO_2 conversion in each test for 7, 28, and 90-day specimens of rutile TiO_2-substituted composites

When the degradation rates of 7-day, 28-day and 90-day-old rutile TiO_2-substituted specimens are evaluated from Figure 4.57 and Figure 4.58, as in the the anatase TiO_2-substituted specimens, regardless of the utilization rate of TiO_2, it can be seen that NO_x and NO reduction rates decreased with the prolonged curing age due to the ongoing hydration reactions. In PSD optimized mixtures, the highest NOx reduction value was obtained from R-Q0.9 composite with 10.4 % at the end of 90-day. There is a similar situation in the system selectivity, and the highest value was obtained from this composite (83.5% for 90-day). As followed from the results, optimizing the PSD of TiO_2 particles did not generally affect the photocatalytic performance/efficiency of rutile TiO_2-substituted specimens positively and system selectivity values of rutile TiO_2-substituted composites decreased continuously with the prolonged curing age, in contrary to the anatase TiO_2-substituted composites. In general, the photocatalytic activity of rutile-containing mixtures lagged far behind anatase TiO_2 containing mixtures. The differences between the photocatalytic activities of the anatase and rutile phases of TiO_2 particles are directly related to their crystal structures. Since the reasons of this were discussed in detail previously, no further comments were made here.

However, the mixture using the PSD modulus of 0.9 had the highest selectivity value (91.1% and 83.5% for anatase and rutile TiO_2-substituted specimens, respectively) at the

conclusion of the 90-day cure period. This means that the highest photocatalytic efficiency was obtained from the PSD modulus of 0.9.

4.3.3.4. Mercury Intrusion Porosimetry Test (MIP)

Since the mixtures with the best results in the cement-binding systems developed within the scope of the study are the mixtures with anatase substituted, the pore size and pore size distribution on the anatase-substituted mixtures were determined by using the mercury porosimetry test (MIP).

MIP was used to test the pore size distributions of 5% anatase-phase TiO_2-substituted cementitious systems containing nano-, submicron- and micron-sized TiO_2 particles individually or in combination and with varying PSD moduli, at the age of 28 days. MIP was also performed on reference specimen for comparison. The current pore size classification proposed by the International Union of Pure and Applied Chemistry (IUPAC) was used to describe the pore structure of the cementitious system (IUPAC, 1971). This proposed classification classifies the pores into three groups according to their sizes, including macropores, over 50 nm; mesopores, from 50 to 2 nm; and micropores, under 2 nm. According to studies available in the literature, voids larger than 50 nm are, more influential on impermeability and strength characteristics of cement-based systems, whereas voids smaller than 50 nm are more influential on drying shrinkage and creep (Jones, 1990; Mehta and Monteiro 1993; Song and Kwon 2007). Therefore, in addition to the IUPAC classification, in this paper, pores were divided into two categories: pores larger than 50 nm termed as pores above 50 nm and pores smaller than 50 nm termed as pores below 50 nm. Total porosity (% of volume) of specimens is presented in Figure 4.59. Pore size distribution percentages and curves of all specimens are illustrated in Figures 4.60-a and 4.60-b, respectively. As indicated in Figure 4.59 and Figure 4.60, reference specimen had the lowest total porosity value (3.9%) and all pores available in this specimen were smaller than 50 nm, evidencing the highest compressive strength results of the reference specimen. The figures also show that almost all pores dispersed throughout nano-sized anatase TiO_2-substituted specimen were smaller than 50 nm. Furthermore, a total porosity value of 4.0% for nano-sized anatase TiO_2-substituted specimen (Figure 4.59) reveals that nano-sized anatase TiO_2-substituted specimen has a relatively low pore volume compared to the other single size TiO_2-substituted specimens

(submicron- and micron-sized anatase TiO_2-substituted specimens). As the size of TiO_2 incorporated to the matrix got coarser, the volume of pores smaller than 50 nm formed in the matrix decreased. The rate of pores, ranged between 0–50 nm, dispersed throughout submicron- and micron-sized anatase TiO_2-substituted specimens was at 87.5% and 47.4% of the total amount of pores, respectively. Moreover, the total porosity values of these mixtures were 8.6% for submicron-sized anatase TiO_2-substituted specimen and 10.4% for micron-sized anatase TiO_2-substituted specimen: higher than that of nano-sized anatase TiO_2-substituted specimen, as previously mentioned. It is therefore reasonable to state that using nano-sized TiO_2, (the much finer fraction of the TiO_2) leads to better packaging of the grains, as expected and consequently improves the compactness of the microstructure of specimens because of its filler effect.

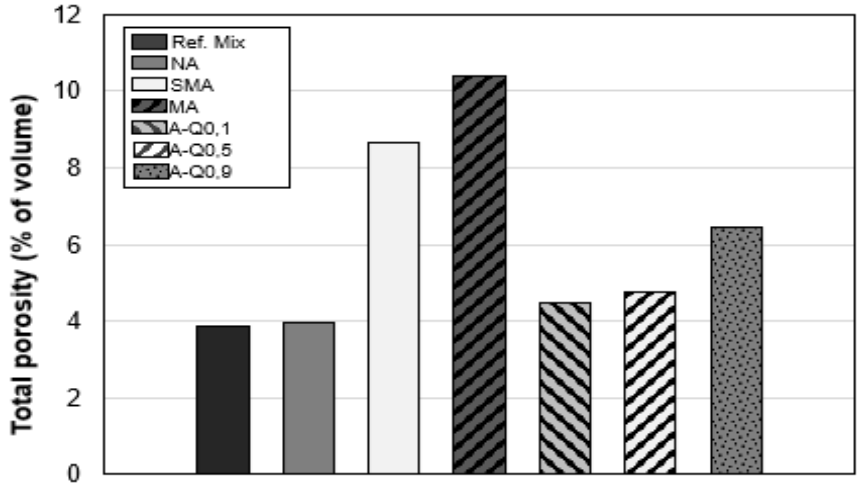

Figure 4.59. Total porosity (% of volume) of the anatase-substituted composites

The MIP test results of PSD-optimized specimens show that the number of pores below 50 nm in the mixtures prepared by using PSD moduli of 0.1 and 0.5 were 100% and the specimen incorporated with TiO_2 using a PSD modulus of 0.9 resulted in a lower rate of pores below 50 nm (64.8%) compared to other PSD-optimized mixtures (Figure 60-a). Total porosity values were 4.5%, 4.8% and 6.4% for the mixtures prepared by using PSD moduli of 0.1, 0.5 and 0.9, respectively; the increase in PSD modulus resulted in an increase in total porosity and proportion of pores above 50 nm. The probable reason for this is that the TiO_2 with the lower PSD modulus (q=0.1) contained a higher proportion of small particles, which can provide more closable smaller interparticle spacing, better

fill the voids between larger particles, and improve the packing density of the powder materials (TiO_2 and cement). Moreover, for the mixture prepared by using PSD moduli of 0.9, which contained the highest proportion of micron-sized TiO_2 particles among the PSD-optimized specimens, the small-sized TiO_2 content was not enough to fill the voids between large particles and thereby prevented significant improvement in packing density of the powder materials compared to other specimens prepared using a smaller PSD modulus. Consequently, these results show that PSD-optimized specimens have a relatively low amount of porosity compared to non-optimized specimens, except nano-sized anatase TiO_2-substituted specimen and PSD optimization significantly contributes to the pore refinement of mixtures, although the use of nano-sized TiO_2 alone performed slightly better.

Figure 4.59 and Figure 4.60 show a low amount of total porosity in NA and more small-size pores compared to the others, both of which indicate good packing density in favor of particle distribution homogeneity and higher compactness. Therefore, the relatively lower difference between NO_x degradation rates of NA and A-Q0.9 was most probably due to the surface of the nano-TiO_2 particles in NA being further covered with hydration products.

MIP test results of A-Q0.9 showed 6.4% total porosity and 64.8% pores below 50 nm, the highest total porosity and lowest number of pores below 50 nm among all the PSD-optimized specimens. This means that the PSD modulus of 0.9 provided a considerably higher number of pores above 50 nm, and that the amount/volume of pores dispersed throughout A-Q0.9 was relatively high compared to the other PSD-optimized specimens. Hence higher photocatalytic degradation capability of the A-Q0.9 compared to the other PSD-optimized specimens may stem from the larger number of pores limiting coverage of the TiO_2 particles with hydration product.

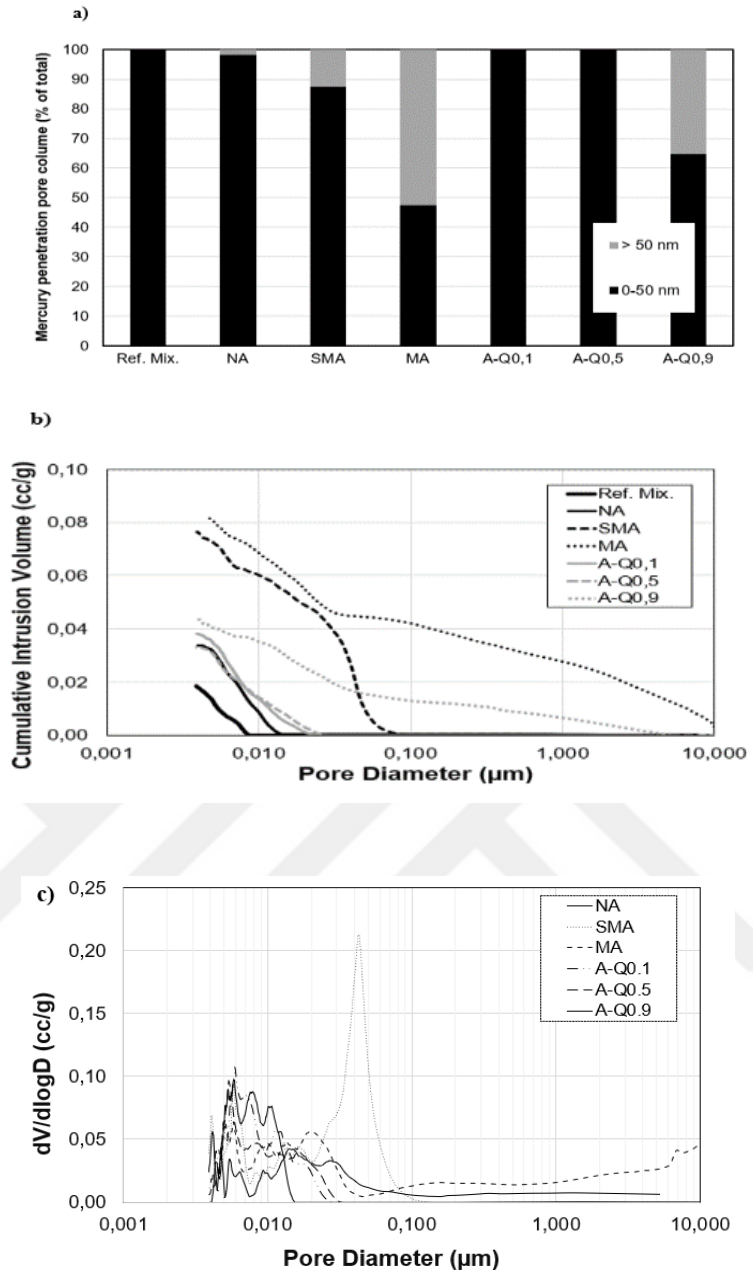

Figure 4.60. a) Mercury penetration pore volume (% of total), b) Pore size distribution curves of specimens, c) dV/dlogD (cc/g)

Figure 4.61 shows the relationship between the total porosity (% of volume) and NO_x degradation rate of specimens. Although MIP tests were carried out on 28-day specimens, total porosity (% of volume) of 28-day old specimens (considering that these reflect the tendency of specimens to 694 form pores), was associated with NO_x degradation results at all ages of relevant specimens. It can be seen from Figures 4.61.a and 4.61.b that the general trends of these two graphs are different from each other. According to Figure

4.61.a (non-optimized specimens), NO_x degradation had an inversely proportional relation to the total porosity of the specimen, whereas the opposite was the case with the PSD-optimized specimens in Figure 4.61.b. Considering the limitations of using trend lines to show the general trend of specimens, as well as the complexity of this situation due to the presence of many factors affecting the characteristics of the specimens, this requires a deeper, more careful assessment. In this regard, if NA is excluded, it can be clearly stated that the increased total porosity value contributes positively to photocatalytic degradation capability. NA not fitting this trend is due to its relatively smaller particle size TiO_2 content, resulting in higher NO_x degradation capability. The photocatalytic efficiency of a cementitious system is significantly related to factors such as physically and chemically effective factors including pore structure and quantity or NO_x degradation capability/efficiency in relation to photocatalyst particle size. When they were more dominant/prominent, the negative effect of comparatively less porosity on photocatalytic efficiency was not dominant enough for NA to cause lower degradation in the positive effect of finer TiO_2 particle content on photocatalytic efficiency compared to SMA or MA. However, this was not the case for PSD-optimized specimens. As mentioned earlier, the relatively higher presence of nano-TiO_2 content could not provide greater NO_x degradation results for PSD-optimized specimens. Increments in total porosity and the presence of pores above 50 nm had a greater effect on NO_x degradation capability of PSD-optimized specimens, indicating that more pores could lead to high photocatalytic efficiency for TiO_2-substituted cementitious systems.

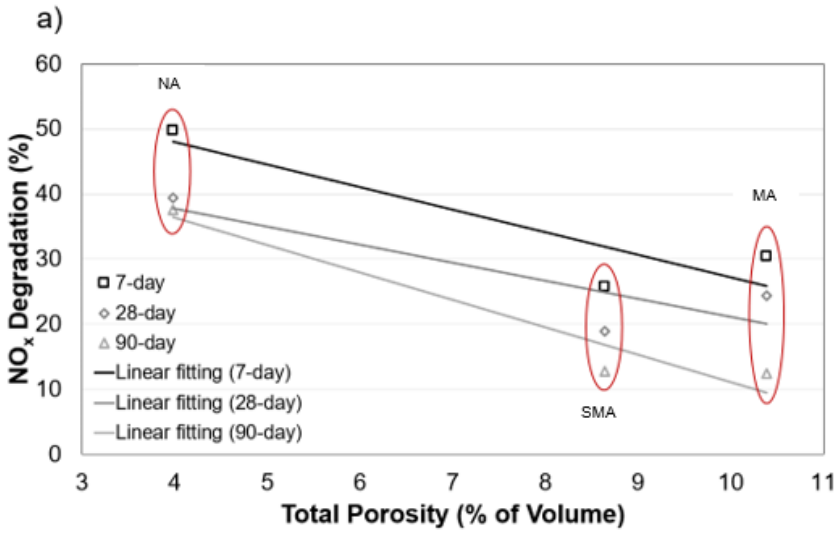

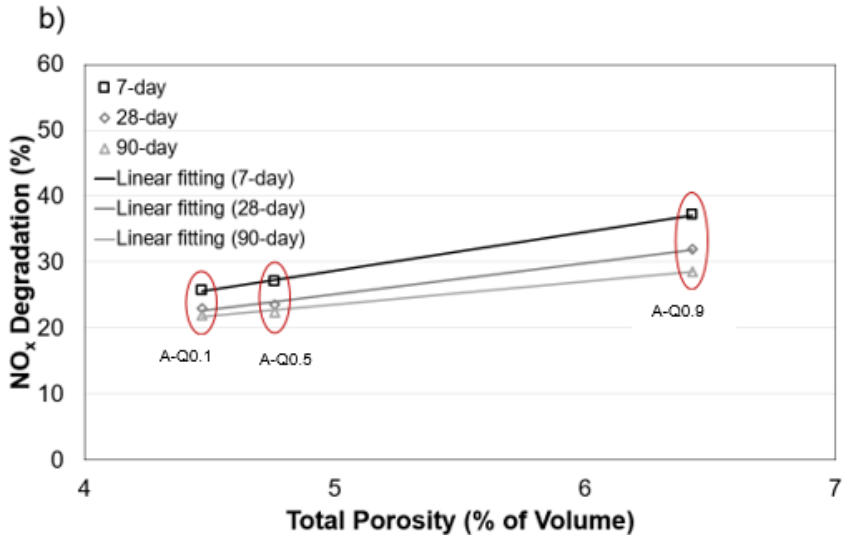

Figure 4.61. Relationship between total porosity (% of volume) and NO_x degradation rate of specimens for (a) PSD non-optimized specimens (b) PSD optimized specimens

Matrix transformations that also take place on the surface of the cementitious matrix with prolonged age mostly affect the photocatalytic activity of the specimens. The results of PSD-optimized specimens showed that optimizing the PSD of TiO_2 particles can limit the decrease in photocatalytic performance with further aging, such limitation was more pronounced for specimens with denser structure. These results revealed that a TiO_2 batch optimized with the proper PSD modulus could be used as a long-term, stable and efficient photocatalyst for air purification, with optimum performance in practical use.

Of the non-optimized specimens, those with denser structure (NA) also showed more stable photocatalytic efficiency over time. This could be because the dense structure of the specimens limits further coating of the already coated TiO_2 particles over time with further hydration and leads to less sensitivity to carbonation because their network of interconnected pores is more significantly developed than in mixtures with dense structure. Low efficiency of SMA and MA in terms of aged photocatalytic efficiency can be also attributed to their relatively high pore volume content. This situation was also valid for PSD-optimized specimens, even though it was more pronounced for non-optimized specimens. A-Q0.9, which has highest pore volume content among the PSD-optimized specimens, also showed more unstable photocatalytic degradation performance over time than denser PSD-optimized specimens.

High porosity allows further penetration of carbonation in deeper layers. By sanding the surface of specimens with lower pore volume, most of the carbonation product can be removed from the UV-reached surface, thereby freeing it of TiO_2 particles. In this way, photocatalytic reactions occurred due to a surface being free from carbonation product, and more stable specimens were obtained depending on time. Further investigations are necessary to clarify the effect of carbonation on NO_x photocatalytic efficiency of cementitious systems by considering its relationship with the pore structure characteristics of these systems.

4.3.3.5. Scanning Electron Microscopy (SEM) and Energy Dispersive X-ray Analysis (EDX)

Since the mixtures with the best results in the cement-binding systems developed within the scope of the study were the mixtures with anatase substituted, microstructural characterization was performed on the anatase substituted mixtures and whether the TiO_2 particles were homogeneously dispersed or not was determined by using scanning electron microscopy (SEM) analysis. In this context, the micron-sized images of the samples under SEM were taken, and the elemental distributions of the scanned areas were determined by Energy Dispersive X-ray Analysis (EDX).

SEM micrographs with EDX analyses, performed to determine the number of Ti elements dispersed throughout a specific section, were obtained for microstructural characterization studies of anatase TiO_2-based cementitious systems. Analyses of non-optimized and PSD-optimized specimens are shown in Figure 4.62 and 4.63, respectively. It can be clearly seen from these figures that carbon (C), oxygen (O), calcium (Ca) and silicon (Si) were the primary elements of all specimens, and substantial part of the chemical content of all specimens was composed of Ca and O. The C contents by weight of all specimens were lower than 9%. The Ti contents (by weight %) of nano-, submicron-, micron-sized anatase TiO_2-substituted specimens were 2.4, 1.7 and 4.9, respectively. When the EDX analyses of NA and MA in Figures 4.62 (a) and 4.62 (c) are evaluated, it is evident that the Ti content (by weight %) dispersed throughout the viewed section of NA (2.4%) was lower than that of MA (4.9%), possibly due to the denser structure of the NA. However, higher amounts of the Ti element throughout MA did not provide higher NO_x degradation results than in NA. This result also confirmed that smaller-size photocatalysts provide a more efficient photocatalytic degradation process than larger

ones. This was not the case when SMA and MA results were compared, which is likely related to the microstructural characteristics of these specimens. However, it should be kept in mind that EDX results of the equivalent specimens can vary according to the section viewed.

For the PSD-optimized specimens, Ti contents (by weight, %) of the mixtures prepared by using PSD moduli of 0.1, 0.5 and 0.9 were 1.9, 2.2, and 4.9, respectively. On the other hand, for PSD-optimized specimens, A-Q0.9 showed better NO_x degradation capability, even though it contained a significantly lower amount of nano-sized TiO_2 than the other PSD-optimized specimens. In addition, whereas the amount of nano-sized TiO_2 in NA was quite a bit larger than in A-Q0.9, a remarkable difference in the nano-sized TiO_2 content was not apparent when comparing NO_x degradation rates of these two specimens. This situation is directly related to specimen microstructure and surface characteristics and may be attributed to the ability of the mixtures, through PSD optimization of TiO_2 particles, to keep distribution and/or the amount of TiO_2 particles optimal throughout the UV-reached surface where photocatalytic reactions occur.

Although the amount of photocatalyst located across the surface reachable by UV-radiation has an undeniable influence on photocatalytic performance of cementitious systems, there was no obvious correlation between the amount of photocatalyst and the photocatalytic degradation rate of specimens. Considering that photocatalytic efficiency of TiO_2 particles can be affected by their crystal structure, surface area and particle size (Cirkva and Žabová, 2010), the NO_x degradation results should be associated with the higher presence of small-sized TiO_2 on the UV-reached surface, which resulted in increments in the number of active surface sites and thereby high separation and transfer efficiency of surface charge carriers.

EDX elemental mapping images of relevant specimens are also illustrated in Figure 4.62-63: red corresponds to Ti atoms and green to Ca atoms. One of the main elements (Ca) was detected in all regions of the specimens. Based on the evidence in these images, Ti elements have more uniformly dispersed throughout the PSD-optimized specimens. For the non-optimized specimens, the distribution of the Ti atoms on the surface of nano-, and micron-sized anatase TiO_2-substituted specimens was also generally homogeneous,

although some irregularities in the distribution of the TiO_2 particles were seen in the microstructure of submicron-sized anatase TiO_2-substituted specimen.

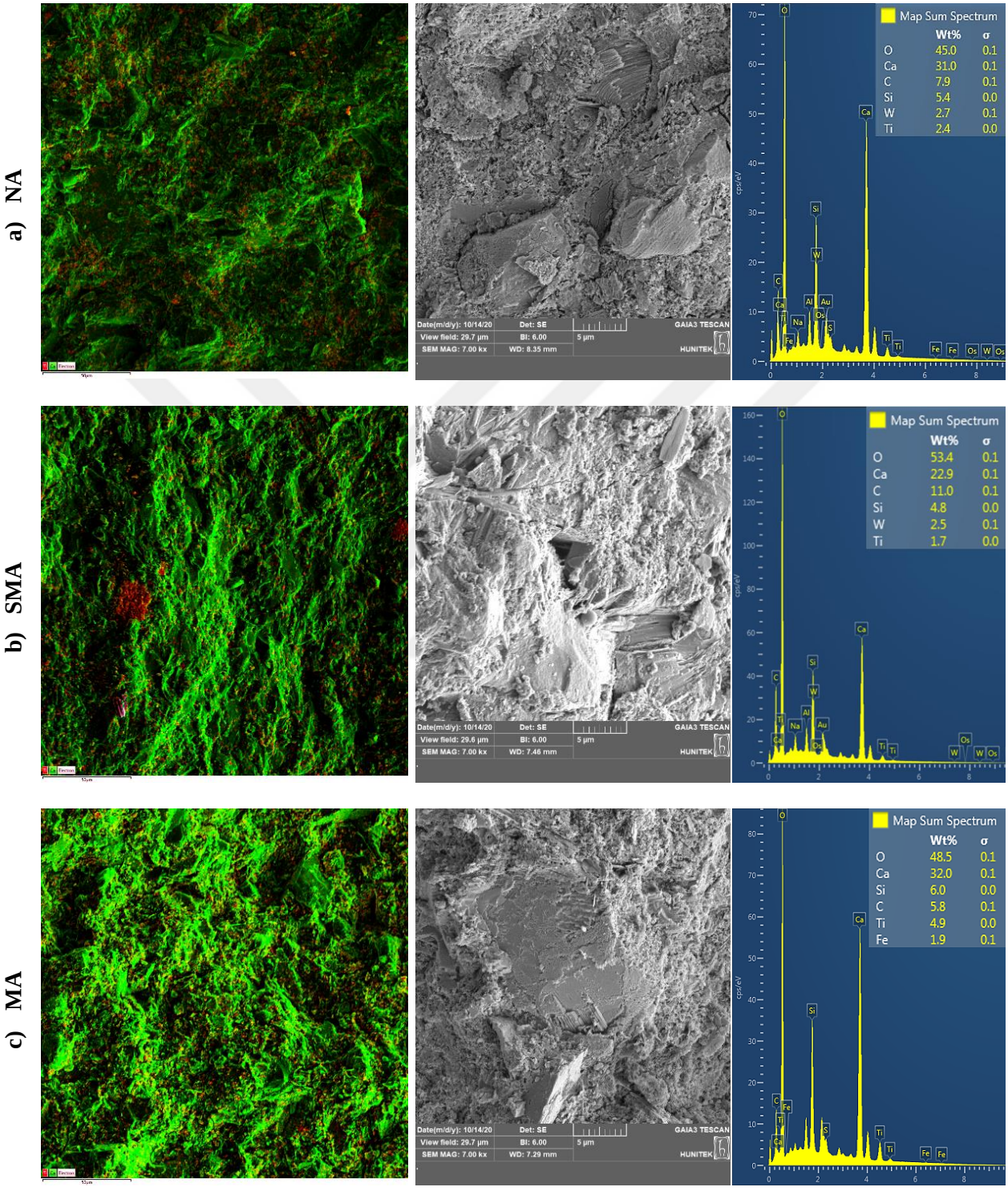

Figure 4.62. Representative EDX elemental mapping images and SEM micrographs with EDX spectra of non-optimized specimens

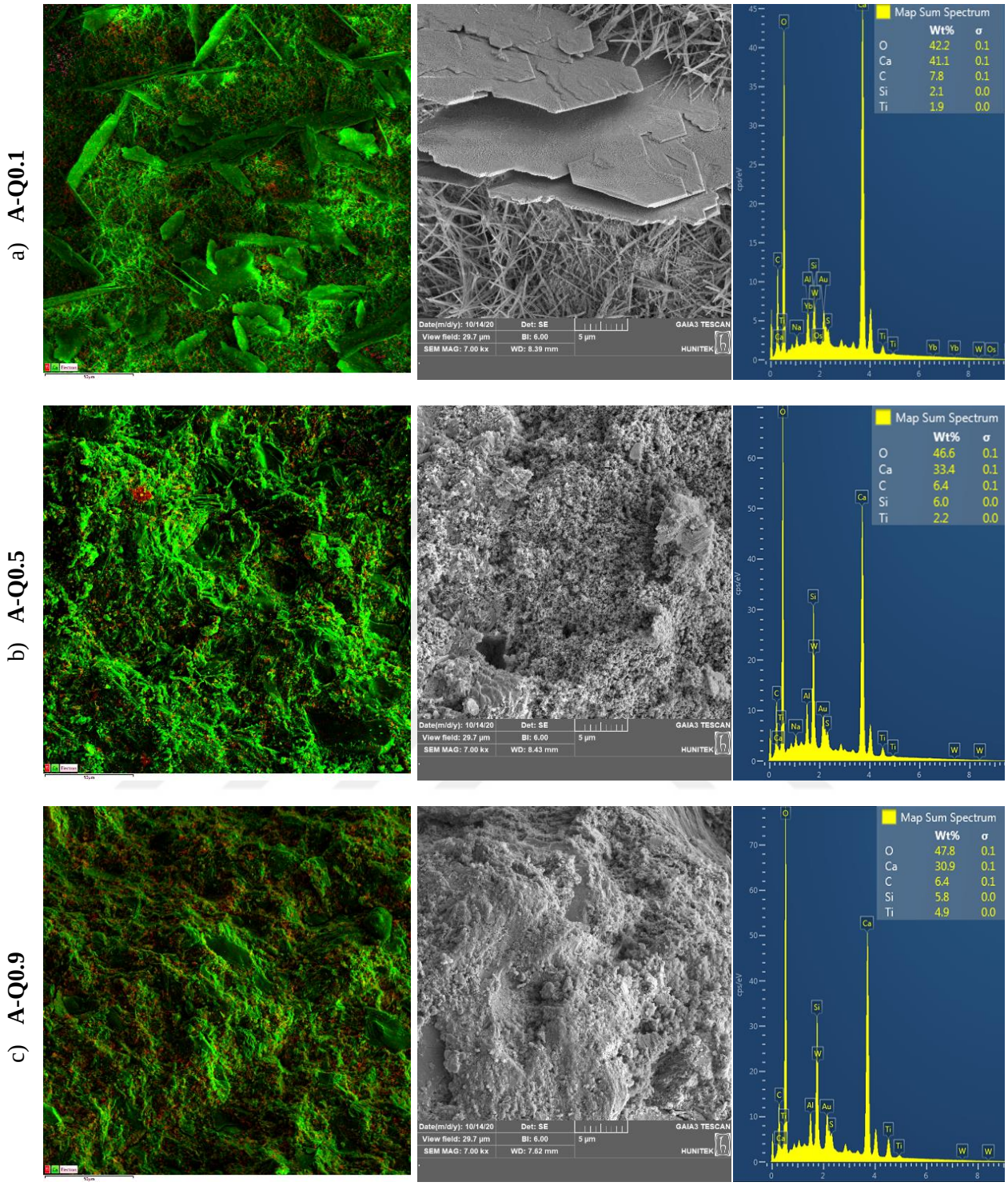

Figure 4.63. Representative EDX elemental mapping images and SEM micrographs with EDX spectra of PSD-optimized specimens

4.4. Determination of the Optimum Combination of Anatase- and Rutile-Phase TiO_2 in Photocatalytic Cement-based Systems

4.4.1. Introduction

Titanium is the fourth most common metal element in the world after aluminum, magnesium and iron. There are three crystalline phases of TiO_2 in nature, under atmospheric pressure; rutile (tetragonal), anatase (tetragonal), and brookite (orthorhombic) (Gamboa and Pasquevich, 1992; Mo and Ching, 1995; Ding et al., 1996; Ghosh et al., 2003; Smith et al., 2009). The generation of brookite phase is more difficult, therefore, its presence is less common compared to other natural phases of TiO_2, which led researchers to focus on more common phases of metastable anatase and stable rutile. Given both anatase and rutile phases of TiO_2 are thermally/chemically stable, have high oxidation capability, permeability against visible rays and high hydrophilic properties, their use as photocatalytic materials in numerous applications has been more common compared to other semi-conductive photocatalysts (Sakai et al., 2004; Banerjee et al., 2006; Ohtani et al., 2010). It is generally reconciled that anatase has a more effective photocatalytic degradation capability (Brown et al., 1985; Sclafani et al., 1990; Tanaka et al., 1991). Despite this general agreement in the literature, it has also been reported by several other researchers that rutile has a better photocatalytic activity than anatase (Mills et al., 2003; Watson et al., 2003; Jia et al., 2018; Vijayarangamuthu et al., 2018). Furthermore, a number of studies have reported that the combined use of anatase and rutile phases leads to a better photoelectrochemical activity and degradation of pollutant compounds than the single use of anatase phase (Bacsa and Kiwi, 1998; Muggli and Ding, 2001; Onho et al., 2001; Poon and Cheung, 2007; Kim and Ehrman, 2009).

As results of several literature studies show, the combined utilization of anatase- and rutile-phase TiO_2 materials in photocatalytic cement-based systems can be beneficial for obtaininig better photocatalytic degradation performance. In this regard, at this stage of the experimental studies, by using experimental-based material design approach, it was aimed to determine the optimum combination of anatase- and rutile-phase TiO_2s to be used in the cement-based systems in favor of higher efficiency.

4.4.2. Experimental Studies

At this step of the experimental studies, mixtures were prepared using the fifth mixing method which was determined as the best mixing method (in Section 4.1). A constant water to powder ratio of 0.35, by weight for all mixtures, TiO_2 utilization rate of %5 (by total weight of powder materials) (determined as optimum utilization rate in Section 4.2) and PSD modulus of 0.9 (determined as optimum PSD modulus in Section 4.3) were used for the preparation of the mixtures. Six different types of TiO_2 (nano-, submicron-, micron-sized anatase and rutile TiO_2 powders) were used in combination.

To study the influence of co-utilization of different-phase TiO_2 particles on the mechanical properties and photocatalytic efficiency of the cementitious systems, each phase of TiO_2 (nano-, submicron-, micron-sized anatase and rutile TiO_2 powders) firslty was combined by using the PSD modulus of 0.9. Then, obtained anatase and rutile-phase TiO_2 powder batches were used in combination to prepare TiO_2-substituted cement-based systems. In this regard, cement paste mixtures containing the combination of anatase- and rutile- TiO_2 particles were produced in different utilization rates (anatase:rutile-"80:20", "50:50", "20:80"). The effects of the co-utilization of different-phase TiO_2 particles on the mechanical properties (compressive strength), and NO_x degradation capability were investigated.

4.4.3. Experimental Study Results and Discussion

4.4.3.1. Compressive Strength

To determine the optimum combination of anatase- and rutile-phase TiO_2s in cement-based systems and the effect of the co-utilization of different-phase TiO_2 particles on the mechanical properties of the cement-based systems, the compressive strength of the mixtures containing anatase-rutile combination of "80:20", "50:50", "20:80" (at the utilization rate of 5% by weight of the powder materials and prepared by using the PSD modulus of 0.9) for different curing ages was determined. The compressive strength results are presented in 4.64. Test results of the mixtures prepared by solely using anatase- and rutile-phase TiO_2s with the PSD modulus of 0.9 (presented in previous section) were also included in this figure for easy comparison of their properties. Considering the differences in compressive strength depending on the combination rates, the mechanical performances of the TiO_2-substituted cement-based systems were evaluated.

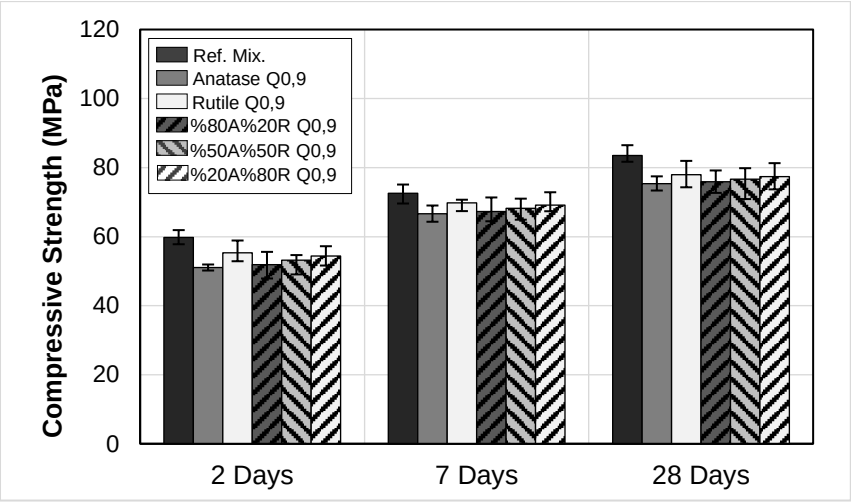

Figure 4.64. Compressive strength results of the mixtures containing anatase-rutile combination

When the compressive strength results of the mixtures containing anatase-rutile combination are evaluated from Figure 4.64, it can be seen that, due to ongoing hydration reactions, the extended aging/curing resulted in continuous increments in the compressive strength results, irrespective of mixture parameters. According to the compressive strength test results of the mixtures produced by using the anatase-rutile combination, generally, differences in compressive strength values of the mixtures were quite low. When the 2-day compressive strength results were examined, the highest compressive strength was obtained with 55.28 MPa in the only rutile-containing composite. In the compressive strengths of 7 and 28-day composites, the highest compressive strengths were also obtained from this composite. These values are respectively; 69.80 and 77.90 MPa. In combination cases, the compressive strength relatively increased with the increase of the rutile substitution ratio. The highest compressive strength results were obtained from the the composite containing 20% anatase and 80% rutile phase for each curing age. Even in this composite, the compressive strength results lagged behind the reference mixture.

4.4.3.2. Photocatalytic Performance

The photocatalytic performance of the mixtures containing anatase-rutile combination of “80:20”, “50:50”, “20:80” (at the utilization rate of 5% by weight of the powder materials and prepared by using the PSD modulus of 0.9) for different curing ages were determined. The NO_x, NO, and NO_2 concentration profiles obtained during the NO_x degradation tests under illumination are presented in Figure 4.65. In addition, NO_x and NO degradation and

NO_2 formation rates (in percentage) of the developed systems together with the system selectivity values are summarized in Figure 4.66. Test results of the mixtures prepared by solely using anatase- and rutile-phase TiO_2s with the PSD modulus of 0.9 (presented in previous section) were also included in this figure for easy comparison of their properties. Considering the differences in NO_x and NO degradation and NO_2 formation rates depending on the combination rates, the performances of the TiO_2-substituted cement-based systems were evaluated.

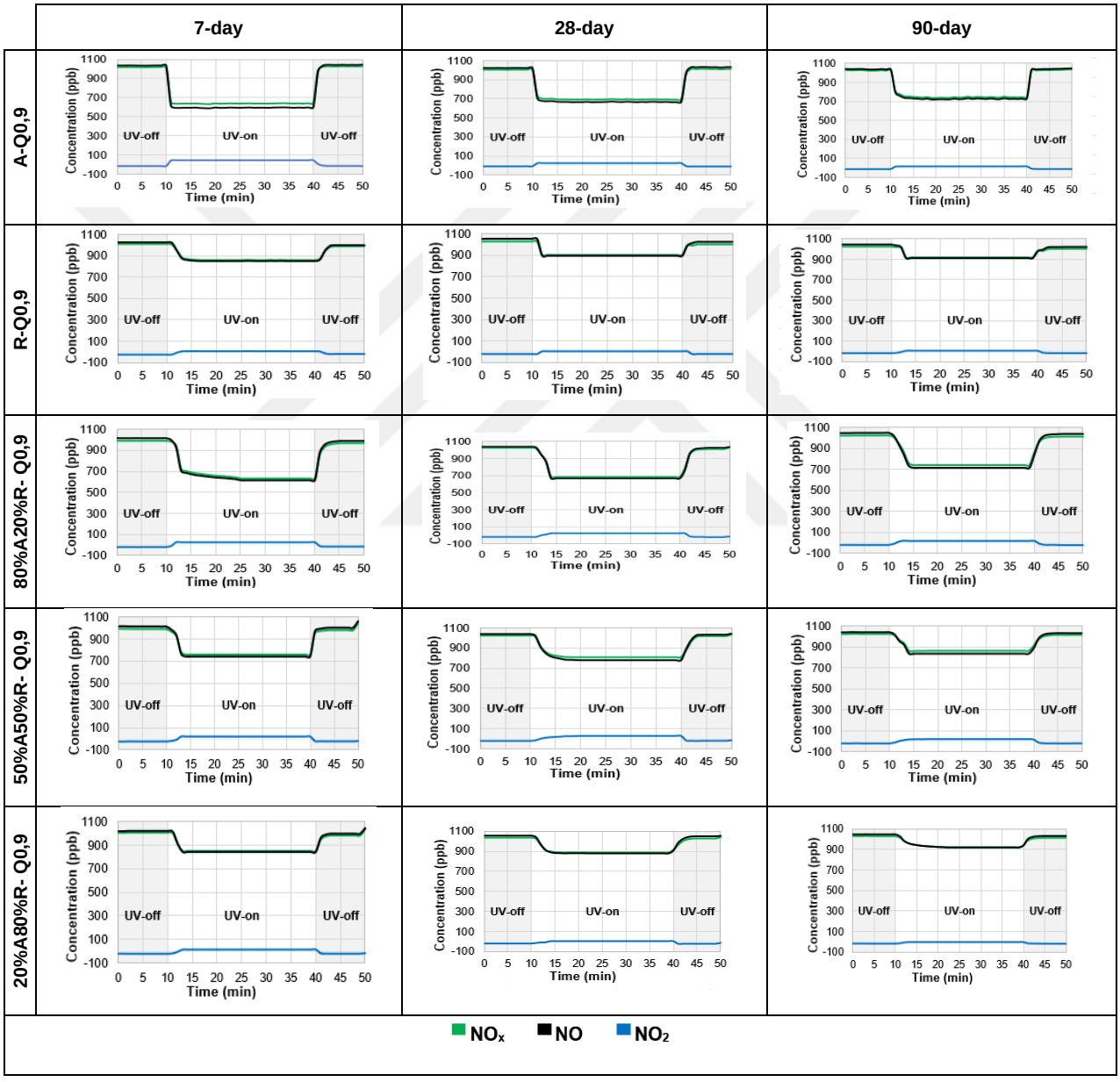

Figure 4.65. Variation of NO_x, NO, and NO_2 concentrations during each test for 7, 28, and 90-day-old specimens of composites containing anatase-rutile combination of "80:20", "50:50", "20:80"

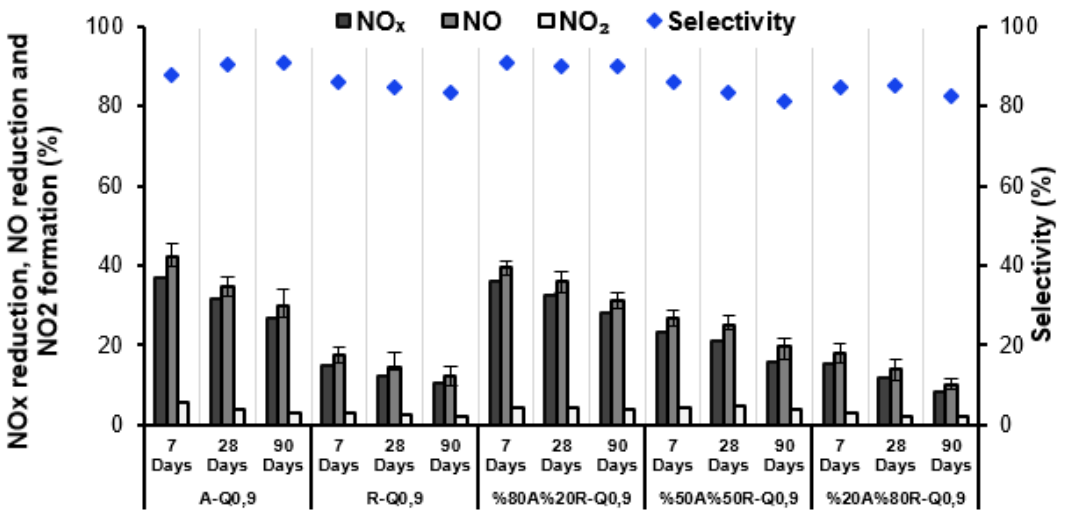

Figure 4.66. For 7, 28, and 90-day-old specimens of composites containing anatase-rutile combination of "80:20", "50:50", "20:80", the rate of NO_x reduction, NO reduction, and NO_2 conversion in each test, and the system selectivity (%).

When the degradation rates of 7-day, 28-day and 90-day-old specimens of composites containing anatase-rutile combination of "80:20", "50:50", "20:80" are evaluated from Figure 4.66, regardless of combination rares, the utilization rate of TiO_2, it can be seen that NO_x and NO reduction rates decreased with the prolonged curing age. At the end of the 7-day curing age, the highest photocatalytic performance (NO_x reduction rate) (36.9 %) was obtained from the anatase TiO_2-substituted mixture prepared with PSD modulus of 0.9. However, at the end of the curing age of 28 and 90 days, the highest photocatalytic performance performances (NO_x reduction rate) were obtained from the mixture containing anatase-rutile combination of "80:20" (32.6 % and 27.9% respectively). This situation is directly related to the excess amount of anatase-phase TiO_2. In addition, as mentioned before, the photocatalytic efficiency (system selectivity) of the anatase TiO_2-substituted mixture increased continuously with the prolonged curing age. In the composite in which only the rutile phase is used and in the composites of the combinations, the selectivity generally decreased with prolonged curing age. The highest selectivity value in 7-day composites was obtained from the mixture containing "80:20" anatase-rutile combination (90.9%). In combinations, highest selectivity at each curing age (7-day, 28-day, and 90-day) was obtained from the mixtures containing the 80:20" anatase-rutile combination. These values are 90.9%, 90.0% and 89.9%, respectively.

Besides, as the rutile substitution rate increased, there was a significant decrease in photocatalytic performance and efficiency.

As a result, at the end of the curing age of 28 and 90 days, the highest photocatalytic performance performances (NO_x reduction rate) were obtained from the mixture containing anatase-rutile combination of "80:20", which is the closest combination to the Degussa P25 in terms of content.

5. CONCLUSION

Within the scope of this thesis study, the main focus was to develop new generation TiO_2-substituted cement-based systems with efficient photocatalytic degradation capability by using a multi-scale design approach without endangering engineering properties. To do this, compherensive experimental studies were performed by producing specimens in different scenarios. Mechanical properties (compressive strength), physical properties (pore volume and pore size distribution), hydration kinetics and NO_x degradation capability of the developed specimens were investigated. In addition, microstructural features of specimens were examined by microstructural characterization analyses. The important results obtained within the scope of the thesis studies are presented under sub-headings.

Determining the Best Mixing Method

At this stage of the thesis, the best mixing method was determined by planning the development of new generation cement-based systems with TiO_2 substituted by using a multi-scale design approach without sacrificing engineering properties. The important results obtained at this stage, where the best mixing method is determined, are presented below.

- The ultrasonic mixer should be operated at 80% amplitude and 1900 J energy level in order to get the best performance from the ultrasonic mixing technique.
- Considering the suspended period of TiO_2 particles, it can be stated that the single use of PAA provides better dispersion and suspension stability than that of PCE at the same utilization rate.
- Considering the zeta potential values and suspension stability properties obtained according to the utilization rates of the surfactant materials, it can be stated that the ideal utilization rates for singly-utilized PCE and PAA are 1% and among 0.5-1%, respectively. In the case of co-utilization of PCE and PAA, it was observed that the suspension is more stable when the total utilization rate is 1-1.5%.
- The co-utilization of PAA and PCE at the utilization rate of 1% (0.5+0.5) resulted that the nanoparticles remain suspended in solution for a very long time.
- The singly utilization of surfactant materials (1% PCE or 0.5% PAA) in the mixture, especially in the early hydration period, delayed the occurrence of peak

of the rate of hydration and caused a decrease in the cumulative heat of hydration released. However, this effect reduced over time.

- Although there are some natural variations when the whole curing ages are taken into account, the highest compressive strength values were obtained from the mixtures prepared with first mixing method while the lowest ones were obtained from those prepared with fourth mixing method (for anatase and rutile, separately).
- Unlike the anatase- and rutile-phase TiO_2-substituted composites, as a striking point, although there are some natural variations when the whole curing ages are taken into account, the Degussa P-25 TiO_2-mixtures made using the fifth mixing technique had the greatest compressive strength values, while those prepared using the fourth mixing method had the lowest.
- At the end of 180-day curing age, the electrical impedance values of nano-anatase TiO_2-substituted cementitious composites prepared by using the first, second and third mixing methods ranged between 10570 Ω and12567 Ω, while those prepared by using fourth and fifth mixing methods were 3630 Ω and 3075 Ω, respectively.
- While the electrical impendance values of 180-day-old specimens prepared with nano-anatase TiO_2-substituted cementitious composites were more than 10000 Ω for the first, second and third mixing methods, the electrical impedance values for the the first, second and third mixing methods in nano-rutile TiO_2-substituted cementitious composites were recorded as 8050 Ω, 6071 Ω and 7500 Ω, respectively. The 180-day electrical impedance values of the nano-rutile TiO_2-substituted cementitious composites prepared by using fourth and fifth methods were recorded as 2650 Ω and 1950 Ω, respectively.
- The fifth mixing method is the most effective in terms of decreasing the electrical impedance of TiO_2-substituted composites.
- The electrical impedance values of nano-rutile TiO_2-substituted specimens were lower than those of nano-anatase- and Degussa P25 (containing approximately 80% anatase- and 20% rutile-phase TiO_2)-substituted specimens.
- Nano-sized TiO_2 particles are more uniformly dispersed throughout the composites prepared by using fifth mixing methos. Because this mixing method resulted in an increase in the electrical conductivity by forming additional conductive paths with semiconductor TiO_2 particles via homogenous dispersion of them throughout the matrix.

- The nano-anatase TiO_2-substituted composites prepared by using fifth mixing method had the largest NO_x reduction rates for each curing age. NO_x reduction rates of the 7-, 28-, and 90-day-old nano-anatase TiO_2-substituted composites prepared by using fifth mixing method were obtained as 47.9%, 38.8%, and 37.3%, respectively. Additionally, at the conclusion of the 90-day curing period, the composites made utilizing the fifth mixing procedure had the greatest system selectivity (85.8 %). Therefore, it is thought that the fifth mixing method among all mixing methods provides a more homogeneous distribution of TiO_2 particles thoroughout TiO2-substituted composites.
- The composites prepared by using fifth mixing method achieved the highest NOx reduction rates for each curing age (for rutile phase). The 7, 28, and 90-day NO_x reduction rates of the composites prepared by using fifth mixing method were recorded as 18.5%, 15.4%, and 8.6%, respectively. At the conclusion of the 90-day curing period, the composites made utilizing the fifth mixing procedure had the greatest system selectivity (85.6%). Therefore, it is thought that the fifth mixing method among all mixing methods provides a more homogeneous distribution of TiO_2 particles thoroughout TiO2-substituted composites.
- When the degradation rates of 7-day, 28-day and 90-day-old Degussa P 25 TiO_2-substituted specimens are evaluated, as in the nano-rutile and nano-anatase TiO_2-substituted specimens, the specimens prepared by using fifth mixing method achieved the highest NO_x reduction rates for each curing age. The 7, 28, and 90-day NO_x reduction rates of the composites prepared by using fifth mixing method were recorded as 38.1%, 31.9%, and 30.5%, respectively. At the conclusion of the 90-day curing period, the composites made utilizing the fifth mixing procedure had the greatest system selectivity (85.9%).
- Considering the compressive strength values, electrical properties, and photocatalytic performances of the specimens prepared by using five different methods, the fifth mixing method was the best method providing more homogeneous dispersion of TiO_2 particles.

Determination of Critical Usage Rate

At this stage of the thesis, it was aimed to determine the optimum usage rates in cases where nano, sub-micron, and micron sizes are used individually. In this context, composites were produced by substituting TiO_2 particles in different phases and with

different particle sizes in the cement binder system at the rates of 2.5%, 5%, 7.5% and 10%. The important results obtained within this section are listed below.

- Nano-sized anatase-phase TiO_2-substituted mixtures had a higher rate of hydration and reached rate of hydration peak earlier compared to the reference mixture (without TiO_2) when the utilization rate of TiO_2 exceeded the rate of 7.5%. As a striking point, although the highest rate of hydration was obtained from the mixture prepared by using 10% nano-sized anatase-phase TiO_2, the mixture prepared by substituting 2.5% nano-sized anatase-phase TiO_2 reached hydration peak earliest.
- Although mixtures with higher rate of hydration were obtained when the utilization rate of nano-sized anatase-phase TiO_2 exceeded 7.5%, higher compressive strength results were obtained from the reference mixture and the mixture prepared by using 2.5% nano-sized anatase-phase TiO_2.
- The composites prepared by using submicron-sized anatase-phase TiO_2 powder exhibited lower hydration peak magnitudes compared to those prepared by using nano-sized one. As with nano- and submicron-sized anatase-phase TiO_2-substituted cement-based materials, the rate of hydration peak values rose as the TiO_2 usage rate increased. However, it was determined that even at the micron-sized anatase-phase TiO_2 utilization rate of 10%, the hydration peak level obtained from the reference mixture (without TiO_2) could not be reached.
- In general, it was determined that utilization of anatase-phase TiO_2 resulted in reaching rate of hydration peak earlier compared to the reference mixture (without TiO_2). This indicates that TiO_2 substitution accelerates early age hydration.
- The increase in the particle size of TiO_2 particles (from nano to micron size) resulted in reaching rate of hydration peak later and a lower rate of hydration.
- As with nano-sized anatase and rutile TiO_2-substituted cement-based systems, the inclusion of submicron- and micron-sized TiO_2 up to a certain point of utilization rate resulted in increased compressive strength values when compared to the reference mixture (without TiO_2). The highest compressive strength values were achieved at a given point of usage rate of 2.5%.
- According to compressive strength results, highest strength was obtained in composites using nano-sized TiO_2. Relatively less strength was obtained in the sub-micron size, and the least strength was obtained in the micron-size substitution.

- Highest 28-day-old electrical impedance results were obtained from the specimens prepared with the TiO_2 utilization rate of the 2.5%, regardless of the particle size range of TiO_2 used. The electrical impedance values decrease as the rate of substitution increases from 2.5% to 7.5%. (For different size of anatase phase). On the other hand, with an increase in the utilization rate from 7.5% to 10%, there was a considerable rise in electrical impedance values (This is valid for the anatase/rutile phase.).
- The increment in the particle size of the anatase or rutile-phase TiO_2 substituted, the electrical impedance results also increased. According to the electrical impedance results of the 28-day-old specimens, the highest values were obtained from the micron-sized anatase TiO_2-substituted composites.
- When the results are evaluated comparatively, it can be observed that lower electrical impedance values (higher conductivity) were obtained from rutile TiO_2-substituted cementitious composites compared to anatase TiO_2-substituted ones.
- At the conclusion of the 90-day cure period, the highest NO_x reduction rate (37.3%) and system selectivity value (85.6%) were obtained from 5% nano-sized TiO_2-substituted cement-based systems. This means that the utilization rate of 5% for nano-sized TiO_2 provides a more effective photocatalytic degradation process.
- In contrast to the presence of a diffraction point where the trend (increase in NO_x reduction rates with the increment in the TiO_2 utilization) reversed after a specific point (at the utilization rate of 5% of the total binder weight) in nano-anatase-substituted mixtures, for the submicron-anatase TiO_2-substituted specimens, NO_x reduction rates increased continuously with the increment in the TiO_2 usage rate.
- At the end of 90 days, the highest NO_x reduction rate (22.3%) was obtained from 10% submicron-sized anatase TiO_2-substituted cement-based system although the highest system selectivity value (87.8%) was obtained from the mixture with 5% TiO_2-substituted one. Although the highest NO_x reduction rate was obtained from 10% submicron-sized TiO_2-substituted cement-based system, considering its higher system selectivity, it can be said that 5% submicron-sized TiO_2-substituted cement-based system exhibited the optimum photocatalytic performance.
- At the end of 90 days, the highest NO_x reduction rate (14.4%) was obtained from 7.5% micron-sized anatase TiO_2-substituted cement-based system although the highest system selectivity value (90.2%) was obtained from the mixture with 5% TiO_2-substituted one. As a result, although the highest NO_x reduction rate was

obtained from 7.5% micron-sized TiO_2-substituted cement-based system, considering its higher system selectivity, it can be said that 5% micron-sized TiO_2-substituted cement-based system exhibited the optimum photocatalytic performance.

- When considering the results obtained from the anatase TiO_2-substituted specimens, it is thought that the TiO_2 substitution rate of 5% was ideal because of superior characteristics of 5% TiO_2-substituted systems in terms of cost effectivenes, mechanical properties and photocataliytic performance-related issues.
- In general, the photocatalytic activity of nano-rutile-containing mixtures lagged far behind nano-anatase TiO_2 containing mixtures. The differences between the photocatalytic activities of the anatase and rutile phases of TiO_2 particles are directly related to their crystal structures.
- At the end of 90-day curing age, the highest NO_x reduction rate (8.6%) and system selectivity value (85.6%) were obtained from 5% nano-sized rutile TiO_2-substituted cement-based systems. This means that the utilization rate of 5% for nano-sized TiO_2 provides a more effective photocatalytic degradation process. (for rutile phase)
- Among the all rutile TiO_2-substituted cement-based composites, the lowest reduction rates were obtained from the micron-size rutile TiO_2-substituted ones.
- NO_x reduction rates of the micron-sized rutile TiO_2-substituted specimens generally increased with the increment in TiO_2 substitution rate up to 5% of the total binder weight. Beyond the 5% TiO_2 substitution rate, the NO_x reduction rates of the micron-sized rutile TiO_2-substituted specimens decreased.
- NO_x reduction rates (in percentage) of the Degussa P25 TiO_2-substituted cement-based systems increased with the increment in TiO_2 usage rate up to 7.5% of total weight of binder and displayed opposite trend after this point.
- At the end of 90 days, the highest NO_x reduction rate (31.3%) and system selectivity value (86.5%) were obtained from the 7.5% Degussa P25 TiO_2-substituted cement-based system. However, the NO_x reduction rate (30.5%) and system selectivity (85.9%) of the the 5% Degussa P25 TiO_2-substituted cement-based system were really close to the those of 7.5% Degussa P25 TiO_2-substituted one.

- Exceeding a certain critical utilization rate resulted in relatively lower photocatalytic degradation caspability because of agglomeration issues with small-sized TiO_2 particles and generated instability throughout the matrix.
- Considering all results, optimum TiO_2 utilization rate was determined as 5%.

Determination of Optimum TiO_2 Particle Size Distribution

At this stage of the thesis, it was aimed to determine the optimum PSD when nano, sub-micron and micron sizes are used together. In this context, the PSDs of TiO_2 particles in different phases were optimized using different PSD modules (Q0,1, Q0,5, and Q0,9). The important results obtained within this section are listed below.

- Although reference specimen non-containing TiO_2 was not the specimen which reached rate of hydration peak earliest, the highest rate of hydration peak value was obtained from this specimen. This result can be attributable to the relatively higher cement content of the reference specimen compared to those of TiO_2-substituted specimens.
- Among the non-optimized specimens (specimens prepared by using nano-, submicron, micron-sized anatase TiO_2 powders, solely), nano-sized anatase TiO_2 addition resulted in an earlier and higher rate of hydration peak compared to submicron- and micron-sized anatase TiO_2s, probably due to a more effective nucleation effect provided by significantly smaller particles of nano-sized anatase TiO_2.
- Incorporating nano materials with extremely small particle size has a hydration agitation and acceleration effect. This caused higher heat of hydration for the cementitious system containing nano-sized anatase TiO_2 than for the pastes with submicron- and micron-sized anatase TiO_2s, especially between 8-48 hours of hydration. However, the heat of hydration values of nano-, submicron-, micron-sized anatase TiO_2-substituted mixtures were similar at the end of 72 hours of hydration.
- The apparent first delay effect-in which a longer induction period is observed but without a decreased rate of peak heights for the mixtures prepared by using three different PSD moduli of 0.1, 0.5 and 0.9 may be attributed to retardation of cement grains dissolution because of residual inorganic substances. However, these retardations were not effective on non-optimized TiO_2 used paste mixtures. This

could be attributed to effects of PSD which lead more densify structure and covering more cement grain in fresh stages, hence results more retardation effects and less dissolution of particles in initial duration.

- When comparing the influence of PSD modulus on the rate and heat of hydration, increasing PSD modulus of TiO_2 particles from 0.1 to 0.9 made no considerable difference. Besides, TiO_2 addition with varying PSD moduli concluded a higher heat of hydration than submicron- and micron-sized anatase TiO_2 for hydration time of up to 48 hours. However, the reverse was true thereafter. This finding indicates that using nano-, submicron- and micron-size particles, mixed to provide varying PSD moduli, is highly effective on the rate and total heat of hydration at early periods before 48 hours.
- Among the non-optimized specimens (specimens prepared by using nano-, submicron, micron-sized anatase TiO_2 powders, solely), it was evident that those containing nano-sized anatase TiO_2 showed the highest compressive strength results for each curing age. The compressive strength values of nano-sized anatase-phase TiO_2-incorporated specimen for 2-day, 7-day and 28-day curing ages were 55.40, 66.00 and 77.63 MPa, respectively. The probable reason for this behavior is that nano-sized powders create higher density due to the filler effect arising from comparatively smaller particle sizes. This behavior can also be attributed to the seeding effect, which is the formation of additional area (nucleation sites) due to the extremely fine particle size of nano materials (and thereby their high surface area) that can pull unhydrated cement particles towards themselves, resulting in more suitable places for the precipitation of hydration product.
- In the PSD-optimized specimens (the mixtures prepared by using three different PSD moduli of 0.1, 0.5 and 0.9), although there was no important difference in their compressive strength values, the mixture prepared by using PSD moduli of 0.1 had the highest compressive strength values at approximately 52.10 (2-day), 65.82 (7-day) and 78.01 MPa (28-day), for almost all curing ages except for 7 days.
- After 28 days, A-Q0.1 had the highest compressive strength of the PSD-optimized specimens. It is worth noting that A-Q0.1 has a greater compressive strength than NA, which may be ascribed to its well-graded PSD reaching a high particle packing density.

- The compressive strength values of the mixture containing nano-sized rutile TiO_2 were recorded as 57.3, 70.10 and 79.0 MPa for the curing ages of 2, 7, and 28-day, respectively. This is because of that the rutile phase TiO_2 contributes much more to strength than the anatase phase TiO_2 at each curing age.
- Apart from nano size, it has been observed that composites using PSD modulus provided better compressive strength compared to single size uses (submicron and micron) (for rutile phase).
- PSD optimization has a positive effect on compressive strength. At the conclusion of 28 days, the compressive strengths of the rutile-substituted samples produced with PSD optimization (Q 0.1, 0.5 and 0.9) were determined as 75.27, 76.74 and 77.90 MPa, respectively. In other words, higher compressive strength was obtained in the composite containing less nano-sized material.
- The compressive strength of the reference mixture without TiO_2 (Ref. Mix.) was the highest among all mixtures, regardless of the curing ages.
- Submicron- and micron-sized anatase-phase TiO_2-substituted composites showed considerably lower photocatalytic degradation performance than nano-sized anatase-phase TiO_2-substituted one, with the differences in degradation results becoming significantly more pronounced with longer curing periods.
- Among the PSD-optimized specimens, photocatalytic degradation rates of the mixture prepared by using PSD moduli of 0.9 were the highest for all curing ages and after that, in decreasing order, those of for the mixture prepared by using PSD moduli of 0.5 and for the mixture prepared by using PSD moduli of 0.1.
- All specimens degraded photocatalytically at a decreasing pace from 7 to 90 days. This time-dependent trend may have come from the ongoing hydration reaction, leading to the coating of TiO_2 particles with further hydration product and thereby reducing the presence of TiO_2 materials on specimen surfaces reached by UV irradiation. A more likely reason is that carbonation products, produced by binding carbon dioxide (CO_2) into solid carbonates on the specimen surface or another possible process, cause the specimen surface to be coated.
- The rate of decrement in photocatalytic degradation results of non-optimized specimens from 7 to 28 days was more evident than in PSD-optimized specimens. With further aging of specimens beyond 28 days, the rate of decrement in photocatalytic degradation results of submicron- and micron-sized anatase-phase TiO_2-substituted composites was significantly higher than in other specimens.

- When the cementitious systems' system selectivity was evaluated, it was clearly evident that the system selectivity of all specimens increased incrementally from 7 to 90 days (Applicable to the anatase phase).
- In terms of NO_x and NO reduction, although the nano-sized anatase-phase TiO_2-substituted specimen was exhibited better performances, the higher selectivity values were obtained from the PSD-optimized specimens. Therefore, it is possible to state that PSD optimization significantly contributed to enhancement in the photocatalytic efficiency of the cementitious systems by increasing the system selectivity.
- In the PSD-optimized specimens (the mixtures prepared by using PSD moduli of 0.1, 0.5 and 0.9), although there was no significant difference in their system selectivity values, the mixture prepared by using PSD moduli of 0.9 had the highest one (% 91.1) at the 90-day cure period's conclusion.
- In PSD optimized mixtures, the highest NO_x reduction value was obtained from R-Q0.9 composite with 10.4 % at the end of 90-day. There is a similar situation in the system selectivity, and the highest value was obtained in this composite (83.5% for 90-day).
- Optimizing the PSD of TiO_2 particles did not generally affect the photocatalytic performance/efficiency of rutile TiO_2-substituted specimens positively and system selectivity values of rutile TiO_2-substituted composites decreased continuously with the prolonged curing age, in contrary to the anatase TiO_2-substituted composites.
- In general, the photocatalytic activity of rutile-containing mixtures lagged far behind anatase TiO_2 containing mixtures. The crystal structures of the anatase and rutile phases of TiO_2 particles are closely connected to their photocatalytic activity.
- The mixture using the PSD modulus of 0.9 had the highest selectivity value (91.1% and 83.5% for anatase and rutile TiO_2-substituted specimens, respectively) at the conclusion of the 90-day cure period. This indicates that a PSD modulus of 0.9 results in the best photocatalytic efficiency.
- The reference specimen had the lowest total porosity value (3.9%) and all pores available in this specimen were smaller than 50 nm, evidencing the highest compressive strength results of the reference specimen.

- Using nano-sized TiO_2, (the much finer fraction of the TiO_2) leads to better packaging of the grains, as expected and consequently improves the compactness of the microstructure of specimens because of its filler effect.
- PSD-optimized specimens have a relatively low amount of porosity compared to non-optimized specimens, except nano-sized anatase TiO_2-substituted specimen and PSD optimization significantly contributes to the pore refinement of mixtures, although the use of nano-sized TiO_2 alone performed slightly better.

Determining the Best Phase Combination (Anatase and Rutile)

At this stage of the thesis, it was aimed to determine the optimum combination of anatase and rutile. The important results obtained within this section are listed below as items.

- It was only in the rutile-containing composite that it had the highest compressive strength of 55.28 MPa after two curing days. In the compressive strengths of 7 and 28-day composites, the highest compressive strengths were obtained from this composite, as well. These values are respectively; 69.80 and 77.90 MPa.
- In combination cases, compressive strength rose proportionately as the rutile substitution ratio increased. The highest compressive strength results were obtained from the the composite containing 20% anatase and 80% rutile phase for each curing age. Even in this composite, the compressive strength results lagged behind the reference mixture.
- When the degradation rates of 7-day, 28-day and 90-day-old specimens of composites containing anatase-rutile combination of “80:20”, “50:50”, “20:80” are evaluated, regardless of combination rares, the utilization rate of TiO_2, it can be seen that NO_x and NO reduction rates decreased with the prolonged curing ages.
- At the conclusion of the 7-day curing period, the highest photocatalytic performance (NO_x reduction rate) (36.9 %) was obtained from the anatase TiO_2-substituted mixture prepared with PSD modulus of 0.9. However, at the end of the curing age of 28 and 90 days, the highest photocatalytic performance performances (NO_x reduction rate) were obtained from the mixture containing anatase-rutile combination of “80:20” (32.6 % and 27.9% respectively). This situation is directly related to the excess amount of anatase-phase TiO_2.

- The highest selectivity value in 7-day composites was obtained from the mixture containing “80:20” anatase-rutile combination (90.9%). In combinations, In combinations, highest selectivity at each curing age (7-day, 28-day, and 90-day) was obtained from the mixtures containing the 80:20” anatase-rutile combination. These values are 90.9%, 90.0% and 89.9%, respectively.
- Besides, as the rutile substitution rate increased, there was a significant decrease in photocatalytic performance and efficiency.
- As a result, at the end of the curing age of 28 and 90 days, the highest photocatalytic performances (NO_x reduction rate) were obtained from the mixture containing anatase-rutile combination of “80:20”, which is the closest combination to the Degussa P25 in terms of content.

6. REFERENCES

A. Fujishima, J. Ohtsuki, T. Yamashita, S. Hayakawa, Behavior of tumor cells on photoexcited semiconductor surface, Photomed. Photobiol. 8 (1986) 45–46. D. Mowbray, et al., Trends in metal oxide stability for nanorods, nanotubes, and surfaces, J. Phys. Chem. C 115 (5) **(2010)** 2244–2252.

A. Ibhadon, P. Fitzpatrick, Heterogeneous photocatalysis: recent advances and applications, Catalysts 3 (1) **(2013)** 189–218.

A.G. Ilie, M. Scarisoareanu, I. Morjan, E. Dutu, M. Badiceanu, I. Mihailescu, Principal component analysis of Raman spectra for TiO2 nanoparticle characterization, Appl. Surf. Sci. 417 **(2017)** 93–103,

Abreu, M., Morgado, E., Jardim, P., & Marinkovic, B. **(2012)**. The effect of anatase crystal morphology on the photocatalytic conversion of NO by TiO_2-based nanomaterials. Open Chemistry, 10(4), 1183-1198.

Aguado, M. A., Anderson, M. A., & Hill Jr, C. G. **(1994)**. Influence of light intensity and membrane properties on the photocatalytic degradation of formic acid over TiO_2 ceramic membranes. Journal of molecular catalysis, 89(1-2), 165-178.

Aïtcin, P. C., & Flatt, R. J. **(2016)**. Science and technology of concrete admixtures, in Woodhead Publishing series in civil and structural engineering number 59. Woodhead Publishing is an Imprint of Elsevier, Cambridge, UK.

Al-Dahawi, A., Öztürk, O., Emami, F., Yıldırım, G., & Şahmaran, M. **(2016)**. Effect of mixing methods on the electrical properties of cementitious composites incorporating different carbon-based materials. Construction and Building Materials, 104, 160-168.

Almquist C.B. & P. Biswas, **(2002)**. Role of synthesis method and particle size of nanostructured TiO_2 on its photoactivity. J. Catal. 212, 145

Al-Najjar, Y., Yeşilmen, S., Al-Dahawi, A. M., Şahmaran, M., Yıldırım, G., Lachemi, M., & Amleh, L. **(2016)**. Physical and Chemical Actions of Nano-Mineral Additives on Properties of High-Volume Fly Ash Engineered Cementitious Composites. ACI Materials Journal, 113(6).

Alqedra, M., Dabbour, B., & Arafa, M. **(2014)**. Influence of several nano minerals on the mechanical properties of fresh and hardened concrete. In Scientific Cooperation's International Workshops on Engineering Branches.

Alrekabi, S., Cundy, A., Whitby, R. L., Lampropoulos, A., & Savina, I. **(2017)**. Effect of undensified silica fume on the dispersion of carbon nanotubes within a cementitious composite. In Journal of Physics: Conference Series (Vol. 829, No. 1, p. 012011). IOP Publishing.

Andreasen, A. H. M., & Andersen, J. **(1930)**. Über die Beziehung zwischen Kornabstufung und Zwischenraum in Produkten aus losen Körnern (mit einigen Experimenten). Kolloid-Zeitschrift, 50(3), 217-228.

Anpo, M., Aikawa, N., & Kubokawa, Y. **(1984)**. Photocatalytic hydrogenation of alkynes and alkenes with water over titanium dioxide. Platinum loading effect on the primary processes. The Journal of Physical Chemistry, 88(18), 3998-4000.

Anpo, M., Yamashita, H., Ichihashi, Y., & Ehara, S. **(1995)**. Photocatalytic reduction of CO_2 with H_2O on various titanium oxide catalysts. Journal of Electroanalytical Chemistry, 396(1-2), 21-26.

Anpo, M.; Shima, T.; Kodama, S.; Kubokawa, Y. Photocatalytic Hydrogenation of CH_3CCH with H_2O on Small-Particle TiO2: Size Quantization Effects and Reaction Intermediates. J. Phys. Chem**. (1987)** 91, 4305

Ao, C. H., Lee, S. C., Mak, C. L., & Chan, L. Y. **(2003)**. Photodegradation of volatile organic compounds (VOCs) and NO for indoor air purification using TiO_2: promotion versus inhibition effect of NO. Applied Catalysis B: Environmental, 42(2), 119-129.

Asiltürk, M., Sayılkan, F., Erdemoglu, S., Akarsu, M., Sayılkan, H., Erdemoglu, M., ve Arpac, E. **(2006)**. Characterization of the hydrothermally synthesized nano-TiO_2 crystallite and the photocatalytic degradation of Rhodamine B. Journal of Hazardous Materials, 129 (1-3), 164-170.

Aslani, F. **(2015)**. Nanoparticles in self-compacting concrete–a review. Magazine of Concrete Research, 67(20), 1084-1100.

Assadi, A. A., Bouzaza, A., & Wolbert, D. **(2012)**. Photocatalytic oxidation of trimethylamine and isovaleraldehyde in an annular reactor: influence of the mass transfer and the relative humidity. Journal of Photochemistry and Photobiology A: Chemistry, 236, 61-69.

ASTM Standard C150. **(2007)**. Standard Specification for Portland Cement. ASTM International, West Conshohocken, PA, USA.

ASTM Standard C39. **(2003)**. Standard test method for compressive strength of cylindrical concrete specimens. ASTM International, West Conshohocken, PA, USA.

ASTM Standard C494. **(1999)**. Standard Specification for Chemical Admixtures for Concrete. ASTM International, West Conshohocken, PA, USA.

Augugliaro V, Baiocchi C, Prevot AB, Garcı´a-Lo´pez E, Loddo V, Malato S et al **(2002)** Azo-dyes photocatalytic degradation in aqueous suspension of TiO_2 under solar irradiation. Chemosphere 49:1223–1230

Augustynski, J. **(1993)**. The role of the surface intermediates in the photoelectrochemical behaviour of anatase and rutile TiO_2. Electrochimica Acta, 38(1), 43-46.

Austin, R. H., & Lim, S. F. **(2008)**. The Sackler Colloquium on promises and perils in nanotechnology for medicine. Proceedings of the National Academy of Sciences, 105(45), 17217-17221.

B. Y. Lee, K. E. Kurtis, Influence of TiO_2 nanoparticles on early C_3S hydration. J. Am. Ceram. Soc. 93(10) **(2010)** 3399-3405.

Bacsa, R. R., & Kiwi, J. **(1998)**. Effect of rutile phase on the photocatalytic properties of nanocrystalline titania during the degradation of p-coumaric acid. Applied Catalysis B: Environmental, 16(1), 19-29.

Bahnemann D **(1999)** Photocatalytic detoxification of polluted waters. In: Boule P (ed) The handbook of environmental chemistry 2. Part L: environmental photochemistry. Springer, Berlin, pp 285–351

Balbuena, J., Cruz-Yusta, M., Pastor, A., & Sánchez, L. **(2018)**. α-Fe2O3/SiO_2 composites for the enhanced photocatalytic NO oxidation. Journal of Alloys and Compounds, 735, 1553-1561.

Ballari, M. M., Hunger, M., Husken, G., & Brouwers, H. J. H. **(2010)**. NOx photocatalytic degradation employing concrete pavement containing titanium dioxide. Applied Catalysis B: Environmental, 95(3-4), 245-254.

Ballari, M. M., Yu, Q. L., & Brouwers, H. J. H. **(2011)**. Experimental study of the NO and NO_2 degradation by photocatalytically active concrete. Catalysis Today, 161(1), 175-180.

Banerjee, S., Dionysiou, D. D., & Pillai, S. C. **(2015)**. Self-cleaning applications of TiO_2 by photo-induced hydrophilicity and photocatalysis. Applied Catalysis B: Environmental, 176, 396-428.

Banerjee, S., Gopal, J., Muraleedharan, P., Tyagi, A. K., & Raj, B. **(2006)**. Physics and chemistry of photocatalytic titanium dioxide: visualization of bactericidal activity using atomic force microscopy. Current science, 90(10), 1378-1383.

Behfarnia, K., Azarkeivan, A., & Keivan, A. **(2013)**. The effects of TiO_2 and ZnO nanoparticles on physical and mechanical properties of normal concrete. Asian Journal of Civil Engineering, 14, 517–531.

Behnajady, M. A., Alizade, B., & Modirshahla, N. **(2011)**. Synthesis of Mg-doped TiO_2 nanoparticles under different conditions and its photocatalytic activity. *Photochemistry and photobiology*, *87*(6), 1308-1314

Beltran, A., Gracia, L., & Andres, J. **(2006)**. Density functional theory study of the brookite surfaces and phase transitions between natural titania polymorphs. The Journal of Physical Chemistry B, 110(46), 23417-23423.

Bengtsson, N., & Castellote, M. **(2010)**. Photocatalytic activity for NO degradation by construction materials: parametric study and multivariable correlations. Journal of Advanced Oxidation Technologies, 13(3), 341-349.

Bengtsson, N., & Castellote, M. **(2014)**. Heterogeneous photocatalysis on construction materials: effect of catalyst properties on the efficiency for degrading NO_x and self cleaning. Material Construction, 64, 1-17.

Bickley, R. I., Gonzalez-Carreno, T., Lees, J. S., Palmisano, L., & Tilley, R. J. **(1991)**. A structural investigation of titanium dioxide photocatalysts. Journal of SolidState Chemistry, 92(1), 178-190.

Blake, D. M., Maness, P. C., Huang, Z., Wolfrum, E. J., Huang, J., & Jacoby, W. A. **(1999)**. Application of the photocatalytic chemistry of titanium dioxide to disinfection and the killing of cancer cells. Separation and purification methods, 28(1), 1-50.

Blimes, S., Mandelbaum, P., Alvarez, F. & Victoria, N. **(2008).** Surface and Electronic Structures of Titanium Dioxide Photocatalyst., Journal of Physical Chemistry B, 104, 9851-9858.

Blimes, S., Mandelbaum, P., Alvarez, F., and Victoria, N. **(2000)**. "Surface and electronic structures of titanium dioxide photocatalyst." J. Phys. Chem. B, 104(42), 9851–9858.

Bolte, G. **(2009)**. Innovative building materials-reduction of pollutants with TioCem. ZKG international, 62(1), 63-70.

Boonen, E., & Beeldens, A. **(2013)**. Photocatalytic roads: from lab tests to real scale applications. European Transport Research Review, 5(2), 79-89.

Boonen, E., & Beeldens, A. **(2014)**. Recent photocatalytic applications for air purification in Belgium. Coatings, 4(3), 553-573.

Brown, J. D., Williamson, D. L., & Nozik, A. J. **(1985)**. Moessbauer study of the kinetics of iron (3+) photoreduction on titanium dioxide semiconductor powders. The Journal of Physical Chemistry, 89(14), 3076-3080.

Brus, L. **(1986)**. Electronic wave functions in semiconductor clusters: experiment and theory. The Journal of Physical Chemistry, 90(12), 2555-2560.

Burdett JK, Hughbanks T, Miller GJ, Richardson JW Jr, Smith JV **(1987)** J Am Chem Soc 109:3639.

Calza, P., Pelizzetti, E., Mogyorósi, K., Kun, R. & Dékány, I. **(2007)**. Size dependent photocatalytic activity of hydrothermally crystallized titania nanoparticles on poorly adsorbing phenol in absence and presence of fluoride ion. Applied Catalysis B: Environmental, 72(3-4), 314-321.

Cárdenas, C., Tobón, J. I., García, C., & Vila, J. **(2012)**. Functionalized building materials: Photocatalytic abatement of NOx by cement pastes blended with TiO_2 nanoparticles. Construction and Building Materials, 36, 820-825.

Cárdenas, C., Tobón, J., & García, C. **(2013)**. Photocatalytic Properties Evaluation Of Portland White Cement Added with TiO2-nanoparticles. La Revista Latinoamericana de Metalurgia y Materiales, RLMM, 33(2).

Carneiro, J. T., Almeida, A. R., Moulijn, J. A., & Mul, G. **(2010)**. Cyclohexane selective photocatalytic oxidation by anatase TiO_2: influence of particle size and crystallinity. Physical chemistry chemical physics, 12(11), 2744-2750.

Carp, O., Huisman, C. L., & Reller, A. **(2004)**. Environmental toxicity and antimicrobial efficiency of titanium dioxide nanoparticles in suspension. Progress Solid State Chemical, 32(1-2), 33-38.

Carrera, R., Vázquez, A., Arce, E., Moran-Pineda, M., & Castillo, S. **(2007)**. Photodecomposition of NO by sol–gel TiO_2 catalysts under atmospheric conditions: Effect of the method on the textural and morphologic properties. Journal of Alloys and Compounds, 434-435, 788-791.

Cassar, L. **(2004)**. Photocatalysis of cementitious materials: clean buildings and clean air. Mrs Bulletin, 29(5), 328-331.

Chen, H., Namdeo, A. ve Bell, M. **(2008)**. Classification of road traffic and roadside pollution concentrations for assessment of personal exposure. Environmental Modelling and Software, 23(3), 282-287.

Chen, J., & Poon, C. S. **(2009a)**. Photocatalytic cementitious materials: influence of the microstructure of cement paste on photocatalytic pollution degradation. Environmental science & technology, 43(23), 8948-8952.

Chen, J., & Poon, C. S. **(2009b)**. Photocatalytic activity of titanium dioxide modified concrete materials–Influence of utilizing recycled glass cullets as aggregates. Journal of Environmental Management, 90(11), 3436-3442.

Chen, J., Kou, S. C., & Poon, C. S. **(2011)**. Photocatalytic cement-based materials: Comparison of nitrogen oxides and toluene removal potentials and evaluation of self-cleaning performance. Building and Environment, 46(9), 1827-1833.

Chen, J., Kou, S. C., & Poon, C. S. **(2012)**. Hydration and properties of nano-TiO_2 blended cement composites. Cement and Concrete Composites, 34(5), 642-649.

Chen, S. J., Qiu, C. Y., Korayem, A. H., Barati, M. R., & Duan, W. H. **(2016)**. Agglomeration process of surfactant-dispersed carbon nanotubes in unstable dispersion: A two-stage agglomeration model and experimental evidence. Powder Technology, 301, 412-420.

Chen, S., & Liu, Y. **(2007)**. Study on the photocatalytic degradation of glyphosate by TiO_2 photocatalyst. Chemosphere, 67(5), 1010-1017.

Chen, X. F., Kou, S. C., & Poon, C. S. **(2020)**. Rheological behaviour, mechanical performance, and NOx removal of photocatalytic mortar with combined clay brick sands-based and recycled glass-based nano-TiO_2 composite photocatalysts. Construction and Building Materials, 240, 117698.

Chen, X. F., Lin, S. R., & Kou, S. C. **(2018)**. Effect of composite photo-catalysts prepared with recycled clay brick sands and nano-TiO_2 on methyl orange and NOx removal. Construction and Building Materials, 171, 152-160.

Cheng, H., Wang, J., Zhao, Y., & Han, X. **(2014)**. Effect of phase composition, morphology, and specific surface area on the photocatalytic activity of TiO_2 nanomaterials. Rsc Advances, 4(87), 47031-47038.

Cheung, J., Jeknavorian, A., Roberts, L., & Silva, D. **(2011)**. Impact of admixtures on the hydration kinetics of Portland cement. Cement and concrete research, 41(12), 1289-1309.

Chong M. N., Jin B., Chow C. W. K., Saint C., **(2010)**, Recent developments in photocatalytic water treatment technology: A review c water research 44, 2997-3027

Chou, T. P., Zhang, Q., Russo, B., Fryxell, G. E., & Cao, G. **(2007)**. Titania particle size effect on the overall performance of dye-sensitized solar cells. The Journal of Physical Chemistry C, 111(17), 6296-6302.

Chun, H., Yizhong, W. ve Hongxiao, T. **(2000)**. Destruction of phenol aqueous solution by photocatalysis or direct photolysis. Chemosphere, 41(8), 1205-1209.

Coleman HM, Vimonses V, Leslie G, et al. Degradation of 1,4–dioxane in water using TiO_2 based photocatalytic and H_2O_2/UV processes. J Hazard Mater. **(2007)**;146(3):496–501.

Cromer, D. T., & Herrington, K. **(1955)**. The structures of anatase and rutile. Journal of the American Chemical Society, 77(18), 4708-4709.

Cunha-Lopes, I.; Martins, V.; Faria, T.; Correia, C.; Almeida, S.M. Children's exposure to sized-fractioned particulate matter and black carbon in an urban environment. Build. Environ. **(2019)**, 155, 187–194).

Curcó, D., Giménez, J., Addardak, A., Cervera-March, S. ve Esplugas, S. **(2002)**. Effects of radiation absorption and catalyst concentration on the photocatalytic degradation of pollutants. Catalysis Today, 76, 177–188.

D.F. Ollis, H. Al-Ekabi, Photocatalytic purification and treatment of water and air, in: Proceedings of the 1st International Conference on TiO_2 Photocatalytic Purification and Treatment of Water and Air, London, Ontario, Canada, 8–13 November, **(1992)**, Elsevier Science Ltd., 1993.

D'Hennezel, O., Pichat, P., Ollis, D.F., **(1998)**. Benzene and toluene gas-phase photocatalytic degradation over H_2O and HCl pretreated TiO_2: by-products and mechanisms. J. Photochem. Photobiol. A: Chem. 118, 197–204.

D'Alessandro, A., Fabiani, C., Pisello, A. L., Ubertini, F., Materazzi, A. L., & Cotana, F. **(2017)**. Innovative concretes for low-carbon constructions: A review. International Journal of Low-Carbon Technologies, 12(3), 289-309.

Daneshvar N, Salari D, Khataee AR **(2003)** Photocatalytic degradation of azo dye acid red 14 in water: investigation of the effect of operational parameters. J Photochem Photobiol A 157:111–116

Dantas, S. R. A., Serafini, R., de Oliveira Romano, R. C., Vittorino, F., & Loh, K. **(2019)**. Influence of the nano TiO_2 dispersion procedure on fresh and hardened rendering mortar properties. Construction and Building Materials, 215, 544-556.

Daude, N., Gout, C., & Jouanin, C. **(1977)**. Electronic band structure of titanium dioxide. Physical Review B, 15(6), 3229.

De Melo, J. V. S., Trichês, G., Gleize, P. J. P., & Villena, J. **(2012)**. Development and evaluation of the efficiency of photocatalytic pavement blocks in the laboratory and after one year in the field. Construction and Building Materials, 37, 310-319.

Demeestere, K., Dewulf, J., Witte, B. D., Beeldens, A. & Langenhove, H. V. **(2008)**. Heterogeneous photocatalytic removal of toluene from air on building materials enriched with TiO_2. Building and Environment, 43(4), 406-414.

Diamanti, M. V., Del Curto, B., Ormellese, M. A. R. C. O., & Pedeferri, M. P. **(2013)**. Photocatalytic and self-cleaning activity of colored mortars containing TiO_2. Construction and Building Materials, 46, 167-174.

Diamanti, M. V., Ormellese, M., & Pedeferri, M. **(2008)**. Characterization of photocatalytic and superhydrophilic properties of mortars containing titanium dioxide. Cement and Concrete Research, 38(11), 1349-1353.

Diebold, U. **(2003)**. The surface science of titanium dioxide. Surface science reports, 48(5-8), 53-229.

Ding, X. Z., Liu, X. H., & He, Y. Z. **(1996)**. Grain size dependence of anatase-to-rutile structural transformation in gel-derived nanocrystalline titania powders. Journal of materials science letters, 15(20), 1789-1791.

Dodd, A. C., McKinley, A. J., Saunders, M., & Tsuzuki, T. **(2006)**. Effect of particle size on the photocatalytic activity of nanoparticulate zinc oxide. Journal of Nanoparticle Research, 8(1), 43.

Duan, P., Yan, C., Luo, W., & Zhou, W. **(2016)**. Effects of adding nano-TiO_2 on compressive strength, drying shrinkage, carbonation and microstructure of fluidized bed fly ash based geopolymer paste. Construction and Building Materials, 106, 115-125.

Einaga, H., Futamura, S., & Ibusuki, T. **(1999)**. Photocatalytic decomposition of benzene over TiO_2 in a humidified airstream. Physical Chemistry Chemical Physics, 1(20), 4903-4908.

Einaga, H., Futamura, S., & Ibusuki, T. **(2002)**. Heterogeneous photocatalytic oxidation of benzene, toluene, cyclohexene and cyclohexane in humidified air: comparison of decomposition behavior on photoirradiated TiO_2 catalyst. Applied Catalysis B: Environmental, 38(3), 215-225.

EN, T. 196-1, **(2016)** Methods of testing cement–Part 1: Determination of strength. Turkish Standard Institution, Ankara.

EN, T. 197-1, **(2012)** Cement – Part 1: Composition, specification and conformity criteria for common cements. Turkish Standard Institution, Ankara.

EPA, **(2010)**. Primary National Ambient Air Quality Standards for Nitrogen Dioxide;Final Rule, in Federal Register, 473-537.

EPA, **(2018)**. Review of the Primary National Ambient Air Quality Standards for Oxides of Nitrogen, Final action, Vol. 83, No.75, 17226-17278.

Erdem, T. K., Demirhan, S., Yıldırım, G., Banyhussan, Q. S., Şahin, O., Balav, M. H., & Şahmaran, M. **(2020)**. Effects of Mixture Design Parameters on the Mechanical Behavior of High-Performance Fiber-Reinforced Concretes. Journal of Materials in Civil Engineering, 32(12), 04020368.

Etacheri, V., Di Valentin, C., Schneider, J., Bahnemann, D., & Pillai, S. C. **(2015)**. Visible-light activation of TiO_2 photocatalysts: Advances in theory and experiments. Journal of Photochemistry and Photobiology C: Photochemistry Reviews, 25, 1-29.

EU, **(2008)**, Directive 2008/50/EC of the European Parliament and of the Council of 21 May 2008 on ambient air quality and cleaner air for Europe, OJ L 152, 11.6.2008 (http://eurlex.europa.eu/LexUriServ/LexUriServ.do?uri=OJ:L:2008:152:0001:0044:EN:PDF) accessed 27 July 2011

European Environment Agency (EEA), **(2011)**, Air quality in Europe — 2011 report, EEA Report No 12/2011, European Commission, European Environment Agency, ISSN 1725-2237 (https://www.eea.europa.eu/publications/air-quality-in-europe-2011)

European Environment Agency (EEA), **(2018)**, Air quality in Europe — 2018 report, EEA Report No 12/2018, European Commission, European Environment Agency, ISSN 1977-8449 (https://www.eea.europa.eu/publications/air-quality-in-europe-2018)

European Environment Agency (EEA), **2020**, European Union emission inventory report 1990-2018, EEA Report No 05/2020, European Commission, European Environment Agency, ISSN 1977-8449 (https://www.eea.europa.eu/publications/european-union-emission-inventory-report-1990-20189)

F IUPAC. (1971). Manual of symbols and terminology for physicochemical quantities and units. Appendix II: definitions, terminology and symbols in colloid and surface chemistry. Everett DH, editor.

Fazli, F. I. M., Ahmad, M. K., Soon, C. F., Nafarizal, N., Suriani, A. B., Mohamed, A., & Murakami, K. **(2017)**. Dye-sensitized solar Cell using pure anatase TiO_2 annealed at different temperatures. Optik, 140, 1063-1068.

Fei, P., Xiong, H., Cai, J., Liu, C., & Yu, Y. **(2016)**. Enhanced the weatherability of bamboo fiber-based outdoor building decoration materials by rutile nano-TiO_2. Construction and Building Materials, 114, 307-316.

Feng, L. C., Gong, C. W., Wu, Y. P., Feng, D. C., & Xie, N. **(2013)**. The study on mechanical properties and microstructure of cement paste with nano-TiO_2. In Advanced Materials Research (Vol. 629, pp. 477-481). Trans Tech Publications Ltd.

Fisher J, Egerton TA **(2001)** Titanium compounds, inorganic, Kirk-Othmer encyclopaedia of chemical technology. Wiley, New York

Folli, A., Jakobsen, U. H., Guerrini, G. L., & Macphee, D. E. **(2009)**. Rhodamine B discolouration on TiO_2 in the cement environment: a look at fundamental aspects of the self-cleaning effect in concretes. Journal of Advanced Oxidation Technologies, 12(1), 126-133.

Folli, A., Pade, C., Hansen, T. B., De Marco, T., & Macphee, D. E. **(2012)**. TiO_2 photocatalysis in cementitious systems: Insights into self-cleaning and depollution chemistry. Cement and concrete research, 42(3), 539-548.

Folli, A., Pochard, I., Nonat, A., Jakobsen, U. H., Shepherd, A. M., & Macphee, D. E. **(2010)**. Engineering photocatalytic cements: understanding TiO_2 surface chemistry to control and modulate photocatalytic performances. Journal of the American Ceramic Society, 93(10), 3360-3369.

Fox, M. A., & Dulay, M. T. **(1993)**. Heterogeneous photocatalysis. Chemical reviews, 93(1), 341-357.

Fu, X., Clark, L.A., Zeltner, W.A. ve Anderson, M.A. **(1996)**. Effects of reaction temperature and water vapor content on the heterogeneous photocatalytic oxidation of ethylene, Journal of Photochemistry and Photobiology A: Chemistry, 97(3), 181-186.

Fu, Y., Lin, G, & Wang, C. **(2009)**. Research on ultrasonic dispersion preparation of epoxy/nano-SiO_2 composites. Eng Plast Appl 2009, 37(5), 5–8.

Fujishima, A. **(2005)**. Discovery and applications of photocatalysis-Creating a comfortable future by making use of light energy. Japan nanonet bulletin, 44, 1-3.

Fujishima, A.; Rao, T.N.; Tryk, D.A. Titanium dioxide photocatalysis. J. Photochem. Photobiol. C Photochem. Rev. (**2000**), 1, 1–21.

Fuller, W. B., and Thompson, S. E. **(1907)**. The laws of proportioning concrete. Transactions of the American Society of Civil Engineers. 33 (1907) 222–298.

Funk, J., D. Dinger, & J. Funk Jr. **(1980)**. Coal Grinding and Particle Size Distribution Studies for Coal-Water Slurries at High Solids Content. Final Report, Empire State Electric Energy Research Corporation, New York.

G. Husken, M. Hunger, H. Brouwers, Experimental study of photocatalytic concrete products for air purification, Build. Environ. 44 (12) **(2009)** 2463-2474. https://doi.org/10.1016/j.buildenv.2009.04.010.

G.K. Mor, et al., Use of highly-ordered TiO_2 nanotube arrays in dye-sensitized solar cells, Nano Lett. 6 (2) **(2006)** 215–218

Gamboa, J. A., & Pasquevich, D. M. **(1992)**. Effect of chlorine atmosphere on the anatase-rutile transformation. Journal of the American Ceramic Society, 75(11), 2934-2938.

Gao, L., & Zhang, Q. **(2001)**. Effects of amorphous contents and particle size on the photocatalytic properties of TiO_2 nanoparticles. Scripta materialia, 44(8-9), 1195-1198.

Garcia, J.C., Takashima, K., **(2003)**. Photocatalytic degradation of imaz-aquin in an aqueous suspension of titanium dioxide. J. Photochem.Photobiol. A: Chem. 155, 215–222

García, L. D., Pastor, J. M., & Peña, J. **(2018)**. Self cleaning and depolluting glass reinforced concrete panels: Fabrication, optimization and durability evaluation. Construction and Building Materials, 162, 9-19.

Gerischer, H., & Heller, A. **(1992)**. Photocatalytic oxidation of organic molecules at TiO_2 particles by sunlight in aerated water. Journal of the Electrochemical Society, 139(1), 113.

Ghosh, T. B., Dhabal, S., & Datta, A. K. **(2003).** On crystallite size dependence of phase stability of nanocrystalline TiO_2. Journal of applied physics, 94(7), 4577-4582.

Giosuè, C., Pierpaoli, M., Mobili, A., Ruello, M. L., & Tittarelli, F. **(2020)**. Multifunctional lightweight mortars for indoor applications to improve comfort and health of occupants: thermal properties and photocatalytic efficiency. Frontiers in Materials, 7, 255.

Giosuè, C., Yu, Q. L., Ruello, M. L., Tittarelli, F., & Brouwers, H. J. H. **(2018)**. Effect of pore structure on the performance of photocatalytic lightweight lime-based finishing mortar. Construction and Building Materials, 171, 232-242.

Gogate, P.R. and Pandit, A.B., A review of imperative technologies for wastewater treatment I: Oxidation technologies at ambient conditions, Advances in Environmental Research, 8, No. 3-4, 501 **(2004)**.

Goguen, C. **(2012)**. ‘’How precast concrete buildings can clean themselves and our air’’, Precast Sol. Mag. published by National Precast Concrete Association.

Gouma, P. I., & Mills, M. J. **(2001)**. Anatase-to-rutile transformation in titania powders. Journal of the American Ceramic Society, 84(3), 619-622.

Grela, M. A., & Colussi, A. J. **(1996)**. Kinetics of stochastic charge transfer and recombination events in semiconductor colloids. Relevance to photocatalysis efficiency. The Journal of Physical Chemistry, 100(46), 18214-18221.

Guo, M. Z., & Poon, C. S. **(2013)**. Photocatalytic NO removal of concrete surface layers intermixed with TiO2. Building and environment, 70, 102-109.

Guo, M. Z., & Poon, C. S. **(2018).** Superior photocatalytic NOx removal of cementitious materials prepared with white cement over ordinary Portland cement and the underlying mechanisms. Cement and Concrete Composites, 90, 42-49.

Guo, M. Z., Ling, T. C., & Poon, C. S. **(2012)**. TiO_2-based self-compacting glass mortar: Comparison of photocatalytic nitrogen oxide removal and bacteria inactivation. Building and environment, 53, 1-6.

Guo, M. Z., Maury-Ramirez, A., & Poon, C. S. **(2015a)**. Photocatalytic activities of titanium dioxide incorporated architectural mortars: Effects of weathering and activation light. Building and Environment, 94, 395-402.

Guo, M. Z., Maury-Ramirez, A., & Poon, C. S. **(2015b)**. Versatile photocatalytic functions of self-compacting architectural glass mortars and their inter-relationship. Materials & Design, 88, 1260-1268.

H. F. W. Taylor, Cement Chemistry, 2nd edition, Thomas Telford, London, **(1997).**

H. He, C. Liu, K. D. Dubois, T. Jin, M. E. Louis, G. Li, Enhanced charge separation in nanostructured TiO_2 materials for photocatalytic and photovoltaic applications, Ind. Eng. Chem. Res. 51(37) **(2012)** 11841-11849

H. He, C. Liu, K. D. Dubois, T. Jin, M. E. Louis, G. Li, Enhanced charge separation in nanostructured TiO_2 materials for photocatalytic and photovoltaic applications, Ind. Eng. Chem. Res. 51(37) **(2012)** 11841-11849.

Han, B., Zhang, L., Zeng, S., Dong, S., Yu, X., Yang, R., & Ou, J. **(2017)**. Nano-core effect in nano-engineered cementitious composites. Composites Part A: Applied Science and Manufacturing, 95, 100-109.

Han, D., & Ferron, R. D. **(2016)**. Influence of high mixing intensity on rheology, hydration, and microstructure of fresh state cement paste. Cement and Concrete Research, 84, 95-106.

Hanaor, D. A., & Sorrell, C. C. **(2011)**. Review of the anatase to rutile phase transformation. Journal of Materials science, 46(4), 855-874.

Hanson, S. & Tikalsky, P. **(2013)**. Influence of Ultraviolet Light on Photocatalytic TiO_2 Materials. Journal of Materials in Civil Engineering, 25(7), 893-898.

Hanson, S. **(2014)**. Evaluation of concrete containing photocatalytic titanium dioxide. The University of Utah.

Harada, H., & Ueda, T. **(1984)**. Photocatalytic activity of ultra-fine rutile in methanol-water solution and dependence of activity on particle size. Chemical physics letters, 106(3), 229-231.

Hashimoto K, Irie H, Fujishima A. TiO_2 photocatalysis: a historical overview and future prospects. Japanese Journal of Applied Physics. **(2005)**;44(1):8269–8285.

Hassan, M. M., Dylla, H., Mohammad, L. N., & Rupnow, T. **(2010b)**. Evaluation of the durability of titanium dioxide photocatalyst coating for concrete pavement. Construction and building materials, 24(8), 1456-1461.

Hassan, M., Dylla, H., Mohammad, L., and Rupnow, T. **(2010a)**. "Effect of application methods on the effectiveness of titanium dioxide as a photocatalyst compound to concrete pavement." Transportation Research Record, Transportation Research Board, Washington, DC

Hay, S. O., Obee, T., Luo, Z., Jiang, T., Meng, Y., He, J., ... & Suib, S. **(2015)**. The viability of photocatalysis for air purification. Molecules, 20(1), 1319-1356.

Hequet, V., Raillard, C., Debono, O., Thévenet, F., Locoge, N., & Le Coq, L. **(2018)**. Photocatalytic oxidation of VOCs at ppb level using a closed-loop reactor: the mixture effect. Applied Catalysis B: Environmental, 226, 473-486.

Hermann, J., Heterogeneous photocatalysis: Fundamentals and applications to the removal of various types of aqueous pollutants, Catalysis Today, 53, No. 1, 115 **(1999)**.

Hernández-Rodríguez, M. J., Santana Rodríguez, R., Darias, R., González Díaz, O., Pérez Luzardo, J. M., Doña Rodríguez, J. M., & Pulido Melián, E. **(2019)**. Effect of TiO2 addition on mortars: characterization and photoactivity. Applied Sciences, 9(13), 2598.

Hou, T. C. **(2008)**. Wireless and Electromechanical Approaches for Strain Sensing and Crack Detection in Fiber Reinforced Cementitious Materials. Doctoral dissertation. University of Michigan, Michigan.

Huang, M., & Wen, X. **(2019)**. Experimental study on photocatalytic effect of nano TiO2 epoxy emulsified asphalt mixture. Applied Sciences, 9(12), 2464.

Hung CH, Yuan C **(2000)** Reduction of Azo-dye via TiO_{2}– photocatalysis. J Chin Inst Environ Eng 10:209–216

Hunger, M., Husken, G., & Brouwers, H. J. H. **(2008)**. Photocatalysis applied to concrete products-Part 2: Influencing factors and product performance. ZKG international, 61(10), 76-84.

Hurum, D. C., Agrios, A. G., Gray, K. A., Rajh, T. & Thurnauer, M. C. **(2003)**. Explaining the enhanced photocatalytic activity of Degussa P25 mixed-phase TiO_2 using EPR. J. Phys. Chem. B 107, 4545–4549.

Husken, G., & Brouwers, H. J. H. **(2008, June)**. Air purification by cementitious materials: Evaluation of air purifying properties. In International Conference on Construction and Building Technology, Kuala Lumpur, Malaysia (Vol. 304).

Hussein, B. S. **(2016)**. ZnO-Assisted Photodegradation of Some Dyes in Aqueous Solutions Under Direct Solar light. DIRASAT TARBAWIYA, 9(36), 273-288.

I.R. Oliveira et al., Particle Dispersion and Packaging, Fazendo Arte, São Paulo, **2000** [in Portuguese].

Ilie, A. G., Scarisoareanu, M., Morjan, I., Dutu, E., Badiceanu, M., & Mihailescu, I. **(2017)**. Principal component analysis of Raman spectra for TiO_2 nanoparticle characterization. Applied Surface Science, 417, 93-103.

Ismail, I., Bakar, N. F. A., Ling, T. H., Ideris, N., Zain, Z. H. M., & Radacsi, N. (2019). Morphology and conductivity evaluation of electrospun polyacrylic acid (PAA) microfiber. Materials Today: Proceedings, 17, 574-583.

J. Jia, L. Mu, Y. Lin, X. Zhou, Rutile versus anatase for quantum dot sensitized solar cell, Electrochim. Acta 266 **(2018)** 103–109,

J. L. Lim, S. N. Raman, M. Safiuddin, M. F. M. Zain, R. Hamid, Autogenous shrinkage, microstructure, and strength of ultra-high performance concrete incorporating carbon nanofibers, Mater. 12(2) **(2019)** 320.

J. Moser, M. Grätzel, R. Gallay, Inhibition of electron-hole recombination in substitutionally doped colloidal semiconductor crystallites, Helv. Chim. Acta 70 **(1987)** 1596–1604.

J. Zhao, X. Yang, Photocatalytic oxidation for indoor air purification: a literature review, Build. Environ. 38 (5) **(2003)** 645-654.

Jang, H. D., Kim, S. K., & Kim, S. J. **(2001)**. Effect of particle size and phase composition of titanium dioxide nanoparticles on the photocatalytic properties. Journal of Nanoparticle Research, 3(2-3), 141-147.

Janus, M., Mądraszewski, S., Zając, K., & Kusiak-Nejman, E. **(2020)**. A New Preparation Method of Cement with Photocatalytic Activity. Materials, 13(23), 5540.

Janus, M., Mądraszewski, S., Zając, K., Kusiak-Nejman, E., Morawski, A. W., & Stephan, D. **(2019)**. Photocatalytic activity and mechanical properties of cements modified with TiO_2/N. Materials, 12(22), 3756.

Jayapalan, A. R., Lee, B. Y. & Kurtis, K. E. **(2009)**. Effect of nano-sized titanium dioxide on early age hydration of Portland cement in nanotechnology in construction. Berlin: Springer, 3(267-273).

Jayapalan, A. R., Lee, B. Y., & Kurtis, K. E. **(2013)**. Can nanotechnology be 'green' Comparing efficacy of nano and microparticles in cementitious materials. Cement and concrete composites, 36, 16-24.

Jenny Schneider, Masaya Matsuoka, Masato Takeuchi, Jinlong Zhang, Yu Horiuchi, Masakazu Anpo, and Detlef W Bahnemann. **(2014)** Understanding TiO2 photocatalysis: mechanisms and materials. Chemical reviews, 114(19):9919–9986.

Jiang J, Oberdorster G, Biswas P. Characterization of size, surface charge, and agglomeration state of nanoparticle dispersions for toxicological studies. JNR **(2008)**;11:77–89.

Jiang, S., Zhou, D., Zhang, L., Ouyang, J., Yu, X., Cui, X., & Han, B. **(2018)**. Comparison of compressive strength and electrical resistivity of cementitious composites with different nano-and micro-fillers. Archives of Civil and Mechanical Engineering, 18(1), 60-68.

Jimenez-Relinque, E., Rodriguez-Garcia, J. R., Castillo, A., & Castellote, M. (2015). Characteristics and efficiency of photocatalytic cementitious materials: Type of binder, roughness and microstructure. Cement and Concrete Research, 71, 124-131.

Jin, Q., Saad, E. M., Zhang, W., Tang, Y., & Kurtis, K. E. **(2019)**. Quantification of NOx uptake in plain and TiO_2-doped cementitious materials. Cement and Concrete Research, 122, 251-256.

Jiu, J., Isoda, S., Adachi, M. & Wang, F. **(2007)**. Preparation of TiO_2 nanocrystalline with 3–5nm and application for dye-sensitized solar cell. Journal of Photochemistry and Photobiology A: Chemistry,189(2-3), 314-321.

Jones, L. **(1990)**. Interference mechanisms in waste stabilization/solidification processes. Journal of hazardous materials, 24(1), 83-88.

Juan Z., ve Xudong Y., **(2003)** Photocatalytic Oxidation for Indoor Air Purification: A Literature Review. Building and Environment 38(5):645-654.

Jun, J., Dhayal, M., Shin, J., Kim, J. ve Getoff, N. **(2006)**. Surface properties and photoactivity of TiO_2 treated with electron beam. Radiation Physics and Chemistry, 75(5), 583-589.

Jung, K. Y., & Park, S. B. **(1999)**. Anatase-phase titania: preparation by embedding silica and photocatalytic activity for the decomposition of trichloroethylene. Journal of Photochemistry and Photobiology A: Chemistry, 127(1-3), 117-122.

K. Vijayarangamuthu, J. Youn, C. Park, K. Jeon, Facile synthesis of core–Shell-Structured rutile TiO_2 with enhanced photocatalytic properties, Catal. Today **(2018)**.

Kabra, K., Chaudhary, R. ve Sawhney, R. L. **(2004)**. Treatment of Hazardous Organic and Inorganic Compounds through Aqueous-Phase Photocatalysis: A Review. Industrial and Engineering Chemistry Research,43(24), 7683-7696.

Kaneco S, Rahman MA, Suzuki T, Katsumata H, Ohta K **(2004)** Optimization of solar photocatalytic degradation conditions of bisphenol A in water using titanium dioxide. J Photochem Photobiol A 163:419–424.

Karapati, S., Giannakopoulou, T., Todorova, N., Boukos, N., Antiohos, S., Papageorgiou, D., ... & Trapalis, C. **(2014)**. TiO_2 functionalization for efficient NOx removal in photoactive cement. Applied surface science, 319, 29-36.

Kavan, L.; Gratzel, M.; Gilbert, S.; Klemenz, C.; Scheel, H. Electrochemical and Photoelectrochemical Investigation of Single-Crystal Anatase. Journal of the American Chemical Society **(1996)**, 118, 6716-6723.

Kim, D. S., Han, S. J., & Kwak, S. Y. **(2007)**. Synthesis and photocatalytic activity of mesoporous TiO2 with the surface area, crystallite size, and pore size. Journal of Colloid and Interface Science, 316(1), 85-91.

Kim, S. B., & Hong, S. C. **(2002).** Kinetic study for photocatalytic degradation of volatile organic compounds in air using thin film TiO_2 photocatalyst. Applied Catalysis B: Environmental, 35(4), 305-315.

Kim, S. B., Hwang, H. T., & Hong, S. C. **(2002)**. Photocatalytic degradation of volatile organic compounds at the gas–solid interface of a TiO2 photocatalyst. Chemosphere, 48(4), 437-444.

Kim, S. J., Lee, E. G., Park, S. D., Jeon, C. J., Cho, Y. H., Rhee, C. K., & Kim, W. W. **(2001)**. Photocatalytic effects of rutile phase TiO_2 ultrafine powder with high specific surface area obtained by a homogeneous precipitation process at low temperatures. Journal of sol-gel science and technology, 22(1), 63-74.

Kim, S., & Ehrman, S. H. **(2009)**. Photocatalytic activity of a surface-modified anatase and rutile titania nanoparticle mixture. Journal of Colloid and Interface Science, 338(1), 304-307.

Kirby, G. H., & Lewis, J. A**. (2004)**. Comb polymer architecture effects on the rheological property evolution of concentrated cement suspensions. Journal of the American Ceramic Society, 87(9), 1643-1652.

Kiriakidou F, Kondarides DI, Verykios XE **(1999)** The effect of operational parameters and TiO2-doping on the photocatalytic degradation of azo-dyes. Catal Today 54:119–130

Kočí, K., Krejčíková, S., Šolcová, O., & Obalová, L. **(2012)**. Photocatalytic decomposition of N_2O on Ag-TiO_2. Catalysis Today, 191(1), 134-137.

Kočí, K., Obalová, L., Matějová, L., Plachá, D., Lacný, Z., Jirkovský, J., & Šolcová, O. **(2009)**. Effect of TiO_2 particle size on the photocatalytic reduction of CO_2. Applied Catalysis B: Environmental, 89(3-4), 494-502.

Kominami H, Murakami S-Y, Kera Y, Ohtani B **(1998)** Titanium(IV) oxide photocatalyst of ultra-high activity: a new preparation process allowing compatibility of high adsorptivity and low electron-hole recombination probability. Catal Lett 56:125–129

Kominami, H., & Ohtani, B. **(2010)**. Preparation of Titanium Oxide-Based Powders and Thin Films of High Photocatalytic Activities Using Solvothermal Methods. In Environmentally Benign Photocatalysts (pp. 113-132). Springer, New York, NY.

Krýsa, J., Keppert, M., Jirkovský, J., Štengl, V. & Šubrt, J. (2004). The effect of thermal treatment on the properties of TiO_2 photocatalyst. Materials Chemistry and Hysics, 86(2-3), 333-339.

Kumar A, Pandey G. Photocatalytic Activity of Co:TiO_2 Nanocomposites and their Application in Photodegradation of Acetic Acid. Chemical Science Transactions. 2017c;6(3):385–392

Kumar A, Pandey G. Photocatalytic degradation of Eriochrome Black- –T by the Ni:TiO_2 nanocomposites. Desalination and Water Treatment. **2017b**;71:406–419.

Kumar A, Pandey G. Photodegradation of Methyl Orange in Aqueous Solution by the Visible Light Active Co:La:TiO_2 Nanocomposite. Chem Sci J. **2017a**;8:164

L. Cao, A. Huang, F. J. Spiess, S. L. Suib, Gas-phase oxidation of 1-butene using nanoscale TiO_2 photocatalysts, J. Catal. 188(1) **(1999)** 48-57.

L. Cao, Z. Gao, S. L. Suib, T. N. Obee, S. O. Hay, J. D. Freihaut, Photocatalytic oxidation of toluene on nanoscale TiO_2 catalysts: studies of deactivation and regeneration. J. Catal. 196(2) **(2000)** 253-261.

L. Gao, Q. Zhang, Effects of amorphous contents and particle size on the photocatalytic properties of TiO_2 nanoparticles, Scr. Mater. 44(8-9) **(2001)** 1195-1198.

L. Znaidi, R. Seraphimova, J. F. Bocquet, C. Colbeau-Justin, C. Pommier, A semi-continuous process for the synthesis of nanosize TiO_2 powders and their use as photocatalysts, Mater. Res. Bull. 36(5-6) **(2001)** 811-825.

Lackhoff, M., Prieto, X., Nestle, N., Dehn, F., & Niessner, R. **(2003)**. Photocatalytic activity of semiconductor-modified cement—influence of semiconductor type and cement ageing. Applied Catalysis B: Environmental, 43(3), 205-216.

Laplaza, A., Jiménez-Relinque, E., Campos, J., & Castellote, M. **(2017)**. Photocatalytic behavior of colored mortars containing TiO_2 and iron oxide based pigments. Construction and Building Materials, 144, 300-310.

Lee, B. Y., Jayapalan, A. R. & Kurtis, K. E. **(2013)**. Effects of nano-TiO_2 on properties of cement-based materials. Magazine of Concrete Research, 65(21), 1293-1302.

Lee, B. Y., Jayapalan, A. R., Bergin, M. H., & Kurtis, K. E. **(2014)**. Photocatalytic cement exposed to nitrogen oxides: Effect of oxidation and binding. Cement and concrete research, 60, 30-36.

LeonaviČIus, D., PundienĖ, I. N. A., PranckeviČIenĖ, J., Girskas, G., & Kligys, M. **(2019)**. The effect of the electrical conductivity of superplasticizers on the fluidity and early hydration parameters of cement paste. Ceramics–Silikáty, 63(4), 390-398.

Lewis, N. S. & Rosenbluth, M. L. **(1989)**. Photocatalysis-Foundamentals and Applications. Wiley Interscience, 20-110.

Leydecker, S. **(2008)**. ‘’Nano Materials in Architecture’’, Interior Architecture and Design, Birkhauser Verlag, Basel, Switzerland.

Li, G., Ciston, S., Saponjic, Z. V., Chen, L., Dimitrijevic, N. M., Rajh, T., & Gray, K. A. **(2008)**. Synthesizing mixed-phase TiO_2 nanocomposites using a hydrothermal method for photo-oxidation and photoreduction applications. Journal of Catalysis, 253(1), 105-110.

Li, G., Lv, L., Fan, H., Ma, J., Li, Y., Wan, Y., & Zhao, X. S. **(2010)**. Effect of the agglomeration of TiO_2 nanoparticles on their photocatalytic performance in the aqueous phase. Journal of colloid and interface science, 348(2), 342-347.

Li, L., Liu, L., Qing, Y., Zhang, Z., Yan, N., Wu, Y., & Tian, C. **(2018)**. Stretchable alkaline poly (acrylic acid) electrolyte with high ionic conductivity enhanced by cellulose nanofibrils. Electrochimica Acta, 270, 302-309.

Li, R., Li, T., & Zhou, Q. (2020). Impact of titanium dioxide (TiO_2) modification on its application to pollution treatment—a review. Catalysts, 10(7), 804.

Li, V. C. **(2019)**. Multi-functional Engineered Cementitious Composites (ECC). In Engineered Cementitious Composites (ECC) (pp. 371-411). Springer, Berlin, Heidelberg.

Li, Z., Ding, S., Yu, X., Han, B., & Ou, J. **(2018)**. Multifunctional cementitious composites modified with nano titanium dioxide: a review. Composites Part A: Applied Science and Manufacturing, 111, 115-137

Li, Z., Han, B., Yu, X., Dong, S., Zhang, L., Dong, X., & Ou, J. **(2017)**. Effect of nano-titanium dioxide on mechanical and electrical properties and microstructure of reactive powder concrete. Materials Research Express, 4(9), 095008.

Lin, H., Huang, C. P., Li, W., Ni, C., Shah, S. I., & Tseng, Y. H. **(2006)**. Size dependency of nanocrystalline TiO_2 on its optical property and photocatalytic reactivity exemplified by 2-chlorophenol. Applied Catalysis B: Environmental, 68(1-2), 1-11.

Lin, J., Wang, B., Sproul, W. D., Ou, Y., & Dahan, I. **(2013)**. Anatase and rutile TiO_2 films deposited by arc-free deep oscillation magnetron sputtering. Journal of Physics D: Applied Physics, 46(8), 084008.

Linsebigler, A. L., Lu, G., & Yates Jr, J. T. **(1995)**. Photocatalysis on TiO_2 surfaces: principles, mechanisms, and selected results. Chemical reviews, 95(3), 735-758.

Lippens, P. E., & Lannoo, M. **(1989)**. Calculation of the band gap for small CdS and ZnS crystallites. Physical Review B, 39(15), 10935.

Liu, Z., Zhang, Y., Liu, L., & Jiang, Q. **(2013)**. An analytical model for determining the relative electrical resistivity of cement paste and C–S–H gel. Construction and Building Materials, 48, 647-655.

Lu, Z., Wang, Q., Yin, R., Chen, B. & Li, Z. **(2016)**. A novel TiO_2 /foam cement composite with enhanced photodegradation of methyl blue. Construction and Building Materials,129, 159-162.

Lucas, S. S. **(2017)**. Influence of operating parameters and ion doping on the photocatalytic activity of mortars containing titanium dioxide nanoparticles. *Materials Today: Proceedings*, *4*(11), 11588-11593.

Lucas, S. S., Ferreira, V. M., & De Aguiar, J. B. **(2013)**. Incorporation of titanium dioxide nanoparticles in mortars—Influence of microstructure in the hardened state properties and photocatalytic activity. Cement and Concrete Research, 43, 112-120.

Luo, Y., Ollis, D.F., **(1996)**. Heterogeneous photocatalytic oxidation of trichloroethylene and toluene mixtures in air: Kinetic promotion and inhibition, time-dependent catalyst activity. J. Catal. 163, 1–11.

M. Xu, Y. Bao, K. Wu, T. Xia, H. L. Clack, H. Shi, V. C. Li, Influence of TiO_2 incorporation methods on NOx abatement in Engineered Cementitious Composites. Constr. Build. Mater. 221 **(2019)** 375-383.

Ma, B., Li, H., Mei, J., Li, X., & Chen, F. **(2015)**. Effects of nano-TiO_2 on the toughness and durability of cement-based material. Advances in Materials Science and Engineering, 1-10.

Ma, H., & Li, Z. **(2013)**. Microstructures and mechanical properties of polymer modified mortars under distinct mechanisms. Construction and Building Materials, 47, 579-587.

Ma, H., Tian, Y., & Li, Z. **(2011)**. Interactions between organic and inorganic phases in PA-and PU/PA-modified-cement-based materials. Journal of materials in civil engineering, 23(10), 1412-1421.

Macphee, D. E., & Folli, A. **(2016)**. Photocatalytic concretes—The interface between photocatalysis and cement chemistry. Cement and Concrete Research, 85, 48-54.

Maggos, T., Bartzis, J. G., Leva, P., & Kotzias, D. **(2007)**. Application of photocatalytic technology for NOx removal. Applied Physics A, 89(1), 81-84.

Maira, A. J., Yeung, K. L., Lee, C. Y., Yue, P. L., & Chan, C. K. **(2000).** Size effects in gas-phase photo-oxidation of trichloroethylene using nanometer-sized TiO_2 catalysts. Journal of Catalysis, 192(1), 185-196.

Mandzy, N., Grulke, E., & Druffel, T. **(2005)**. Breakage of TiO_2 agglomerates in electrostatically stabilized aqueous dispersions. Powder technology, 160(2), 121-126.

Mark, R.N., William, A.J., Danial, M.B., Thomas, A.M., **(1993)**. Detection of intermediates from the gas phase photocatalytic oxidation of TCE. In: Photocatalytic purification and treatment of water and air. Elsevier Science Publisher, Amsterdam, pp. 387–391.

Martinez, T., Bertron, A., Ringot, E., & Escadeillas, G. **(2011)**. Degradation of NO using photocatalytic coatings applied to different substrates. *Building and Environment*, *46*(9), 1808-1816.

Martyanov, I. N. ve Klabunde, K. J. **(2003)**. Photocatalytic Oxidation of Gaseous 2-Chloroethyl Ethyl Sulfide over TiO_2. Environmental Science and Technology, 37(15), 3448-3453.

Maruska, H. P., & Ghosh, A. K. **(1978)**. Photocatalytic decomposition of water at semiconductor electrodes. Solar Energy, 20(6), 443-458.

Matějka, V., Matějková, P., Kovář, P., Vlček, J., Přikryl, J., Červenka, P., ... & Kukutschová, J. **(2012)**. Metakaolinite/TiO_2 composite: Photoactive admixture for building materials based on Portland cement binder. Construction and Building Materials, 35, 38-44.

Mateos, R., Vera, S., Valiente, M., Díez-Pascual, A. M., & San Andrés, M. P. **(2017)**. Comparison of anionic, cationic and nonionic surfactants as dispersing agents for graphene based on the fluorescence of riboflavin. Nanomaterials, 7(11), 403.

Mayabadi, A. H., Waman, V. S., Kamble, M. M., Ghosh, S. S., Gabhale, B. B., Rondiya, S. R., ... & Gosavi, S. W. **(2014)**. Evolution of structural and optical properties of rutile TiO2 thin films synthesized at room temperature by chemical bath deposition method. Journal of Physics and Chemistry of Solids, 75(2), 182-187.

Mazierski, P., Nadolna, J., Lisowski, W., Winiarski, M. J., Gazda, M., Nischk, M., ... & Zaleska-Medynska, A. **(2017)**. Effect of irradiation intensity and initial pollutant concentration on gas phase photocatalytic activity of TiO_2 nanotube arrays. Catalysis Today, 284, 19-26.

McLendon, G. Energy Resources through Photochemistry and Catalysis; Grátzel, M,, Ed.; Academic Press: New York, **(1983)**; p 117.

Mehta, P.K., Monteiro, P.J.M. **(1993)**. Concrete Structure, Properties and Materials, vol. 2, Prentice Hall, New Jersey.

Melo, J. V. S., Trichês, G., Gleize, P. J. P., & Villena, J. **(2012)**. Development and evaluation of the efficiency of photocatalytic pavement blocks in the laboratory and after one year in the field. Construction and Building Materials, 37, 310-319.

Mendoza, O., Sierra, G., & Tobón, J. I. **(2013)**. Influence of super plasticizer and $Ca(OH)_2$ on the stability of functionalized multi-walled carbon nanotubes dispersions for cement composites applications. Construction and Building Materials, 47, 771-778.

Mendoza, O., Sierra, G., & Tobón, J. I. **(2014)**. Effect of the reagglomeration process of multi-walled carbon nanotubes dispersions on the early activity of nanosilica in cement composites. Construction and Building Materials, 54, 550-557.

Meng, C., Dong, P., Tian, H., Cheng, T., Li, J., Liu, Y., ... & Xi, X. **(2020)**. Photocatalytic concrete paving block reinforced by TiO_2 nanotubes for NO removal. Journal of Materials Science, 55(29), 14280-14291.

Meng, T., Yu, Y., Qian, X., Zhan, S., & Qian, K. **(2012)**. Effect of nano-TiO_2 on the mechanical properties of cement mortar. Construction and Building Materials, 29, 241-245.

Mills, A., & Elouali, S. **(2015)**. The nitric oxide ISO photocatalytic reactor system: measurement of NO_x removal activity and capacity. Journal of Photochemistry and Photobiology A: Chemistry, 305, 29-36.

Mills, A., Lee, S. K., & Lepre, A. **(2003)**. Photodecomposition of ozone sensitised by a film of titanium dioxide on glass. Journal of Photochemistry and Photobiology A: Chemistry, 155(1-3), 199-205.

Minero, C., Catozzo, F., & Pelizzetti, E. **(1992)**. Role of adsorption in photocatalyzed reactions of organic molecules in aqueous titania suspensions. Langmuir, 8(2), 481-486.

Mo, S. D., & Ching, W. Y. **(1995)**. Electronic and optical properties of three phases of titanium dioxide: Rutile, anatase, and brookite. Physical review B, 51(19), 13023.

Mohseni, E., Miyandehi, B. M., Yang, J., & Yazdi, M. A. **(2015)**. Single and combined effects of nano-SiO_2, nano-Al_2O_3 and nano-TiO_2 on the mechanical, rheological and durability properties of self-compacting mortar containing fly ash. Construction and Building Materials, 84, 331-340.

Moore, V. C., Strano, M. S., Haroz, E. H., Hauge, R. H., Smalley, R. E., Schmidt, J., & Talmon, Y. **(2003)**. Individually suspended single-walled carbon nanotubes in various surfactants. Nano letters, 3(10), 1379-1382.

Muggli DS, Ding L **(2001)** Photocatalytic performance of sulfated TiO_2 and Degussa P-25 TiO_2 during oxidation of organics. Appl Catal B 32:181–194

Musso, S., Tulliani, J. M., Ferro, G., & Tagliaferro, A. **(2009)**. Influence of carbon nanotubes structure on the mechanical behavior of cement composites. Composites Science and Technology, 69(11-12), 1985-1990.

Nakajima, H., Mori, T., Shen, Q., & Toyoda, T. **(2005)**. Photoluminescence study of mixtures of anatase and rutile TiO_2 nanoparticles: Influence of charge transfer between the nanoparticles on their photoluminescence excitation bands. Chemical Physics Letters, 409(1-3), 81-84.

National Air Pollutants Emission Service of Korea. Emission Rate Inquiry. Available online: https: //airemiss.nier.go.kr **(accessed on 22 July 2020).**

Nazari, A., & Riahi, S. **(2011)**. TiO_2 nanoparticles effects on physical, thermal and mechanical properties of self compacting concrete with ground granulated blast furnace slag as binder. Energy Build., 43, 995–1002.

Nazari, A., Riahi, S., Riahi, S., Shamekhi, S. F., & Khademno, A. **(2010).** Improvement the mechanical properties of the cementitious composite by using TiO_2 nanoparticles. Journal of American Science, 6(4), 98-101.

Negim, E. S. R., Bekbayeva, N., Akmaral, L., Herki, U., Merey, B. M., Rinat, N., & I Yeligbayeva, G. **(2017)**. Effect of methyl cellulose/poly (acrylic acid) blends on physico-mechanical properties of Portland cement pastes.

Neppolian, B., Choi, H. C., Sakthivel, S., Arabindoo, B., & Murugesan, V. **(2002)**. Solar light induced and TiO_2 assisted degradation of textile dye reactive blue 4. Chemosphere, 46(8), 1173-1181.

Newlands, M. D., Jones, M. R., Kandasami, S., & Harrison, T. A. **(2008)**. Sensitivity of electrode contact solutions and contact pressure in assessing electrical resistivity of concrete. Materials and structures, 41(4), 621-632.

Nishikawa, H. ve Takahara, Y. (2001). Adsorption and photocatalytic decomposition of odor compounds containing sulfur using TiO_2/SiO_2 bead. Journal of Molecular Catalysis A: Chemical, 172(1-2), 247-251.

Noorvand, H., Ali, A. A. A., Demirboga, R., Farzadnia, N., & Noorvand, H. **(2013)**. Incorporation of nano TiO_2 in black rice husk ash mortars. Construction and Building Materials, 47, 1350-1361.

Ohama, Yoshihiko & Van Gemert, Dionys. **(2011)**. Applications of Titanium Dioxide Photocatalysis to Construction Materials: State-of-the-Art Report of the RILEM Technical Committee 194-TDP. 10.1007/978-94-007-1297-3.

Ohno T, Sarukawa K, Tokieda K, Matsumura M **(2001)** Morphology of a TiO2 photocatalyst (Degussa, P-25) consisting of anatase and rutile crystalline phases. J Catal 203:82–86

Ohtani, B., Prieto-Mahaney, O., Li, D. & Abe, R. **(2010)**. What is Degussa (Evonik) P25 Crystalline composition analysis, reconstruction from isolated pure particles and photocatalytic activity test. Journal of Photochemistry and Photobiology A: Chemistry, 216(2-3), 179-182.

Oi, L. E., Choo, M. Y., Lee, H. V., Ong, H. C., Abd Hamid, S. B., & Juan, J. C. **(2016)**. Recent advances of titanium dioxide (TiO_2) for green organic synthesis. Rsc Advances, 6(110), 108741-108754.

Ollis DF, Pelizzetti E, Serpone N **(1992)** Photocatalyzed destruction of water contaminants. Environ Sci Technol 25:1522–1529

Ollis, D. F., Pelizzetti, E., & Serpone, N. **(1989)**. Photocatalysis: fundamentals and applications. Edited by Serpone N. and Pelizzetti E., Wiley Intersicence, New York, p603-634.

Ö. Sevim, İ. Demir, Optimization of fly ash particle size distribution for cementitious systems with high compactness, Constr. Build. Mater. 195 **(2019a)** 104-114. https://doi.org/10.1016/j.conbuildmat.2018.11.080

Ö. Sevim, İ. Demir, Physical and permeability properties of cementitious mortars having fly ash with optimized particle size distribution, Cem. Concr. Compos. 96 **(2019b)** 266-273. https://doi.org/10.1016/j.cemconcomp.2018.11.017

Park, J. J., Kim, S., Shin, W., Choi, H. J., Park, G. J., & Yoo, D. Y. **(2020)**. High-Performance Photocatalytic Cementitious Materials Containing Synthetic Fibers and Shrinkage-Reducing Admixture. Materials, 13(8), 1828.

Parveen, S., Rana, S., & Fangueiro, R. **(2013)**. A review on nanomaterial dispersion, microstructure, and mechanical properties of carbon nanotube and nanofiber reinforced cementitious composites. Journal of Nanomaterials.

Pellegrino, F., Pellutiè, L., Sordello, F., Minero, C., Ortel, E., Hodoroaba, V. D., & Maurino, V. **(2017)**. Influence of agglomeration and aggregation on the photocatalytic activity of TiO_2 nanoparticles. Applied Catalysis B: Environmental, 216, 80-87.

Peral J, Domenech X, Ollis DF. Heterogeneous photocatalysis for purification, decontamination and deodorization of air. Journal of Chemical Technology Biotechnology. **(1997)**;70(2):117–140.

Pérez-Nicolás, M., Balbuena, J., Cruz-Yusta, M., Sánchez, L., Navarro-Blasco, I., Fernández, J. M., & Alvarez, J. I. **(2015)**. Photocatalytic NOx abatement by calcium aluminate cements modified with TiO_2: Improved NO_2 conversion. Cement and Concrete Research, 70, 67-76.

Pérez-Nicolás, M., Navarro-Blasco, I., Fernández, J. M., & Alvarez, J. I. **(2017)**. Atmospheric NOx removal: Study of cement mortars with iron-and vanadium-doped TiO_2 as visible light–sensitive photocatalysts. Construction and Building Materials, 149, 257-271.

Pérez-Nicolás, M., Plank, J., Ruiz-Izuriaga, D., Navarro-Blasco, I., Fernández, J. M., & Alvarez, J. I. **(2018)**. Photocatalytically active coatings for cement and air lime mortars: Enhancement of the activity by incorporation of superplasticizers. Construction and Building Materials, 162, 628-648.

Peters G, Vill V **(1989)** Index of modern inorganic compounds. Subvolume A. Landolt-Bo¨rnstein numerical data and functional relationships in science and technology. Verlag, Berlin 15.

Pichat, P., Hermann, J.M., **(1989)**. Adsorption–desorption,related mobility and reactivity in photocatalysis. In: Ser-pone, N., Pelizzetti, E. (Eds.), Photocatalysis: Fundamentalsand Applications. John Wiley & Sons, NTC, pp. 217–250

Poon, C. S., & Cheung, E**. (2006, November)**. Performance of photo-catalytic paving blocks made from waste. In Proceedings of the Institution of Civil Engineers-Waste and Resource Management (Vol. 159, No. 4, pp. 165-171). Thomas Telford Ltd

Poon, C. S., & Cheung, E**. (2007)**. NO removal efficiency of photocatalytic paving blocks prepared with recycled materials. Construction and Building Materials, 21(8), 1746-1753.

PRODESP. Arquivo: frota circulante **2009** [Archive: current fleet 2009]. Companhia de Processamento de Dados do Estado de São Paulo, Detran – Departamento de Análises, São Paulo, Brasil; 2010 [in Portuguese].

Qamar M, Saquib M, Muneer M **(2005)** Photocatalytic degradation of two selected dye derivatives, chromotrope 2B and amido black 10B, in aqueous suspensions of titanium dioxide. Dyes Pigments 65:1–9

R. Cai, K. Hashimoto, K. Itoh, Y. Kubota, A. Fujishima, Photokilling of malignant cells with ultra-fine TiO2 powder, Bull. Chem. Soc. Jpn. 64 **(1991)** 1268–1273.

R. Cai, K. Hashimoto, Y. Kubota, A. Fujishima, Increment of photocatalytic killing of cancer cells using TiO2 with the aid of superoxide dismutase, Chem. Lett. **(1992)** 427–430.

R. Feret, Sur la compacité des mortiers hydrauliques. Annales des Ponts et Chaussees, 4 **(1892)** 5-16.

R. Han, R. Andrews, C. O'Rourke, S. Hodgen, A. Mills, Photocatalytic air purification: Effect of HNO3 accumulation on NOx and VOC removal. Catalysis Today. 380 **(2021)** 105-113.

Ragesh, P., Ganesh, V. A., Nair, S. V., & Nair, A. S. **(2014)**. A review on 'self-cleaning and multifunctional materials'. Journal of Materials chemistry A, 2(36), 14773-14797.

Rahim, A., & Nair, S. R. **(2016)**. Influence of nano-materials in high strength concrete. J. Chem. Pharm. Sci, 974, 15-21.

Reddy, K. M., Manorama, S. V., & Reddy, A. R. **(2003)**. Bandgap studies on anatase titanium dioxide nanoparticles. Materials Chemistry and Physics, 78(1), 239-245.

Retamoso, C., Escalona, N., González, M., Barrientos, L., Allende-González, P., Stancovich, S., & Lopez, M. **(2019)**. Effect of particle size on the photocatalytic activity of modified rutile sand (TiO_2) for the discoloration of methylene blue in water. Journal of photochemistry and photobiology A: Chemistry, 378, 136-141.

Reza, K. M., Kurny, A. S. W., & Gulshan, F. **(2017)**. Parameters affecting the photocatalytic degradation of dyes using TiO_2: a review. Applied Water Science, 7(4), 1569-1578

Rhee, I., Lee, J. S., Kim, J. B., & Kim, J. H. **(2018).** Nitrogen oxides mitigation efficiency of cementitious materials incorporated with TiO_2. Materials, 11(6), 877.

Rismanchian, M., Akbari, J., & Keshavarzi, R. **(2014).** Photocatalytic removal of gaseous toluene by titanium dioxide coated on nickel foam: Influence of relative humidity and

toluene concentration. International Journal of Environmental Health Engineering, 3(1), 29.

Ruot, B., Plassais, A., Olive, F., Guillot, L., & Bonafous, L. **(2009)**. TiO_2-containing cement pastes and mortars: Measurements of the photocatalytic efficiency using a rhodamine B-based colourimetric test. Solar Energy, 83(10), 1794-1801.

S. Arunmetha, P. Manivasakan, A. Karthik, N.R. Dhinesh Babu, S.R. Srither, V. Rajendran, Effect of processing methods on physicochemical properties of titania nanoparticles produced from natural rutile sand, Adv. Powder Technol. 24 **(2013)** 972–979, https://doi.org/10.1016/j.apt.2013.01.011.

S. Garcia-Segura, E. Brillas, Applied photoelectrocatalysis on the degradation of organic pollutants in wastewaters, J. Photochem. Photobiol. C Photochem. Rev. 31 (2017) 1–35, https://doi.org/10.1016/j.jphotochemrev.2017.01.005.

S. Hager, R. Bauer, G. Kudielka, Photocatalytic oxidation of gaseous chlorinated organics over titanium dioxide, Chemosphere 41 (8) **(2000)** 1219-1225.

S. Kawashima, J.-W.T. Seo, D. Corr, M.C. Hersam, S.P. Shah, Dispersion of $CaCO_3$ nanoparticles by sonication and surfactant treatment for application in fly ash–cement systems, Mater. Struct. 47 (6) **(2014)** 1011-1023.

Saafi, M., Andrew, K., Tang, P. L., McGhon, D., Taylor, S., Rahman, M., ... & Zhou, X. **(2013)**. Multifunctional properties of carbon nanotube/fly ash geopolymeric nanocomposites. Construction and Building Materials, 49, 46-55.

Safarzadeh-Amiri, A., Bolton, J. R., & Cater, S. R. **(1996)**. The use of iron in advanced oxidation processes. Journal of Advanced Oxidation Technologies, 1(1), 18-26.

Saggioro EM, Oliveira AS, Pavesi T, Maia CG, Ferreira LFV, Moreira JC **(2011)** Use of titanium dioxide photocatalysis on the remediation of model textile wastewaters containing azo dyes. Molecules 16:10370–10386

Sahin, O., Bay, S., İlcan, H., Yıldırım, G., & Şahmaran, M. **(2021)**. Influence of mixing methods on the NOx reduction capability and electrical properties of photocatalytic cementitious systems. Cement and Concrete Composites, 115, 103840.

Sakai, N., Ebina, Y., Takada, K. ve Sasaki, T. **(2004)**. Electronic band structure of titania semi-conductor nanosheets revealed by electrochemical and photochemical studies. Journal of American Chemical Society. 126, 5851-5858.

Sakthivel S, Neppolian B, Shankar MV, Arabindoo B, Palanichamy M, Murugesan V **(2003)** Solar photocatalytic degradation of azo dye: comparison of photocatalytic efficiency of ZnO and TiO_2. Sol Energy Mater Sol Cells 77:65–82

Salemi, N., Behfarnia, K., & Zaree, S. A. **(2014)**. Effect of nanoparticles on frost durability of concrete. Asian Journal of Civil Engineering (BHRC), 15, 411–420.

Salman, M. M., Eweed, K. M., & Hameed, A. M. **(2016)**. Influence of partial replacement TiO_2 nanoparticles on the compressive and flexural strength of ordinary cement mortar. Al-Nahrain Journal for Engineering Sciences, 19(2), 265-270.

Sanchez, F., & Sobolev, K. **(2010)**. Nanotechnology in concrete–a review. Construction and building materials, 24(11), 2060-2071.

Saquib, M. **(2003)**. TiO_2-mediated photocatalytic degradation of a triphenylmethane dye (gentian violet), in aqueous suspensions. Dyes and Pigments, 56(1), 37-49.

Sayilkan F., **(2007)**. Synthesis of Nano-TiO_2 Photocatalyst and Determination of Photocatalytic Activity. PhD Thesis. Inonu University. Graduate School of Natural and Applied Sciences

Schindler, K. M., & Kunst, M. **(1990)**. Charge-carrier dynamics in titania powders. Journal of Physical Chemistry, 94(21), 8222-8226.

Sclafani, A., Palmisano, L., & Schiavello, M. **(1990)**. Influence of the preparation methods of titanium dioxide on the photocatalytic degradation of phenol in aqueous dispersion. Journal of Physical Chemistry, 94(2), 829-832.

Senff, L., Tobaldi, D. M., Lucas, S., Hotza, D., Ferreira, V. M., & Labrincha, J. A. **(2013)**. Formulation of mortars with nano-SiO_2 and nano-TiO_2 for degradation of pollutants in buildings. Composites Part B: Engineering, 44(1), 40-47.

Seo, D., & Yun, T. S. **(2017)**. NOx removal rate of photocatalytic cementitious materials with TiO_2 in wet condition. Building and Environment, 112, 233-240.

Serpone, N. **(2006)**. Is the band gap of pristine TiO_2 narrowed by anion-and cation-doping of titanium dioxide in second-generation photocatalysts.

Serpone, N., Lawless, D., & Khairutdinov, R. **(1995)**. Size effects on the photophysical properties of colloidal anatase TiO2 particles: size quantization versus direct transitions in this indirect semiconductor?. The Journal of Physical Chemistry, 99(45), 16646-16654.

Si, H., Zhou, M., Fang, Y., He, J., Yang, L., & Wang, F. **(2021)**. Photocatalytic concrete for NO_x degradation: Influence factors and durability. Construction and Building Materials, 298, 123835.

Sikora, P., Augustyniak, A., Cendrowski, K., Nawrotek, P., & Mijowska, E. **(2018)**. Antimicrobial activity of Al_2O_3, CuO, Fe_3O_4, and ZnO nanoparticles in scope of their further application in cement-based building materials. Nanomaterials, 8(4), 212.

Sivalingam G, Nagaveni K, Hegde MS, Madras G **(2003)** Photocatalytic degradation of various dyes by combustion synthesized nano anatase TiO_2. Appl Catal B 45:23–38

Smith, S. J., Ste&ns, R., Liu, S., Li, G., Navrotsky, A., Boerio-Goates, J., & Woodfield, B. F. **(2009)**. Heat capacities and thermodynamic functions of TiO_2 anatase and rutile: Analysis of phase stability. American Mineralogist, 94(2-3), 236-243.

Smith, S. J., Stevens, R., Liu, S., Li, G., Navrotsky, A., Boerio-Goates, J., & Woodfield, B. F. **(2009)**. Heat capacities and thermodynamic functions of TiO_2 anatase and rutile: Analysis of phase stability. American Mineralogist, 94(2-3), 236-243.

So, C. M., Cheng, M. Y., Yu, J. C., & Wong, P. K. **(2002)**. Degradation of azo dye Procion Red MX-5B by photocatalytic oxidation. Chemosphere, 46(6), 905-912.

Soares, E. T., Lansarin, M. A., & Moro, C. C. **(2007)**. A study of process variables for the photocatalytic degradation of rhodamine B. Brazilian Journal of Chemical Engineering, 24(1), 29-36.

Sobolkina, A., Mechtcherine, V., Khavrus, V., Maier, D., Mende, M., Ritschel, M., & Leonhardt, A. **(2012)**. Dispersion of carbon nanotubes and its influence on the mechanical properties of the cement matrix. Cement and Concrete Composites, 34(10), 1104-1113.

Sohrabi MR, Davallo M, Miri M **(2009)** Influence of operational parameters on eliminating azo dyes from wastewater by advanced oxidation technology. Int J ChemTech Res 1:446–451

Sohrabi MR, Ghavami M **(2008)** Photocatalytic degradation of direct red 23 dye using UV/TiO2: effect of operational parameters. J Hazard Mater 153:1235–1239

Song, H. W., & Kwon, S. J. **(2007)**. Permeability characteristics of carbonated concrete considering capillary pore structure. Cement and Concrete Research, 37(6), 909-915.

Spragg, R. P., Castro, J., Nantung, T., Paredes, M., & Weiss, J. **(2012)**. Variability analysis of the bulk resistivity measured using concrete cylinders. Advances in Civil Engineering Materials, 1(1), 1-17.

Spragg, R., Bu, Y., Snyder, K., Bentz, D., & Weiss, J. **(2013)**. Electrical testing of cement-based materials: Role of testing techniques, sample conditioning, and accelerated curing. Publication FHWA/IN/JTRP-2013/28. Joint Transportation Research Program, Indiana Department of Transportation and Purdue University, West Lafayette, Indiana.

Strini, A., Roviello, G., Ricciotti, L., Ferone, C., Messina, F., Schiavi, L., ... & Cioffi, R. **(2016)**. TiO_2-based photocatalytic geopolymers for nitric oxide degradation. Materials, 9(7), 513.

Su, R., Bechstein, R., Sø, L., Vang, R. T., Sillassen, M., Esbjörnsson, B. & Besenbacher, F. **(2011)**. How the Anataz-to-Rutil Ratio Influences the Photoreactivity of TiO_2. The Journal of Physical Chemistry C, 115(49), 24287-24292.

Sugrañez, R., Álvarez, J. I., Cruz-Yusta, M., Mármol, I., Morales, J., Vila, J., & Sánchez, L. **(2013)**. Enhanced photocatalytic degradation of NOx gases by regulating the microstructure of mortar cement modified with titanium dioxide. Building and Environment, 69, 55-63.

Supeno, M. & Siburian, R.. **(2018)**. Effect of TiO2 For Generation of H_2/O_2 Gases, Based on Splited water and UV as Inisiator. Oriental Journal of Chemistry. 34. 973-980. 10.13005/ojc/340247.

Suttiponparnit K, Jiang J, Sahu M, Suvachittanont S, Charinpanitku T, Biswas P. Role of surface area, primary particle size, and crystal phase on titanium dioxide nanoparticle dispersion properties. Nanoscale Res Lett **(2011)**.

T. Chernet, Effect of Mineralogy and Texture in the TiO_2 Pigment Production Process of the Tellnes Ilmenite Concentrate. Mineral. Petrol. 67 **(1999)** 21–32.

Tanaka K, Capule MFV, Hisanaga T **(1991)** Effect of crystallinity of TiO_2 on its photocatalytic action. Chem Phys Lett 187:73–76

Tayeb, A. M., & Hussein, D. S. **(2015)**. Synthesis of TiO_2 nanoparticles and their photocatalytic activity for methylene blue. *American Journal of Nanomaterials*, *3*(2), 57-63.

Thennarasu, G., & Sivasamy, A. **(2016)**. Enhanced visible photocatalytic activity of cotton ball like nano structured Cu doped ZnO for the degradation of organic pollutant. *Ecotoxicology and environmental safety*, *134*, 412-420.

Tian, Y., Jin, X. Y., Jin, N. G., Zhao, R., Li, Z. J., & Ma, H. Y. **(2013)**. Research on the microstructure formation of polyacrylate latex modified mortars. Construction and Building Materials, 47, 1381-1394.

Turcry, P., & Loukili, A. **(2003)**. A study of plastic shrinkage of self-compacting concrete. In Proceedings of the 3rd international RILEM symposium on self-compacting concrete. Reykjavik: RILEM Publications SARL (pp. 576-585).

V. Cirkva, H.Žabová, Thin nanoporous titania films on the electrodeless discharge lamps for photocatalysis. Handbook of Photocatalysts: Preparation, Structure and Applications, **(2010)**.

V. Etacheri, C. Di Valentin, J. Schneider, D. Bahnemann, S.C. Pillai, Visible-light activation of TiO_2 photocatalysts: advances in theory and experiments, J. Photochem, Photobiol. C Photochem. Rev. 25 **(2015)** 1–29.

V. Johansen, P. J. Andersen, Particle Packing and Concrete Properties,in J. Skalny and S.Mindess (Eds) Materials Science of Concrete II, Westerville, OH: The American Ceramic Society, **(1991)**.

V. Matějka, P. Matějková, P. Kovář, J. Vlček, J. Přikryl, P. Červenka, Z.Lacný, J. Kukutschová, Metakaolinite/TiO_2 composite: Photoactive admixture for building materials based on Portland cement binder. Constr. Build. Mater. 35 **(2012)** 38-44.

Vittoriadiamanti, M.; Pedeferri, M. Concrete, mortar and plaster using titanium dioxide nanoparticles: Applications in pollution control, self-cleaning and photo sterilization. In Nanotechnology in Eco-Efficient Construction; Elsevier: Amsterdam, The Netherlands, **(2013)**; pp. 299–326.

Vorontsov, A. V., Kabachkov, E. N., Balikhin, I. L., Kurkin, E. N., Troitskii, V. N., & Smirniotis, P. G. **(2018)**. Correlation of surface area with photocatalytic activity of TiO_2. Journal of Advanced Oxidation Technologies, 21(1), 20170063.

Wang, C. C., Zhang, Z., & Ying, J. Y. **(1997)**. Photocatalytic decomposition of halogenated organics over nanocrystalline titania. Nanostructured Materials, 9(1-8), 583-586.

Wang, H., & Lewis, J. P. **(2005)**. Second-generation photocatalytic materials: anion-doped TiO_2. Journal of Physics: Condensed Matter, 18(2), 421.

Wang, K.H., Tsai, H.H., Hseieh, Y.H., **(1998**). The kinetics of photocatalytic degradation of trichloroethylene in gas phase over TiO_2 supported on glass bead. Appl. Catal. B: Environ. 17, 313–320.

Wang, S., Ang, H. ve Tade, M. O. **(2007)**. Volatile organic compounds in indoor environment and photocatalytic oxidation: State of the art. Environment International, 33(5), 694-705.

Wang, X., Hu, H., Yang, Z., Kong, Y., Fei, B., & Xin, J. H. **(2015)**. Visible light-active sub-5 nm anatase TiO_2 for photocatalytic organic pollutant degradation in water and air, and for bacterial disinfection. Catalysis Communications, 72, 81-85.

Wang, X., Wang, K., Tanesi, J., & Ardani, A. **(2014)**. Effects of nanomaterials on the hydration kinetics and rheology of portland cement pastes. Advances in Civil Engineering Materials, 3(2), 142-159.

Wang, Y., Cheng, H., Zhang, L., Hao, Y., Ma, J., Xu, B. ve Li, W. **(2000)**. The Preparation, Characterization, Photoelectrochemicaland Photocatalytic Properties of Lanthanide Metal-İon-Doped TiO_2 Nanoparticles. Journal of Molecular Catalysis A, 151, 205-216.

Watson, S. S., Beydoun, D., Scott, J. A., & Amal, R. **(2003)**. The effect of preparation method on the photoactivity of crystalline titanium dioxide particles. Chemical Engineering Journal, 95(1-3), 213-220.

Wei, T. Y., & Wan, C. C. **(1991)**. Heterogeneous photocatalytic oxidation of phenol with titanium dioxide powders. Industrial & engineering chemistry research, 30(6), 1293-1300.

WHO, (**2000**), Air quality guidelines for Europe, World Health Organization, Regional Office for Europe, Copenhagen (http://www.euro.who.int/__data/assets/pdf_file/0005/74732/E71922.pdf) accessed 18 February 2021.

World Health Organization. **(2020)**. https://www.who.int/health-topics/air-pollution#tab=tab_1 (Accesible date:09/01/2021)

X. Wang, H. Hu, Z. Yang, Y. Kong, B. Fei, J.H. Xin, Visible light-active sub-5 nm anatase TiO_2 for photocatalytic organic pollutant degradation in water and air, and for bacterial disinfection, Catal. Commun. 72 **(2015)** 81–85.

Xiao, Q., Si, Z., Yu, Z. ve Qiu, G. **(2007)**. Sol–gel auto-combustion synthesis of samarium-doped TiO_2 nanoparticles and their photocatalytic activity under visible light irradiation. Materials Science and Engineering: B, 137(1-3), 189-194

Xiong, G., Deng, M., Xu, L., & Tang, M. **(2006)**. Properties of Cement-Based Composites by Doping Nano-TiO_2. Journal-Chinese Ceramic Society, 34(9), 1158.

Xu, M., Bao, Y., Wu, K., Shi, H., Guo, X., & Li, V. C. **(2019)**. Multiscale investigation of tensile properties of a TiO_2-doped Engineered Cementitious Composite. Construction and Building Materials, 209, 485-491.

Xu, M., Clack, H., Xia, T., Bao, Y., Wu, K., Shi, H., & Li, V. **(2020b)**. Effect of TiO_2 and fly ash on photocatalytic NOx abatement of engineered cementitious composites. *Construction and Building Materials*,

Xu, M.; Gao, Y.; Moreno, E.; Kunst, M. Photocatalytic Activity of Bulk TiO_2 Anatase and Rutile Single Crystals using Infrared Absorption Spectroscopy. American Physical Society **2011**, 106, 1-4.

Xu, N., Shi, Z., Fan, Y., Dong, J., Shi, J., & Hu, M. Z. C. **(1999)**. Effects of particle size of TiO_2 on photocatalytic degradation of methylene blue in aqueous suspensions. Industrial & Engineering Chemistry Research, 38(2), 373-379.

Xu, Y., Jin, R., Hu, L., Li, B., Chen, W., Shen, J., ... & Fang, J. **(2020a)**. Studying the mix design and investigating the photocatalytic performance of pervious concrete containing TiO_2-Soaked recycled aggregates. Journal of Cleaner Production, 248, 119281.

Y. Ohama, D. Van Gemert, Application of titanium dioxide photocatalysis to construction materials: state-of-the-art report of the RILEM Technical Committee 194-TDP (Eds.), **(2011)**, (Vol. 5), Springer Science and Business Media.

Yamashita, H.; Ichihashi, Y.; Harada, M.; Stewart, G.; Fox, M. A.; Anpo, M. Photocatalytic Oxidation of 1-Octanol on Anchored Titanium Oxide and on TiO2 Powder Catalysts. J. Catal. **1996**, 158, 97.

Yang, L. Y., Jia, Z. J., Zhang, Y. M., & Dai, J. G. **(2015)**. Effects of nano-TiO_2 on strength, shrinkage and microstructure of alkali activated slag pastes. Cement and Concrete Composites, 57, 1-7.

Yang, L., Hakki, A., Wang, F., & Macphee, D. E. **(2018)**. Photocatalyst efficiencies in concrete technology: The effect of photocatalyst placement. Applied Catalysis B: Environmental, 222, 200-208.

Yang, L., Hakki, A., Zheng, L., Jones, M. R., Wang, F., & Macphee, D. E. **(2019)**. Photocatalytic concrete for NOx abatement: Supported TiO_2 efficiencies and impacts. Cement and Concrete Research, 116, 57-64

Yang, R., Wang, M., Shen, Z., Wang, W., Ma, H. ve Gu, J. **(2007)**. The degradation and mineralization of 4-chlorophenol in aqueous solutions by electron beam irradiation in the presence of TiO_2 nanoparticles. Radiation Physics and Chemistry, 76(7), 1122-1125.

Yeşilmen, S., Al-Najjar, Y., Balav, M. H., Şahmaran, M., Yıldırım, G., & Lachemi, M. **(2015)**. Nano-modification to improve the ductility of cementitious composites. Cement and Concrete Research, 76, 170-179.

Yeung, K. L., Yau, S. T., Maira, A., Coronado, J. M., Soria, J. ve Yue, P. L. **(2003)**. The influence of surface properties on the photocatalytic activity of nanostructured TiO_2. Journal of Catalysis, 219(1), 107-116.

Yousefi, A., Allahverdi, A., & Hejazi, P. **(2013)**. Effective dispersion of nano-TiO_2 powder for enhancement of photocatalytic properties in cement mixes. Construction and building materials, 41, 224-230.

Yu, Q. L., & Brouwers, H. J. H. **(2009)**. Indoor air purification using heterogeneous photocatalytic oxidation. Part I: experimental study. Applied Catalysis B: Environmental, 92(3-4), 454-461.

Yuangpho, N., Le, S. T. T., Treerujiraphapong, T., Khanitchaidecha, W., & Nakaruk, A. **(2015)**. Enhanced photocatalytic performance of TiO_2 particles via effect of anatase–rutile ratio. Physica E: Low-dimensional Systems and Nanostructures, 67, 18-22.

Zeltner WA, Hill CG Jr and Anderson MA, Supported titania for photodegradation. Chemtech 23:21±28 **(1993)**

Zhang L Y, You J, Dong Z H, Zhong Y J, Li Q W, You Y H, Liu Y W, Sun X. Preparation and photocatalytic properties of Ag modified fluorinated titanium dioxide. J Synth Cryst, **(2019)**, 48(10): 1898–1906+1919.

Zhang T, Oyama T, Horikoshi S, Hidaka H, Zhao J, Serpone N **(2002)** Photocatalyzed N-demethylation and degradation of methylene blue in titania dispersions exposed to concentrated sunlight. Sol Energy Mater Sol Cells 73:287–303

Zhang Z., C.-C. Wang, R. Zakaria & J.Y. Ying, **(1998).** Role of particle size in nanocrystalline TiO_2-based photocatalysts. J. Phys. Chem. B. 102, 10871.

Zhang, L., Anderson, W. A., Sawell, S., & Moralejo, C. **(2007)**. Mechanistic analysis on the influence of humidity on photocatalytic decomposition of gas-phase chlorobenzene. Chemosphere, 68(3), 546-553.

Zhang, L., Moralejo, C., & Anderson, W. A. **(2020)**. A review of the influence of humidity on photocatalytic decomposition of gaseous pollutants on TiO_2-based catalysts. The Canadian Journal of Chemical Engineering, 98(1), 263-273.

Zhao, A., Yang, J., & Yang, E. H. **(2015)**. Self-cleaning engineered cementitious composites. Cement and Concrete Composites, 64, 74-83.

Zhao, Y., Li, C., Liu, X. ve Gu, F. **(2007)**. Highly enhanced degradation of dye with well-dispersed TiO_2 nanoparticles under visible irradiation. Journal of Alloys and Compounds, 440(1-2), 281-286.

Zhu, B., Xia, P., Li, Y., Ho, W., & Yu, J. **(2017)**. Fabrication and photocatalytic activity enhanced mechanism of direct Z-scheme g-C_3N_4/Ag_2WO_4 photocatalyst. Applied Surface Science, 391, 175-183.

Zhu, D., & Zhou, Q. **(2019)**. Action and mechanism of semiconductor photocatalysis on degradation of organic pollutants in water treatment: A review. Environmental Nanotechnology, Monitoring & Management, 12, 100255.

Znaidi, L., Seraphimova, R., Bocquet, J., Colbeau-Justin, C. ve Pommier, C. **(2001)**. Continuous process for the synthesis of nano-size TiO_2 powders and their use as photocatalysts. Materials Research Bulletin., 36(5–6), 811–825)

Zou, L., Luo, Y., Hooper, M., & Hu, E. **(2006).** Removal of VOCs by photocatalysis process using adsorption enhanced TiO_2–SiO_2 catalyst. Chemical Engineering and Processing: Process Intensification, 45(11), 959-964.

APPENDICES

APPENDIX 1 – Published articles from thesis work

Construction and Building Materials 318 (2022) 125992

Contents lists available at ScienceDirect

Construction and Building Materials

journal homepage: www.elsevier.com/locate/conbuildmat

Role of inclusion size distribution of titanium dioxide on the nitrogen oxides reduction capability and microstructural characteristics of cementitious systems

Emrah Bahçi [a], Oğuzhan Şahin [b], Hüseyin İlcan [a,c], Burak Uzal [d], Muhammed Faruk Günal [c], Gürkan Yıldırım [c], Mustafa Şahmaran [c,*]

[a] Institute of Science, Hacettepe University, Ankara, Turkey
[b] Department of Civil Engineering, Kırşehir Ahi Evran University, Kırşehir, Turkey
[c] Department of Civil Engineering, Hacettepe University, Ankara, Turkey
[d] Department of Civil Engineering, Abdullah Gül University, Kayseri, Turkey

ARTICLE INFO

Keywords:
Titanium dioxide (TiO_2)
Photocatalytic activity
Cementitious systems
Nitrogen oxides (NO_x) degradation
Inclusion size distribution
Hydration

ABSTRACT

This paper explores the effect of the inclusion size of titanium dioxide (TiO_2) particles on a variety of performance properties of cementitious systems via experimental studies. In addition to comprehensive microstructural analysis including pore size distribution and scanning electron microscopy with energy-dispersive X-ray spectroscopy (SEM-EDX) analyses, particular consideration was given to the effect of particle size distribution (PSD) of TiO_2 particles on mechanical and photocatalytic properties and hydration kinetics of cementitious systems. Nano-sized, submicron-sized and micron-sized anatase-phase TiO_2 powders were utilized as photocatalysts at a dosage of 5% by total weight of powder material. In addition to the single use of TiO_2 particles with three different size ranges (nano, submicron and micron), they were also used in combination by adjusting their PSDs with three different PSD moduli (q): 0.1, 0.5, and 0.9. Test results show that techniques for achieving optimal microstructural characteristics of cementitious systems also help design and improve their performance in favor of multifunctionality. As a result of PSD optimization of TiO_2 particles with three different size ranges, which was significantly influential on the microstructure of the cementitious systems, superior photocatalytic degradation results were obtained from mixtures containing lower amounts of nano-sized TiO_2 particles. Cementitious composites with denser microstructure showed lower performance in terms of being able to maintain photocatalytic degradation capability for a prolonged period, whereas the opposite was the case for compressive strength.

1. Introduction

Air pollution has become a major global issue with negative environmental, economic and health impacts. To overcome this problem, many approaches have been taken to eliminate or reduce polluting emissions such as carbon monoxide, sulfur oxides and nitrogen oxides (NO_x) sustained in air [1–8]. Nitrogen oxide (NO_x [NO and NO_2]) leads to the formation of ozone gases and acid rain [9–10], and is particularly detrimental to the health of living things. To reduce its negative effects, it should be captured and permanently stored as harmless substances, using efficient process facilities/methods. In that regard, multifunctional advanced materials with NO_x reduction capability have been gaining importance with sectors looking to improve air quality: the construction industry is one of those sectors. Their focus is shifting towards use of NO_x-reducing materials (photocatalysts) in cementitious systems to provide air purifying properties and decrease environmental burden. In this regard, materials such as titanium dioxide (TiO_2), zinc oxide (ZnO) and cadmium oxide (CdO) are photocatalysts frequently used by the construction sector worldwide [11–12]. Among all the available materials capable of reducing NO_x under ultraviolet (UV) radiation, TiO_2 is recommended for use in cementitious systems due to its cost-effectiveness, high photocatalytic degradation capability [13], chemical stability, non-toxicity in the cement matrix and remaining in an inert state unless exposed to UV radiation [12,14–15].

* Corresponding author at: Department of Civil Engineering, Hacettepe University, Ankara, Turkey.
E-mail address: sahmaran@hacettepe.edu.tr (M. Şahmaran).

https://doi.org/10.1016/j.conbuildmat.2021.125992
Received 4 September 2021; Received in revised form 9 November 2021; Accepted 1 December 2021
Available online 10 December 2021
0950-0618/

Photocatalytic degradation capability of the TiO_2-incorporated cementitious systems is directly related to the surface morphology, specific surface area and particle size of TiO_2 utilized and the number of photocatalyst particles on UV-reached surfaces of photocatalytic cementitious systems. Considering that the particle size of TiO_2 is a significantly influential factor on the activity of photocatalytic systems, studies addressing the relationship between the particle size of TiO_2 incorporated into the cement-based systems and photocatalytic activity of such systems have been performed. Seo and Yun [16] used 35 nm- and 100 nm-sized TiO_2 particles, and obtained higher NO removal rate from mortar mixtures produced with smaller TiO_2 particles (35 nm) compared to those with larger ones (100 nm). Their results were found attributable to the fact that (i) smaller-size particles mean the presence of larger number of particles and thereby large surface area beneficial for NO absorption capability, and (ii) smaller-size particles provide higher amount of active surface areas. Similarly, Chen and Poon [17], Husken et al., [18]; Hunger et al., [19], Meng et al., [20] and Folli et al., [21] found results indicating that TiO_2 particles with higher surface area exhibits better photocatalytic degradation capability compared to TiO_2 with lower surface area. Although high photocatalytic efficiency of nano-sized TiO_2 particles compared to larger-sized TiO_2 particles [22–27], considering the fact that obtaining nano-sized particles requires a costly, demanding and intense production process, to ensure more sustainable and cost-effective air cleaning through photocatalytic reactions stimulated in TiO_2-incorporated cementitious systems, cheaper larger-sized TiO_2 particles should be included in the photocatalytic cement-based systems along with nano-sized ones to improve performances of cementitious systems other than photocatalytic performance in favor of multifunctionality. Although the properties of TiO_2 used as photocatalyst in cement-based systems have significant effects on the NO_x degradation capability, the microstructure of such systems (the number of voids and pores and pore size distribution) undeniably affects the activity as well. Pérez-Nicolás et al. [28] manufactured mortars with different types of binders namely, Portland cement, high-alumina cement, low-alumina cement and dry slaked lime and obtained relatively higher photocatalytic degradation activity from mortars prepared by using high-alumina cement and lime separately, which contained higher amounts of pores with diameters above 0.05 μm allowing easier reach of NO molecules into the more in-depth parts of the mortars in favour of further contact between the surface of photocatalytic materials and pollutants. Lucas et al. [29] prepared several mortars by using different types of binders (e.g. lime, cement and gypsum) and established links between the microstructure and photocatalytic performance of these mortars. They emphasized that high porosity promotes the photocatalytic activity through facilitating the gas diffusion in an effort to assist the contact between the photocatalyst and NO_x gas at the irradiated surface, and the diameter of pores should not be less than 1 μm (nanopores) to restrict the gas diffusion, as also reported by Giosuè et al. [30]. Similarly, Sugranez et al. [31] stated that the formation of higher amount of hydration products provides a denser microstructure through the filling of the pores, while lower amount of hydration products and the amount of adsorbed water filling the space between the cement grains provide a more porous structure, which is beneficial for higher photocatalytic activity. They also concluded that photocatalytic activity is enhanced as the total porosity increases due to higher possibility of having larger number of active sites accessible to the molecules needed for the photocatalytic reactions and increasing in the generation/amount of hydroxyl radicals to react with NO_x, and they proposed that poor packaging of aggregate particles [through modification of particle size distribution (PSD)] is a method that can be used to create a macro-porosity structure. In order to achieve improved photocatalytic activity through altering the porosity of cementitious materials, Chen and Poon [17,32] and Poon and Cheung [33] recommended changing the PSD of aggregates or decreasing the cement content of the mixtures. Meng et al. [20], Matějka et al. [34], Lee et al. [35], Guo et al. [36], Xu et al. [37–38] and Boonen and Beeldens [39] observed increments in the NO removal rate with increased porosity as well. Chen et al. [40] also noted the positive contribution of porosity to the photocatalytic activity, as it provides a channel for pollutants to easily flow through, more surface area for the deposition of photocatalysts and more space for holding/accumulation of final products, which prevents the covering of the surface of the photocatalyst. Jin et al. [41] stated that the presence of larger amount of micropores (less than 5 nm) in cement-based mortars is beneficial for NO_x uptake.

In the case of co-utilization of TiO_2 particles of different sizes, optimizing PSD of all TiO_2 particles can be essential for optimum performance and/or improvement in performance of systems in several ways. Feret [42] first studied the PSD to obtain more economical concrete mixture designs by filling in voids among particles. The Fuller and Thompson method has also been used for a long time in determining the extent to which concrete aggregates should be mixed during PSD optimization [43]. In 1980, the "minimum particle diameter" technique, which considers the size of the smallest grain used as well as the largest one, was used by Funk et al. [44] to create mixtures with the highest packing density. There have also been other methods used to ensure high compactness of aggregates [45–46]. On the other hand, in addition to PSD optimization of aggregates, proper gradation of powdery materials such as cement or mineral admixtures can fill entire voids among different particles. There are number of studies related to the effects of optimizing the PSD of some powder materials on several properties of cementitious systems. Sevim and Demir [47] studied the effect of optimizing the PSD of fly ash on the performance of cement-based systems in terms of mechanical and durability perspectives. They concluded that optimizing the PSD of fly ash particles in a proper manner provided much better performance for cementitious systems. Another study of Sevim and Demir [48] investigated changes in physical and permeability properties of cementitious mortars through optimizing the PSD of fly ash. They found that modifying the PSD of fly ash particles as a pozzolanic material has an undeniable effect on the properties of cement-based systems, due to proper PSD playing a major role in filler effect and providing a good distribution of solid concentration. Lim et al. [49] also studied the effects of particle grading on autogenous shrinkage and strength of ultra-high-performance concrete, and they reported that PSD is reasonably influential on these concrete properties.

As results of several literature studies show, the PSD of powder materials has a significant influence on several properties of cementitious systems. However, until now, there have been no specific studies on using different-sized TiO_2 materials with optimized PSD in cementitious systems to improve microstructures in favor of optimum photocatalytic efficiency. In this instance, optimization of the PSD of TiO_2 particles in a wide range of sizes (inert ingredients that can be considered filling materials along with their photocatalytic efficiency) is necessary to improve the engineering properties of cementitious systems and/or the degree of photocatalytic reactions in favor of NO_x degradation capability. Therefore, due to the absence of relevant studies, the authors set out to investigate the effects of PSD of TiO_2 with ternary use of nano-sized, submicron-sized and micron-sized TiO_2 particles on photocatalytic performance and mechanical properties of cementitious systems. The effects of PSD optimization on mechanical properties (compressive strength), physical properties (pore volume and pore size distribution), hydration kinetics and NO_x degradation capability were investigated using different distribution modules. In addition, microstructural features of specimens were examined by microstructural characterization analyses including scanning electron microscopy with energy-dispersive X-ray spectroscopy (SEM/EDX).

2. Experimental program

2.1. Materials

Considering its lower light absorption ability compared to that of Ordinary Portland Cement (OPC), CEM I 52.5R type White Portland

Cement (WPC) conforming to the EN 197–1 cement standard was used as the main binder material in all mixtures. Its chemical composition and physical properties are summarized in Table 1. Nano-sized, submicron-sized and micron-sized anatase-phase (NA, SMA and MA) TiO_2 powders were used as photocatalysts to degrade the NO in the presence of UV light. Physical properties of different sizes of anatase-phase TiO_2 powders used in this study are presented in Table 2. Different-sized TiO_2 used as photocatalyst material in this study was characterized by using scanning electron microscope (SEM) (Tescan GAIA 3 FIB-SEM operated at 3.0 kV) and X-Ray diffraction measurement (XRD) (Rigaku Ultima-IV diffractometer at 40 kV, within a scan range of 2θ = 5–80° and 30 mA with Cu-Kα (λ = 1.5405Å) radiation.). To prevent any error in results, a representative sample of powder was obtained from the inside of the premixed powder batch of TiO_2 powders and was dried overnight in an oven before analyzes. X-ray diffraction (XRD) patterns of NA, SMA and MA TiO_2 powders are shown in Fig. 1. The morphology and microstructure of NA, SMA and MA TiO_2 powders obtained by SEM for each size of TiO_2 are presented in Fig. 2.

Two different surfactants were used in this experimental study, namely polycarboxylic ether-based superplasticizer (PCE) and polyphosphates and aminocarboxylate-based liquid polyacrylic acid (PAA). The PCE was liquid, conforming with ASTM-C494/C494M standard [50], with 40% solid material content and a specific gravity of 1.1. The PAA was used to provide particle surface charges with its polyelectrolyte dispersant ability [51]. White, milky liquid PAA contained 48% solid material, with a density of 1.22 kg/l and pH value of in the range of 3–4.5.

2.2. Mixture proportions

All mixtures were prepared at a constant water to powder ratio of 0.35, by weight. Preliminary studies were performed for determining optimum TiO_2 content to be utilized in this study. Specimens prepared with different TiO_2 contents, ranging from 1% to 20% of total weight of powder material, were subjected to NO degradation tests and there was not significant increase in NO removal rate beyond TiO_2 utilization rate of 5% and even declines after a certain point. Therefore, utilization rate of TiO_2 powders was kept constant at 5% of total weight of powder material for all mixtures. NA, SMA and MA TiO_2 powders were used as ternary and their incorporation rates were determined in accordance with the PSD equation proposed by Funk et al. [24]. Various PSD moduli (0.1, 0.5, 0.9) representative of a wide region were used. NA, SMA and MA TiO_2 powders were also used solely. To ensure homogeneous distribution of TiO_2 particles throughout matrix without compromising any other properties of the mixtures, the proper amounts of PCE (around 0.5% of the total weight of powder materials) and PAA (0.5% of total weight) were used as binary surfactant materials in all mixtures. These utilization rates for surfactant materials were chosen based on a previously conducted study by the authors [51].

2.2.1. Particle size distribution of TiO_2 particles

To study the influence of optimizing the PSD of TiO_2 particles in co-utilization of different-sized TiO_2 particles on the mechanical properties and photocatalytic efficiency of the cementitious systems, PSD Equation (1) proposed by Funk et al. [44], was adapted to this study. When using this equation to calculate incorporation rates of TiO_2 powders with different particle size fractions, three sieve diameters of 50 nm, 255 nm and 1110 nm were considered: the maximum grain sizes of each TiO_2 powder batch classified by particle size (NA, SMA, MA; respectively) and the limit values separating the TiO_2 materials from each other in accordance with particle size.

$$P(D) = \frac{D^q - D^q_{min}}{D^q_{max} - D^q_{min}} \quad (1)$$

where P(D) is the passing percentage of TiO_2 particles passing through relevant sieve, D is the diameter of relevant sieve opening, D_{min} is the minimum particle diameter in all TiO_2 powders and D_{max} is the maximum, and q is the PSD modulus. Three different PSD moduli of 0.1, 0.5 and 0.9 were used. It should be noted that mixtures containing relatively higher proportion of particles with larger grain size were obtained when the numerical value of the PSD modulus increased. NA, SMA and MA TiO_2 powders were also used solely to observe their individual influences on the performance of cementitious systems. In addition, a reference mixture was manufactured without TiO_2 powder content for comparison. PSD curves were plotted using the equation above for values of q: 0.1, q: 0.5 and q: 0.9. These PSD curves and those of NA, SMA and MA TiO_2 powders are displayed in Fig. 3. A total of 7 different mixtures were manufactured: their proportions can be seen in Table 3.

Mixtures are denominated with letters and numbers based on ingredients used in production. M0 is the reference mixture. The second, third and fourth mixtures (MNA, MSMA, MMA) were prepared using TiO_2 powders solely according to their particle size. For example, MNA was prepared using only NA TiO_2 powder. The fifth, sixth and seventh mixtures (MQ0.1, MQ0.5, MQ0.9) were prepared by ternary use of NA, SMA and MA TiO_2 powders with different PSD moduli. For example, MQ0.1 was prepared using a PSD modulus of q = 0.1.

Table 2
Physical properties of different sized anatase-phase TiO_2 powders.

Physical Properties	Nano-sized Anatase (NA)	Submicron-sized Anatase (SMA)	Micron-sized Anatase (MA)
Purity (%)	99.86	99.89	99.87
Density (g/cm³)	3.55	3.55	3.60
Maximum Grain Size (nm)	50	255	1110
Minimum Grain Size (nm)	0.4	50	255

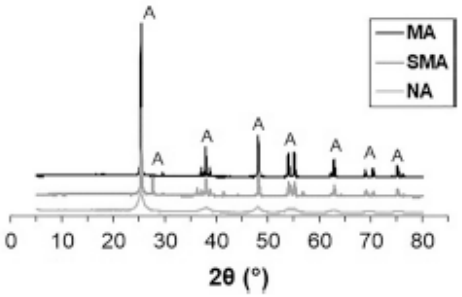

Fig. 1. XRD analysis of MA, SMA and NA TiO_2 (Anatase: A).

Table 1
Chemical composition and physical properties of CEM I 52.5 R WPC.

Chemical Composition, %						Physical Properties		
SiO_2	Al_2O	Fe_2O_3	CaO	MgO	SO_3	Loss on ignition	Density (g/cm³)	Specific surface, Blaine (cm²/g)
21.39	3.37	0.89	62.6	2.39	4.55	3.1	3.15	4650

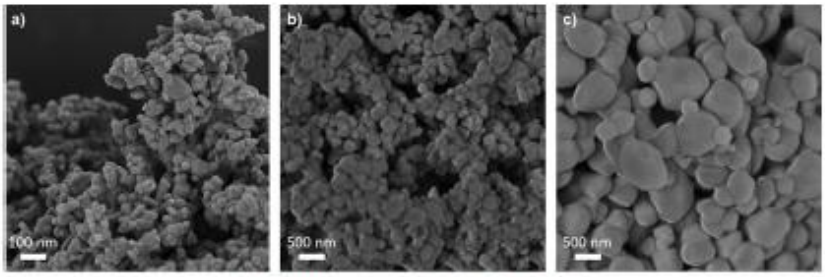

Fig. 2. SEM images of a) NA, b) SMA and c) MA TiO_2.

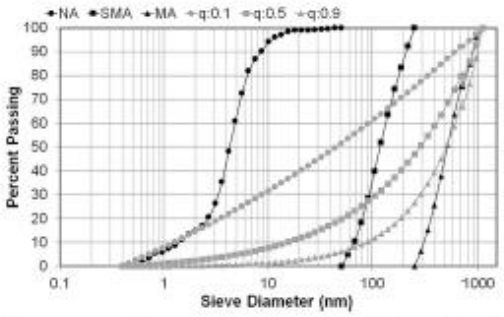

Fig. 3. PSD curves of NA, SMA, MA TiO_2 powders and TiO_2 powders with varying PSD moduli.

2.3. Mixing Process, specimen preparation and testing

All mixing was conducted with an Vibra-Cell ultrasonic mixer with a 25 mm diameter (Fig. 4.a) and a planetary-type laboratory mixer with a 4-liter capacity (Fig. 4.b). To investigate the effects of PSD accurately by providing more homogenous dispersion of TiO_2 in system, the mixing procedure developed/determined in the study of [51] has been followed in this study. The overall mixing process included the following steps: (i) To uniformly disperse powder materials throughout the matrix, surfactant materials (PCE, PAA), TiO_2 powders and water were initially mixed with an ultrasonic mixer for 10 min at a working amplitude of 80% and an energy input of 1900 Joules; (ii) The suspension obtained after ultrasonic mixing was slowly added to a simultaneously operating planetary-type laboratory mixer containing WPC at 100 rpm over 30 s; (iii) Mixing speed was increased to 300 rpm and all ingredients (WPC, TiO_2, water, PCE and PAA) were mixed for another 10 min at 300 rpm.

Mixture performance was evaluated by measuring compressive strength, photocatalytic degradation capability (NO reduction in percentage), hydration kinetics, pore size distribution, and microstructural characterization. For the compressive strength and photocatalytic degradation tests, mixtures were poured into pre-oiled molds and compacted using a vibration table. All specimens were then demolded after curing for 24 h in the laboratory environment and moisture cured in plastic bags at 95 ± 5% RH, 23 °C until testing age. The compressive strength of all mixtures was evaluated according to the ASTM C109 standard. 50 mm cubic specimens were prepared to determine uniaxial compressive strength. Tests were conducted using a loading rate of 0.9 kN/s and the average compressive strength value of three cubic specimens was reported for each curing age of 2, 7, and 28 days.

The dynamic test method was used as in study of [51] to obtain the NO degradation capability of the specimens. In this method, gas passes continuously throughout a test unit at a constant flow rate by interacting with the surface of the specimen and the difference in gas concentration between the system inlet and outlet, which is directly related to photocatalytic efficiency, is monitored by measuring simultaneously in real time. Details of the equipment used to measure NO reduction capability can be found in Fig. 5. To determine photocatalytic efficiency of the mixtures, 50 × 100 × 100 mm prismatic specimens were prepared separately for each curing age of 7, 28 and 90 days. A flow of 1000 ± 50 ppb of NO gas was introduced at a rate of 3.0 l/min, from a 5 mm spacing between the 50 ± 1 cm^2 specimen surface and UV permeable quartz glass positioned above a closed reaction cabinet. UV light with an intensity of 10 W/m^2 was dropped on the specimen surface with two 18 W UV-A blue lamps and one 36 W (UVA-1) white lamp. NO gas entering the system was moistened with a humidifying bottle to reach 50–60% humidity level. In addition, NO gas flowing through the system was diluted

Fig. 4. a) Ultrasonic mixer and b) planetary-type laboratory mixer.

Table 3
Mixture Proportions (values are in g).

Mixture #	ID	PSD Modulus (q)	WPC	TiO_2 MA	SMA	NA	Water	PAA	PCE
1	M0	–	2000	–	–	–	700	10	10
2	MNA	–	1900	–	–	100	700	10	10
3	MSMA	–	1900	–	100	–	700	10	10
4	MMA	–	1900	100	–	–	700	10	10
5	MQ0.1	0.1	1900	25.0	23.5	51.5	700	10	10
6	MQ0.5	0.5	1900	53.1	27.1	19.8	700	10	10
7	MQ0.9	0.9	1900	73.5	20.4	6.1	700	10	10

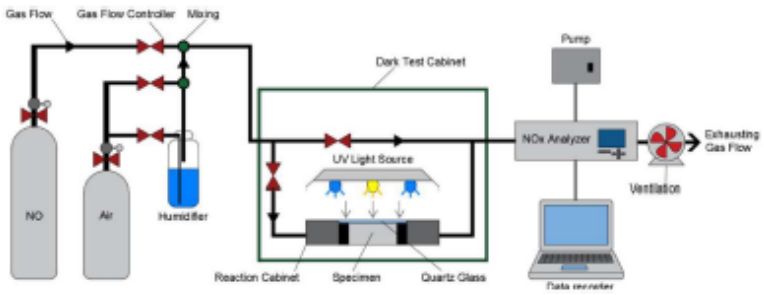

Fig. 5. Schematic view of the photocatalytic testing system.

from 100 ppm to 1 ppm using dry air to ensure proper flow rate. Thermo Scientific Model 42i NO analyzer was used continuously to measure change in NO concentration. To ensure reliable testing under consistent conditions and to prevent the manipulative effects of humidity on photocatalytic efficiency reported by Cassar et al. [52], Dylla et al. [53], and Seo and Yun [16], all specimens were dried in an oven at 45 °C for 48 h before testing. The testing surface of the specimen was then sanded and cleaned, and the specimen was placed in the reaction cabinet, where its upper surface could be illuminated with UV light. To adapt the specimen to the test environment, it was kept under active UV-light sources for four hours without any gas flow through the system. After this process, UV light sources were switched off and pre-adjusted gas flow was introduced to the system. The UV light sources were turned on at least 10 min after the gas concentration remained constant. Under the influence of UV irradiation, photocatalytic specimens started to reduce the NO concentration of flow. The test was performed until the lowest point at which NO concentration remained constant as a result of photocatalytic degradation reactions on the specimen. After that point, UV lights were turned off and gas flow was continued until NO concentration reached its initial level again. At the end of the tests, in order to determine the photocatalytic performance of the cementitious systems, the NO_x and NO reduction, and NO_2 formation (%) values, which were calculated according to Equations (2), (3), and (4), respectively, were obtained. Furthermore, for the purpose of determining the photocatalytic efficiency of the system, selectivity that expresses the ratio of degraded NO that ends up as innocuous nitrate rather than toxic nitrogen dioxide is used and is derived according to Equation (5) [54–55].

$$NO_{xred}(\%) = \frac{NO_{xi} - NO_{xf}}{NO_{xi}} \times 100, \quad (2)$$

$$NO_{red}(\%) = \frac{NO_i - NO_f}{NO_i} \times 100, \quad (3)$$

$$NO_{2for}(\%) = \frac{NO_{2f} - NO_{2i}}{NO_i} \times 100, \quad (4)$$

$$S(\%) = \frac{NO_{xred}(\%)}{NO_{red}(\%)} \times 100, \quad (5)$$

where NO_{xred} (%), NO_{red} (%), and NO_{2for} (%) are NO_x reduction, NO reduction and NO_2 formation, respectively; NO_{xi}, NO_i, and NO_{2i} are of the initial concentrations in order of NO_x, NO, and NO_2; and NO_f, NO_f, and NO_{2f} are the final concentrations of the NO, NO, and NO_2, respectively; finally, S (%) is the system selectivity.

Hydration kinetics of cementitious mixtures were examined using a TAM Air Microcalorimeter in isothermal conditions at 25 °C, in accordance with the practice of ASTM C 1679–17. The fresh pastes were immediately placed in plastic with closed lids and the ampoules were transferred into the calorimeter. Ampoules were placed into the calorimeter within 2 min of the end of mixing. Thermal power (as mW/g of total powder present in the cement paste) was recorded for 72 h to measure rate of hydration (rate of heat evolution). Cumulative heat of hydration curves of the cementitious pastes were also obtained as area under rate of hydration vs. time curves.

The mercury intrusion porosimetry (MIP) technique was used to characterize porosity and pore size distribution of TiO_2-based cementitious systems. First, 28-day-old prismatic specimens used for photocatalytic degradation tests were broken into small pieces, with sizes between 7 and 10 mm. The specimens were then dried in an oven at 50 °C for 1 day and the MIP test was conducted on the dry specimens. The instrument used for MIP testing (Quantachrome Corporation, Poremaster 60) had a pressure capacity of 380 MPa (55000 psia) with a contact angle of 140°.

Microstructural characterization of TiO_2-based cementitious systems were investigated with scanning electron microscopy observations coupled with energy-dispersive X-ray spectroscopy (SEM/EDX) (Tescan-GAIA3 + Oxford XMax 150 EDS) to clarify their morphologies and elemental compositions. For this purpose, specimens were obtained from 28-day-old prismatic specimens used for photocatalytic degradation tests. To do that, tested surface of the photocatalytic specimen was firstly sanded and cleaned. After that, the specimen was broken into small pieces and samples were randomly selected from among the broken pieces. SEM/EDX analyses were conducted on these specimens after being oven-dried overnight. SEM micrographs were captured, and the elemental compositions of the sections viewed were analyzed by SEM-EDX mapping.

3. Experimental results

3.1. Hydration kinetics

Isothermal calorimetry was used to examine the hydration of cementitious pastes, using 0.35 water-to-powder ratio at 25 °C to observe the influence of the PSD of anatase-phase TiO_2 on hydration kinetics. Hydration rate and cumulative heat of hydration of cementitious pastes are presented in Fig. 6. As seen from Fig. 6-a, although M0 (reference specimen non-containing TiO_2) was not the specimen which reached rate of hydration peak earliest, the highest rate of hydration peak value was obtained from this specimen. This result can be attributable to the relatively higher cement content of the reference specimen compared to those of TiO_2-substituted specimens, which will be detailed in compressive strength results section (Section 3.2).

Among the non-optimized specimens (MNA, MSMA, MMA), NA addition resulted in an earlier and higher rate of hydration peak than SMA and MA, probably due to a more effective nucleation effect provided by significantly smaller particles of NA (Table 2). Incorporating nano materials with extremely small particle size has a hydration agitation and acceleration effect [56–59]. This caused higher heat of hydration for the cementitious system containing NA than for the pastes

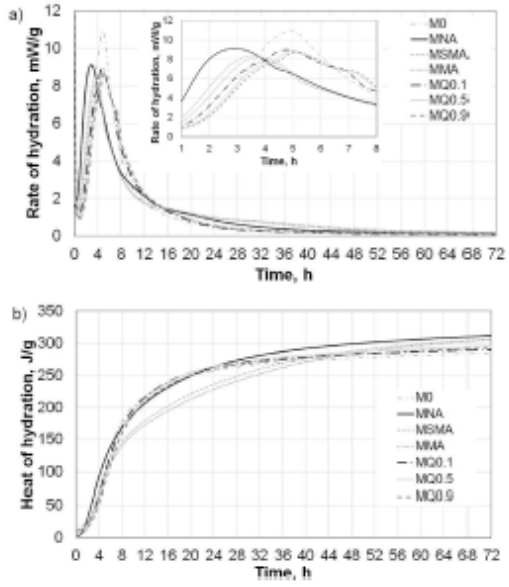

Fig. 6. a) Rate of hydration and b) heat of hydration of cementitious systems with variable PSD of anatase TiO_2.

with SMA and MA, especially between 8 and 48 h of hydration (Fig. 6-b). However, the NA, SMA and MA heat of hydration values were similar at the end of 72 h of hydration. On the other hand, cementitious systems containing a combination of NA, SMA, and MA TiO_2 particles with varying PSD moduli exhibited a maximum rate of hydration comparable to that of the paste with only NA indicating similar seeding/nucleation effects. However, the apparent initial retardation effect—where a longer induction period is observed but without a reduction rate of peak heights for the MQ0.1, MQ0.5 and MQ0.9 may be attributed to retardation of cement grains dissolution because of residual inorganic substances. Knowing that some inorganic (SO_4^{2-}, CO_3^{2-}, PO_4^{3-}, and F^-) materials have an adverse effect on early dissolution rate [60]. In this regard, sulfate ions, coming from extracting and purifying process, on TiO_2's surface may be dissolved into C_3S particles, causing dissolution to be delayed [61–62]. The reason why shifted peak observed by MQ0.1, MQ0.5 and MQ0.9 were related with retardation effects of residual inorganic materials. However, these retardations were not effective on non-optimized TiO_2 used paste mixtures. This could be attributed to effects of PSD which lead more densify structure and covering more cement grain in fresh stages, hence results more retardation effects and less dissolution of particles in initial duration.

When comparing the influence of PSD modulus on the rate and heat of hydration, increasing PSD modulus of TiO_2 particles from 0.1 to 0.9 made no considerable difference. Besides, TiO_2 addition with varying PSD moduli resulted in a higher heat of hydration than SMA and MA TiO_2 for hydration time of up to 48 h. However, the reverse was true thereafter. This finding indicates that using nano-, submicron- and micron-size particles, mixed to provide varying PSD moduli, is highly effective on the rate and total heat of hydration at early periods before 48 h. Furthermore, anatase-TiO_2 with varying PSD moduli caused a small shoulder formation in the rate of hydration curves at around 8 h. This kind of shoulder formation in the deceleration stage of the main hydration peak is generally associated with the conversion of AFt to AFm [63]. Earlier conversion of AFt to AFm, in the case of anatase-TiO_2 with varying PSD moduli, could be attributed to the specific influence of PSD on the hydration of calcium aluminates, which cause earlier conversion of AFt to AFm.

3.2. Compressive strength

Fig. 7 illustrates the compressive strength test results of each mixture for different curing ages. MNA, MSMA, MMA were designed to reveal the effect of the particle size of TiO_2 powders on the performance of cementitious systems. In addition, MQ0.1, MQ0.5, MQ0.9 were designed to better understand the effects of PSD optimization on TiO_2 particles. Due to ongoing hydration reactions, the extended aging/curing resulted in continuous increments in the compressive strength results, irrespective of mixture parameters. MSMA showed the highest strength increase at 33.7%, from 2-day to 7-day curing age. Between 7-day and 28-day curing ages, strength increases slowed for all mixtures. The highest compressive strength test results were recorded from M0 specimen (reference specimen non-containing TiO_2) for each curing age with the values reaching 59.32 MPa for 2-day-old specimens, 71.33 MPa for 7-day-old specimens and 85.30 MPa for 28-day-old specimen. In the available literature, it was reported that the mechanical performance of cementitious systems can be improved with the incorporation of different nano materials up to a certain nano-material utilization rate beyond which decrements or negligible increments can be noted [64–65]. In the study of Jimenez-Relinque et al. [66], incorporation of 2% TiO_2 (by mass of cement) reduced the compressive strength of the cementitious systems. In this regard, considering relatively higher incorporation rate of TiO_2 powder in this study (5% of total weight of powder material), the relatively lower compressive strength results of the TiO_2-incorporated systems (especially of MNA) compared to that of reference specimen (M0) can be attributed to the dilution effect (diminution of cement). The addition of inert TiO_2 powders resulted a less amount of presence of reactive cement (in percentage) in the mixtures decreasing the rate/amount of hydration products manufactured and causing lower compressive strength [65–67].

Among the non-optimized specimens (MNA, MSMA, MMA), it was evident that those containing nano-sized TiO_2 (MNA) showed the highest compressive strength results for each curing age. The compressive strength values of MNA for 2-day, 7-day and 28-day curing ages were 55.40, 66.00 and 77.63 MPa, respectively. The probable reason for this behavior is that nano-sized powders create higher density due to the filler effect arising from comparatively smaller particle size [68]. This behavior can also be attributed to the seeding effect, which is the

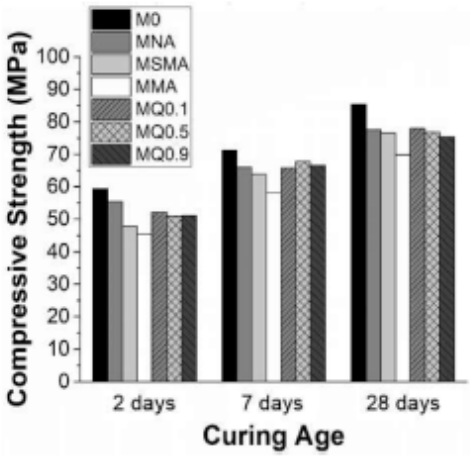

Fig. 7. Compressive strength test results.

formation of additional area (nucleation sites) due to the extremely fine particle size of nano materials (and thereby their high surface area) that can pull unhydrated cement particles towards themselves, resulting in more suitable places for the precipitation of hydration product [69–70].

MMA showed the lowest compressive strength performance among all tested mixtures for each curing age, most probably because of the lower capability of the micron-sized TiO_2 particles in terms of refinement of pore size structure in the paste due to their coarser structure and thereby lower surface areas. In the PSD-optimized specimens (MQ0.1, MQ0.5, MQ0.9), although there was no significant difference in their compressive strength values, MQ0.1 had the highest compressive strength values at approximately 52.10 (2-day), 65.82 (7-day) and 78.01 MPa (28-day), for almost all curing ages except for 7 days. The lowest compressive strength obtained after 28 days of curing among PSD-optimized specimens was 75.37 MPa for MQ0.9. When all results (obtained from TiO_2-incorporated mixtures) are evaluated together and MMA results are excluded, the differences in compressive strength results of mixtures at 28 days was not significantly evident, and compressive strength test results were 76–79 MPa for tests carried out on all TiO_2-incorporated mixtures after 28 days.

3.3. Photocatalytic performance

The photocatalytic activity of 5% anatase-phase TiO_2-substituted cementitious systems was tested to assess the effects of single or combined utilization of three different size ranges of TiO_2 particles on the photocatalytic degradation capability of cementitious systems. Fig. 8 shows NO_x, NO, and NO_2 concentration profiles obtained during the NO degradation tests under illumination. In addition, NO_x and NO degradation and NO_2 formation rates (in percentage) of the developed systems together with the system selectivity values are summarized in Fig. 9 for easy comparison of photocatalytic performances of the specimens. When the degradation rates of 7-day, 28-day and 90-day-old specimens are evaluated, it can be clearly seen that the NO_x degradation rates of MNA were the highest for each curing age. Although using nano-sized materials in the cementitious systems triggers agglomeration problems caused by the high surface interactions due to the particles' high surface area and energy [71], specimens containing nano-sized TiO_2 powder had comparatively high photocatalytic degradation capability. This can be attributed to the easy current transfer capability of the nano-sized TiO_2 from its surface, especially when uniform distribution was guaranteed [9,12,72].

Due to the fact that photocatalytic reactions occur at the surface of the photocatalyst and photons are captured from the surface of materials [73], it is also possible to state that the photocatalytic activity directly depends on the total surface area of the photocatalyst where UV irradiation is reached and on the grain size of the photocatalyst affecting this area, and therefore nano particles can provide maximal photocatalytic surface area accessible to polluting substances. However, the microstructure of cementitious systems incorporating TiO_2 particles is significantly influential on the dispersion of TiO_2 particles throughout the surface where the photocatalytic reactions occur and thereby on the performance of these systems. On the other hand, MSMA and MMA showed considerably lower photocatalytic degradation performance than MNA, with the differences in degradation results becoming significantly more pronounced with longer curing periods. Among the PSD-optimized specimens, photocatalytic degradation rates of MQ0.9 were the highest for all curing ages and after that, in decreasing order, those of MQ0.5 and MQ0.1. Photocatalytic degradation rates of all specimens exhibited a decremental trend starting from 7 to 90 days. This time-dependent trend may have come from the ongoing hydration reaction, leading to the coating of TiO_2 particles with further hydration product and thereby reducing the presence of TiO_2 materials on specimen surfaces reached by UV irradiation. A more likely reason is that carbonation products, produced by binding carbon dioxide (CO_2) into solid carbonates on the specimen surface or another possible process, cause the specimen surface to be coated [17,33,74]. The rate of decrement in photocatalytic degradation results of non-optimized specimens from 7 to 28 days was more evident than in PSD-optimized specimens. With further aging of specimens beyond 28 days, the rate of decrement in photocatalytic degradation results of MSMA and MMA was significantly higher than in other specimens.

As followed from Fig. 9, different NO_2 formation levels were obtained from the specimens at the end of the photocatalytic reactions. The formation of NO_2 in photocatalytic reactions can be related to the HNO_3 and NO_3^- accumulation on the TiO_2 surface over time, reacting with NO, beyond a threshold value, to form NO_2 [75–76]. Besides, the reactions between NO and O_2 and/or HNO_2 and *OH could be another possible reason of the formation of NO_2 [75–77]. Considering the fact that the toxicity of NO_2 is significantly higher than the primary pollutant NO [78], it was critical to monitor the change of NO_2 levels throughout the photocatalytic reactions, and the system selectivity. When evaluating the system selectivity of the cementitious systems, it was clearly observed that the system selectivity of all specimens exhibited an incremental trend starting from 7 to 90 days. In terms of NO_x and NO reduction, although the MNA specimen containing nano-sized TiO_2 was exhibited better performances, the higher selectivity values were obtained from the PSD-optimized specimens. Therefore, it is possible to state that PSD optimization significantly contributed to enhancement in the photocatalytic efficiency of the cementitious systems by increasing the system selectivity. In the PSD-optimized specimens (MQ0.1, MQ0.5, MQ0.9), although there was no significant difference in their system selectivity values, MQ0.9 had the highest one (%91.1) at the end of the 90-day curing age.

3.4. Pore size distribution

MIP was used to test the pore size distributions of 5% TiO_2-substituted cementitious systems containing NA, SMA, MA TiO_2 particles individually or in combination and with varying PSD moduli, at the age of 28 days. MIP was also performed on reference specimen (M0) for comparison. The current pore size classification proposed by the International Union of Pure and Applied Chemistry (IUPAC) was used to describe the pore structure of the cementitious system [79]. This proposed classification classifies the pores into three groups according to their sizes, including macropores, over 50 nm; mesopores, from 50 to 2 nm; and micropores, under 2 nm. According to studies available in the literature, voids larger than 50 nm are, more influential on impermeability and strength characteristics of cement-based systems, whereas voids smaller than 50 nm are more influential on drying shrinkage and creep [80–82]. Therefore, in addition to the IUPAC classification, in this paper, pores were divided into two categories: pores larger than 50 nm termed as pores above 50 nm and pores smaller than 50 nm termed as pores below 50 nm. Total porosity (% of volume) of specimens is presented in Fig. 10. Pore size distribution percentages and curves of all specimens are illustrated in Fig. 11-a and 11-b, respectively. As indicated in Fig. 10 and Fig. 11, reference specimen (M0) had the lowest total porosity value (3.9%) and all pores available in this specimen were smaller than 50 nm, evidencing the highest compressive strength results of the M0 specimen. The figures also show that almost all pores dispersed throughout MNA were smaller than 50 nm. Furthermore, a total porosity value of 4.0% for MNA (Fig. 10) reveals that MNA has a relatively low pore volume compared to the other single-size TiO_2-substituted specimens (MSMA and MMA). As the size of TiO_2 incorporated to the matrix got coarser, the volume of pores smaller than 50 nm formed in the matrix decreased. The rate of pores, ranged between 0 and 50 nm, dispersed throughout MSMA and MMA was at 87.5% and 47.4% of the total amount of pores, respectively. Moreover, the total porosity values of these mixtures were 8.6% for MSMA and 10.4% for MMA: higher than that of MNA, as previously mentioned. It is therefore reasonable to state that using NA TiO_2, (the much finer fraction of the TiO_2) leads to better packaging of the grains, as expected and

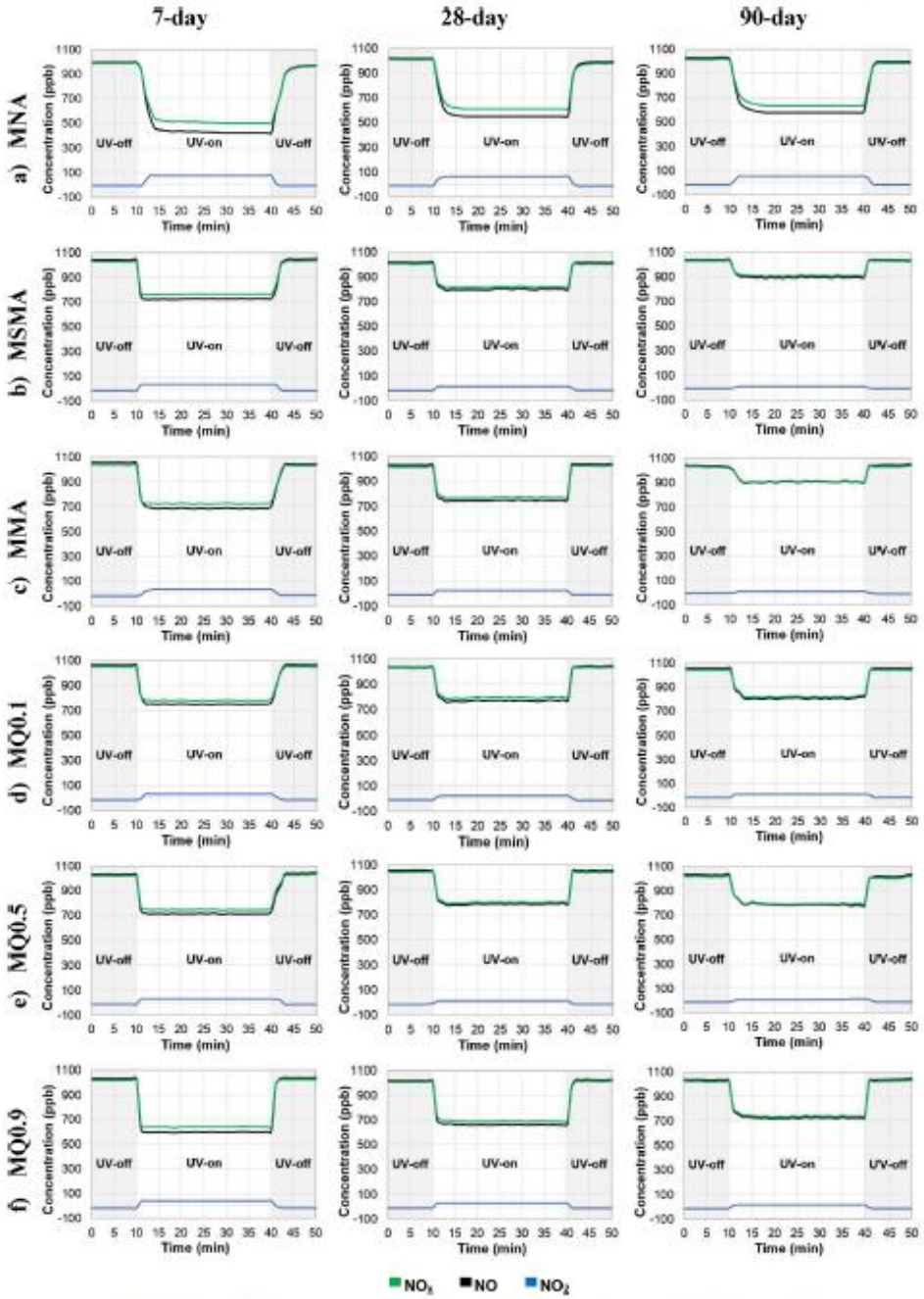

Fig. 8. Variation of NO_x, NO, and NO_2 concentration during each test for 7, 28, and 90 days old specimens.

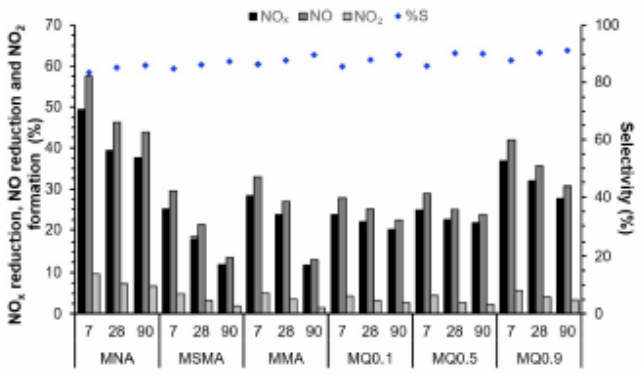

Fig. 9. Variation of NO_x reduction, NO reduction, and NO_2 formation (%) each test for 7-, 28-, and 90-days old specimens and the system selectivity (%).

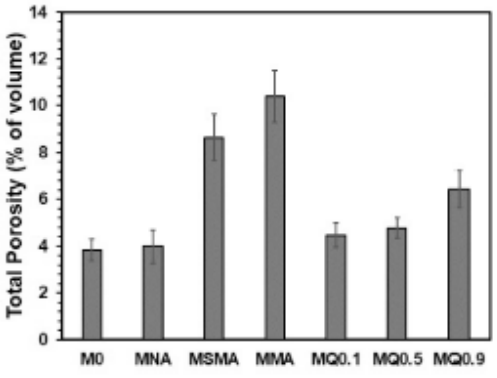

Fig. 10. Total porosity (% of volume) of the specimens.

consequently improves the compactness of the microstructure of specimens because of its filler effect.

The MIP test results of PSD-optimized specimens show that the number of pores below 50 nm in MQ0.1 and MQ0.5 were 100% and the specimen incorporated with TiO_2 using a PSD modulus of 0.9 (MQ0.9) resulted in a lower rate of pores below 50 nm (64.8%) compared to other PSD-optimized mixtures (Fig. 11a). Total porosity values were 4.5%, 4.8% and 6.4% for MQ0.1, MQ0.5 and MQ0.9, respectively; the increase in PSD modulus resulted in an increase in total porosity and proportion of pores above 50 nm. The probable reason for this is that the TiO_2 with the lower PSD modulus (q = 0.1) contained a higher proportion of small particles, which can provide more closable smaller interparticle spacing, better fill the voids between larger particles, and improve the packing density of the powder materials (TiO_2 and cement). On the other hand, for MQ0.9, which contained the highest proportion of micron-sized TiO_2 particles among the PSD-optimized specimens, the small-sized TiO_2 content was not enough to fill the voids between large particles and thereby prevented significant improvement in packing density of the powder materials compared to other specimens prepared using a smaller PSD modulus. Consequently, these results show that PSD-optimized specimens have a relatively low amount of porosity compared to non-optimized specimens, except MNA and PSD optimization significantly contributes to the pore refinement of mixtures, although the use of nano-sized TiO_2 alone performed slightly better.

3.5. Microstructural characterization

SEM micrographs with EDX analyses, performed to determine the number of Ti elements dispersed throughout a specific section, were obtained for microstructural characterization studies of TiO_2-based cementitious systems. Analyses of non-optimized and PSD-optimized specimens are shown in Fig. 12 and Fig. 13, respectively. It can be clearly seen from these figures that carbon (C), oxygen (O), calcium (Ca) and silicon (Si) were the primary elements of all specimens, and substantial part of the chemical content of all specimens was composed of Ca and O. The C contents by weight of all specimens were lower than 9%. The Ti contents (by weight %) of MNA, MSMA and MMA were 2.4, 1.7 and 4.9, respectively. For the PSD-optimized specimens, Ti contents (by weight, %) of MQ0.1, MQ0.5 and MQ0.9 were 1.9, 2.2, and 4.9, respectively. Although the amount of photocatalyst located across the surface reachable by UV-radiation has an undeniable influence on photocatalytic performance of cementitious systems, there was no obvious correlation between the amount of photocatalyst and the photocatalytic degradation rate of specimens. Considering that photocatalytic efficiency of TiO_2 particles can be affected by their crystal structure, surface area and particle size [83], the NO degradation results should be associated with the higher presence of small-sized TiO_2 on the UV-reached surface, which resulted in increments in the number of active surface sites and thereby high separation and transfer efficiency of surface charge carriers.

EDX elemental mapping images of relevant specimens are also illustrated in Figs. 12-13: red corresponds to Ti atoms and green to Ca atoms. One of the main elements (Ca) was detected in all regions of the specimens. Based on the evidence in these images, Ti elements have more uniformly dispersed throughout the PSD-optimized specimens. For the non-optimized specimens, the distribution of the Ti atoms on the surface of MNA and MMA was also generally homogeneous, although some irregularities in the dispersion of the TiO_2 particles were seen in the microstructure of MSMA specimens.

4. Discussions

In term of mechanical properties, in the non-optimized specimens, the compressive strength of the MNA surpassed all other mixtures for all curing ages. This finding has been reported by several other researchers in the literature. They attributed it to various enhancement influences of nano-scale materials on microstructural and mechanical properties in favor of obtaining a denser matrix. Well-graded ingredients stimulate the hydration process due to their high surface area, resulting in nucleation sites bonding with cement hydrates [58,84], hydration

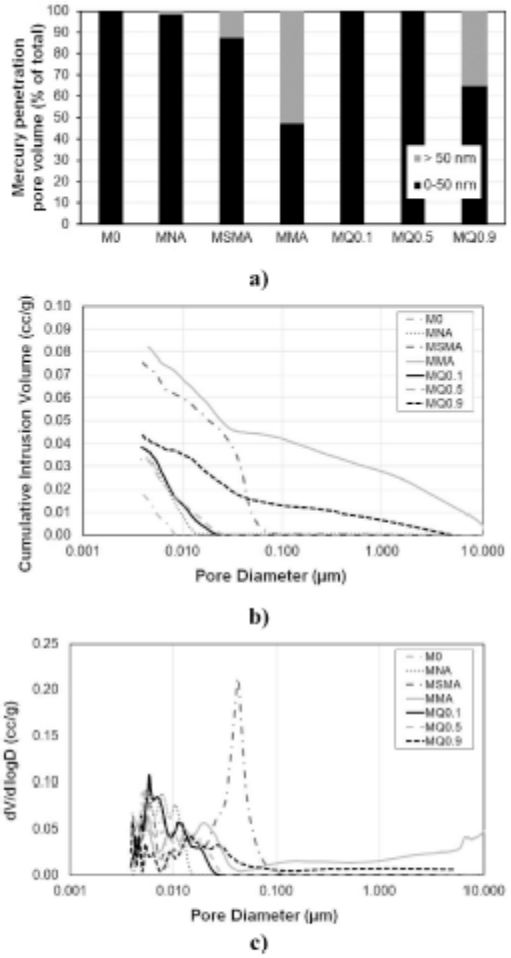

Fig. 11. a) Mercury penetration pore volume (% of total), b) Pore size distribution curves of specimens, c) dV/dlogD (cc/g).

agitation, acceleration effect [56–59] and filler effect, resulting in relatively better particle packing of constituents [56–57]. The hydration kinetics results of cementitious pastes shown in Fig. 6 show that using nano-sized TiO_2 (NA) caused an enhanced/accelerated degree of hydration reaction (kinetics) of the cementitious paste (larger peak magnitude and earlier time of peak occurrence) owing to its considerably fine structure providing significant surface energy. This acceleration confirms that using nanoparticles (NA) provides higher early-age strength. As the particle size of the TiO_2 in cementitious systems increased (among specimens characterized by single use of TiO_2 particles), the peak occurrence time increased and the peak magnitude decreased. This situation is in accordance with the results of compressive strength, which determined that increasing particle size decreases strength. Although the MNA showed highest compressive strength performances among non-optimized specimens for each curing age, the incorporation of nano-sized TiO_2 reduced the compressive strength results of the cementitious system considering relatively higher compressive strength performance of the TiO_2 non-containing specimen (M0). In this regard, it is possible to state that the decremental effect of the decrease in the reactive cement content of MNA, because of replacement of cement with inert TiO_2, on mechanical performance was more dominant than the enhancing effects of the nano materials (detailed above) incorporation into cementitious systems. It should be also stated that although, at the end of the 48 h, heat of hydration released from MNA was higher than the reference mixture, the compressive strength results were inconsistent with this case. The possible reason of this situation can be related with (i) differences in the consistency of the mixtures due to the different sized TiO_2 content, (ii) formation of heterogenous reaction product for faster hydration at the early age and (iii) differences in the hydration products because the possible effects of TiO_2 existence.

Of the PSD-optimized specimens, MQ0.1 showed better compressive strength results than the other mixtures at the end of 28 days. It is especially noteworthy that the compressive strength of MQ0.1 is higher than that of MNA, which can be attributed to its well-graded PSD achieving high particle packing density. When the hydration kinetics results shown in Fig. 6 are evaluated, it can be clearly seen that using TiO_2 with varying PSD moduli resulted in a retardation of peak occurrence compared to the single-sized TiO_2 (longer time of peak occurrence) due to retardation of early dissolution as a result of residual inorganic chemicals [62] and better covering capability of PSD-optimized TiO_2 particles. As the PSD modulus increased, the peak occurrence time increased and also its magnitude decreased due to decrement in seeding and nucleation capability with increased coarser TiO_2 particles. The 28-day compressive strength results of optimized specimens were consistent with these results. Peak magnitude values (maximum rate of hydration) of cementitious systems containing a combination of NA, SMA, and MA TiO_2 particles with varying PSD moduli were higher than those in systems containing SMA or MA TiO_2, and lower than in those containing NA TiO_2. The cumulative heat of hydration values of single-size TiO_2-substituted cementitious systems at the end of 72 h of hydration were higher than those of systems containing a combination of NA, SMA, and MA TiO_2 particles with varying PSD moduli. As a result, considering the higher peak magnitude value, the earlier peak occurrence and the higher cumulative heat of hydration of cementitious system containing NA TiO_2 at the end of 72 h of hydration, it can be clearly stated that MQ0.1's relatively high compressive strength compared to MNA was geometry-related (physical) rather than chemistry-related (chemical), and PSD optimization with PSD modulus of 0.1 provided the highest particle packing density, as mentioned earlier.

Considering all of these results, it can be clearly stated that although the difference between compressive strength results was not significantly prominent, meaningful differences were noted for 28-day-old specimens. Less pronounced effect of the modification/optimization of the PSD of TiO_2 powders on the compressive strength of specimens containing PSD-optimized powders can be attributed to the relatively wide range of particle sizes of NA and SMA TiO_2 batches, resulting in naturally good particle grading, thereby positively affecting the mechanical properties of specimens. Although it was minimally effective in increasing compressive strength for this study, the advantages of PSD-optimization of TiO_2 powders in tailoring microstructural properties are also likely to improve compressive strength results of mixtures with PSD-optimized powders over those containing TiO_2 powders with a narrower range of particle sizes.

The most important element of this study is the enhancement of the NO_x degradation efficiency of mixtures through optimization of the PSD of TiO_2 powders. As mentioned earlier, the photocatalytic activity of TiO_2 is highly dependent on its size, shape, type, phase and on changes in particle properties [85], and the photocatalytic degradation capability of the nano-sized TiO_2 particles is higher compared to the larger ones [22–27]. It is therefore not surprising that the highest performance in NO_x degradation capability was obtained from MNA for all curing ages. When the EDX analyses of MNA and MMA in Fig. 12(a) and 12(c) are

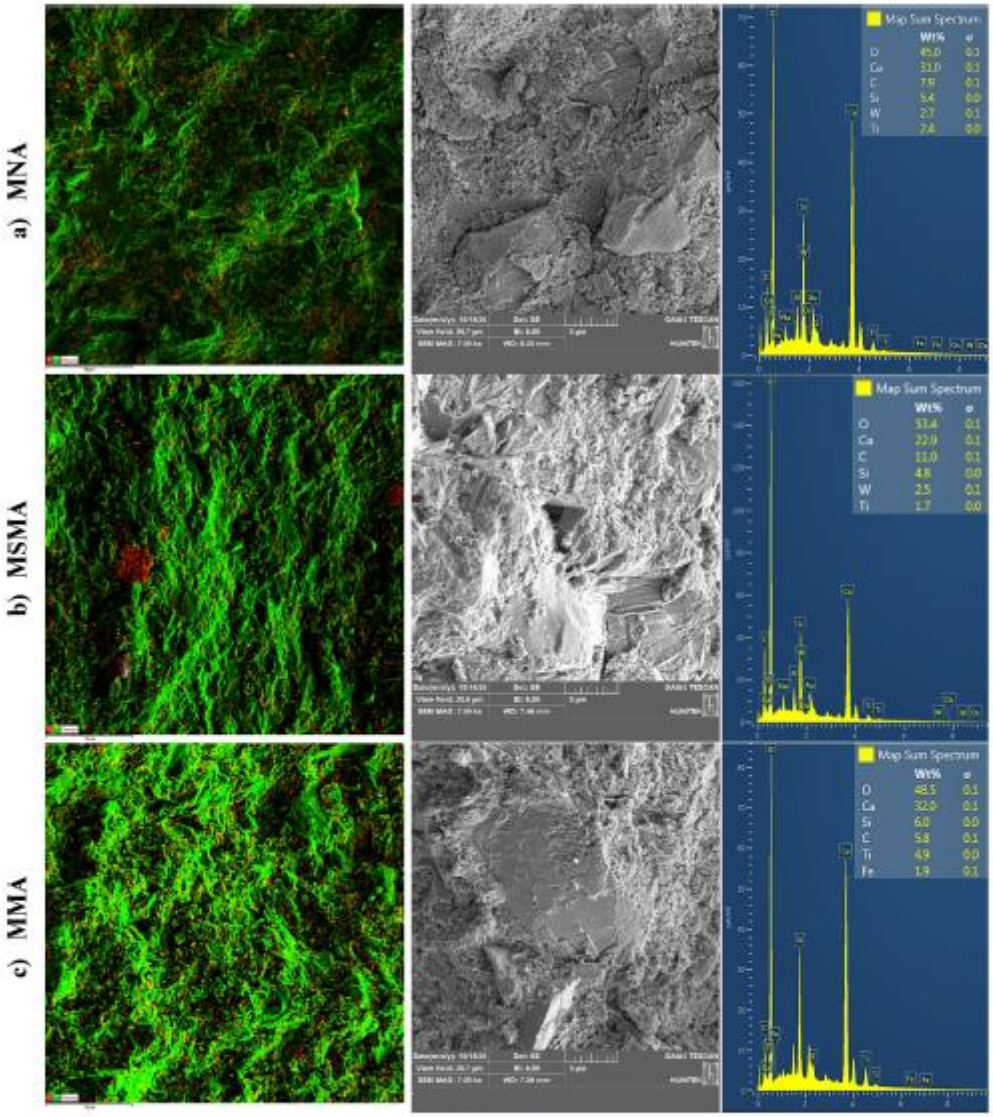

Fig. 12. Representative EDX elemental mapping images and SEM micrographs with EDX spectra of non-optimized specimens.

evaluated, it is evident that the Ti content (by weight %) dispersed throughout the viewed section of MNA (2.4%) was lower than that of MMA (4.9%), possibly due to the denser structure of the MNA. However, higher amounts of the Ti element throughout MMA did not provide higher NO degradation results than in MNA. This result also confirmed that smaller-size photocatalysts provide a more efficient photocatalytic degradation process than larger ones. This was not the case when MSMA and MMA results were compared, which is likely related to the microstructural characteristics of these specimens (explained below). However, it should be kept in mind that EDX results of the equivalent specimens can vary according to the section viewed. On the other hand, for PSD-optimized specimens, MQ0.9 showed better NO_x degradation capability, even though it contained a significantly lower amount of nano-sized TiO_2 than the other PSD-optimized specimens. In addition, whereas the amount of nano-sized TiO_2 in MNA was quite a bit larger than in MQ0.9, a remarkable difference in the nano-sized TiO_2 content was not apparent when comparing NO_x degradation rates of these two specimens. This situation is directly related to specimen microstructure and surface characteristics and may be attributed to the ability of the mixtures, through PSD optimization of TiO_2 particles, to keep distribution and/or the amount of TiO_2 particles optimal throughout the UV-reached surface where photocatalytic reactions occur. Fig. 10 and Fig. 11 show a low amount of total porosity in MNA and more small-size pores compared to the others, both of which indicate good packing

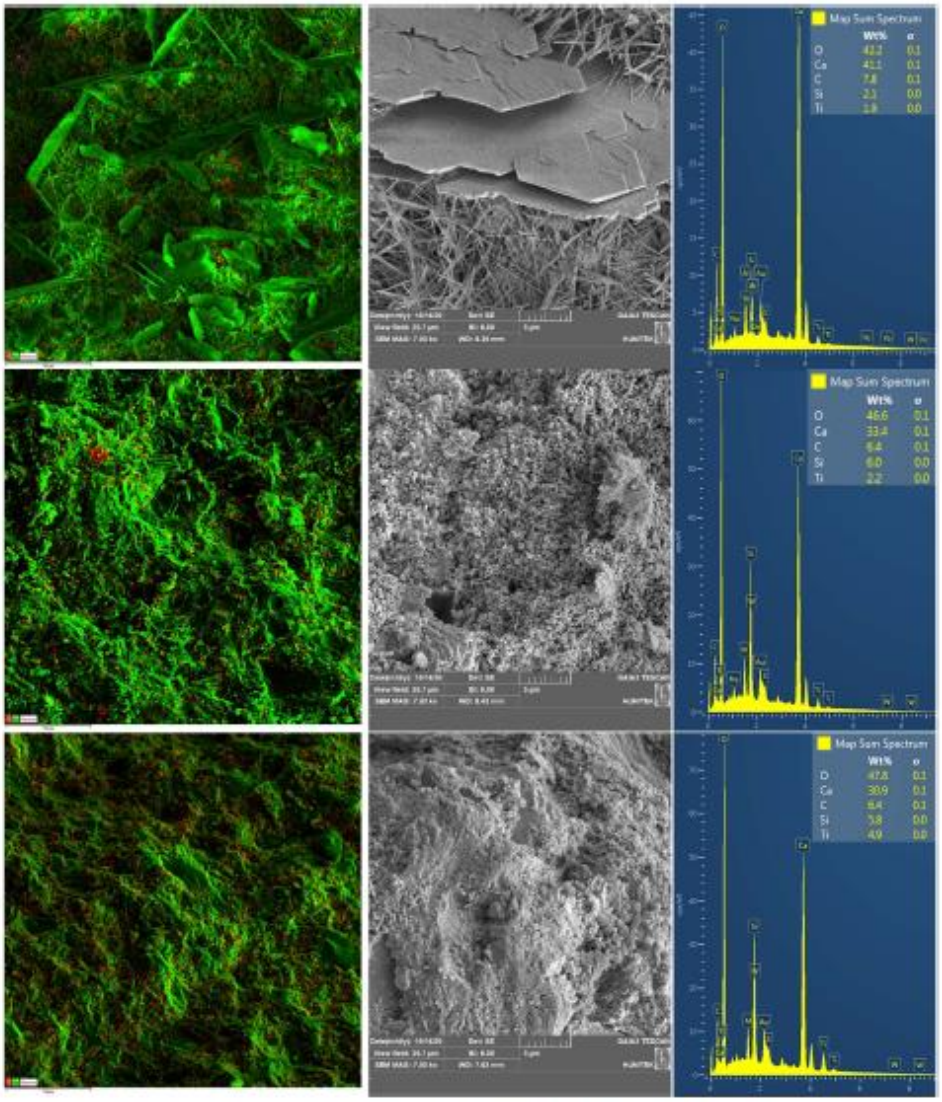

Fig. 13. Representative EDX elemental mapping images and SEM micrographs with EDX spectra of PSD-optimized specimens.

density in favor of particle distribution homogeneity and higher compactness. Therefore, the relatively lower difference between NO_x degradation rates of MNA and MQ0.9 was most probably due to the surface of the nano-TiO_2 particles in MNA being further covered with hydration products. As a result, nano-TiO_2 particles are likely to remain in the dark depths of the denser specimens, resulting in insufficient contact with UV-light and TiO_2 particles and preventing photocatalytic reactions. This situation was also valid for PSD-optimized specimens. Moreover, when evaluating the system selectivity of the cementitious systems, it can be clearly seen that MQ0.9 exhibited relatively higher performance, which means a more efficient NO_x degradation capability.

Although a refined pore structure due to good particle grading caused relatively greater compressive strength, this negatively affected the photocatalytic activity of the mixtures, thereby causing NO_x degradation with low efficiency. Furthermore, the optimal TiO_2 quantities from different-sized TiO_2 batches sufficient for efficient photocatalytic activity were different than those sufficient for mechanical property. In this regard, the most favorable particle packing was provided at a PSD modulus of 0.1 with well-graded TiO_2 particles (MQ0.1), which achieved higher strength results than the other PSD-optimized mixtures, although some natural variations were observed. This can be attributed to the improvement/optimization of the PSD of powder materials in a proper manner, which promoted pore refinement of the microstructure of the cementitious systems, thereby obtaining a relatively denser matrix.

Although MQ0.1 contains higher amounts of more active nano-sized TiO_2, its dense structure resulted in lower photocatalytic efficiency compared to other PSD-optimized specimens. On the other hand, MQ0.9 showed superior photocatalytic efficiency among all PSD-optimized specimens, despite having a small amount of nano-TiO_2. Therefore, it is plausible that the NO_x degradation capability of the mixtures is strongly related to the microstructure characteristics of matrix (as mentioned earlier) although their relationship is quite different than the relationship between microstructure and compressive strength.

MIP test results of MQ0.9 showed 6.4% total porosity and 64.8% pores below 50 nm, the highest total porosity and lowest number of pores below 50 nm among all the PSD-optimized specimens. This means that the PSD modulus of 0.9 provided a considerably higher number of pores above 50 nm, and that the amount/volume of pores dispersed throughout MQ0.9 was relatively higher compared to the other PSD-optimized specimens. Hence higher photocatalytic degradation capability of the MQ0.9 compared to the other PSD-optimized specimens may stem from the larger number of pores limiting coverage of the TiO_2 particles with hydration product. Another possible reason for the better photocatalytic efficiency of MQ0.9 is due to the multiple pore-structure of MQ0.9 homogeneously spread throughout the surface morphology, which causes a large number of TiO_2 particles to be dispersed throughout pore walls for maximum photocatalytic surface area. In addition, larger pores can allow pollutant gas (NO gas) to diffuse into the cementitious matrix more easily, thereby more pollutants participate in the photocatalytic reactions and provide easily reaching of photons to the TiO_2-containing inner parts of the specimens in favor of further contact between the surface of photocatalytic materials and UV irradiation. This situation also evident for MMA and MSMA. Although MSMA contained submicron-sized TiO_2 particles with photocatalytic efficiency that is expected to be higher than in micron-sized TiO_2, the NO degradation capability of MMA at 7 and 28 days was higher than that of MSMA. This can also be attributed to the fact that MMA contained a relatively higher volume of pores, the large majority of which were pores above 50 nm. Fig. 14 shows the relationship between the total porosity (% of volume) and NO degradation rate of specimens. Although MIP tests were carried out on 28-day specimens, total porosity (% of volume) of 28-day old specimens (considering that these reflect the tendency of specimens to form pores), was associated with NO_x degradation results at all ages of relevant specimens.

It can be seen from Fig. 14a and 14b that the general trends of these two graphs are different from each other. According to Fig. 14a (non-optimized specimens), NO_x degradation had an inversely proportional relation to the total porosity of the specimen, whereas the opposite was the case with the PSD-optimized specimens in Fig. 14b. Considering the limitations of using trend lines to show the general trend of specimens, as well as the complexity of this situation due to the presence of many factors affecting the characteristics of the specimens, this requires a deeper, more careful assessment. In this regard, if MNA is excluded, it can be clearly stated that the increased total porosity value contributes positively to photocatalytic degradation capability. MNA not fitting this trend is due to its relatively smaller particle size TiO_2 content, resulting in higher NO_x degradation capability. The photocatalytic efficiency of a cementitious system is significantly related to factors such as physically and chemically effective factors including pore structure and quantity or NO_x degradation capability/efficiency in relation to photocatalyst particle size. When they were more dominant/prominent, the negative effect of comparatively less porosity on photocatalytic efficiency was not dominant enough for MNA to cause lower degradation in the positive effect of finer TiO_2 particle content on photocatalytic efficiency compared to MSMA or MMA. However, this was not the case for PSD-optimized specimens. As mentioned earlier, the relatively higher presence of nano-TiO_2 content could not provide greater NO_x degradation results for PSD-optimized specimens. Increments in total porosity and the presence of pores above 50 nm had a greater effect on NO_x degradation capability of PSD-optimized specimens, indicating that more

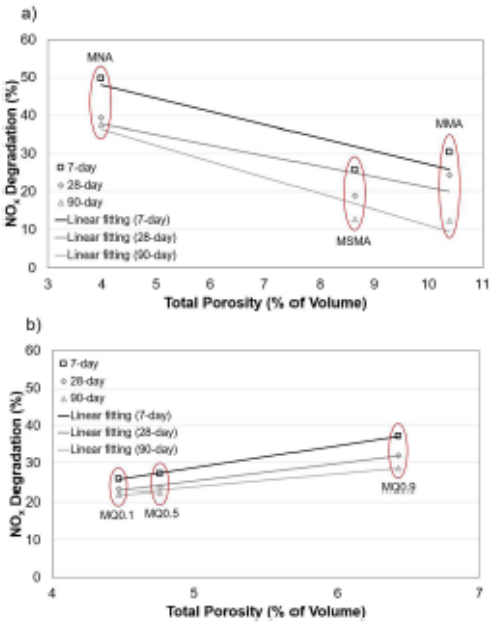

Fig. 14. Relationship between total porosity (% of volume) and NO degradation rate of specimens for (a) PSD non-optimized specimens (b) PSD optimized specimens.

pores could lead to higher photocatalytic efficiency for TiO_2-substituted cementitious systems.

Matrix transformations that also take place on the surface of the cementitious matrix with prolonged age mostly affect the photocatalytic activity of the specimens. The results of PSD-optimized specimens showed that optimizing the PSD of TiO_2 particles can limit the decrease in photocatalytic performance with further aging, such limitation was more pronounced for specimens with denser structure. These results revealed that a TiO_2 batch optimized with the proper PSD modulus could be used as a long-term, stable and efficient photocatalyst for air purification, with optimum performance in practical use.

Of the non-optimized specimens, those with denser structure (MNA) also showed more stable photocatalytic efficiency over time. This could be because the dense structure of the specimens limits further coating of the already coated TiO_2 particles over time with further hydration and leads to less sensitivity to carbonation because their network of interconnected pores is more significantly developed than in mixtures with denser structure. Low efficiency of MSMA and MMA in terms of aged photocatalytic efficiency can be also attributed to their relatively high pore volume content. This situation was also valid for PSD-optimized specimens, even though it was more pronounced for non-optimized specimens. MQ0.9, which has highest pore volume content among the PSD-optimized specimens, also showed more unstable photocatalytic degradation performance over time than denser PSD-optimized specimens.

High porosity allows further penetration of carbonation in deeper layers. By sanding the surface of specimens with lower pore volume, most of the carbonation product can be removed from the UV-reached surface, thereby freeing it of TiO_2 particles. In this way, photocatalytic reactions occurred due to a surface being free from carbonation product, and more stable specimens were obtained depending on time. Further

investigations are necessary to clarify the effect of carbonation on photocatalytic efficiency of cementitious systems by considering its relationship with the pore structure characteristics of these systems.

5. Conclusions

This study investigated the effect of particle size distribution (PSD) and optimization of TiO_2 particles on the mechanical and photocatalytic efficiency of cementitious systems. Specimens were prepared with single-use nano-sized, submicron-sized and micron-sized TiO_2 particles and co-utilizing them with different PSD moduli. This assessed the effects of PSD optimization with different PSD moduli on mechanical and physical properties of mixtures based on compressive strength, porosity and pore size distribution, hydration kinetics and NO_x degradation capability of cementitious systems. The following conclusions are based on the findings of this study:

- The compressive strength of the reference mixture without TiO_2 (M0) was the highest among all mixtures, regardless of the curing ages. Among the TiO_2-incorporated mixtures, modification/optimization of the PSD of TiO_2 powders with a proper PSD modulus provided relatively better mechanical performance by ensuring high compactness. Specimens prepared by using TiO_2 powder optimized with the PSD modulus of 0.1 performed comparatively better under compressive strength test than other non-optimized and PSD-optimized specimens at the end of 28 days.
- Although specimens containing nano-sized TiO_2 particles showed the highest photocatalytic activity, a comparatively high efficiency cementitious system in terms of NO_x degradation capability was obtained with PSD optimization of TiO_2 powders, probably due to the pore structure. High photocatalytic efficiency was obtained by using a considerably smaller number of nano TiO_2 particles, which have higher photocatalytic activity than larger ones. By optimizing the PSD of TiO_2 particles, lower decrements in NO_x degradation of mixtures over curing time were also achieved. Furthermore, PSD optimization increased the system selectivity, which proves that PSD optimization contributes to the enhancement in photocatalytic efficiency of the TiO_2-incorporated cementitious systems.
- When results related to hydration kinetics are evaluated separately for the optimized and non-optimized cementitious systems, the system with higher peak magnitude value, earlier peak occurrence, and higher cumulative heat of hydration (at the end of 72 h of hydration) showed lower total porosity formation (% of volume) and less pores above 50 nm formation. A more pronounced enhanced/accelerated hydration process was obtained by using nano-sized TiO_2 particles, resulting in the decrease of total volume of pores and the formation of pores above 50 nm. When all results are compared, it is clear that although an enhanced/accelerated hydration reaction (kinetics) was not obtained, the formation of a dense structure with proper particle packaging through ideal PSD optimization (for $q = 0.1$) prevented the formation of pores above 50 nm and thereby provided higher compressive strength.
- The pore structure of the TiO_2-substituted cementitious systems is significantly influential on their mechanical and photocatalytic properties. Although higher volume of pores (especially pores above 50 nm) increases the NO_x degradation capability of specimens, it causes higher rate of decrements in photocatalytic degradation capability with increasing curing time. In addition, a higher proportion of pores reduces compressive strength of the cementitious systems. The optimum PSD value may differ depending on the performance expected from the specimens. While the PSD value, which causes an optimum packing density and very dense microstructure, was beneficial in terms of compressive strength, it provided a less effective photocatalytic activity.
- Increasing the number of TiO_2 particles across the surface of specimens that UV rays can reach, is the key parameter in improving the photocatalytic efficiency of cementitious systems, and is significantly related to specimen microstructure. Therefore, the PSD of TiO_2 particles, which is also effective on microstructure, must be considered for the design of photocatalytic cementitious systems.

CRediT authorship contribution statement

Emrah Bahşi: Investigation, Methodology, Writing – original draft. **Oğuzhan Şahin:** Investigation, Methodology, Writing – original draft. **Hüseyin İlcan:** Investigation, Methodology, Writing – original draft. **Burak Uzal:** Funding acquisition, Writing – review & editing. **Muhammed Faruk Günal:** Investigation, Methodology, Writing – original draft. **Gürkan Yıldırım:** Funding acquisition, Data curation, Conceptualization, Writing – review & editing. **Mustafa Şahmaran:** Funding acquisition, Project administration, Supervision, Writing – review & editing.

Declaration of Competing Interest

The authors declare that they have no known competing financial interests or personal relationships that could have appeared to influence the work reported in this paper.

Acknowledgement

The authors gratefully acknowledge the financial assistance of the Scientific and Technical Research Council (TUBITAK) of Turkey provided under projects: 118M197. This publication is a part of doctoral dissertation work by the first author in the Academic Program of Civil Engineering, Institute of Science, Hacettepe University.

References

[1] D. Tristantini, R. Mustikasari, Modification of TiO_2 nanoparticle with PEG and SiO_2 for anti-fogging and self-cleaning application, Int. J. Eng. Technol. 11 (2) (2011) 73–78.
[2] D.M. Chien, N.N. Viet, N.T.K. Van, N.T.P. Phong, Characteristics modification of TiO_2 thin films by doping with silica and alumina for self-cleaning application, J. Exp. Nanosci. 4 (3) (2009) 221–232, https://doi.org/10.1080/17458080902920506.
[3] T.K. Tseng, Y.S. Lin, Y.J. Chen, H. Chu, A review of photocatalysts prepared by sol-gel method for VOCs removal, Int. J. Mol. Sci. 11 (6) (2010) 2336–2361, https://doi.org/10.3390/ijms11062336.
[4] Q. Zhang, J.B. Joo, Z. Lu, M. Dahl, D.Q. Oliveira, M. Ye, Y. Yin, Self-assembly and photocatalysis of mesoporous TiO_2 nanocrystal clusters, Nano Res. 4 (1) (2011) 103–114, https://doi.org/10.1007/s12274-010-0058-9.
[5] S. Anandan, T. Narasinga Rao, M. Sathish, D. Rangappa, I. Honma, M. Miyauchi, Superhydrophilic graphene-loaded TiO_2 thin film for self-cleaning applications, ACS Appl. Mater. Interfaces. 5(1) (2013) 207-212. 10.1021/am302557z.
[6] B.M. Kim, H.M. Yadav, J.S. Kim, Self-cleaning performance of sol–gel-derived TiO_2/SiO_2 double-layer thin films, J. Coat Technol. Res. 13 (5) (2016) 905–910, https://doi.org/10.1007/s11998-016-9804-6.
[7] H.E. Çamurlu, Ö. Kesmez, E. Burunkaya, N. Kiraz, Z. Yeşil, M. Asiltürk, E. Arpaç, Sol-gel thin films with anti-reflective and self-cleaning properties, Chem. Pap. 66 (5) (2012) 461–471, https://doi.org/10.2478/s11696-012-0144-4.
[8] Z. Yuan, B. Li, J. Zhang, C. Xu, J. Ke, Synthesis of TiO_2 thin film by a modified sol-gel method and properties of the prepared films for photocatalyst, J. Sol-gel Sci. Technol. 39 (3) (2006) 249–253, https://doi.org/10.1007/s10971-006-8164-6.
[9] O. Carp, C.L. Huisman, A. Reller, Photoinduced reactivity of titanium dioxide, Prog. in Solid State Chem. 32 (1–2) (2004) 33–177, https://doi.org/10.1016/j.progsolidstchem.2004.08.001.
[10] V. Zivica, A. Bajza, Acidic attack of cement-based materials - a review, Constr. Build. Mater. 15 (8) (2001) 331–340, https://doi.org/10.1016/S0950-0618(01)00012-5.
[11] H. Chen, A. Namdeo, M. Bell, Classification of road traffic and roadside pollution concentrations for assessment of personal exposure, Environ. Model. Softw. 23 (3) (2008) 282–287, https://doi.org/10.1016/j.envsoft.2007.04.006.
[12] J. Zhao, X. Yang, Photocatalytic oxidation for indoor air purification: a literature review, Build. Environ. 38 (5) (2003) 645–654, https://doi.org/10.1016/S0360-1323(02)00212-3.
[13] S. Hager, R. Bauer, G. Kudielka, Photocatalytic oxidation of gaseous chlorinated organics over titanium dioxide, Chemosphere 41 (8) (2000) 1219–1225, https://doi.org/10.1016/S0045-6535(99)00558-5.

[14] G. Hüsken, M. Hunger, H.J.H. Brouwers, Experimental study of photocatalytic concrete products for air purification, Build. Environ. 44 (12) (2009) 2463–2474, https://doi.org/10.1016/j.buildenv.2009.04.010.
[15] S. Wang, H. Ang, O. Tade, Volatile organic compounds in indoor environment and photocatalytic oxidation: State of the art, Environ. Int. 33 (5) (2007) 694–705, https://doi.org/10.1016/j.envint.2007.02.011.
[16] D. Seo, T.S. Yun, NO removal rate of photocatalytic cementitious materials with TiO_2 in wet condition, Build. Environ. 112 (2017) 233–240, https://doi.org/10.1016/j.buildenv.2016.11.037.
[17] J. Chen, C.S. Poon, Photocatalytic cementitious materials: Influence of the microstructure of cement paste on photocatalytic pollution degradation, Environ. Sci. Technol. 43 (23) (2009) 8948–8952, https://doi.org/10.1021/es902359e.
[18] G. Husken, H.J.H. Brouwers, Air purification by cementitious materials: Evaluation of air purifying properties. In International Conference on Construction and Building Technology, Kuala Lumpur, Malaysia, 2008.
[19] M. Hunger, G. Husken, H.J.H. Brouwers, Photocatalysis applied to concrete products-Part 2: Influencing factors and product performance, ZKG international 61 (10) (2008) 76–84.
[20] C. Meng, P. Dong, H. Tian, T. Cheng, J. Li, Y. Liu, X. Yang, M. Xie, X. Chen, X. Xi, Photocatalytic concrete paving block reinforced by TiO2 nanotubes for NO removal, J. Mater. Sci. 55 (29) (2020) 14280–14291, https://doi.org/10.1007/s10853-020-05048-w.
[21] A. Folli, I. Pochard, A. Nonat, U.H. Jakobsen, A.M. Shepherd, D.E. Macphee, Engineering photocatalytic cements: understanding TiO2 surface chemistry to control and modulate photocatalytic performances, J. Am. Ceram. Soc. 93 (10) (2010) 3360–3369, https://doi.org/10.1111/j.1551-2916.2010.03838.x.
[22] M. Anpo, T. Shima, S. Kodama, Y. Kubokawa, Photocatalytic Hydrogenation of CH3CCH with H2O on Small-Particle TiO_2: Size Quantization Effects and Reaction Intermediates, J. of Phys. Chem. 91 (1987) 4305.
[23] L. Cao, A. Huang, F.J. Spiess, S.L. Suib, Gas-phase oxidation of 1-butene using nanoscale TiO_2 photocatalysts, J. Catal. 188 (1) (1999) 48–57, https://doi.org/10.1006/jcat.1999.2596.
[24] L. Cao, Z. Gao, S.L. Suib, T.N. Obee, S.O. Hay, J.D. Freihaut, Photocatalytic oxidation of toluene on nanoscale TiO_2 catalysts: studies of deactivation and regeneration, J. Catal. 196 (2) (2000) 253–261, https://doi.org/10.1006/jcat.2000.3050.
[25] L. Cao, Q. Zhang, Effects of amorphous contents and particle size on the photocatalytic properties of TiO_2 nanoparticles, Scr. Mater. 44 (8–9) (2001) 1195–1198, https://doi.org/10.1016/S1359-6462(01)00681-9.
[26] Y. Ohama, D. Van Gemert, Application of titanium dioxide photocatalysis to construction materials: state-of-the-art report of the RILEM Technical Committee 194-TDP (Eds.), (2011), (Vol. 5), Springer Science and Business Media.
[27] H. He, C. Liu, K.D. Dubois, T. Jin, M.E. Louis, G. Li, Enhanced charge separation in nanostructured TiO_2 materials for photocatalytic and photovoltaic applications, Ind. Eng. Chem. Res. 51 (37) (2012) 11841–11849, https://doi.org/10.1021/ie300510n.
[28] M. Pérez-Nicolás, I. Navarro-Blasco, J.M. Fernández, J.I. Alvarez, Atmospheric NOx removal: Study of cement mortars with iron-and vanadium-doped TiO2 as visible light–sensitive photocatalysts, Constr. Build. Mater. 149 (2017) 257–271, https://doi.org/10.1016/j.conbuildmat.2017.05.132.
[29] S.S. Lucas, V.M. Ferreira, J.B. De Aguiar, Incorporation of titanium dioxide nanoparticles in mortars—Influence of microstructure in the hardened state properties and photocatalytic activity, Cem. Concr. Res. 43 (2013) 112–120, https://doi.org/10.1016/j.cemconres.2012.09.007.
[30] C. Gionis, Q.L. Yu, M.L. Ruello, F. Tittarelli, H.J.H. Brouwers, Effect of pore structure on the performance of photocatalytic lightweight lime-based finishing mortar, Constr. Build. Mater. 171 (2018) 232–242, https://doi.org/10.1016/j.conbuildmat.2018.03.106.
[31] R. Sugrañez, J.I. Alvarez, M. Cruz-Yusta, I. Marmol, J. Morales, J. Vila, L. Sánchez, Enhanced photocatalytic degradation of NOx gases by regulating the microstructure of mortar cement modified with titanium dioxide, Build. Environ. 69 (2013) 55–63, https://doi.org/10.1016/j.buildenv.2013.07.014.
[32] J. Chen, C.S. Poon, Photocatalytic activity of titanium dioxide modified concrete materials–Influence of utilizing recycled glass cullets as aggregates, J. Environ. Manage. 90 (11) (2009) 3436–3442, https://doi.org/10.1016/j.jenvman.2009.05.029.
[33] C.S. Poon, E. Cheung, NO removal efficiency of photocatalytic paving blocks prepared with recycled materials, Constr. Build. Mater. 21 (8) (2007) 1746–1753, https://doi.org/10.1016/j.conbuildmat.2006.05.018.
[34] V. Matějka, P. Matějková, P. Kovář, J. Vlček, J. Pitkryl, P. Červenka, Z. Lacný, J. Kukutschová, Metakaolinite/TiO2 composite: Photoactive admixture for building materials based on Portland cement binder, Constr. Build. Mater. 35 (2012) 38–44, https://doi.org/10.1016/j.conbuildmat.2012.02.086.
[35] B.Y. Lee, A.R. Jayapalan, M.H. Bergin, K.E. Kurtis, Photocatalytic cement exposed to nitrogen oxides: Effect of oxidation and binding, Cem. Concr. Res. 60 (2014) 30–36, https://doi.org/10.1016/j.cemconres.2014.03.003.
[36] M.Z. Guo, A. Maury-Ramirez, C.S. Poon, Photocatalytic activities of titanium dioxide incorporated architectural mortars: Effects of weathering and activation light, Build. Environ. 94 (2015) 395–402, https://doi.org/10.1016/j.buildenv.2015.08.027.
[37] M. Xu, Y. Bao, K. Wu, T. Xia, H.L. Clack, H. Shi, V.C. Li, Influence of TiO2 incorporation methods on NOx abatement in Engineered Cementitious Composites, Constr. Build. Mater. 221 (2019) 375–383, https://doi.org/10.1016/j.conbuildmat.2019.06.063.
[38] M. Xu, H. Clack, T. Xia, Y.i. Bao, K. Wu, H. Shi, V. Li, Effect of TiO2 and fly ash on photocatalytic NOx abatement of engineered cementitious composites, Constr. Build. Mater. 236 (2020) 117559, https://doi.org/10.1016/j.conbuildmat.2019.117559.
[39] E. Boonen, A. Beeldens, Recent photocatalytic applications for air purification in Belgium, Coatings. 4 (3) (2014) 553–573, https://doi.org/10.3390/coatings4030553.
[40] X.F. Chen, S.C. Kou, C.S. Poon, Rheological behaviour, mechanical performance, and NOx removal of photocatalytic mortar with combined clay brick sands-based and recycled glass-based nano-TiO2 composite photocatalysts, Constr. Build. Mater. 240 (2020), 117698, https://doi.org/10.1016/j.conbuildmat.2019.117698.
[41] Q. Jin, E.M. Saad, W. Zhang, Y. Tang, K.E. Kurtis, Quantification of NOx uptake in plain and TiO2-doped cementitious materials, Cem. Concr. Res. 122 (2019) 251–256, https://doi.org/10.1016/j.cemconres.2019.05.010.
[42] R. Feret, Sur la compacité des mortiers hydrauliques, Annales des Ponts et Chaussees 4 (1892) 5–16.
[43] W.B. Fuller, S.E. Thompson, The laws of proportioning concrete, Trans. Am. Soc. Civil Eng. 33 (1907) 222–298.
[44] J. Funk, D. Dinger, J.E. Funk Jr., Coal Grinding and Particle Size Distribution Studies for Coal-Water Slurries at High Solids Content, Final Report, Empire State Electric Energy Research Corporation, New York, (1980).
[45] A.H.M. Andreasen, J. Andersen, Über die Beziehung zwischen Kornabstufung und Zwischenraum in Produkten aus losen Körnern (mit einigen Experimenten), Colloid Polym. Sci. 50 (3) (1930) 217–228.
[46] V. Johansen, P.J. Andersen, Particle Packing and Concrete Properties, in: J. Skalny, S. Mindess (Eds.), Materials Science of Concrete II, The American Ceramic Society, Westerville, OH, 1991.
[47] Ö. Sevim, İ. Demir, Optimization of fly ash particle size distribution for cementitious systems with high compactness, Constr. Build. Mater. 195 (2019) 104–114, https://doi.org/10.1016/j.conbuildmat.2018.11.080.
[48] Ö. Sevim, İ. Demir, Physical and permeability properties of cementitious mortars having fly ash with optimized particle size distribution, Cem. Concr. Compos. 96 (2019) 266–273, https://doi.org/10.1016/j.cemconcomp.2018.11.017.
[49] J.L. Lim, S.N. Raman, M. Safiuddin, M.F.M. Zain, R. Hamid, Autogenous shrinkage, microstructure, and strength of ultra-high performance concrete incorporating carbon nanofibers, Mater. 12 (2) (2019) 320, https://doi.org/10.3390/ma12020320.
[50] ASTM C494 / C494M-19, Standard Specification for Chemical Admixtures for Concrete, ASTM International, West Conshohocken, PA, 2019, www.astm.org 10.1520/C0494_C0494M-19.
[51] O. Şahin, S. Bay, H. Ilcan, G. Yıldırım, M. Şahmaran, Influence of mixing methods on the NO reduction capability and electrical properties of photocatalytic cementitious systems, Cem. Concr. Compos. 115 (2021), 103840, https://doi.org/10.1016/j.cemconcomp.2020.103840.
[52] L. Cassar, A. Beeldens, N. Pimpinelli, G. L. Guerrini, Photocatalysis of cementitious materials. In International RILEM Symposium on Photocatalysis, Environ. Constr. Mater. 1 (2007) 131-145.
[53] H. Dylla, M.M. Hassan, L.N. Mohammad, T. Rupnow, E. Wright, Evaluation of environmental effectiveness of titanium dioxide photocatalyst coating for concrete pavement, Transp. Res. Rec. 2164 (1) (2010) 46–51, https://doi.org/10.3141/2164-06.
[54] J. Balbuena, M. Cruz-Yusta, A. Pastor, L. Sánchez, α-Fe2O3/SiO2 composites for the enhanced photocatalytic NO oxidation, J. Alloys Compd. 735 (2018) 1553–1561, https://doi.org/10.1016/j.jallcom.2017.11.259.
[55] H. Si, M. Zhou, Y. Fang, J. He, L.u. Yang, F. Wang, Photocatalytic concrete for NOx degradation: Influence factors and durability, Constr. Build. Mater. 298 (2021) 123835, https://doi.org/10.1016/j.conbuildmat.2021.123835.
[56] E. Mohseni, B.M. Miyandehi, J. Yang, M.A. Yazdi, Single and combined effects of nano-SiO_2, nano-Al_2O and nano-TiO_2 on the mechanical, rheological and durability properties of self-compacting mortar containing fly ash, Constr. Build. Mater. 84 (2015) 331–340, https://doi.org/10.1016/j.conbuildmat.2015.03.006.
[57] Z. Li, B. Han, X. Yu, S. Dong, L. Zhang, X. Dong, J. Ou, Effect of nano-titanium dioxide on mechanical and electrical properties and microstructure of reactive powder concrete, Mater. Res. Express 4 (9) (2017), 095008, https://doi.org/10.1088/2053-1591/aa87db.
[58] J. Chen, S.C. Kou, C.S. Poon, Hydration and properties of nano-TiO_2 blended cement composites, Cem. Concr. Compos. 34 (5) (2012) 642–649, https://doi.org/10.1016/j.cemconcomp.2012.02.009.
[59] B. Han, L. Zhang, S. Zeng, S. Dong, X. Yu, R. Yang, J. Ou, Nano-core effect in nano-engineered cementitious composites, Compos. Part A: Appl. Sci. Manuf. 95 (2017) 100–109, https://doi.org/10.1016/j.compositesa.2017.01.008.
[60] H.F.W. Taylor, Cement Chemistry, 2nd edition, Thomas Telford, London, 1997.
[61] T. Chernet, Effect of Mineralogy and Texture in the TiO2 Pigment Production Process of the Tellnes Ilmenite Concentrate, Mineral. Petrol. 67 (1999) 21–32.
[62] B.Y. Lee, K.E. Kurtis, Influence of TiO2 nanoparticles on early C3S hydration, J. Am. Ceram. Soc. 93 (10) (2010) 3399–3405, https://doi.org/10.1111/j.1551-2916.2010.03868.x.
[63] P.C. Aïtcin, R.J. Flatt, Science and technology of concrete admixtures, in Woodhead Publishing series in civil and structural engineering number 59, Woodhead Publishing is an imprint of Elsevier, Cambridge, UK, 2016.
[64] T.K. Erdem, S. Demirhan, G. Yıldırım, Q.S. Bazyhussan, O. Şahin, M.H. Balav, M. Şahmaran, Effects of Mixture Design Parameters on the Mechanical Behavior of High-Performance Fiber-Reinforced Concretes, J. Mater. Civil Eng. 32 (12) (2020) 04020368, https://doi.org/10.1061/(ASCE)MT.1943-5533.0003459.
[65] M. Xu, Y. Bao, K. Wu, H. Shi, X. Guo, V.C. Li, Multiscale investigation of tensile properties of a TiO_2-doped Engineered Cementitious Composite, Constr. Build. Mater. 209 (2019) 485–491, https://doi.org/10.1016/j.conbuildmat.2019.03.112.

[66] E. Jiménez-Relinque, J.R. Rodríguez-García, A. Castillo, M. Castellote, Characteristics and efficiency of photocatalytic cementitious materials: Type of binder, roughness and microstructure, Cem. Concr. Res. 71 (2015) 124–131, https://doi.org/10.1016/j.cemconres.2015.02.003.
[67] A.R. Jayapalan, B.Y. Lee, K.E. Kurtis, Can nanotechnology be 'green'? Comparing efficacy of nano and microparticles in cementitious materials, Cem. Concr. Compos. 36 (2013) 16–24, https://doi.org/10.1016/j.cemconcomp.2012.11.002.
[68] A. Al-Dahawi, O. Öztürk, F. Emami, G. Yıldırım, M. Şahmaran, Effect of mixing methods on the electrical properties of cementitious composites incorporating different carbon-based materials, Constr. Build. Mater. 104 (2016) 160–168, https://doi.org/10.1016/j.conbuildmat.2015.12.072.
[69] S. Yeşilmen, Y. Al-Najjar, M.H. Balav, M. Şahmaran, G. Yıldırım, M. Lachemi, Nano-modification to improve the ductility of cementitious composites, Cem. Concr. Res. 76 (2015) 170–179, https://doi.org/10.1016/j.cemconres.2015.05.026.
[70] Y. Al-Najjar, S. Yeşilmen, A. M. Al-Dahawi, M. Şahmaran, G. Yıldırım, M. Lachemi, L. Amleh, Physical and chemical actions of nano-mineral additives on properties of high-volume fly ash engineered cementitious composites, ACI Mater. J. 113(6) (2016) 791-801. 10.14359/51689114.
[71] S. Kawashima, J.W.T. Seo, D. Corr, M.C. Hersam, S.P. Shah, Dispersion of CaCO3 nanoparticles by sonication and surfactant treatment for application in fly ash–cement systems, Mater. Struct. 47 (6) (2014) 1011–1023, https://doi.org/10.1617/s11527-013-0110-9.
[72] C.B. Almquist, P. Biswas, Role of Synthesis Method and Particle Size of Nanostructured TiO_2 on Its Photoactivity, J. Catal. 212 (2) (2002) 145–156, https://doi.org/10.1006/jcat.2002.3783.
[73] C. Minero, F. Catozzo, E. Pelizzetti, Role of adsorption in photocatalyzed reactions of organic molecules in aqueous titania suspensions, Langmuir. 8 (2) (1992) 481–486.
[74] M. Lackhoff, X. Prieto, N. Nestle, F. Dehn, R. Niessner, Photocatalytic activity of semiconductor-modified cement-influence of semiconductor type and cement ageing, Appl. Catal. B: Environ. 43 (3) (2003) 205–216, https://doi.org/10.1016/S0926-3373(02)00303-X.
[75] A. Mills, S. Elouali, The nitric oxide ISO photocatalytic reactor system: measurement of NO removal activity and capacity, J. of Photochem. Photobiol. A: Chem. 305 (2015) 29–36, https://doi.org/10.1016/j.jphotochem.2015.03.002.
[76] H. Wang, Z. Wu, W. Zhao, B. Guan, Photocatalytic oxidation of nitrogen oxides using TiO2 loading on woven glass fabric, Chemosphere 66 (1) (2007) 185–190, https://doi.org/10.1016/j.chemosphere.2006.04.071.
[77] R. Han, R. Andrews, C. O'Rourke, S. Hodgen, A. Mills, Photocatalytic air purification: Effect of HNO3 accumulation on NOx and VOC removal, Catalysis Today. 380 (2021) 105–113, https://doi.org/10.1016/j.cattod.2021.04.017.
[78] L. Yang, A. Hakki, F. Wang, D.E. Macphee, Photocatalyst efficiencies in concrete technology: The effect of photocatalyst placement, Appl. Catal. B: Environ. 222 (2018) 200–208, https://doi.org/10.1016/j.apcatb.2017.10.013.
[79] F IUPAC. (1971). Manual of symbols and terminology for physicochemical quantities and units. Appendix II: definitions, terminology and symbols in colloid and surface chemistry. Everett DH, editor.
[80] L. Jones, Interference mechanisms in waste stabilization/solidification processes, J. Hazard. Mater. 24 (1) (1990) 83–88, https://doi.org/10.1016/0304-3894(90)80005-O.
[81] P.K. Mehta, P.J.M. Monteiro, Concrete Structure, Properties and Materials vol. 2 (1993) 548.
[82] H.W. Song, S.J. Kwon, Permeability characteristics of carbonated concrete considering capillary pore structure, Cem. Concr. Res. 37 (6) (2007) 909–915, https://doi.org/10.1016/j.cemconres.2007.03.011.
[83] V. Cirkva, H. Žabová, Thin nanoporous titania films on the electrodeless discharge lamps for photocatalysis, Preparation, Structure and Applications, Handbook of Photocatalysts, 2010.
[84] X. Wang, K. Wang, J. Taerwe, A. Ardani, Effects of nanomaterials on the hydration kinetics and rheology of Portland cement pastes, Adv. Civil Eng. Mater. 3 (2) (2014) 142–159, https://doi.org/10.1520/ACEM20140021.
[85] L. Znaidi, R. Seraphimova, J.F. Bocquet, C. Colbeau-Justin, C. Pommier, A semi-continuous process for the synthesis of nanosize TiO_2 powders and their use as photocatalysts, Mater. Res. Bull. 36 (5–6) (2001) 811–825, https://doi.org/10.1016/S0025-5408(00)00482-7.